A REFLECTING TIME-OF-FLIGHT MASS SPECTROMETER

BY

XUEJUN TANG

A Thesis Submitted to

the Faculty of Graduate Studies

In Partial Fulfillment of the Requirements

for the Degree of

DOCTOR OF PHILOSOPHY

University of Manitoba

Winnipeg, Manitoba, Canada

March 1991

ISBN 0-315-76798-7

A REFLECTING TIME-OF-FLIGHT MASS SPECTROMETER

BY

XUEJUN TANG

A thesis submitted to the Faculty of Graduate Studies of
the University of Manitoba in partial fulfillment of the requirements
of the degree of

DOCTOR OF PHILOSOPHY

ACKNOWLEDGEMENTS

I would like to thank my advisor, Dr. Ken Standing, for directing the research described in this thesis, and for his valuable advice and tremendous insight. The concept for the work outlined in the thesis was his, including the design of the reflecting spectrometer; my part was the realization of the idea. I am grateful to Dr. John Westmore for his helpful advice on the chemistry involved in this thesis, including assistance in the interpretation of the mass spectra. I would also like to thank Dr. Werner Ens for his contributions to the development of the data system used for the work and for his helpful advice in the experiments.

I am grateful to my wife, Ying, for her tremendous support of my work, particularly during the period of writing this thesis.

Finally, I wish to thank Francois Lafortune, John Martens, Nancy Poppe-Schriemer, Henry Schriemer, Gillis Roy and Drs. Franz Mayer, Dennis Main, Bruno Schueler, Ron Beavis, Gerard Bolbach, and many others, each in a special way, for making this such a memorable experience.

Financial assistance in the form of a graduate fellowship and a research assistantship was provided by the University of Manitoba and the U.S. National Institutes of Health (GM-30605).

ABSTRACT

The design, construction and operation of Manitoba TOF II, a reflecting time-of-flight mass spectrometer is described. In particular, the details of design and construction of the ion mirror are discussed. The principle of velocity focusing with a single-stage ion mirror and the effect of the acceleration region are described and discussed.

The performance of the reflecting instrument is described. Its detection limit is illustrated by observation of $[M+H]^+$ ions from ~5-35 femtomoles of various peptides. The factors that affect the resolution are discussed; a mass resolving power of $(m/\Delta m)_{FWHM} \approx 13\ 000$ has been achieved with the single-stage mirror.

The principle and operation of the reflecting instrument as a tandem mass spectrometer is described; this involves correlated detection of neutral and ionized fragments. The efficiency, resolution, sensitivity, and mass determination of daughter ions by this method are described and discussed.

Methods of sample preparation are described. By using a nitrocellulose substrate, organic molecular ions as large as bovine insulin (MW 5733) were detected for the first time with low energy (keV) ion bombardment of a solid surface. Many daughter ion spectra resulting from metastable decay of parent ions have been studied. Secondary ions $[(CsI)_nCs]^+$ with n up to ~50 were detected; all the clusters were found to be metastable, with most lifetimes $\ll$100 μs, and for n>10 the daughter ions are dominant in the mass spectrum. Peptides of mass up to ~2000 u have been studied with the correlated method; the daughter ion spectra were found to be strongly influenced by the identity of the bound

cation (H^+, Na^+, K^+, or Ag^+). Many daughter ions formed by known reactions yield structure and sequence information about the peptides. In addition, the $[M+Na]^+$ and $[M+Ag]^+$ ions decompose by a previously unreported pathway, namely, rearrangement of a C-terminal carboxyl oxygen onto the daughter ion containing the N-terminus. Both the reflected spectra and daughter ion spectra were found useful in peptide sequencing. The applications of the correlated method to analysis of peptide mixtures and to nucleotides are also described and discussed.

CONTENTS

APPENDIX Page

LIST OF FIGURES

LIST OF TABLES

CHAPTER 1

INTRODUCTION

Mass spectrometry, one of the most generally applicable of all the analytical techniques, provides qualitative and quantitative information about the atomic and molecular composition of inorganic and organic materials. It has grown in the past eighty years from a research technique of basic physics to a powerful analytical tool which can provide useful data for all branches of science from physics to chemistry and from oceanography to space science. The fundamental principle of mass spectrometry (the production, the separation and recording of the mass of an ionized particle) was first demonstrated by J. J. Thompson in 1912 [1]. In his work the existence of two isotopes of neon, masses 20 and 22, was found by using a magnetic deflection instrument. The first precision mass spectrometers were constructed by J. Dempster in 1918 [2] and by F. W. Aston in 1919 [3], to measure the relative abundances of some isotopes.

Until 1940 the mass spectrometer was only used for the analysis of gases and for the mass determination of the stable isotopes of chemical elements [4,5]. It was later used to carry out quick and accurate analyses of complex mixtures of hydrocarbons from petroleum fractions; then, when it was demonstrated that a complex molecule could give rise to a well-defined and reproducible mass spectrum, interest in its application to the

determination of organic structures was established.

The coupling of gas chromatography with mass spectrometry (GC/MS) has extended the applications of both techniques. These two methods are in fact highly complementary. Gas chromatograph is very efficient for the separation of the constituents of a mixture, whereas the mass spectrometer is excellent for identification. A very important factor is the comparable sensitivity of the two techniques.

The main advantages of mass spectrometry as an analytical technique are its increased sensitivity over many other analytical techniques and its specificity in identifying unknowns or confirming the presence of suspected compounds. Sample size requirements for solids and liquids may range from a few milligrams to subnanogram quantities as long as the material can be volatilized and can exist in the gaseous state at the temperature and pressure in the ion source, where the molecules of the substance become ionized. The most widely used ionization method is that of electron impact (EI).

Ions formed by the exchange of energy during the collision of the electron beam and sample molecules are usually in a high state of electronic and vibrational excitation. With organic samples, the large amount of electronic and vibrational excitation leads to the dissociation of the molecular ions, thus resulting in complex mass spectra, often without molecular weight information. Several alternative ionization methods can be used in order to reduce fragmentation following ionization. The most successful alternatives to EI have been chemical ionization (CI) and field ionization (FI).

CI was first introduced by Munson and Field in 1962 [6]. It is accomplished by an ion-molecule charge transfer occurring between a preionized reactant gas and the sample gas. The reaction takes place at a relatively high pressure (typically reagent gas pressure of ~1 torr and sample pressures of $\sim 10^{-3}$ torr in the ion source). When little

energy is released in the ion-molecule reaction the fragmentation may be substantially less than in electron impact.

FI was first used in mass spectrometry by Inghram and Gomer in 1954 [7] and a comprehensive treatment of field ionization sources was subsequently prepared by Beckey [8]. FI utilizes a high local electrical field of ~10^8 V/cm to generate ions near the tip of thin filaments, the edges of metal blades, or grown microstructures. Ionization is assumed to occur at a distance of several angstroms in front of the tip due to quantum mechanical tunnelling of an electron from a gas molecule to the metal surface. Because FI involves small amounts of energy transfer, fragile molecules can be analyzed without appreciable dissociation.

Although CI and FI offer some improvement of the molecular ion signal over EI, the requirement of volatilization of samples for these ionization methods causes problems when the sample molecules are involatile or thermolabile, i.e. the temperature at which they would evaporate is higher than that at which they decompose. There are many organic compounds which are too involatile, either because their molecular mass is too high or because they are highly polar, to be studied by mass spectrometry with the above mentioned ionization methods. Such compounds, including proteins, are often very important to many life-science-related disciplines such as biochemistry and biotechnology.

1.1 DEVELOPMENT OF MASS SPECTROMETRIC METHODS FOR LARGE INVOLATILE ORGANIC MOLECULES

Much progress has been made over the past twenty years towards the mass

spectrometry of these large involatile compounds. The success is largely due to the development of desorption ionization techniques.

1.1.1 Field Desorption

The first technique used to produce molecular ions of large organic molecules was field desorption (FD), which was introduced by Beckey in 1969 [9]. Field desorption is a special case of field ionization; here a sample solution of interest is coated onto the emitting surface, a fine tungsten wire (10 μm diameter) on which microneedles have been grown. After careful evaporation of the solvent, the emitter is introduced into the field ionization source where positively charged sample ions are ejected from the surface of the emitter under the action of a strong electric field. This is in contrast to field ionization where the sample reaches the vicinity of the field tip as a vapour. The special applicability of the field desorption ion source to the analysis of biologically important compounds, large molecules and samples that are thermally involatile, was successful in attracting wide attention, but the handling of the process of needle growth and sample coating is difficult, and the reproducibility of the emitters is often poor. These factors have limited the analytical application of this technique.

1.1.2 Particle Induced Desorption

There are other ionization methods that have been applied very successfully to produce large intact organic molecular ions from the condensed phase. In these techniques, bombardment of samples with ion, atom, fission fragment or photon beams

may be used to desorb and ionize molecules from a thin solid or liquid layer deposited on a surface.

1.1.2.1 ^{252}Cf Fission fragment plasma desorption

The first of these techniques, which revolutionized the mass spectrometry of large organic molecules, is plasma desorption mass spectrometry (PDMS). This method, using ^{252}Cf fission fragments as the impacting particles, was first discovered by Macfarlane and Torgerson in 1974 [10] from a chance observation made when these authors studied recoil ions from ß decay using a time-of-flight spectrometer. In the experiment, they found additional peaks representing adsorbed molecules on the surface. To check on the origin of the background, they replaced the beta emitters with fission fragments from a ^{252}Cf-source to increase the energy deposition in the surface to determine whether the desorption yields of molecular ions increased. This, in fact, happened, and the first PDMS spectrum was recorded [11]. This new approach, to desorb and ionize non-volatile molecules from a solid surface, was termed plasma desorption because the fission fragments were speculated to lose energy in the solid through the production of microplasmas. Californium-252 is a spontaneously fissioning nucleus with a half-life of 2.65 years, 3% of the decays taking place by spontaneous fission and the remaining 97% by emission of alpha particles [12,14]. Each fission event produces two fragments travelling in almost opposite directions. A typical pair of fission fragments is $^{142}Ba^{18+}$ and $^{106}Te^{22+}$, which have kinetic energies of about 79 to 104 MeV, respectively [13,14]. These fission fragments also have a very short range in solids due to their high energy loss in passing through the solid (0.1-1 keV/Å). Thus it is important that the source be

thin if the fission fragments are incident from behind. A typical source strength is 10 μCi spread over a circular area of 3-5 mm diameter [15].

To obtain a mass spectrum the sample solution is deposited on a thin foil, (e.g. aluminized polypropylene film) over an area ca 1 cm^2. It is important for the sample and backing to be thin enough (less than ~ 10 μm) [14] for the fission fragment to be transmitted; if the fission fragment stops in the sample because it is too thick, no ions are detected. After preparation, the sample foil is precisely aligned in close proximity to the ^{252}Cf source in a time-of-flight spectrometer. In most systems used so far, both associated fission fragments from a fission event are used. One fission fragment penetrates the sample from the back of the sample foil, producing desorbed ions, which emerge from the opposite face and are accelerated by a uniform electric field into the spectrometer. The other fission fragment, travelling in the opposite direction, is detected and serves as a time zero marker. By using fast timing electronics originally designed for nuclear physics, the flight time of the individual ions can be recorded. The spectral data are obtained in the pulsed mode with a flux of about 2000 fission fragments per second hitting the target. Because each ion pulse is generated by a discrete event that generates only a few ions, the signal can be accumulated over a considerable period of time from a few minutes to many hours to produce a reasonable mass spectrum.

The development of ^{252}Cf plasma desorption mass spectrometry has given a considerable boost to the mass spectrometry of large involatile and thermolabile organic molecules. ^{252}Cf fission fragment plasma desorption was the most effective means for producing molecular ions of involatile species of mass above 10 000 u [15] until the recent emergence of two new techniques described below. The high mass range and sensitivity have made PDMS an interesting candidate for certain aspects of biochemistry,

particularly for direct molecular weight determinations of large biomolecules such as small proteins, carbohydrates and polynucleotides. The largest involatile molecular ion observed with this technique is from ovalbumin with a molecular weight of 45,000 u [16]. Commercial instruments equipped with a time-of-flight mass analyzer and a ^{252}Cf fission fragment source were made available by Bio-Ion Nordic AB, Uppsala Sweden. Progress in PDMS has been reviewed by Sundqvist and Macfarlane [15].

1.1.2.2 High energy ion bombardment

Although ^{252}Cf PDMS has been used successfully for many large biomolecules, it is difficult to study the fundamentals of the primary processes, since the parameters relating to the incident ion cannot be controlled. A technique similar to ^{252}Cf fission fragment bombardment, but more flexible in several respects was developed independently by Dück et al [17], and Sundqvist and co-workers [18]. The technique is based on bombardment by heavy ions with energies in the order of MeV u^{-1}, produced in a tandem accelerator. The spectra obtained by high energy ion bombardment are similar to those produced by fission fragment induced desorption, but offer further insight into the desorption process because the energy, charge state, angle of incidence and mass of the primary ions are adjustable parameters. Desorption yields have been measured as a function of these variables, allowing some tentative conclusions to be drawn concerning the role of electronic energy loss and the desorption mechanism [19-22].

1.1.2.3 Low energy ion bombardment-SIMS

Several alternative approaches for identification of large involatile and thermolabile molecules were developed a little later. One such approach is low energy (keV) ion bombardment, which is also the method most relevant to this thesis.

The production of secondary ions by ion bombardment, or sputtering is one of the most important methods for the analysis of solids; when a solid surface is bombarded by energetic ions, there will be an emission of secondary particles (positive and negative ions, neutrals and electrons) and photons. Mass analysis of the secondary ions is the basis of secondary ion mass spectrometry (SIMS).

Virtually all secondary ions originate from the uppermost layers of the bombarded surface. This results in one of the most important features of SIMS, i.e. its surface sensitivity. The m/z spectrum of secondary ions emitted from the bombarded surface supplies direct information obtained on the chemical composition of the bombarded area. By applying a finely-focused primary particle beam, and by scanning this beam over a limited surface area, information about the lateral surface distribution of the secondary ion emission and thus of the chemical composition can be obtained.

The removal of atomic and molecular surface species by sputtering results in the erosion of the surface. Under the condition of high primary ion current densities ($>10^{-6}A/cm^2$), the lifetime of a monolayer is less than a few seconds [23]. This fast surface erosion continuously moves the actual surface into the bulk material, thus supplying information on the chemical composition of originally deeper layers of the bombarded sample (depth profiling). The mode of operation that uses high primary ion current density is known as "Dynamic SIMS". Dynamic SIMS with a focused scanning

ion beam allows a three-dimensional analysis of the sample.

SIMS has a long history but had a slow, hesitant start. Although the first observation of emission of ion-induced neutral species and positive ions was made by J. J. Thomson in 1910 [24], the first complete SIMS instrument was reported only in 1958 [25], almost half a century later. During the following years, SIMS started to gain momentum, and beginning in the middle 1960's, rapid development took place both in instrumentation and analytical applications. However, the early applications of SIMS were limited almost exclusively to inorganic samples, and they mainly used dynamic SIMS for obtaining concentration profiles in depth and for identifying trace impurities of semiconductor materials [26].

The use of low energy ion bombardment for desorption of organic molecules was pioneered by Benninghoven [27] and was regarded as an unexpected development of so called static SIMS, which he introduced in 1969 [28]. In static SIMS, it is the intention to get information on the composition of the uppermost monolayer, virtually without disturbing its composition and structure. This is achieved by using very low primary ion current densities ($\leq 10^{-9} A/cm^2$) and limiting the total dose of primary ions to 10^{12}~$10^{13}/cm^2$ to insure that most of the secondary ions are emitted from areas not previously damaged. This dose corresponds to an aggregate bombarded area amounting to 1-10% of the total area. Typical bombardment conditions are: primary current densities of $10^{-9} A/cm^2$ or less for about 1000s; the lifetime of a monolayer is of the order of some hours under such conditions. To increase the sensitivity of the method, it is necessary to work with large sample areas. Initially, static SIMS was applied to monomolecular layers adsorbed on metals [28-30], and later, beginning in 1976 [27], to the desorption and analysis of organic molecules with a ~3 keV Ar^+ primary ion beam and a magnetic sector

instrument. In their investigations of secondary ion emission from amino acids, Benninghoven and co-workers found a strong emission of protonated or deprotonated molecules $[M+H]^+$ and $[M-H]^-$ from the corresponding molecular layer on a silver substrate. Soon afterwards, they demonstrated similar results for various other families of small organic molecules [31,32]. The mass range ($m/z \leq 300$) was then limited because of the type of mass spectrometer used in the experiments. The appearance of quasimolecular ion peaks in the secondary ion mass spectrum of such organic molecules was an unexpected result at that time [23]. Organic molecules are very sensitive to ion bombardment; sputtering had been regarded as extremely destructive and only small fragments were expected to be emitted even for large surface molecules. This is the case in dynamic SIMS, where higher primary ion current densities used in sputtering rapidly damage the surface and destroy the desorbed molecules in the process, before a mass spectrum can be accumulated. The success of organic SIMS attracted wide attention, the main reason being its analytical capabilities; submonolayers of nonvolatile and thermolabile organic compounds can be detected and identified with rather simple SIMS equipment. Depending on the mass spectrometer used, sensitivities in the picomole to femtomole range can be achieved.

1.1.2.4 Fast atom bombardment

Another approach, called fast atom bombardment (FAB), has found wide acceptance and is widely used, mostly in combination with double focusing magnetic sector or quadrupole mass analyzers.

FAB, a variant of the SIMS technique, was introduced by Barber et al in 1981

[33-35]. It uses a beam of keV energy neutral atoms rather than ions as bombarding particles. This reduces charging of organic samples, which are usually insulators, and also allows an easier transfer of the primary beam into the ion source, which is, in general, at a high potential in commercial magnetic sector instruments. Since a beam of neutral atoms is undisturbed by either electric or magnetic fields, some of ion optics problems are avoided and the adaptation of a FAB source to various types of existing double focusing magnetic sector instruments is relatively simple.

A feature distinguishing FAB from other ion production methods is the use of a liquid matrix [36] such as glycerol, containing the sample molecules, instead of assaying thin solid films or coatings. It is now well established that the presence or absence of charge on the impacting primary particle has little effect on the desorption process. Since the ion may be neutralized by long range electron transfer as it approaches the surface, the major effect of the impact is the same for neutral species as for singly charged ions [14]. The similarity in spectra obtained by SIMS and FAB confirms the similarity in mechanism, but the use of the liquid matrix has some pronounced effects.

As mentioned earlier, it is necessary that the investigation of organic secondary ion emission from a simple solid surface be carried out in the static mode of SIMS to avoid radiation damage to molecules on the surface. However, the very low secondary ion currents produced under static SIMS conditions prevents the application of organic SIMS to instruments with relatively low overall efficiency, such as double-focusing magnetic sector instruments. If a sample of a nonvolatile organic compound is first dissolved in a liquid with very low vapour pressure, such as glycerol, then exposed to the primary particle beam, the surface of the liquid will be damaged as in the solid case. However, the solution presents a mobile, constantly renewed, surface to the bombarding beam

because of sputtering of the glycerol matrix. This provides continuous replenishment of undamaged sample molecules to be desorbed and ionized. The liquid also promotes the formation of a favourable precursor. As a result of using the liquid matrix, the requirement for working at low primary current densities to avoid damage of molecules on the surface is removed. Current densities several orders of magnitude larger than those suggested by Benninghoven's static SIMS work [27] have been used routinely; concomitantly, higher and more stable secondary ion currents can be obtained as long as a liquid phase is present on the sample holder. This gives long-lasting spectra (up to 30 min or more) even when the sample is bombarded with high-flux primary beams [36] and allows the application of organic SIMS to low transmission instruments.

The compatibility of FAB or liquid SIMS sources with high resolution and high mass range double focusing sector field instruments has made it very popular with many laboratories, and these techniques have considerably extended the scope of applications of mass spectrometry. FAB has become the usual method for the mass spectrometric analysis of most polar, nonvolatile compounds with mass up to ~5 000 u. The early extensive applications of FAB in organic analysis were reviewed by Fenselau [37], Turner et al [38] and Burlingame et al [39]. A large number of more recent FAB publications have been reviewed by Biemann et al [40], Burlingame et al [41] and Tomer [42]; these attest to the continuing popularity of FAB/MS.

1.1.3 Laser Desorption

The last desorption method to be discussed involves the use of lasers, in a technique related to particle desorption, that has revolutionized the mass spectrometry of

very large organic molecules in the last two years.

The first use of a laser beam to produce ions in a mass spectrometer ion source was reported by Honig and Woolston in 1963 [43,44], shortly after the invention of the laser. They demonstrated that sufficiently high surface temperatures were generated with a ruby laser to produce vaporization and ionization from metals, semiconductors and insulators. A few years later, Vastola and his co-workers started a program of laser induced vaporization of solids, including organic compounds [45,46]. However, the real development of laser desorption mass spectrometry (LDMS) of organic specimens, including bioorganic molecules and biological samples, only began in the mid-seventies.

In 1976, the use of nanosecond pulsed lasers with sophisticated time-of-flight mass spectrometers to study biological materials was reported by Hillenkamp and co-workers [47]. In 1978, the potential for laser desorption mass spectral analysis of large, non-volatile, thermally labile organic molecules was demonstrated by Kistemaker et al [48], using a magnetic sector instrument capable of recording simultaneously a limited spectral range with a channel-plate array. Since then, a number of laboratories have conducted laser desorption experiments with a variety of mass analyzers [49-53], and LDMS has been widely applied to many problems. Commercial instruments for microanalysis have also been developed, such as the LAMMA 500 and 1000 [54,55] by Leybold-Heraeus under the acronym of laser Microprobe Mass Analyzer (LAMMA). In LAMMA instruments, organic or inorganic sample molecules from a small area are desorbed and ionized by a short pulse of a well-focused laser beam. The ions produced are then analyzed by a time-of-flight mass spectrometer with an electronic transient recorder. The laser microprobe has become an important instrument for the analysis of metals, polymers, and inorganic and biological specimens. The early work on LDMS was

reviewed in detail by Conzemius and Capellen in 1980 [53], and more recent laser desorption work has been reviewed by Hillenkamp in 1983 and 1985 [56,57], with particular emphasis on laser-induced ion formation from organic solids. Various experimental and instrumental approaches were discussed, and mechanisms of ion formation, attempting to explain the mass spectra obtained with the different techniques, were given. These processes are:

1. Thermal evaporation of ions from the solid.
2. Thermal evaporation of neutral molecules from the solid followed by ionization in the gas phase.
3. "True" laser desorption.
4. Ion formation in a laser-generated plasma.

The first two processes are referred to as thermal, because they can also be induced by classical Joule or non-laser radiative heating, usually in conjunction with heat conduction to the sample surface. In the case of "true" laser desorption, the laser induced ions show properties that exclude a thermal process of generation. The ions have initial kinetic energies of more than 10 eV and often even 50-100 eV. The mechanisms that lead to such "true" laser desorption are believed to be collective, non-equilibrium processes in the condensed phase [56,58].

At high laser power densities [$\geq 10^{10} W/cm^2$], dense plasmas are formed from the solid, molecules will be broken down to their atomic constituents, multiply charged atomic ions will grow in abundance with increasing laser power density, and ion initial energies will typically be in the range of kiloelectron volts. The plasma mode is certainly not suited for organic mass spectrometry, but has decided advantages for inorganic analysis because the ion yields become nearly uniform for all elements throughout the

periodic table. It is quite likely that the actual experimental results have to be explained by more than a single process, since one can simultaneously create a plasma in the center of the non-uniformly irradiated area, and get "true" laser desorption from the periphery, and even thermal ion emission from the heated substrate from times longer than the laser pulse duration.

Compared with particle desorption methods, laser desorption may offer the advantage of more free variables for adjustment in a given analytical problem. At the same time, this makes intercomparison of laser desorption results difficult because of the wide range of experimental parameters used by different groups [56,57].

The laser desorption mass spectrometry technique has been hampered by its poor spectrum reproducibility for both fragmentation patterns and absolute intensities owing to the complicated set of processes contributing to ion formation. The probabilities of these processes may well depend on various experimental parameters, such as laser power densities, wavelengths, pulse lengths and the absorption characteristics of the sample matrix. Among them, the most critical parameter appears to be the laser power density. On changing it, the laser desorption technique can provide elemental analyses of the most nonvolatile samples and can also yield molecular weight and structure information on quite fragile biological molecules. This extreme dependence on laser power density (more properly energy density absorbed by the sample) is also the source of its poor reproducibility. The factors affecting the energy density absorbed by the sample may vary between laser shots, making it difficult to obtain reproducible spectra.

Apart from its poor reproducibility, application of laser desorption mass spectrometry to non-volatile organic compounds had been limited by its relatively low mass range (up to ~1000 u) [59,79].

In laser desorption, high irradiances, (10^6-10^8 W/cm^2) [57] that are necessary for desorption also cause an appreciable degree of internal excitation (vibrational and rotational) of the desorbed molecular ions. As a result, the ions produced by laser desorption have not only higher initial translational energies than those produced by particle desorption but also a large degree of internal excitation, and the spectra of large organic molecules (without matrix) usually show a large amount of fragmentation with little or no molecular ion information.

Efforts have been made to overcome the lack of "softness" of the laser desorption technique and to improve its applicability to larger organic molecules.

One general finding in laser desorption is that neutral organic molecules are desorbed at much lower laser irradiance than that necessary for the desorption of ions, and the yield of neutral molecules is much higher than that of the ions [60-62], as also found in FAB, SIMS and PDMS [63,64]. Typical values for the ratio of neutral molecules to ions is about 10^4:1 in laser desorption experiments [60,61].

This result has recently spurred some interesting developments in which ultraviolet lasers have been used for postionization of neutral molecules desorbed by pulsed infrared (IR) or ultraviolet (UV) lasers, with or without cooling in a supersonic jet [62]. Schlag et al [65,66], and subsequently Tembreull and Lubman [67-69], demonstrated with time-of-flight mass spectrometers that resonant multiphoton ionization after cooling of IR-laser desorbed molecules in a supersonic molecular beam is a useful method of soft ionization of involatile bioorganic molecules of masses up to ~1000 u. The main advantage of this technique results from the separation of the desorption and the ionization processes, allowing the optimization of both processes independently. The ionization, in particular, can be very controllable. Tuning the laser wavelength into an

electronic transition of one particular component in a mixture of substances will lead to its selective ionization, thereby often improving the signal-to-background ratio. Also, the degree of fragmentation of molecular species can be influenced by changing the laser power density, thereby increasing the yield of molecular ions or large ionic fragments. A disadvantage of this method is the relatively low useful yield, due to the geometrical losses in the transport process. Successful detection of IR-laser desorbed PTH-amino acids without the use of supersonic cooling has been reported by Engelke et al [70], but attempts to postionize UV-laser desorbed neutrals of mass above ~500 u without fragmentation and without cooling in a supersonic beam have not been successful [62].

In the last decade, the accessible mass range of thermally labile and involatile organic molecules has been continuously extended with the development of these so called "soft" ionization methods. While FAB, or liquid SIMS, finds its main application in the mass range below 5,000 u, PDMS was more useful in the mass range above 10,000 u [15]. Although PDMS has been used to observe proteins with masses up to 45,000 u [16], it is routinely used below 15,000 u only [71,72].

Several years ago, two exciting new methods of producing quasi-molecular ions of very large organic species by laser desorption mass spectrometry were published. Both of these new techniques use pulsed ultraviolet (UV) lasers to desorb molecules embedded in a matrix, and time-of-flight mass measurement. The significant common feature of the two techniques is the use of a sample matrix, rather than a pure substance, and the essential difference between them is the type of matrix used. Tanaka et al [73,74] first reported laser desorption/ionization of molecular ions of proteins with masses up to 34,000 u by using a matrix of an ultra fine metal powder dispersed in glycerol and irradiating the mixture of analyte and matrix with a pulsed nitrogen laser at 337 nm.

For a number of years, Hillenkamp and co-workers had been investigating the effect of matrix-assisted ion desorption using UV lasers [57,75,76] and found that the use of resonantly absorbing matrices enabled an effective and controllable coupling of the laser energy into the condensed phase. As a result, the degree of internal excitation of the desorbed quasimolecular ions may remain limited; hence a "very soft" desorption can be achieved even for molecules lacking absorption at the wavelength used. The matrix-assisted laser desorption spectra show not only an increase in quasimolecular ion abundances but also great improvement in reproducibility over the pure substance spectra. Biomolecules up to a molecular weight of ~3000 u could then be successfully desorbed without any fragmentation, and with considerable sensitivity, by using a resonantly absorbing solid or liquid matrix [75].

After some systematic studies, a real breakthrough towards the analysis of very large bioorganic molecules was achieved. In 1988 Karas and Hillenkamp reported preliminary results on protein desorption ionization up to a molecular weight of 67,000 u by using a relatively volatile nicotinic acid (3-pyridine carboxylic acid) matrix and irradiating the dried mixture of the sample and nicotinic acid (a strong UV absorber at 266nm) with a UV laser at 266nm [77]. Subsequently, the same group demonstrated that molecular ions of biological compounds with masses up to 230,000 u could be desorbed and detected by this technique [62,78,79].

The mass spectrometer used in their experiments was the LAMMA 1000, a reflecting time-of-flight mass spectrometer equipped with a Q switched quadrupled Nd-YAG-laser (pulse length 10 ns, wave length 266 nm) for desorption and ionization. Typical laser parameters are focus diameters between 10-50 μm and irradiances of $1-5\times10^7$ W/cm^2. Ions were extracted by a voltage of 3kV and post-accelerated to about

20 keV to improve the sensitivity of the electron multiplier in the high mass range. The intense ion signals for each laser pulse were recorded and stored with a transient recorder.

Samples were dissolved in water at a concentration of about 10^{-5} M. One microliter of sample solution (10^{-11} mol) was mixed with 1 μL of a more concentrated aqueous solution of nicotinic acid as matrix in a molar ratio of 1:100-10,000. The mixture is dripped onto a metallic substrate and air-dried. It is typically spread over an area of 5 mm^2. A large number of intact quasimolecular ions are generated upon impact of a laser pulse, and clearly detectable ion signals are detected in all cases, even for single shot spectra. Usually 10-30 single spectra are accumulated for a better signal-to-noise ratio. They can be obtained by repeatedly irradiating the same area. The accumulation time is 1-5 min, limited by the laser repetition frequency of 1 Hz and by PC data-processing time.

Although the process by which these monster molecular ions are produced is still not well understood, nevertheless, matrix assisted laser desorption appears to be a very soft and very efficient ionization technique. The spectra are characterized by singly and doubly charged molecular ions; usually the singly charged molecular ion is the base peak of the analyte signal. No fragment ions are observed in the mass range above 1000 u, and the intense signals in the mass range below 1,000 u are caused exclusively by the matrix. All spectra show a very good signal-to-noise ratio with a sample amount in the picomole range.

The capability and unique features of the matrix-assisted laser desorption technique demonstrated by Karas and Hillenkamp have attracted a lot of attention. The successful application of this technique with other matrices such as cinnamic acid derivatives and

different lasers, with wavelengths ranging from 266 nm to 355 nm, on a linear time-of-flight mass spectrometer has been reported recently by Beavis and Chait [80-82]. They have also shown that, by choosing a suitable matrix, mixtures can be analyzed without the suppression effects observed in other techniques [83].

These exciting developments promise that matrix-assisted laser desorption will become a valuable tool in the field of high-mass molecular weight determination and structure analysis, and will certainly be a hot topic of research in the next few years.

1.1.4 Electrospray Ionization

Apart from the desorption ionization methods discussed above, another significant advance has occurred in mass spectrometry of large involatile organic molecules during the last two years. This is largely due to the efforts made by Fenn and co-workers [84-86] during the early 1980's in developing the electrospray ionization method.

About twenty years ago, Dole and his colleagues [87,88] carried out some pioneering experiments that produced isolated gas-phase ions from high molecular weight polymers by electrospraying a polymer solution into a bath gas at atmospheric pressure. Because he was concerned with macroions whose masses were larger than could be accommodated by conventional mass analyzers then available, Dole resorted to a low accuracy energy analysis for mass determination. This was done by measuring the retarding potential required to stop the ions from reaching a Faraday cage.

Recently, Fenn and co-workers [86,89-92] overcame the difficulties encountered by Dole by interfacing an atmospheric pressure electrospray ionization source to a quadrupole mass analyzer. In their technique, an analyte solution of flow rate between

1–40 μL/min enters the electrospray chamber through a stainless steel hypodermic needle at ground potential.

The field at the needle tip charges the surface of the emerging liquid, dispersing it by Coulomb forces into a fine spray of charged droplets. Driven by the electric field, the droplets migrate toward the metallized inlet end of a glass capillary through a counter current flow (100 mL/s) of heated bath gas, typically at 800 Torr. The solvent vapour from the evaporating droplets, along with any other uncharged material, is swept away from the capillary inlet by the bath gas flow. Some of the desorbed ions are entrained in the flow of dry bath gas that enters the capillary, to emerge at the metallized exit end as a supersonic free jet in the first of two vacuum chambers. A core portion of this free jet passes through a skimmer into a second vacuum chamber, delivering ions to a quadrupole mass analyzer. Fenn et al discovered that the electrospray ionization process exhibits a strong propensity for producing very highly charged ions from large organic molecules. This is a considerable advantage, because the mass range of any analyzer is increased by a factor equal to the number of charges per ion. Furthermore, the multiple charging is so extensive that mass-to-charge ratios are usually less than about 2500 [92], no matter how massive the parent species, so very large molecules may be examined in quadrupole or magnetic sector mass spectrometers of limited m/z range. Another advantage of the multiple charging is that under the same acceleration voltage, the kinetic energy of the multicharged ions is higher than that of singly charged ions with same mass by a factor equal to the multiplicity. Thus, the detection efficiency of the electron multiplier for the multiply charged ions will be improved considerably for large molecules. This technique also appears to be very "soft"; the spectra are characterized by a group of multiply charged molecular ions with very little, or no fragmentation.

In the last two years, a variety of biopolymers, especially proteins and peptides, have been examined by electrospray ionization with quadrupole mass analyzers [91-95]. Very recently, proteins with molecular weights ranging to 133,000 u have been observed by Loo et al [94], by this technique. This combination has also been incorporated into commercial instruments by Sciex (Thornhill, Ontario, Canada) and other companies. The progress of electrospray ionization has been reviewed by Fenn [92] last year.

1.1.5 Influence of Sample Preparation

In the desorption ionization techniques discussed above, the spectra produced have some common characteristics in spite of the very different types of primary excitation. Even-electron pseudomolecular ions (protonated, deprotonated or cationized molecules) are present and there is a pronounced influence of the physico-chemical properties of the surrounding matrix and, thereby, of the sample preparation. The formation and emission of sample-specific ions, and the degree of fragmentation, depend critically on the analyte chemical environment. The intensity ratio of pseudomolecular ions $[M+H]^+/[M-H]^-$ can be changed by an order of magnitude by changing the acidity of the sample solution [23], and traces of ionic impurities such as alkali metal can suppress formation of protonated molecules, distort fragmentation patterns, and produce new ions due to the cationization of the molecules that often dominate the mass spectra. The intensity of quasimolecular ions can be greatly increased, the fragmentation decreased, and larger involatile molecular ions can be produced by choosing the right sample/substrate or sample/matrix combination. For instance, the desorption of intact organic species by high intensity keV ion or atom beams was made possible only after the introduction of glycerol as a liquid

matrix [36]. PDMS and static SIMS were significantly improved for protein and peptide desorption by the use of a nitrocellulose substrate to adsorb analyte molecules [96,97], and the latest revolutionary advance in laser desorption/ionization of very large organic molecules was made by the discovery of a solid matrix of nicotinic acid [77-79].

More about sample preparation methods will be discussed later in this thesis.

1.2 DEVELOPMENT OF TIME-OF-FLIGHT MASS SPECTROMETRY

During the first half of this century, the development of mass spectrometry after the pioneering work of J.J.Thomson [1] was limited to instruments based on deflecting electric and magnetic fields to energy-select and momentum-analyze ions.

In the late 1940's and early 1950's, several new concepts in mass analyzers began to evolve, which used dynamic or time-varing electric fields; consequently, these instruments are referred to as dynamic mass spectrometers.

The use of the time-of-flight (TOF) principle for mass separation of a pulsed ion packet was first suggested by Stephens [98] in 1946, and two years later, such an apparatus, which was called an ion "Velocitron", later to be known as the time-of-flight mass spectrometer, was reported by Cameron and Eggers [99]. The omegatron, forerunner to the ion cyclotron resonance mass spectrometer and Fourier transform mass spectrometer, was reported by Hipple and coworkers [100] in 1949. The concept of the strong focusing effect with quadrupole fields was reported by Courant et al [101] and Blewett [102] in the early 1950's, and soon thereafter Paul and Steinwedel recognized the potential of electric quadrupole fields for mass analysis [103].

TOF mass spectrometers operate on the simple principle that a packet of ions of different mass-to-charge (m/z) ratio, if rapidly accelerated to the same kinetic energy, or momentum, will possess individual velocities that depend on their m/z ratio; if z=1, the dependence is essentially with respect to mass. When the ions are projected into a drift space, they will separate according to their mass; the light ions, having the higher velocity, will arrive at the end of the drift space before the heavier ions of low velocity. For the constant energy case, the TOF of an ion is given by $t=L(m/2qV)^{1/2}$, where L is the length of the flight path and qV is the energy of the ion. To utilize this TOF separation as a mass spectrometer, the ions must be formed in the source as a discrete packet and pulsed into the flight tube. Each packet reaching the detector at the end of a flight tube will result in a series of detector outputs at various arrival times; these give information concerning the mass of the ion being detected, while the amplitude of the signal is a measure of the corresponding ion abundance. Thus, a complete mass spectrum is generated for each cycle--acceleration, flight separation and detection--of the instrument.

A TOF mass spectrometer has some unique advantages, such as: compatibility with event-driven measurements, fast recording of the associated mass spectra, simple open source structure, and high transmission since it does not require mass scanning. These advantages were recognized by researchers in the early days, and this type of instrument has been chosen for studies of ion/molecule reactions and very fast monitoring of reactions such as explosions [105]. The unique features of a TOF mass spectrometer also suggest that the instrument may be ideal for use in GC/MS work; indeed, the first GC/MS instrument utilized a TOF spectrometer [106].

In spite of its attractiveness, the application of the TOF mass spectrometer was

limited, mainly by its poor resolution. Historically, the resolution of TOF mass spectrometers has been really poor; the first prototype instrument had a resolving power of only "about 2"! [99,104]. Subsequent models reported had much higher resolution, although still very low by today's standard. For example, a resolving power of about 100 was demonstrated by Katzenstein and Friedland [107] in 1955 on their instrument, which incorporated many important features.

The limitation to the ultimate resolution of a TOF mass spectrometer is that, the ion packets of identical m/z are not infinitely thin discs. This limitation arises because molecules in gas phase ionization ion sources (such as electron impact) have different initial velocity (or kinetic energy) and space distributions at the time of ionization and acceleration. If the ions were formed in a plane perpendicular to the source drawout and acceleration fields, and with no initial velocity components, then the flight time would be exactly the same for all ions of the same m/z, and the resolution would be high.

Considerable improvements were made in the TOF mass spectrometer, particularly in its resolution, with the appearance the of the Wiley and Mclaren instrument in 1955 [108]. In their design, a pulsed ion source containing two acceleration regions was employed, the first accelerating field was pulsed while the second one was constant in time. Ions are formed in different regions of the ionization space inside the first accelerating region and with different initial velocities under pulsed transverse electron bombardment. Disregarding the velocity effect, those ions initially closer to the exit grid acquire less energy than, and are eventually overtaken by, those initially farther away from the exit grid. This constitutes a space focusing or "bunching" effect, which can be achieved by varying the ratio of the two accelerating fields.

The effect of initial velocities can be reduced by introducing a suitable delay

between the electron ionization pulse and the ion acceleration pulse. An ion initially travelling away from the collector would normally arrive at the collector later than an ion initially travelling towards it. However, during the time lag, the ions having different initial velocities move to new positions in the ion source. When the ion acceleration pulse is turned on sometime later, the ions with velocity components away from the exit grid, that is, those ions located farther away from the exit grid, will acquire greater energy, and hence will have larger final velocities than those ions that moved towards the exit grid during the time lag. Thus it is possible to adjust the time lag so that the initially slower moving ions can overtake or catch up to the initially higher velocity ions. Consequently, this velocity or energy focusing method is referred to as time lag focusing. However, space and velocity focusing cannot be obtained simultaneously, but a reasonable compromise can be achieved [105,109,110]. Wiley and McLaren reported resolving powers of about 300 by using this innovative technique. Their design, which still forms the basis of some present day instruments, was commercialized by Bendix in 1957 and later by CVC Products (Rochester, NY) [111]. Designed for electron impact ionization of volatile species in the gas phase, these instruments could produce mass spectra at a high rate and achieve a resolving power (ΔM measured at 10% of peak height) of 300–400 for organic molecules, and 500–800 for inorganic species (for which there is less fragmentation and a smaller contribution to kinetic energy spread of the ions from kinetic energy release upon fragmentation).

In the late 1960's the quadrupole mass spectrometer became commercially available. Soon after, it surpassed the TOFMS technique in popularity, in part, because it has some similar features, namely, compactness, simplicity, economy, a fast-scanning capability (although not nearly as fast), while it has higher resolution (which is

independent of initial energy spread). It also allowed a higher operating pressure, which could be important when an ion source is required to operate at higher pressure, such as in GC/MS and CI.

There have been a number of attempts to develop alternative TOF mass spectrometers to that of Wiley and McLaren in order to improve the performance and, particularly, the resolution of the instruments further, but most of them did not offer a significant improvement in performance [105,109,111]. However, one approach that has attracted much attention recently is based on a reflecting spectrometer proposed by Mamyrin over twenty years ago [112], although his work was not generally known until several years later [113-115]. Mamyrin and co-workers [113] described a new energy focusing method in ion time-of-flight devices, using an electrostatic system (an ion reflector) to compensate for the initial ion kinetic energy spread, which is the main factor limiting the resolution of the time-of-flight mass spectrometer. The concept is simple. There is an electrostatic ion reflector at the normal detector position that reflects the ion beam to a detector mounted beside the ion source. For ions of the same m/z ratio, those with higher energy penetrate deeper into the reflector than do low energy ions. As a consequence, the faster, more energetic ions have a longer flight time in the reflector than do the slower less energetic ions. This compensates for the reverse behaviour in the field-free flight path. Thus fast and slow ions can be focused in time at the detector if the electrostatic field in the reflector is chosen correctly.

In their experiments, Mamyrin et al showed that this system provides a relative variation in time-of-flight within 0.01% for ions with a few percent spread in initial energies. The "Mass-reflectron", a reflecting time-of-flight mass spectrometer equipped with an EI source was reported by Mamyrin et al shortly afterwards in 1973, and a mass

resolving power up to 3,500 (FWHM) was obtained for some simple inorganic compounds [114].

While the new focusing methods were being developed, there was renewed interest in using the time-of-flight technique for mass analysis upon the appearance of new ionization techniques such as ^{252}Cf plasma desorption and laser desorption/ionization. These pulsed ionization methods are ideally suited for TOFMS, not only because a complete mass spectrum can be obtained instantaneously for each ionization event, but also because the ion formation process can take place on a plane equipotential surface perpendicular to the acceleration field. Thus, the spatial distribution of ions is no longer a problem, theoretically leaving only the initial kinetic energy distributions of the desorbed ions to affect the ultimate resolution.

Furthermore, if only a very limited number of sample molecules is available for an analysis (e.g. many biomolecules are available only in sub-picomole quantities), or the ion current generated is very low because of the nature of the ionization methods (e.g. ^{252}Cf plasma desorption, static SIMS), a maximum use of the ions generated may be necessary. The sensitivities of conventional mass spectrometers (sector, quadrupole mass spectrometers) suffer from the need to scan the mass spectra; only one mass can be examined at a time. The time-of-flight instruments can examine the full mass range at the same time, and also have excellent transmission so high sensitivity is obtained. Benninghoven has estimated that these combined factors increase the TOF sensitivity by a factor $\sim 10^5$ compared to a typical quadrupole mass spectrometer [116], so TOF methods offer significant advantages in such cases.

The development of these so called soft ionization techniques, starting with ^{252}Cf plasma desorption, generated much interest among those interested in characterizing

biologically important, high mass molecules. The unlimited mass range of a TOF analyzer offers another advantage for analyzing these massive molecules, which may be difficult for other types of mass spectrometer. As a matter of fact, mass spectrometry of the largest molecules (>200,000 u) has so far been achieved only by TOF methods [79]. In the early 1980s, interest accelerated in the particle and laser induced desorption techniques and many independent studies were carried out by using pulsed sources such as lasers, fission fragments and ion beams combined with TOF mass spectrometers [104]. In subsequent developments, the resolutions of TOF instruments have also been greatly improved by the use of ion reflectors. Traditionally, a time-of-flight mass spectrometer has been regarded as a low resolution instrument. Now resolving powers (FWHM) in and above the 10,000 range have been achieved in reflecting TOF instruments using a variety of ionization methods: laser excitation [117,118], particle induced desorption [119-121] and electron impact ionization [122]

The current revival of interest in TOFMS is a consequence of developments in ionization techniques, such as ^{252}Cf fission fragment, laser and ion induced desorption. The progress in TOFMS was reviewed in 1984 by Price and Milnes [111]. More recent developments have been reviewed by Standing [123] and described at SIMS V, VI [124,125], at IFOS III-V [126-128] and in a special issue of "Analytical Instrumentation" devoted to this topic [129].

1.3 THE DEVELOPMENT OF TOF-SIMS IN MANITOBA

About ten years ago, Manitoba TOF I, a linear time-of-flight mass spectrometer

was constructed in our laboratory [130]. It was originally designed to use fission fragments to induce desorption, but after the discovery of similar results (for some low mass organic molecules) with keV primary ions, a pulsed ion gun was designed to take advantage of the convenience and versatility of keV ions [32,131]. The instrument is similar to that of Macfarlane and Torgerson [132], but it produces secondary ions by bombardment with a pulsed beam of low-energy primary ions (normally ~10 keV Cs^+) instead of fission fragments. In this instrument, the secondary ions are ejected from a thin film of sample deposited on a flat metallic surface (an equipotential plane). They are accelerated by an electrostatic field across a narrow gap between the target and grid, then travel in straight lines to a detector at the end of the flight tube.

In linear TOF spectrometers like this, the transmission is high and is determined simply by the transverse velocity spread of the secondary ions, the accelerating voltage, and the size of the detector. No slits are necessary. This allows extremely low primary ion currents (~pA) to be used without sacrificing sensitivity. The products of unimolecular decay in the flight tube are also detected with high efficiency. They have almost the same velocity as their parent ion so they appear in the mass spectrum centred at the same position as the parent, but the peak is broadened due to the energy release. Thus, including these daughters in the parent ion peak is equivalent to including the parent ions that decay in free flight, i.e. it is equivalent to measuring the mass spectrum at a time immediately after acceleration (normally ≤100 ns after ejection from the target) [133,134]. In most other types of spectrometer, the time scale is longer by a factor $\geq 10^3$, since the intensity of a given peak is measured at the time the ions arrive at the detector.

Such instruments have several advantages. Their mass range is essentially unlimited. They have high efficiency, even for ions of short lifetime. Their simple

geometry makes ion yield measurements relatively easy to interpret. Mass spectra measured are much closer to the spectra actually emitted than in spectrometers that operate on a longer time scale; striking effects of such differences have been observed [133-135].

On the other hand, the resolution of linear TOF mass spectrometers is limited by the initial velocity spread of the secondary ions ejected from the target. Manitoba TOF I gives a resolving power $M/\Delta M_{FWHM}\approx 3200$ at mass ~500 u [121] (see Fig.1.1) or ~700 u [148], for negative ion clusters in the mass spectrum of CsBr, considerably better than the value obtainable in most earlier TOF spectrometers, but still lower than the resolution

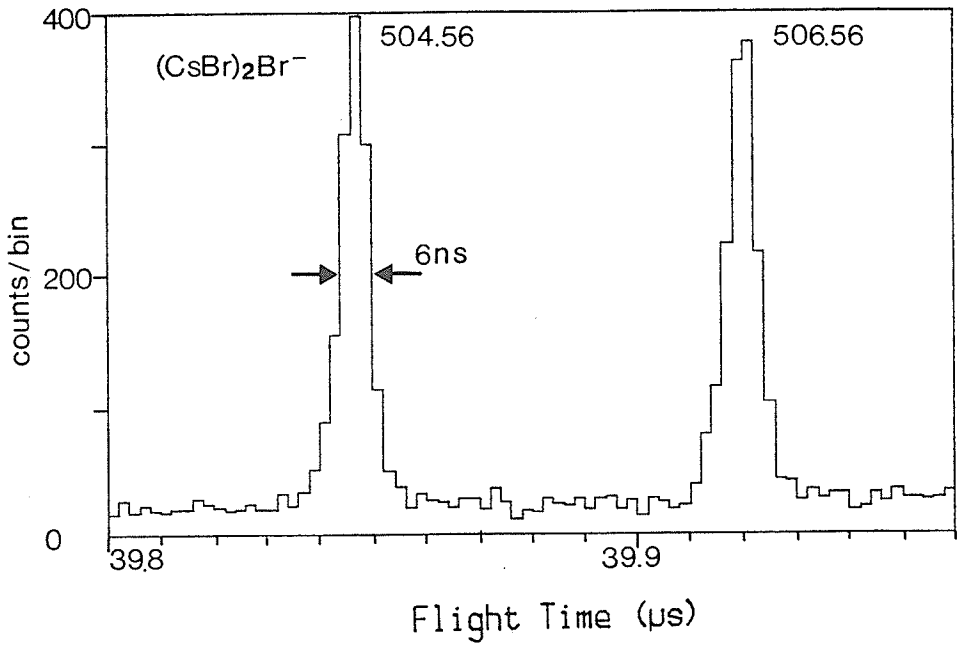

Figure 1.1 Negative ion TOF spectrum of CsBr near the second cluster, measured in the linear TOF mass spectrometer (Manitoba TOF I). Here, $(t/\Delta t)_{FWHM}\approx 6400$ so $(m/\Delta m)_{FWHM}\approx 3200$.

commonly used in sector-field instruments. Perhaps more serious is the high background under the parent ion peaks for large organic molecules (see Fig. 3.3); this arises from the products of metastable decay in the flight tube. Detection of the fragments increases the parent ion detection efficiency since the parents that decay in the flight tube are included in the measured peaks, and it also enables measurement on a short time scale, as remarked above. However, the resulting background sets an undesirable limit on the signal/noise ratio, and for most organic molecules with $m/z \geq 200$ the mass resolution is much poorer than that of inorganic species [131].

Manitoba TOF II [121,136,137], a reflecting time-of-flight mass spectrometer, was constructed in 1985 to overcome the difficulties in the linear TOF instrument. It incorporates an ion mirror to compensate the initial velocity spread of the secondary ions, as proposed by Mamyrin [112-115]. Compared to the linear spectrometer, the instrument gives not only considerable improvements in resolution for both inorganic and organic molecules but also in signal/noise ratio. It retains most of the advantages of the linear instrument, such as unlimited mass range, high transmission, and high sensitivity, as discussed above. It also can be used as a linear instrument simply by turning off the electric field in the ion mirror. Its construction and operation are described in detail in Chapter 2 and its performance is reported in Chapter 3.

A molecular ion peak from bovine insulin, produced by using low energy primary ions and a nitrocellulose substrate, was first reported on Manitoba TOF II [97,121,138]. It has also been used to study a number of compounds of biological interest, particularly peptides and nucleotides, supported on various substrates, of masses up to ~6000 u, including an unknown peptide. The results will be presented and discussed in subsequent chapters.

Many of the large molecular and cluster ions produced by particle-induced desorption are found to be metastable. The pattern of metastable decay may be studied in linear instruments by using retarding grids in front of a detector at the end of the flight tube [131,139-141], or by incorporating a small movable ion mirror to separate the parent ions from the products of metastable decay [143,144]. In the Manitoba TOF I instrument, retarding grids were used to investigate the stability of CsI clusters [131], and later a movable detection system incorporating a small ion mirror was inserted into the spectrometer [142]. It consists of an electrostatic mirror with grids at 45^0 to the spectrometer axis and detectors at 0^0 and 90^0, as in the design of Danigel et al [144]. The parent ion and the charged fragments are bent through 90^0 into one detector, while the neutral fragments pass through the mirror into the other detector. Such dual-detector systems enable measurement of decay lifetimes and of correlations between the daughters [121,137,142,143]. However, the mirror is too short (~1cm) to give much separation between the various charged fragments and the parent ions. Thus the measurements of the daughter masses from metastable decay are very limited in accuracy if these are estimated from flight time differences. For the same reason, the mirror is not capable of giving much improvement in resolution.

In Manitoba TOF II, a much longer ion mirror is used, which gives significant improvement in resolution, both for the parent ion and for the charged fragments from unimolecular decay. It also introduces much greater time dispersion between the daughter ions and their parents; consequently the masses of the daughter ions can be determined much more accurately.

This instrument, like the 45^0 mirror described above and like the Orsay "reflex" spectrometer [145-147], uses two detectors. Undissociated parent ions and charged

daughters are reflected into one detector by the electrostatic mirror, while the undeviated neutral fragments pass through the mirror into a second detector, which serves also to measure the overall spectrum when the electric field in the mirror is removed.

The dual-detector system, combined with a data system developed in this laboratory [148,149], enables examination of the correlations between the charged daughter ions and the corresponding neutral fragments if the counting rate is kept sufficiently low, so the probability of detecting randomly correlated events is small. Since the neutral fragment has approximately the same velocity as its parent, the time of arrival of the neutral fragment serves to identify the parent ion; this specifies which parent ion gives rise to a given daughter and vice versa. Thus the method gives information similar to that obtained in the various forms of tandem mass spectrometry (MS/MS) [150,151]. In most such methods only one parent/daughter pair can be examined at a time, but with the present method, decompositions of all parents may be examined at the same time. The number of such simultaneous measurements is limited only by the computer memory available for data storage. No scanning is performed for both parents and daughters. Therefore, the sensitivity of the present MS/MS technique is much higher.

The principle of the correlated measurements and the operation of the reflecting time-of-flight mass spectrometer as a "tandem" mass spectrometer will be described in detail in Chapter 4, in which the performance of the MS/MS instrument, including the resolution, sensitivity, efficiency and accuracy of the daughter ion measurements, is also reported and discussed.

Many compounds, both organic and inorganic, particularly peptides up to mass ~2,000 u have been studied with the technique described in Chapter 4. Measurements of various daughter ion mass spectra resulting from metastable ion decomposition in the first

leg of free flight, and their application to obtaining structural or sequence information of molecules, decay patterns and pathways, and the analysis of simple mixtures are presented in Chapter 5.

CHAPTER 2

MANITOBA TOF II: A REFLECTING TIME-OF-FLIGHT MASS SPECTROMETER

2.1 INTRODUCTION

Following the work of Mamyrin [112-115], a number of TOF spectrometers incorporating ion reflectors have been constructed [104,111,152,153]. Until recently, most such instruments were built to compensate large initial velocity spreads (e.g. from electron beam ionization in the gas phase or from laser desorption) and seldom gave mass resolution ≥1000. New problems arise when one starts from a resolution ~3000, as in our case, but some encouraging progress has been made over last few years. Several groups have reported mass resolving power $m/\Delta m_{FWHM}$ in and above the 10 000 range using ion mirrors for a variety of ionization techniques: laser ionization [117] and laser induced surface ionization [118], particle induced desorption [119-121] and electron bombardment [122].

A spectrometer of this type has also been designed and constructed at our laboratory. This reflecting TOF mass spectrometer, shown schematically in Figure 2.1 has

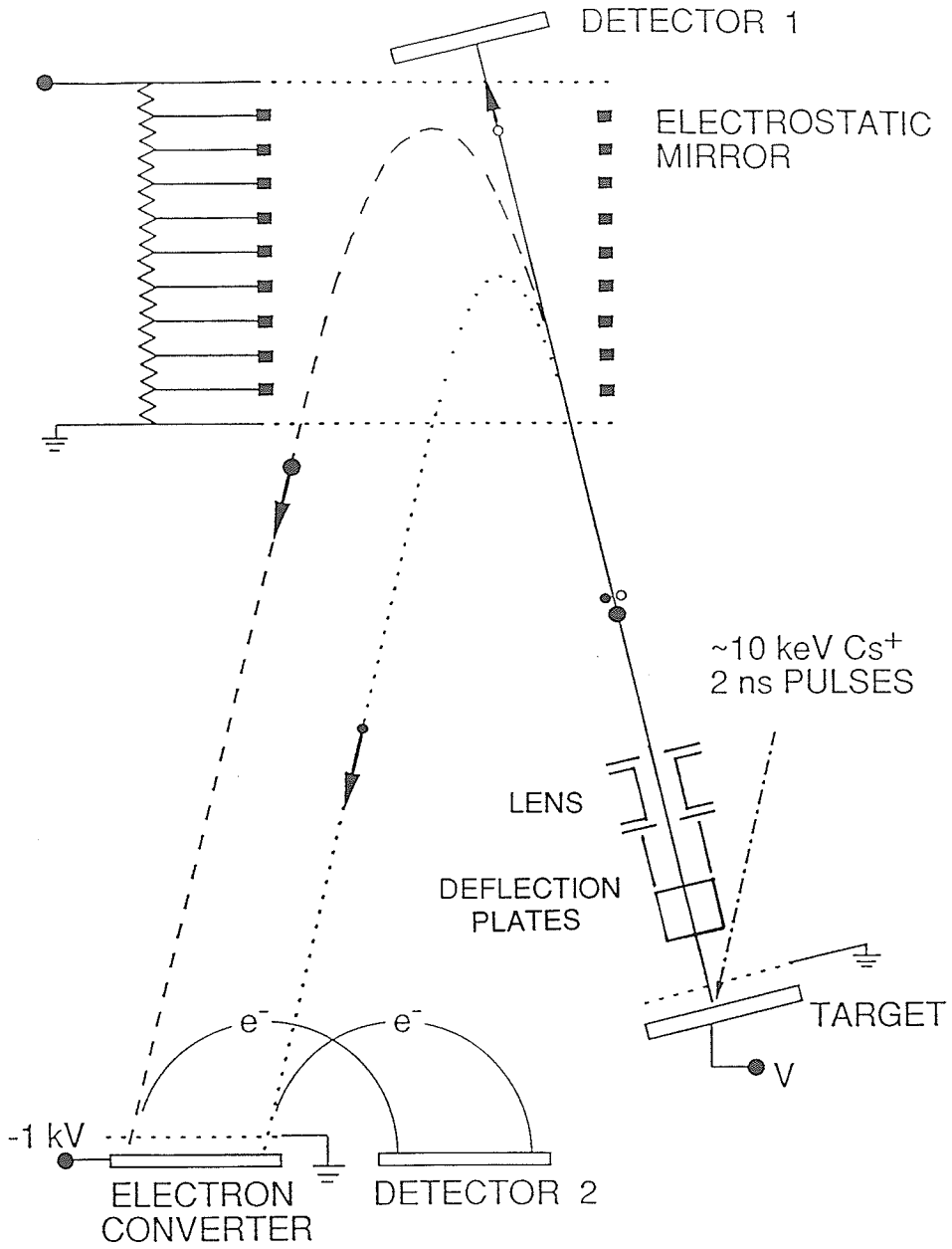

Figure 2.1 Schematic diagram of the reflecting time-of-flight mass spectrometer (Manitoba TOF II), not to scale. The angle between the spectrometer axis and the secondary ion path has been exaggerated for clarity; the actual angle is ≈1.4°. The accelerating field must be at this angle to the axis so that the reflected ions will hit the detector. However, the face of the detector 2 must be perpendicular to the spectrometer (mirror) axis, *not* perpendicular to the ion trajectory. The solid line shows the path of a neutral fragment observed in detector 1. The dashed and dotted lines indicate the respective paths of a parent ion and a daughter ion of mass $m'=m/2$, when the mirror is optimized for the parent ion.

been already reported in the literature [121,137]. Here, an ion gun produces ~2 ns pulses of Cs^+ ions with energy up to 25 keV and at a repetition rate of 2-5 kHz. The primary ions strike a thin layer of sample material deposited on the target backing at an angle of 20° to the normal. The secondary ions produced by the bombardment are accelerated across a potential difference, V (usually 5-15 keV), between the target and a grounded grid, which is typically 4 mm away. The polarity of the secondary ion to be analyzed is selected by the polarity of the acceleration voltage on the target. The secondary ions then pass down the flight tube into the electrostatic ion mirror. After reflection through ~177°, the ions again traverse the flight tube and return to a detector assembly beside the target. The total effective flight path is ~2.5 m. Two pairs of deflection plates mounted above the acceleration grid are used for steering the beam to optimize the counting rate on the bottom detector, and an Einzel lens on the top of the deflection plate assembly is sometimes used for improving the transmission. Neutral fragments resulting from decay of the parent ions in the first section of free flight are detected by a microchannel plate detector behind the mirror. Both charged particles and neutral fragments are detected simultaneously and correlations between them may also be examined with our data system to yield the daughter ion spectrum.

Photographs of the instrument and data system are shown in Fig. 2.2. The apparatus is constructed of non-magnetic stainless steel, and has a vertical flight tube which has a length of ~1 m and an internal diameter of ~24 cm. The system is sealed by Viton "O" rings and an operating pressure of $(0.5\text{-}5)\times10^{-7}$ Torr is maintained by a sublimation pump and an ion pump, which has a pumping speed of 140 litres/s. Rough pumping is done by sorption pumps and a venturi pump so that clean vacuum conditions are maintained throughout evacuation. A vacuum lock is provided at the bottom of the

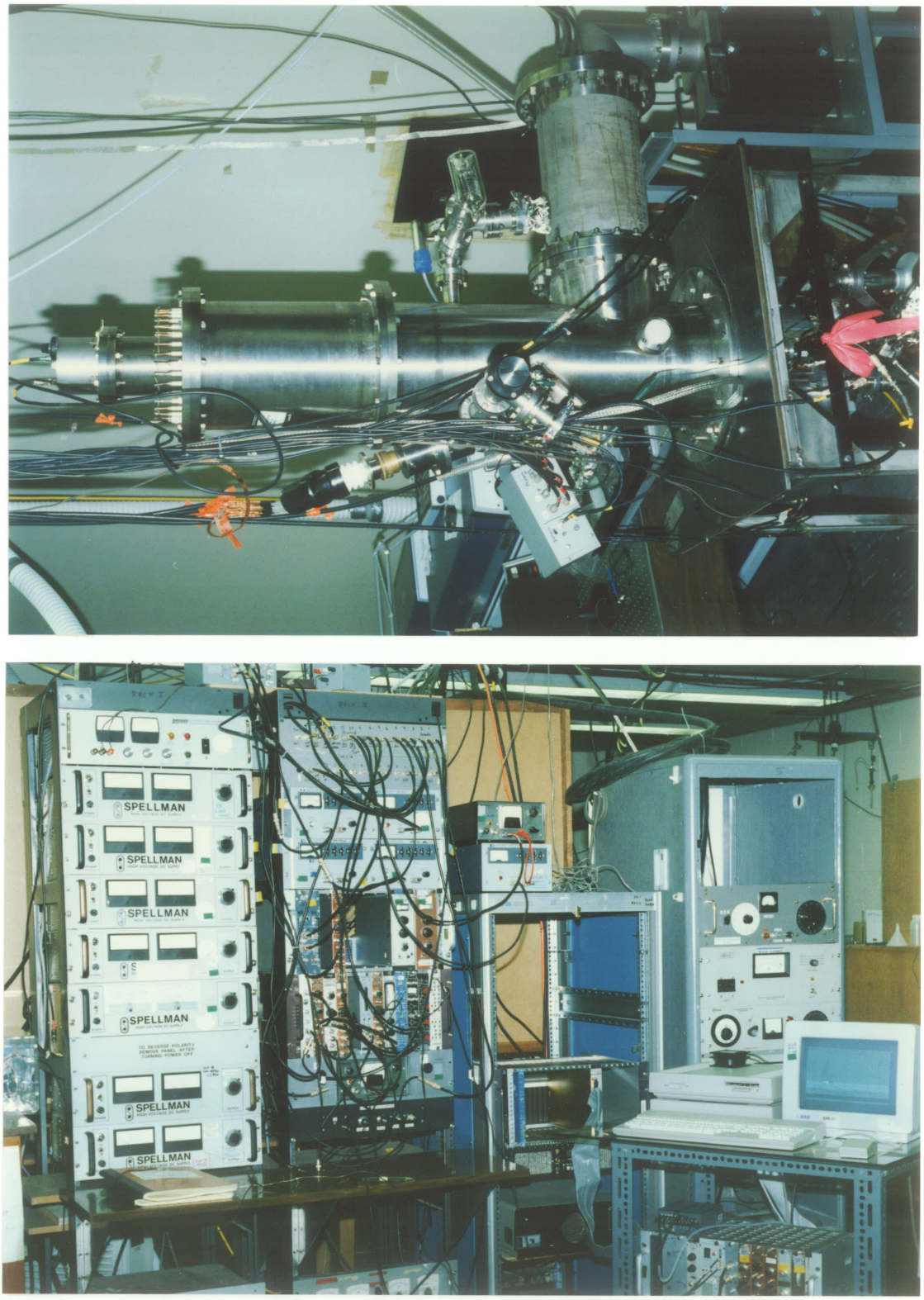

Figure 2.2 The reflecting time-of-flight mass spectrometer (Manitoba TOF II) at top, and data system at bottom.

spectrometer for the operation of a direct inlet sample probe, so that a target may be changed without disturbing the vacuum in the main system. Two quartz windows on the main flight tube permit introduction of a laser beam into the spectrometer to dissociate the desorbed ions.

2.2 PRINCIPLE OF THE ELECTROSTATIC ION MIRROR (REFLECTOR)

2.2.1 Principle of Velocity Focusing with a Single-stage Electrostatic Mirror

As discussed in §1.2 and 1.3, an intrinsic limit on the resolution of linear TOF spectrometers is set by the axial velocity spread of the ions ejected from the target, but this difficulty may be circumvented by the use of a relatively long ion mirror, as proposed by Mamyrin [112-115]. The principle is straightforward. An ion of higher velocity penetrates more deeply into the mirror so it spends more time there. This may compensate the shorter time it spends in free flight, if the electrostatic field in the mirror is chosen correctly.

Although the original proposal treated a more complicated case [112-115], the principle of operation may be seen most clearly for a simple plane single-stage mirror, as illustrated in Fig. 2.3. The results shown below can, of course, be obtained from the more general development [112-115,154], but it is instructive to derive them directly.

In Fig. 2.3, the constant electric field $\vec{E}$ within the mirror defines the spectrometer axis, here taken as the z axis, i.e. $E_z=E$ for $z<0$ and $E_z=0$ for $z>0$. Note that the ion velocity component perpendicular to the axis does not affect the flight time and that this

component is constant for an ideal mirror; it simply determines whether or not the ion will hit the detector. Thus, we need consider only the axial component v_z, with v_z determined by $v_z^2=v^2+v_{iz}^2$, where v_{iz} is the initial axial velocity and v is the axial velocity component after acceleration for an ion ejected from the target with zero velocity, i.e. $mv^2/2=qVcos^2\theta=qU$ (see Fig. 2.3), where q is the charge, m the mass and V the accelerating voltage.

We first calculate the flight time neglecting the initial velocity (i.e. $v_z=v$ for $v_{iz}=0$). It is convenient to define a reference plane perpendicular to the axis just outside the accelerating grid (denoted the "object plane" in Fig. 2.3). We calculate the total flight

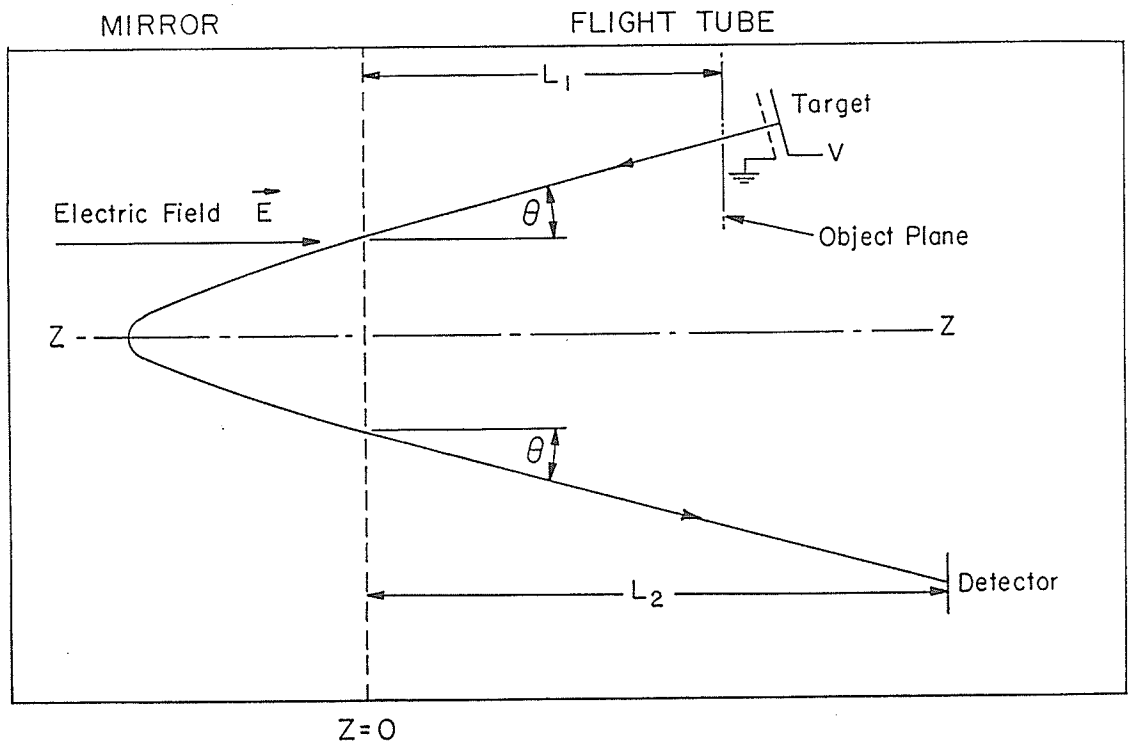

Figure 2.3 Schematic diagram (not to scale) showing the flight path of an ion in a single-stage reflecting TOF mass spectrometer.

time of an ion from the time it passes through this reference plane to the time it arrives at the detector; corrections due to the finite distance between the target and the reference plane will be considered later. Since the axial velocity component is simply reversed by reflection, its magnitude is the same for L_1 and L_2 (see Fig. 2.3), so the time spent in free flight is $t_F=L/v$ where $L=L_1+L_2$. The time spent in the mirror is $t_M=2v/a$, where the acceleration $a=qE/m$. The total flight time, t, is then

$$t=t_M+t_F=\frac{2m}{qE}v+\frac{L}{v} \tag{2-1}$$

For variations in v (resulting from changes in accelerating voltage V), the flight time is minimum for $\partial t/\partial v=0$, or

$$\frac{2mv_0}{qE}=\frac{L}{v_0}, \qquad i.e. \qquad E=\frac{2mv_0^2}{qL}=\frac{4U_0}{L} \tag{2-2}$$

where v_0 corresponds to the optimum value of accelerating voltage V_0 ($mv_0^2/2=qV_0cos^2\theta=qU_0$), i.e. for a given value of the mirror electric field E, the flight time (Eq. (2-1)) is minimum if $v=v_0$. For this value of E, $t_M=t_F=L/v_0$, i.e. the ion spends the same amount of time in the mirror as in free flight. Also

$$t=\frac{2L}{v_0}=\left[\frac{2L}{\sqrt{2qU_0}}\right]\sqrt{m} \tag{2-3}$$

so the flight time is proportional to $\sqrt{m}$, as in a simple linear TOF instrument. The stopping distance, l, in the mirror is given by $qU_0=lqE=lq4U_0/L$, so $l=L/4$ specifies the minimum length of mirror required. Since the average axial velocity in the mirror is $v_0/2$, this corresponds to an *effective* mirror length $2\times L/4=L/2$.

In the more general case, ions have a velocity spread due to their initial velocity distribution; the velocity spread can also be caused due to changes in accelerating voltage. The axial velocity v_z after acceleration may be expressed as $v_z=v_0+\delta$, where the δ specifies the velocity spread. The flight time excluding the acceleration region is then

$$t=\frac{2m}{qE}(v_0+\delta)+\frac{L}{v_0+\delta}$$

Expanding the second term as a function of δ gives

$$t=\frac{2m}{qE}(v_0+\delta)+\frac{L}{v_0}-\delta\frac{L}{v_0^2}+\delta^2\frac{L}{v_0^3}-\delta^3\frac{L}{v_0^4}+\cdots$$

$$t=\left[\frac{2mv_0}{qE}+\frac{L}{v_0}\right]+\frac{\delta}{v_0}\left[\frac{2mv_0}{qE}-\frac{L}{v_0}\right]+\left(\frac{\delta}{v_0}\right)^2\frac{L}{v_0}-\left(\frac{\delta}{v_0}\right)^3\frac{L}{v_0}+\cdots \qquad (2\text{-}4)$$

The linear term in this expression vanishes for

$$\frac{2mv_0}{qE}=\frac{L}{v_0}, \qquad or \qquad E=\frac{2mv_0^2}{qL}=\frac{4U_0}{L} \qquad (2\text{-}2)$$

As might be expected, this is the condition for minimum flight time discussed above. For this value of the mirror field, the flight time is independent of axial velocity to first order for parent ions of every mass, i.e.

$$t=\frac{L}{v_0}\left[2+\left(\frac{\delta}{v_0}\right)^2-\left(\frac{\delta}{v_0}\right)^3+\cdots\right] \qquad (2\text{-}5)$$

The relative flight time variation $\Delta t/t$ of Eq. (2-5) resulting from changes in acceleration voltage can be seen in Fig. 2.5, which is presented later in §2.2.3.

2.2.2 Unimolecular Decay and Flight Time of the Daughter Ions

Metastable decay in the flight tube can be investigated using the correlation method which has been briefly described in chapter 1 and will be described in detail in chapter 4. It is convenient to compare the total flight time, t^*, of a daughter ion of mass m' with the total flight time, t, of its parent ion (mass m). In zeroth order, both ions have the same velocity v_0. From Eqs. (2-1) and (2-2), $t=2L/v_0$ and

$$t^* = \frac{L}{v_0} + \frac{2m'v_0}{qE} = \frac{L}{v_0}\left(1+\frac{m'}{m}\right) \tag{2-6}$$

so

$$\frac{t^*}{t} = \frac{m+m'}{2m} \tag{2-7}$$

The daughter peak position lies between the parent ion flight time (for large fragments) and half the parent ion flight time [i.e. apparent mass $=m/4$; see Eq. (2-3)] for small fragments. It is clear that the daughter will be much better separated from the parent than with the small mirror discussed in §1.3.

The velocity spread of the daughter ions is not completely compensated, but a first-order calculation shows that some improvement in resolution is obtained for them too. Consider a parent ion (mass m and axial velocity $v_0+\delta$) that decays in free flight with emission of a daughter ion (mass m' and axial velocity $v_0+\delta'$) after travelling a distance $(1-\alpha)L$, where $0.5\leq\alpha<1$. For the daughter ion

$$t^* = \frac{L(1-\alpha)}{v_0+\delta} + \frac{\alpha L}{v_0+\delta'} + \frac{2m'(v_0+\delta')}{qE}$$

$$t^* = \left[\frac{L}{v_0} + \frac{2m'v_0}{qE}\right] + \frac{\delta}{v_0}\left[\frac{2m'v_0}{qE} - \frac{L}{v_0}\right] + \frac{\delta'-\delta}{v_0}\left[\frac{2m'v_0}{qE} - \frac{\alpha L}{v_0}\right] + \ldots \qquad (2\text{-}8)$$

where the second and third terms give the first-order time spread, Δt^*_{lin}, produced by δ and δ'. From Eqs. (2-2) and (2-6)

$$\frac{\Delta t^*_{lin}}{t^*} = -\frac{\delta}{v_0}\left(\frac{m-m'}{m'+m}\right) + \frac{\delta'-\delta}{v_0}\left(\frac{m'-\alpha m}{m'+m}\right) \qquad (2\text{-}9)$$

With the mirror off

$$\frac{\Delta t^*_{lin}}{t^*} = -\frac{\delta}{v_0} + \frac{\delta'-\delta}{v_0}(1-2\alpha)$$

The improvement in resolution depends on the values of the parameters in these equations; for the most probable condition (α=1, i.e. decay at the accelerating grid), the relative time spread is reduced by a factor $(m+m')/(m-m')$, e.g. a factor of 7 for m'=0.75m. If Δt^*_{lin} is reduced below the intrinsic time spread determined by various defects in the spectrometer (see below), the resolution for the daughter will be comparable with the value obtained for the parent ion.

It is possible to optimize the mirror for examination of a particular daughter ion. For this purpose, the electric field, E, in the mirror is reduced until the linear term in the *fragment* flight time vanishes, i.e. the field is reduced to the value E' where

$$\frac{2m'v_0}{qE'} = \frac{L}{v_0}$$

or

$$E' = \frac{2m'v_0^2}{qL} = \frac{m'}{m}\frac{4U_0}{L} \tag{2-10}$$

This condition is achieved when the flight time, t^*, of the fragment reaches a value

$$t^* = \frac{2m'v_0}{qE'} + \frac{L}{v_0} = 2\frac{L}{v_0} \tag{2-11}$$

i.e. the same flight time as that measured for its parent with a field E in the mirror. Under this condition

$$\frac{m'}{m} = \frac{E'}{E} \tag{2-12}$$

so the ratio of mirror voltages gives a determination of the mass of the fragment. With the field E', the parent ions will pass through a mirror of length $L/4$ into the 0° detector behind the mirror and the mirror will be optimized only for fragments of the given mass. Under this condition, the second term in Eq. (2-8) vanishes, but the third term will still give some peak broadening for $\alpha<1$.

It is useful to compare the flight time t^* of the daughter with that of a parent ion of the *same* mass m', since such ions are often produced directly at the target. This parent ion m' has a velocity $v_0' = v_0\sqrt{m/m'}$ and flight time $t' = 2L/v_0' = (2L/v_0)\sqrt{m'/m}$, so

$$\frac{t^*}{t'} = \frac{m+m'}{2m\sqrt{m'/m}} \tag{2-13}$$

The ratios t^*/t and t^*/t' are plotted in Fig. 2.4 (curves A) along with the corresponding ratios for a two-stage mirror (curve B). Note that large fragments (i.e. $m'/m \approx 1$) have nearly the same flight time as parent ions of the same mass m', as might be expected,

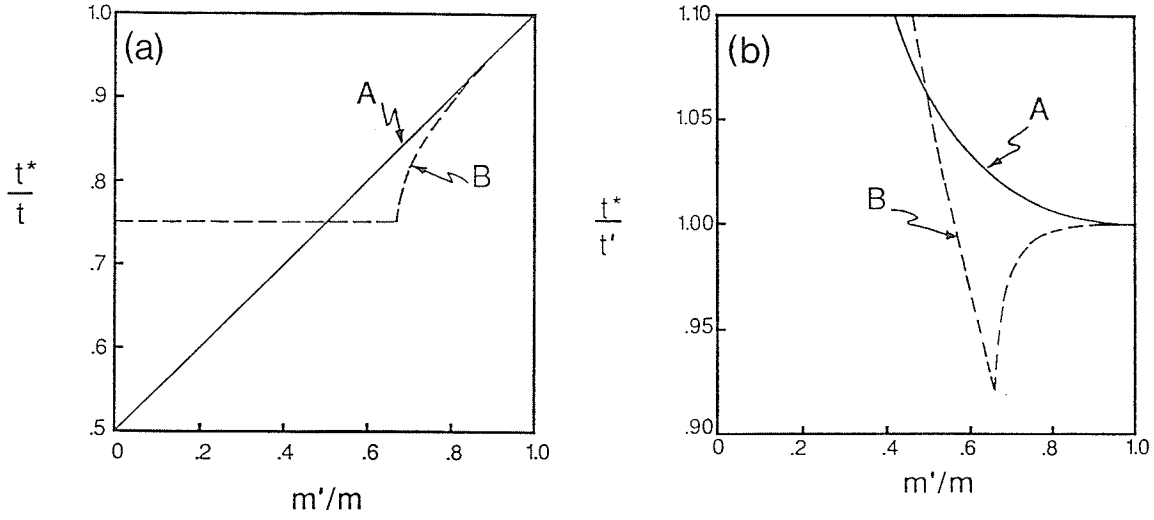

Figure 2.4 Ratios of the total flight times for the parent ion, t, the charged daughter from decay in region L_1 of Fig. 2.3, t^*, and an ion of the same mass as the daughter but produced at the target surface, t'. Ratios t^*/t and t^*/t' are plotted in (a) and (b), respectively. In each case the solid curve, **A**, shows the ratio calculated for the single stage mirror described in the text. The broken curve, **B**, shows the ratio calculated for a two-stage mirror, which will be discussed later (in the limiting case of an infinitesimal decelerating gap, for which the voltage across the gap to give second-order correction is $2V/3$ [112-115,154]).

since the effect of their different velocities is compensated to first order.

Parent ions of mass m that decay during acceleration will give charged daughters of mass m' with velocities between v_0 and v'. Thus, the flight times of the charged fragments resulting from decay of this parent in the acceleration region form a continuum between t' and t^* [141,155,156].

2.2.3 Effects of Acceleration Region and Velocity Focusing

From the calculation shown in §2.2.1, we obtain the first order velocity focusing conditions for an ion packet starting from the reference plane (after acceleration). This

gives a simple picture of the principle of velocity focusing by an ion mirror and also yields a good approximation for the value of the electric field and minimum length of the mirror required for compensation of the first order velocity spread. However, as remarked above, corrections arising from the finite distance between the target and the initial reference plane, must be considered when higher accuracy is required. In particular, the ion flight time in the acceleration region has also to be taken into account in the calculation. As has been shown recently by Brunelle et al in the case of a two stage ion mirror [158], a significant time spread may be produced in a finite acceleration region by the ion initial energy distribution.

2.2.3.1 Time variation due to changes in acceleration voltage and velocity focusing

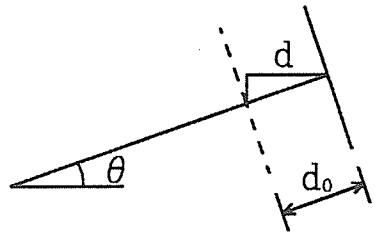

We first consider a velocity spread δ due to changes in the acceleration voltage. For ions ejected from the target with zero initial velocity, the time spent in the acceleration region is $t_A=2d/v$, where $d=d_0\cos\theta$, d_0 is the distance between the target and the acceleration grid (see the diagram), and v is the axial component of the velocity *after* acceleration. In all the calculations performed below, practical parameters of d=4 mm, and L=1250 mm are used unless indicated. The total flight time t_0 for ions starting from the target is then

$$t_0=t_M+t_F+t_A=\frac{2m}{qE}v+\frac{L}{v}+\frac{2d}{v}=\frac{2m}{qE}v+\frac{L+2d}{v} \qquad (2\text{-}14)$$

where t_A is the time spent in the acceleration region, i.e. between the target and the

reference plane. Comparing Eq. (2-14) with Eq. (2-1), we can see, if L in the Eq. (2-1) derived previously is replaced with $L+2d$, the results obtained before are still valid. Thus, the effect of the acceleration region in this case is simply to extend the effective length of free flight by 2d. The minimum length of mirror required is then $l=(L+2d)/4$ corresponding to an effective total flight path $2L+4d$.

When the ion velocity changes from v_0 to $v=v_0+\delta$ due to changes in the accelerating voltage, the flight time changes from t_0 to $t_0+\Delta t$. The relative time variation can be written as

$$\frac{\Delta t}{t_0} = \frac{t_0+\Delta t-t_0}{t_0} = \frac{(\Delta t)_{reflex}}{t_0} + \frac{(\Delta t)_{accel}}{t_0}$$

where $(\Delta t)_{reflex}/t_0$ corresponds to the contributions of time variation in mirror and free flight, and $(\Delta t)_{accel}/t_0$ corresponds to the contribution in acceleration region.

The flight time variations $\Delta t/t_0$ under the first order focusing condition (Eq. (2-2) with L replaced by $L+2d$.) can be calculated from Eq. (2-14) or from Eq. (2-5) with L replaced by $L+2d$, ($\Delta t/t_0$ can also be obtained from more general calculations given in Appendix A.1). For convenience of discussion, here the flight time was calculated in terms of ion energy qU that corresponds to the axial velocity v (i.e. $qU=mv^2/2$), if the velocity spread δ is due to changes in accelerating voltage, then we have $\delta/v_0=\Delta v/v_0=\Delta U/2U_0$. The calculated curves of the time variation versus acceleration voltage variations are plotted in Fig. 2.5. It can be seen that the time variation due to the changes in acceleration voltage can be well compensated by a single stage ion mirror, for example, a ±1% variation in acceleration voltage produces a total time variation $\Delta t/t_0$ of only $\sim 1.25\times10^{-5}$, this means that a resolution of 40,000 can still be achieved in principle

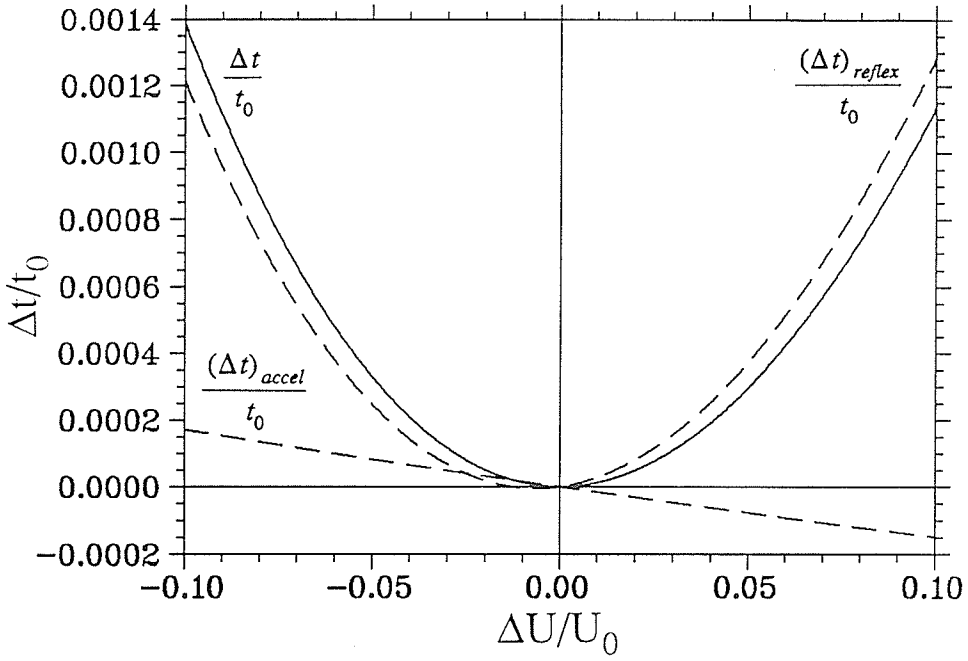

Figure 2.5 Calculated time variations $\Delta t/t_0$, versus the accelerating voltage variations $(\Delta U/U_0=\Delta V/V_0)$, under the first order velocity focusing condition described in Eq. (2-2) (with L replaced by $L+2d$). The broken lines represent the respective time variations induced in acceleration region $(\Delta t)_{accel}/t_0$ and in free flight and mirror $(\Delta t)_{reflex}/t_0$, the solid line represents the total time variation $\Delta t/t_0$, i.e. sum of the two terms above.

if there is a ±100 eV ion energy fluctuation in a total energy of 10 keV.

Generally, ions are ejected from the target with an initial kinetic energy or velocity distribution. As before, if an ion has an initial energy qU_i corresponding to an initial axial velocity v_{iz} along the spectrometer axis, then the axial velocity v_z of the ion after acceleration is determined by

$$\frac{1}{2}mv_z^2=\frac{1}{2}mv_{iz}^2+qV\cos^2\theta=\frac{1}{2}mv_{iz}^2+\frac{1}{2}mv^2$$

or

$$v_z=v_0+\delta=\sqrt{v^2+v_{iz}^2}=\sqrt{2q(U+U_i)/m} \qquad (2\text{-}15)$$

where

$$qU_i=\frac{1}{2}mv_{iz}^2;\quad qU=\frac{1}{2}mv^2=qV\cos^2\theta$$

so the velocity of an ion is a function of ion initial velocity and the acceleration voltage, i.e. $v_z=f(v_{iz},V)$, and the flight time of an ion with initial axial velocity v_{iz} is then

$$t=t_M+t_F+t_A=\frac{2m}{qE}v_z+\frac{L}{v_z}+\frac{2d}{v_z+v_{iz}} \tag{2-16}$$

Eqs. (2-15) & (2-16) include all the physics of the problem, but some more detailed analysis of the equations may be necessary to see the effects of the acceleration region. As before, if there is a variation in v_z due to changes in accelerating voltage V, the flight time is minimum for

$$\frac{\partial t}{\partial V}=\frac{\partial t}{\partial v_z}\frac{\partial v_z}{\partial V}=0;\quad but\quad \frac{\partial v_z}{\partial V}=\frac{q\cos^2\theta}{mv_z}$$

so

$$0=\frac{\partial t}{\partial v_z}=\frac{2m}{qE}-\frac{L}{v_z^2}-\frac{2d}{(v_z+v_{iz})^2},\quad or\quad \frac{2m}{qE}v_z=\frac{L}{v_z}+\frac{2d}{v_z}\frac{1}{(1+v_{iz}/v_z)^2}$$

i.e.

$$E=\frac{2mv_z^2}{q\left[L+\dfrac{2d}{(1+v_{iz}/v_z)^2}\right]}=\frac{4U_0(1+k)}{L+2d(1+k)(\sqrt{1+k}-\sqrt{k})^2} \tag{2-17}$$

where $k=U_i/U_0$. So when the acceleration region taken into consideration, the value of E required for first order compensation of velocity spread due to the changes in the acceleration voltage depends on ion initial velocity or energy. Note that this dependence

is weak for $k=U_i/U_0 \ll 1$, e.g. for qU_i=5 eV, and qU_0=5 keV, the focusing value of E required is increased only by ~0.14% comparing with the value required for zero initial ion energy, i.e. qU_i=0, so the shift is not significant. The flight time under the focusing condition for a given value of v_{iz} is readily obtained from Eqs. (2-16) & (2-17), which is

$$t=\frac{1}{v_z}\left[2L+2d\left(\frac{1}{1+v_{iz}/v_z}+\frac{1}{(1+v_{iz}/v_z)^2}\right)\right] \tag{2-18}$$

The time variation due to changes in acceleration voltage has been given in Fig. 2.5 for ions with zero initial energy. Now, such time variations can also be calculated for ions with a given value of initial energy. The detailed calculations are given in Appendix A.1. The results are similar to that for ions with zero initial energy. For example, for initial energy $qU_i=0.01qU_0$ and for acceleration voltage variation $\Delta U/U_0 \leq 5\%$, the calculated time variations are essentially the same as those for zero initial energy (see Fig. 2.5), so the effect of the initial energy is negligible in this case.

From discussion above, we know the first order velocity focusing including acceleration region can be achieved in case of acceleration voltage changes for a given value of initial energy. However, the value of mirror electric field required for focusing is dependent on the ion initial energy. In practice, the ions with different initial energy are recorded in a spectrum under the same mirror field, so the compensation would be different for ions with different initial energy. If we take ions with zero initial axial velocity as reference ions, i.e. chose the value of the mirror electric field corresponding to the focusing condition of these ions (Eq. (2-17) with v_{iz}=0), then the time variation due to changes in both acceleration voltage and ion initial energy can be calculated (see Appendix A.2).

From Equation 6 and 7 in Appendix A, we can see that the acceleration voltage variation and ion initial energy distribution are equivalent in "reflex" region (i.e. free flight and mirror) , but in the acceleration region, the initial energy spread induces more time spread. Fig. 2.6 shows the calculated curves of $\Delta t_{t0}/t_0$ verses $\Delta U/U_0$ for different ion initial energy and for the reference value of E, we can see the curves of non-zero initial energy are shifted with respect to the origin, and the compensation of the acceleration voltage changes for ions with non-zero initial energy are usually not as good as the ions of zero initial energy under the mirror field selected. However, the time variations caused by the change of the acceleration voltage for a given initial energy qU_i are still not

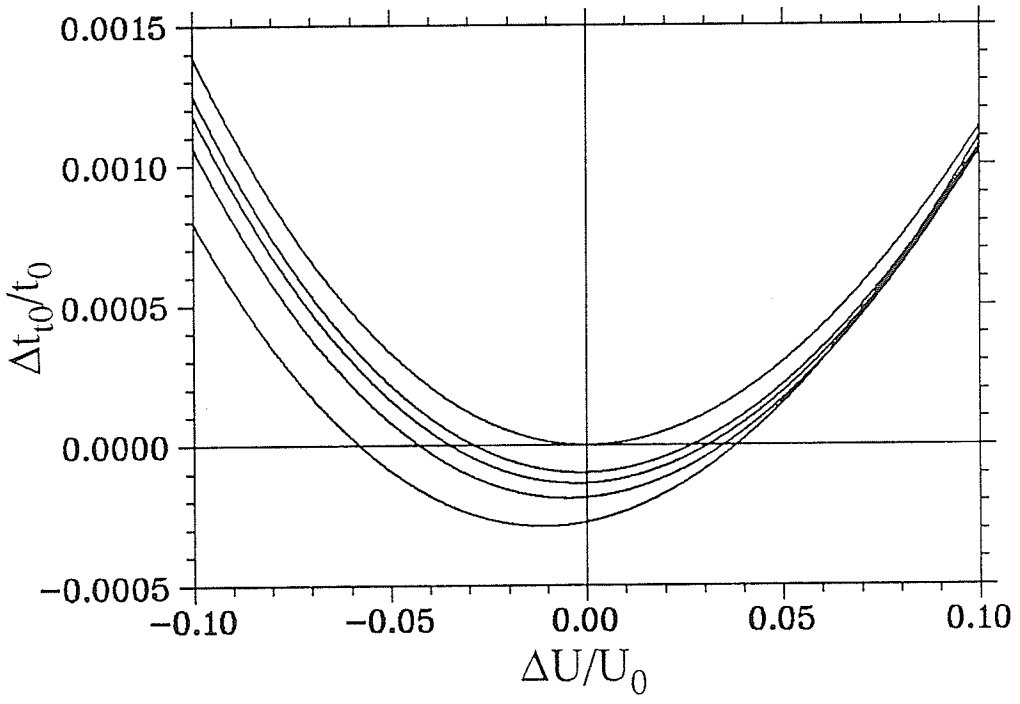

Figure 2.6 The calculated time variations $\Delta t_{t0}/t_0$ verses the acceleration voltage variations $\Delta U/U_0$ for different initial energy. The value of the mirror field is corresponding to the optimum for ions with zero initial energy (Eq. (2-17) with k=U_i/U_0=0). The curves from top to bottom are corresponding to ion initial energy of 0, 0.001, 0.002, 0.004 and 0.01 qU_0 respectively.

significant. For examples, for ±1% variation in acceleration voltage, i.e. $\Delta U/U_0=\pm 1\%$, the time variation is within ~1.6×10^{-5} for $U_i/U_0=0.1\%$, very close to the case of $U_i/U_0=0$. The worst case in Fig. 2.6. is $U_i/U_0=1\%$, but the time variation is still within ~5.5×10^{-5}.

2.2.3.2 Time variation due to initial energy distribution

The above discussion has described the time variation caused by a change in acceleration voltage, but the primary purpose of an ion mirror is to compensate the velocity spread caused by the ion initial energy distribution. The time variation caused by the initial energy spread is represented by the vertical distance between the curves in Fig. 2.6 at a given U ($U=U_0+\Delta U$), and this may be much bigger than the time variation induced by changes in acceleration voltage (the change in flight time as U changes).

The time variation caused by initial energy spread can be seen more clearly by plotting $\Delta t/t_0$ against U_i/U_0. For simplicity, we assume the acceleration voltage is stable here, and set w=0 i.e. ΔU=0 in Eq. 6 and 7 in Appendix A. The calculated curve of the time variation versus ion initial energy is shown in Fig. 2.7(a). Comparing the curves with those in Fig. 2.5 (where the time variation is caused by acceleration voltage change), it can be seen that the time variation produced after acceleration has the same behaviour in both cases, but the time variation produced in the acceleration region has a different behaviour and its magnitude is considerably larger in the case of an initial energy spread, which results in a bigger total time variation. For examples, a $U_i/U_0=1\%$ induces a $\Delta t/t_0$ of 2.8×10^{-4} and even $U_i/U_0=0.1\%$ induces $\Delta t/t_0$ of 1×10^{-4}. So the time spread in the acceleration region is significant in the case of initial energy spread. The time width of a peak depends not only on the width of the initial energy distribution, but also on the

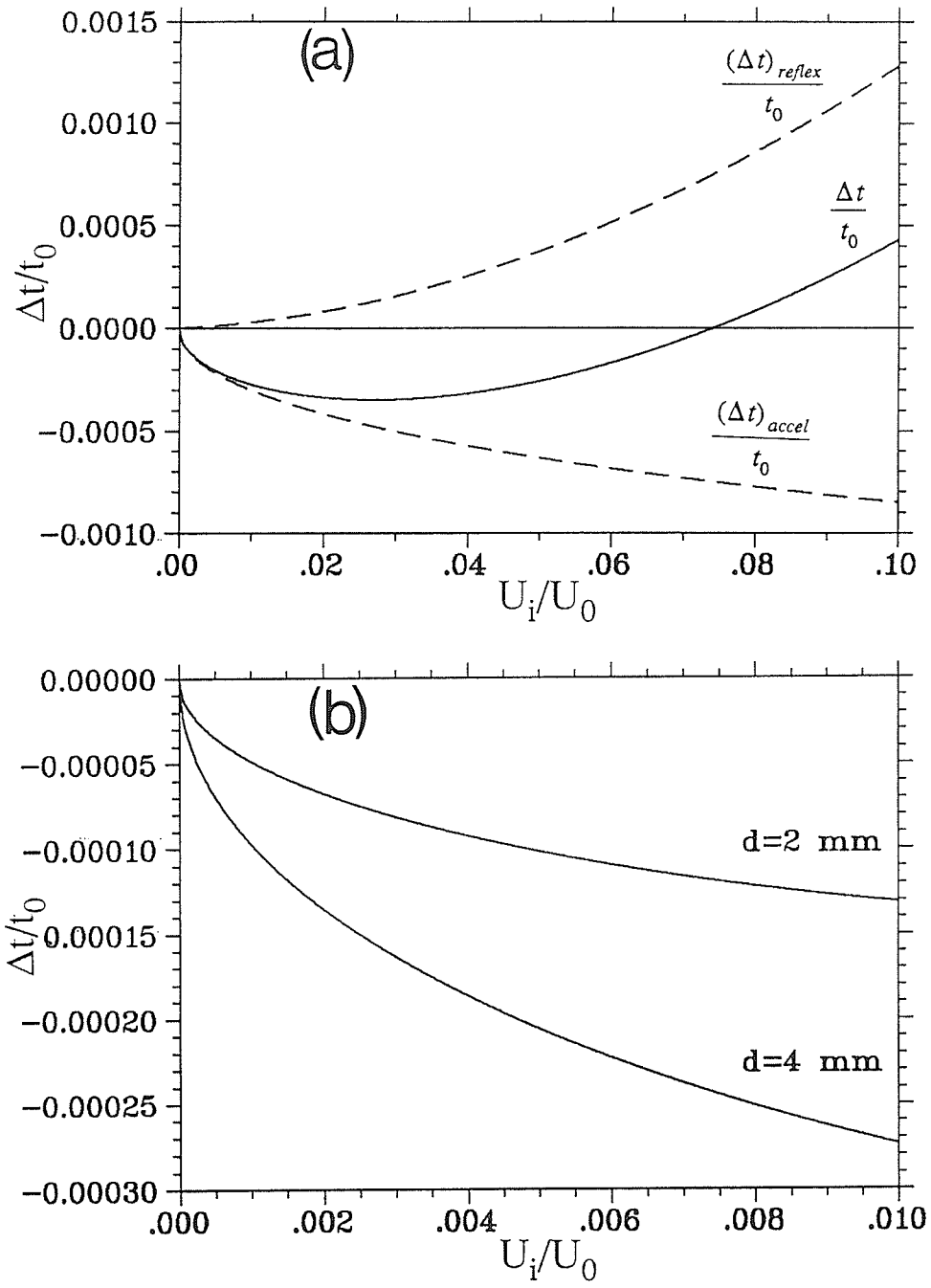

Figure 2.7 Calculated time variations ($\Delta t/t_0$) versus the ion initial energy (actually qU_i/qU_0). The value of mirror field corresponds to optimum for ions with zero initial energy. (a) The dashed curves correspond to the time variations induced in acceleration region $(\Delta t)_{accel}/t_0$, and in free fight and mirror $(\Delta t)_{reflex}/t_0$; the solid curve corresponds to the sum of the two terms above. (b) Show the total time variations with acceleration gap d=2 and 4 mm respectively.

mean energy value. For a given initial energy width in the energy range, ca $0 \le U_i/U_0 \le 1\%$, the time spread is maximum if the initial energy distribution includes $qU_i=0$. For example, for an initial energy width $qU_i=2$ eV at $qU_0=5$ keV (0.04% of qU_0), the total time variation produced is 6.24×10^{-5} if the initial energy is distributed between 0 and 2 eV, and is 3.8×10^{-5} if the initial energy is distributed between 0.5 and 2.5 eV; if the initial energy width is 0.1% of qU_0 (5 keV), then the time variations of $\sim9.7\times10^{-5}$ and 5.6×10^{-5} are produced for initial energy distributions of 0-5 eV, and 1-6 eV respectively. So the time variations produced in the acceleration region may be significant if the initial energy distribution is large and a high resolution (e.g. 10,000) is required. Since the time spread depends on relative initial energy spread $\Delta U_i/U_0$, it can be reduced by using higher accelerating voltage, e.g. for initial energy distribution of qU_i=0-2 ev, if qU_0 is increased from 5 keV to 10 keV, the time spread will be reduced from 6.24×10^{-5} to 4.44×10^{-5}, and a resolution of >10,000 can still be expected.

From the discussion above, we can see that the time spread in the acceleration region due to ion initial energy distribution imposes a rather tight restriction on high resolution measurements. One way to ease this restriction is to reduce the time variation in the acceleration region by reducing the acceleration gap width. Fig. 2.7(b) shows the plots similar to that in Fig. 2.7(a) with d=2 mm, and 4 mm respectively. So if the acceleration gap is reduced to 2 mm, the time spread will be reduced by a factor of ~2. For example, for initial energy distribution of qU_i=0-2 eV, the time spread will be reduced to 3.13×10^{-5} and 2.22×10^{-5} respectively for qU_0=5 and 10 keV and a resolution of >20,000 can be expected in the latter case. This gives a factor of 2 improvement in resolution over 4 mm gap width and for a given resolution requirement (e.g. 10,000) and accelerating voltage (qU_0=10 keV), a larger initial energy distribution (e.g. qU_i=0-10 eV)

can be tolerated. However, a small gap width that is too small may cause high voltage sparking or breakdown.

From Fig. 2.7, we know the time variations in the "reflex" and acceleration regions have opposite behaviour, so a practical way of dealing with larger initial energy spread is to increase the time variation in the "reflex" region to increase the compensation for the variations induced in the acceleration region. This may be achieved by reducing the value of the mirror electric field specified by the focusing condition in Eq. (2-17) to increase the time variations in the mirror. If the value of mirror electric field specified by Eq. (2-17) is reduced, the $(\Delta t)_{accel}/t_0$ is not affected by this change, but the minimum of the $(\Delta t)_{reflex}/t_0$ is shifted to correspond to a lower initial energy or acceleration voltage (see Fig. 2.6, since after acceleration the effect of the initial energy distribution and changes in the acceleration voltage are identical), and the originally upper and more steep part of the curve move to near the zero point. Fig. 2.8 (a) shows the curves similar to those in Fig. 2.7(a) but the strength of the mirror field (e.g. the mirror voltage) is reduced by 20% with respect to the value specified by Eq. (2-17) for U_i=0. It can be seen that a time variation $\Delta t/t_0$ of ~5×10^{-5} or a resolution of ~10,000 can be obtained for relative initial energy spread of U_i/U_0=0-0.35% or less. Thus a 35 eV initial energy spread can be tolerated for 10 kV acceleration; this can be quite satisfactory since the initial energy spread is usually only few eV in our case [160]. As shown in Fig. 2.8 (b), further reduction of the time spread for ions with initial energies distributed at lower energy range can also be achieved by reducing the mirror voltage further, but there are practical limits to this procedure dictated by the finite length of the mirror.

A drawback of this method is that under reduced mirror field, the flight time minimum is shifted to a corresponding lower acceleration voltage (see Fig. 2.6), so the

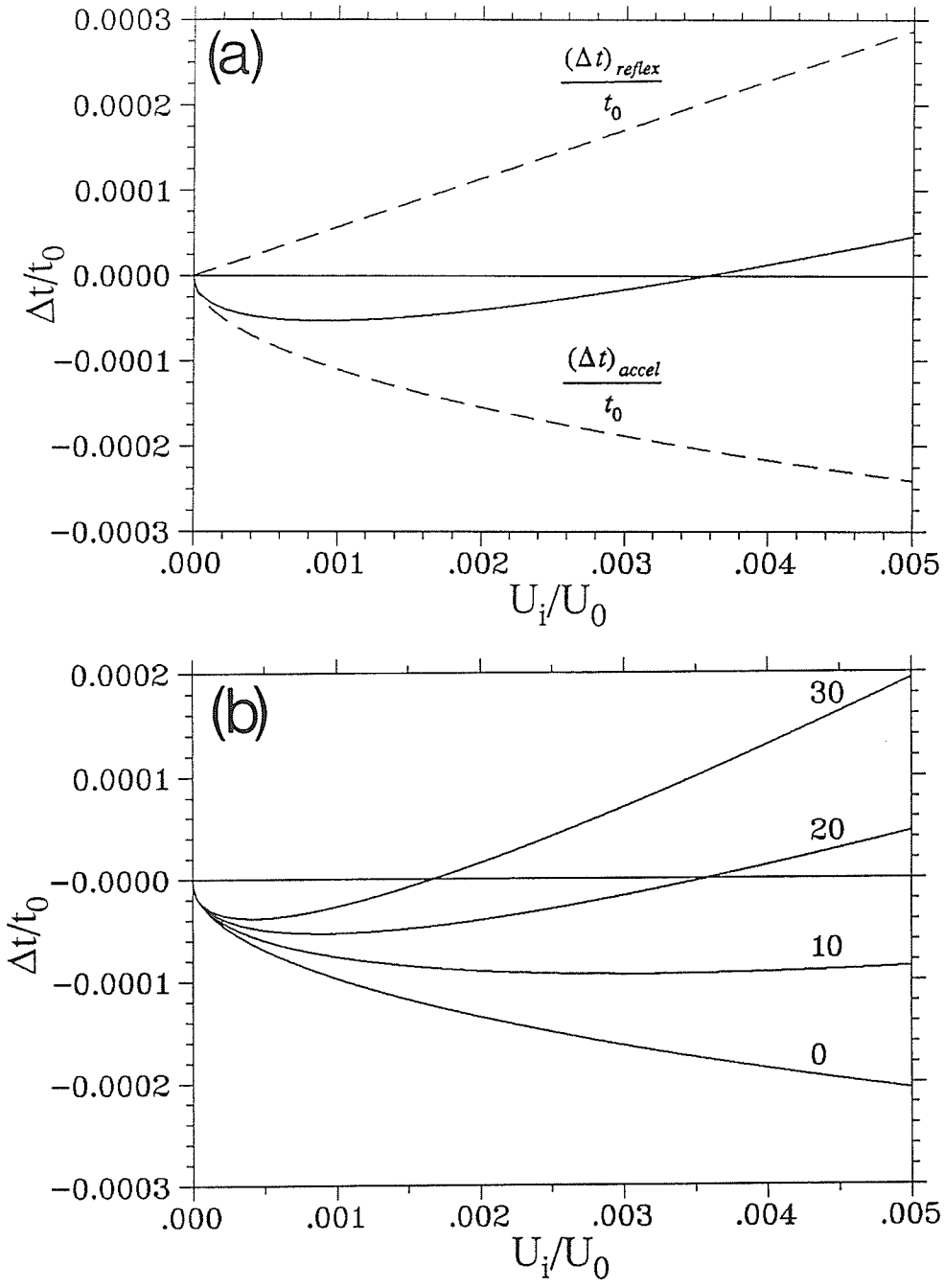

Figure 2.8 Calculated time variations ($\Delta t/t_0$) verses U_i/U_0, plots similar to those in Fig. 2.7, but the value of mirror electric field is reduced with respect to the focusing value specified by Eq. (2-17). (a) 20% reduction of mirror voltage from the focusing value, (b) the curves labelled 0, 10, 20, and 30 correspond to 0%, 10%, 20%, and 30% reductions of mirror voltage.

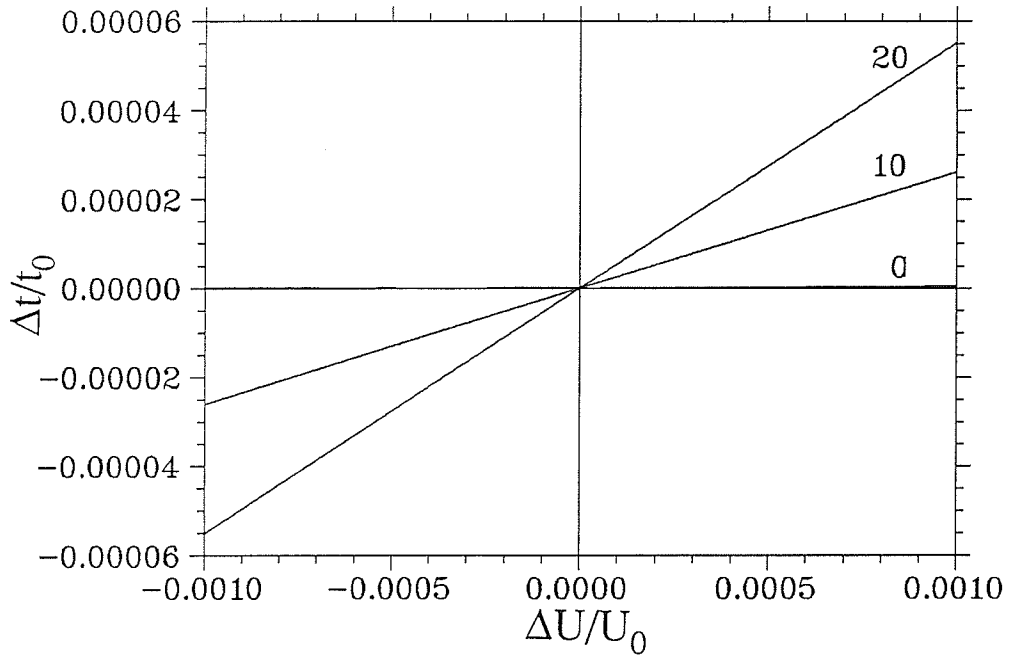

Figure 2.9 Calculated total time variations verses changes in acceleration voltage, curve 0, the value of mirror field is set according to focusing condition Eq. (2-17) for U_i=0; for curve 10 and 20, the value of mirror field is reduced by 10% and 20% with respect to that in curve 0.

system does not compensate acceleration voltage variations as well as before; as a result, the ion flight time will be more sensitive to the variations of the acceleration voltage. The comparison is shown in Fig. 2.9, and time variation of $\pm 5.5\times10^{-5}$ could be induced by a ±0.1% changes in acceleration voltage if the mirror electric field is reduced 20% from its focusing value, so a more stable power supply is required for acceleration in this case. However, this is a relatively trivial requirement, as commercial power supplies with these specifications are readily available. In fact the requirements here are much less stringent than those for the mirror power supply discussed in §3.3.1.2. This might however be a problem in the case of charging of the target since the surface potential due to the primary ion bombardment of insulating material can be quite high (~100 V) [242].

2.2.3.3 Correction on the daughter ion measurement

In section 2.2.2, we obtained the formula for daughter ion mass determination i.e.

$$\frac{t^*}{t}=\frac{1}{2}\frac{m'}{m}+\frac{1}{2} \tag{2-7}$$

since the daughter ions considered here are produced after acceleration, the acceleration region has no direct effect on daughter ion mass determination. However, when the acceleration region and initial energy distribution are taken into consideration, the value of the mirror electric field required for focusing is different from the value specified by Eq. (2-2), so this may affect the formula for daughter ion mass determination. In zeroth order, the time difference between a daughter and its parent is produced due to the different energy they have when they travel in the mirror. Since the electric field in a single stage mirror is linear, a linear equation similar to Eq. (2-7) is expected, but the slope and constant in Eq. (2-7) may change. Generally, we may have

$$\frac{t^*}{t}=a\frac{m'}{m}+b \tag{2-19}$$

If the mirror field is chosen according to the focusing condition Eq.(2-17) with $U_i=U_{i0}$, U_{i0} is the average ion initial energy, then we have

$$a=\frac{\frac{1}{2}+\frac{d}{L}\left(\frac{1}{1+j}\right)^2}{1+\frac{d}{L}\left[\frac{1}{1+j}+\left(\frac{1}{1+j}\right)^2\right]}\;;\quad b=\frac{\frac{1}{2}+\frac{d}{L}\left(\frac{1}{1+j}\right)}{1+\frac{d}{L}\left[\frac{1}{1+j}+\left(\frac{1}{1+j}\right)^2\right]} \tag{2-20}$$

where $j=[k_0/(1+k_0)]^{1/2}$ and $k_0=U_{i0}/U_0$. For an initial energy distribution peaking at 0.1%, i.e. $U_{i0}/U_0=k_0=0.1\%$, which is close to our case, we obtain a=0.4999527, b=0.5000472, so the

correction to Eq. (2-7) is very small. If we still use Eq. (2-7) to calculate the mass of the daughter, the error arising is

$$\Delta\left(\frac{m'}{m}\right) = \left(\frac{m'}{m}\right)_{a,b} - \left(\frac{m'}{m}\right)_{\frac{1}{2}} = \left(\frac{1}{a}-2\right)\frac{t^*}{t} - \left(\frac{b}{a}-1\right) \qquad (2\text{-}21)$$

for the values of a ,b above, we have $\Delta(m'/m)=0.0001892(t^*/t)$ -0.000189

since the value of t^*/t ranges from 1/2 to 1, corresponding to daughter ion masses of 0 to m, the maximum error is ~10^{-4} occurring at daughter ion mass close to zero. So the effect is not significant.

If the field E deviated from the focusing value E_f specified in Eq.(2-17) (for simplicity, take E_f corresponding to zero initial energy here), then we have

$$\frac{t^*}{t} = \frac{1}{1+f}\frac{m'}{m} + \frac{f}{1+f} \qquad (2\text{-}22)$$

where $f=E/E_f$. For example, for f=0.999, we have a=0.5002501, and b=0.4997498, the maximum error of Δ(m′/m) is 5×10^{-4} at daughter ion mass close to zero, so if the field E set 0.1% away from the focusing value, e.g. 10 V away from 10 kV mirror voltage, then a maximum calculation error of 0.5 mass unit in daughter ion mass is expected for a parent ion mass of 1000. Such errors are expected to be larger, if the mirror field E is set farther away from its focusing value, however, the values of a and b can be determined experimentally with known daughter and parent ion masses.

2.2.4 Single-Stage Versus Two-Stage Ion Mirror

As Mamyrin has shown [112-115], it is possible to make the second-order term

of the velocity spread [see Eq.(2-4)] vanish as well by the use of a two stage mirror (with two grids). Similar arguments have been given by Gohl et al.[154]. Most TOF mirrors constructed to date employ this prescription [111-115,117-120,129,137,152,155-159]. The second-order term can be important when the ions have a large velocity spread. However, in SIMS applications, the energy spread of secondary organic ion and clusters is usually a few eV [160], e.g. a typical velocity spread of $\delta/v_0=\Delta t/t=1/6400$ is illustrated in Fig. 1.1 in our case. Compared with other factors degrading the resolution, the second-order term is therefore small ($\sim 10^{-12}$ s for the conditions of Fig.1.1) and the two-stage mirror is unnecessary (for $m/\Delta m \approx 10^4$). It may, however, be convenient for added flexibility or to reduce the overall length of the apparatus. Moreover, similar to the case of a single stage mirror discussed in last section, the time spread induced in the acceleration region due to the initial energy distribution is not well compensated by a two stage mirror either. This may in fact limit the resolution of a two stage mirror instrument to a much lower value than expected [120,158].

The discussion in §2.2.2 has treated the behaviour of daughter ions in a single-stage mirror. It is interesting to compare this with their behaviour in a two-stage mirror (Mamyrin), which has been extensively investigated by the Munich group [155-157]. The broken curves, B, in Fig. 2.4 show the ratios t^*/t and t^*/t' for this case. The ratio t^*/t' is closer to 1 for large fragments ($m'/m \rightarrow 1$) than in the single stage mirror as a result of the additional correction provided by the second stage. Thus, the flight time of the largest fragments are almost identical to the flight times of ions of the same mass produced directly at the target or by decay in the acceleration region [155-157]. This is often a considerable advantage, since it simplifies the spectrum in the high mass region and facilitates identification of the daughter ions.

However, accurate measurement of daughter ion masses appears to be more difficult in the two stage configuration. The simplicity of the linear equation [Eq.(2-7)] is lost, since the corresponding relation for the two-stage mirror is more complicated [see Fig. 2.4(a)]. and does not determine daughter ion masses for $m'/m \leq 2/3$. This is a more serious problem; it arises because in a two stage mirror, the first stage acts as a retarding stage with a narrow gap (typically several mm) and a large potential difference (e.g. 2/3 of acceleration voltage of the ions) [114,115,154]. Thus if the mass of a daughter ion is less than two-thirds of its parent mass, it will be reflected in the retarding stage. Since the gap is very small, the time dispersion it introduced is not large enough to differentiate the daughter ions reflected in the first stage.

An alternative method of mass determination is by measuring the kinetic energies of daughter ions, which can be done by reducing the mirror voltage until the reflected peaks disappear one by one. This is analogous to measurements with retarding grids in linear TOF instruments [133,134,141] and has also yielded valuable information when used in reflecting spectrometers [155-157]. However, it lacks the capability of examining a number of mass peaks simultaneously, so is limited in sensitivity compared with the present technique. It also appears to be somewhat limited in accuracy (Kühlwind et al. quote <0.5% [156]).

Another disadvantage of a two-stage mirror here is its reduced transmission; some of the ions are lost when they pass through the extra metal grid which is used to define the second region of the mirror. This has spurred some interest recently in developing gridless ion mirrors [122,161-163]. However, the operation and optimization of such a device can be more complicated because the electric field in it is no longer homogeneous. The transmission is expected to be higher in a single-stage mirror because ions need pass

only one grid twice rather than two grids twice in a two-stage mirror.

From the considerations discussed above, a single stage ion mirror has been chosen for our reflecting instrument. Some preliminary experiments however were performed in the two stage mirror configuration [136,137] because the ion mirror was then not long enough to operate in a single stage configuration.

2.2.5 Construction of the Ion Mirror

A photograph of the ion mirror used in our reflecting spectrometer is shown in Fig. 2.10 (a). As in most such devices, the "uniform" electric field is produced by a finite set of rings spaced uniformly along its length. The ion mirror is made of non-magnetic stainless steel; In the present configuration, it consists of two end plates and 28 rings (8.79 mm thick, 11.75 cm I.D.) spaced 3.25 mm apart using ceramic balls and has a length of 34.9 cm between the two grids on the end plates. Both the front plate (ground) and the back plate (high potential) have 5.7 cm diameter apertures covered with 90% transmission nickel grids (Buckbee Mears Co.) The opening on the back plate provides a passage for neutrals when the mirror is "turned on" or to the ions and neutrals when the mirror is "turned off". The two grids are used in order to maintain field uniformity between the plates. Although the mirror is made for a single-stage configuration, it can be converted to a two-stage mirror by simply adding one more plate similar to those described above to the front to create a retarding field.

A constant potential difference between the adjacent rings was provided by a voltage divider consisting of a string of ordinary metal film resistors (1 MΩ, 0.5 W). The resistors have an accuracy of 0.11% and were picked out from one hundred such resistors

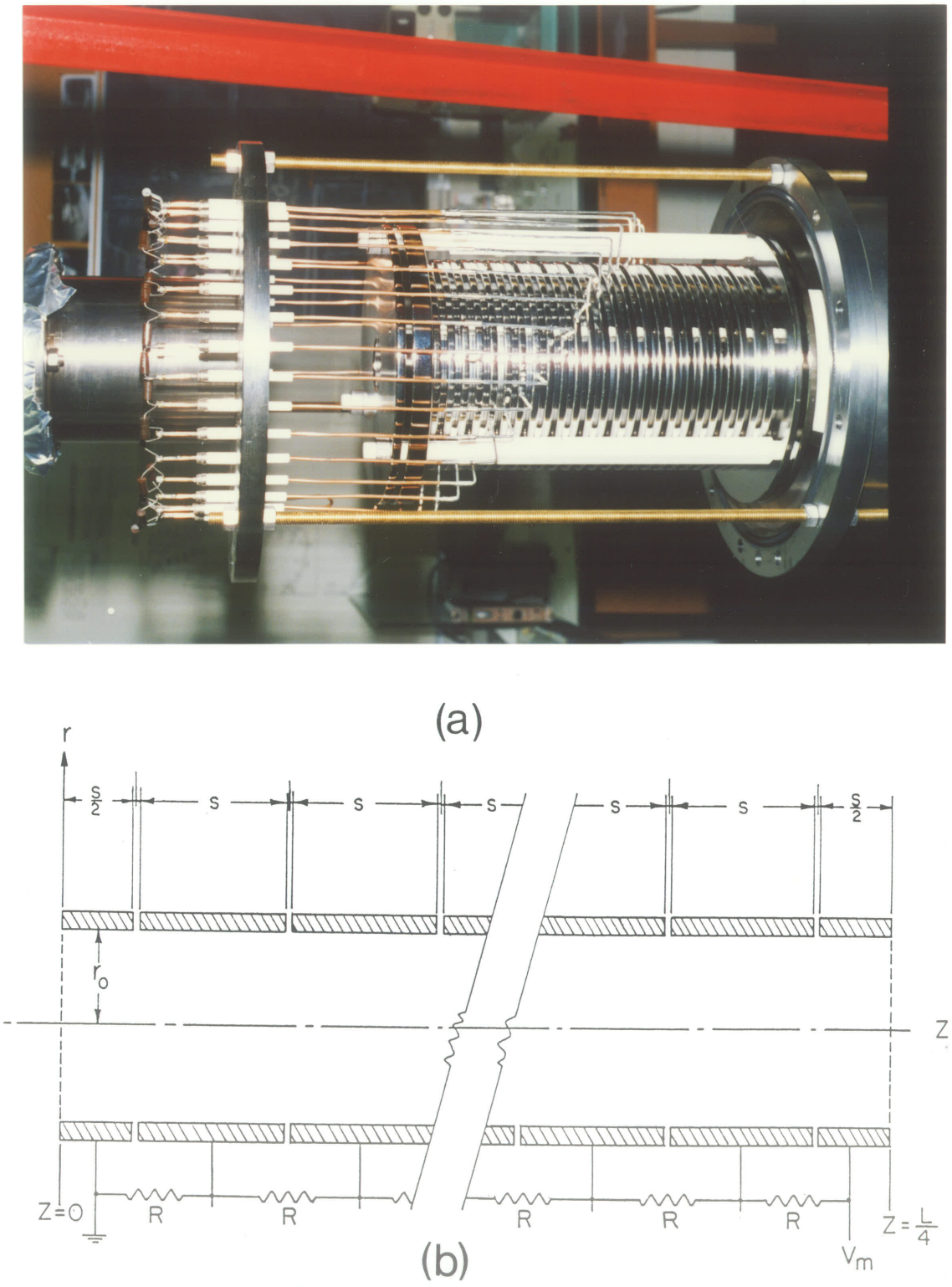

Figure 2.10 (a) Photograph of the ion mirror used in the reflecting spectrometer; (b) Cross-sectional view of the ion mirror (not to scale).

with a labelled accuracy of ±1%. The resistors were mounted on a flange outside the vacuum and connected to the rings through the vacuum electric feed throughs, so the potentials fed to each ring can be checked easily on the divider and any defective resistor can be replaced conveniently without venting the system.

In such an ion mirror, the field on the axis is expected to be constant, but at the rings the potential changes in steps at the junctions between rings, so the field is highly non-uniform at the outside.

For the ring geometry shown in Fig. 2.10 (b), an analytical solution for the potential ϕ inside the mirror may be obtained from Laplace's equation and the appropriate boundary conditions.

For cylindrical symmetry, Laplace's equation is

$$0=\nabla^2\phi=\frac{1}{r}\frac{\partial}{\partial r}\left[\frac{r\partial\phi}{\partial r}\right]+\frac{\partial^2\phi}{\partial z^2}$$

where r and z are cylindrical coordinates [see Fig. 2.10 (b)], and the boundary conditions are

$\phi=0$ at $z=0$

$\phi=V_m$ at $z=L/4$ (the length of the mirror)

$\phi=0$ at $r=r_0$ for $0<z<(s/2)$, $\phi=4V_m s/L$ for $s/2<z<3s/2\cdots$

where r_0 is the inner radius of a ring.

The potential ϕ may be solved as a superposition of potentials ϕ_1 and ϕ_2, i.e. $\phi=\phi_1+\phi_2$, where ϕ_1 and ϕ_2 satisfy Laplace's equation and their boundary conditions respectively. The obvious way to solve ϕ is to chose ϕ_1 as a uniform field solution and ϕ_2 as a solution periodic in z, that is

$\nabla^2\phi_1=0$

$\phi_1=0$ at $z=0$

$\phi_1=V_m$ at $z=L/4$

$\phi_1=(4V_m/L)z$ at $r=r_0$ and $0\le z\le L/4$ [see Fig. 2.11]

which has a uniform field solution

$\phi_1=\alpha+\beta z$

and the coefficients can be easily determined as $\alpha=0$ and $\beta=4Vm/L$. Hence

$$\phi_1=(4V_m/L)z$$

For ϕ_2, the problem can be expressed as

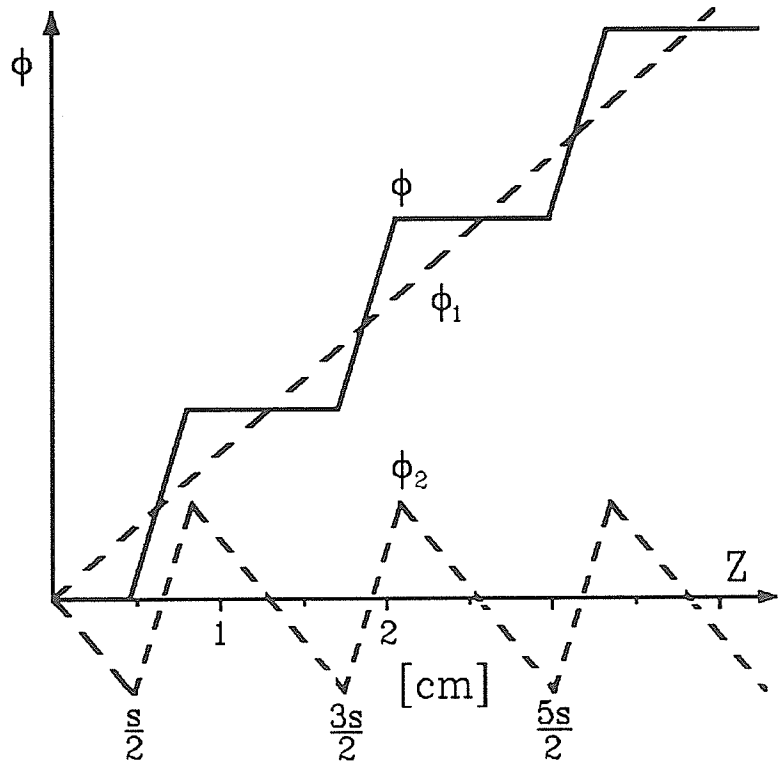

Figure 2.11 Boundary conditions (solid line) of the potential ϕ inside the mirror, for the purpose of computations, the potential ϕ may be taken as a superposition of two components ϕ_1 and ϕ_2 with their respective boundary conditions shown in dashed lines.

$\nabla^2\phi_2=0$

$\phi_2=0$ at $z=0$ and $z=L/4$

$\phi_2=-(4V_m/L)z$ at $r=r_0$ and $0<z<s/2$; $\phi_2=-(4V_m/L)(z-s)$ for $s/2<z<3s/2$···

i.e. at $r=r_0$, ϕ_2 has a sawtooth wave boundary function with a period of s along the z axis [see Fig.2.11]. It has a solution of the form

$$\phi_2=\sum_{n=1}^{\infty} A_n I_0\left[\frac{n2\pi r}{s}\right]\sin\left[\frac{n2\pi z}{s}\right]$$

where s is the thickness of a ring and $I_0(x)=J_0(ix)$ is a modified Bessel function [164]. The coefficients A_n can be determined from the boundary condition, that is

$$A_n=\frac{1}{I_0(n2\pi r_0/s)}\frac{4}{s}\int_0^{s/2}(-\frac{4V_m}{L}z)\sin(n2\pi z/s)dz=\frac{1}{I_0(n2\pi r_0/s)}\frac{4V_m s}{\pi L}\frac{(-1)^n}{n}$$

so

$$\phi_2=\frac{4V_m s}{\pi L}\left[\sum_{n=1}^{\infty}\frac{(-1)^n}{n}\frac{I_0(n2\pi r/s)}{I_0(n2\pi r_0/s)}\sin(n2\pi z/s)\right]$$

and

$$\phi=\phi_1+\phi_2=\frac{4V_m}{L}z+\frac{4V_m s}{\pi L}\left[\sum_{n=1}^{\infty}\frac{(-1)^n}{n}\frac{I_0(n2\pi r/s)}{I_0(n2\pi r_0/s)}\sin(n2\pi z/s)\right] \qquad (2\text{-}23)$$

The corresponding electric field, E_z, is

$$E_z=-\frac{\partial\phi}{\partial z}=-\frac{4V_m}{L}-\frac{8V_m}{L}\left[\sum_{n=1}^{\infty}(-1)^n\frac{I_0(n2\pi r/s)}{I_0(n2\pi r_0/s)}\cos(n2\pi z/s)\right] \qquad (2\text{-}24)$$

For large x, it has been shown [165] that

$$I_0(x)\rightarrow\frac{e^x}{\sqrt{2\pi x}}\left(1+\frac{1^2}{1!8x}+\frac{1^2\cdot3^2}{2!(8x)^2}+\cdots\right)$$

In our case, r_0=5.875 cm, $s\approx$1.2 cm, for n=1, $I_0(2\pi r_0/s)\approx1.65\times10^{12}$, so at r=1 cm

$$\frac{I_0(2\pi r/s)}{I_0(2\pi r_0/s)}\approx2.04\times10^{-11}$$

since the second order term is much smaller, i.e. for n=2 and at r=1 cm

$$\frac{I_0(4\pi r/s)}{I_0(4\pi r_0/s)}\approx1.65\times10^{-22}$$

Therefore, the electric field is mainly determined by the first order term (n=1). Hence

$$E_z=-\frac{4V_m}{L}[1-4.1\times10^{-11}\cos(2\pi z/s)]$$

Thus

$\Delta E_z/E_z\approx4.1\times10^{-11}$, at r=1 cm, similarly

$\Delta E_z/E_z\approx5.3\times10^{-9}$, at r=2 cm, and

$\Delta E_z/E_z\approx8.2\times10^{-7}$, at r=3 cm,

so the field is highly uniform around the axis. The region that the ions can traverse inside the mirror has a radius of <3 cm; the inhomogeneity of the field inside this cylinder is $\Delta E_z/E_z<8.2\times10^{-7}$, which is much better than what is required in this application.

From the calculations shown above, the field homogeneity in such a device is determined by the ratio of the modified Bessel function $I_0(n2\pi r/s)/I_0(n2\pi r_0/s)$; for a given radius of the rings, r_0, the homogeneity decreases with increase in s as might be expected.

2.3 PULSED ION GUN

The pulsed primary ion gun used in the reflecting instrument is shown schematically in Fig.2.12. It is very similar to the one employed in Manitoba TOF I, which was thoroughly described in the literature [130,131]. The Cs^+ primary ions are emitted thermionically from a small glassy bead of cesium aluminosilicate melted onto the end of a tungsten hairpin filament. The ions are accelerated up to 25 keV by the electric field between the shield and cathode, then they are collimated and focused by the Einzel lens onto a slit. The focused beam is swept rapidly across the 50 μm wide slit by a high voltage pulse (with amplitude up to 1 kV) applied to the deflection plates A. This results in a short pulse of ions beyond the slit with a time width (FWHM) of 2 to 3 ns. A second ion burst appearing on the falling edge of the voltage pulse is removed by applying a delayed voltage pulse to the deflection plates B, oriented at right angles to the deflection plates A. The pulse of ions then goes through the secondary ion accelerating

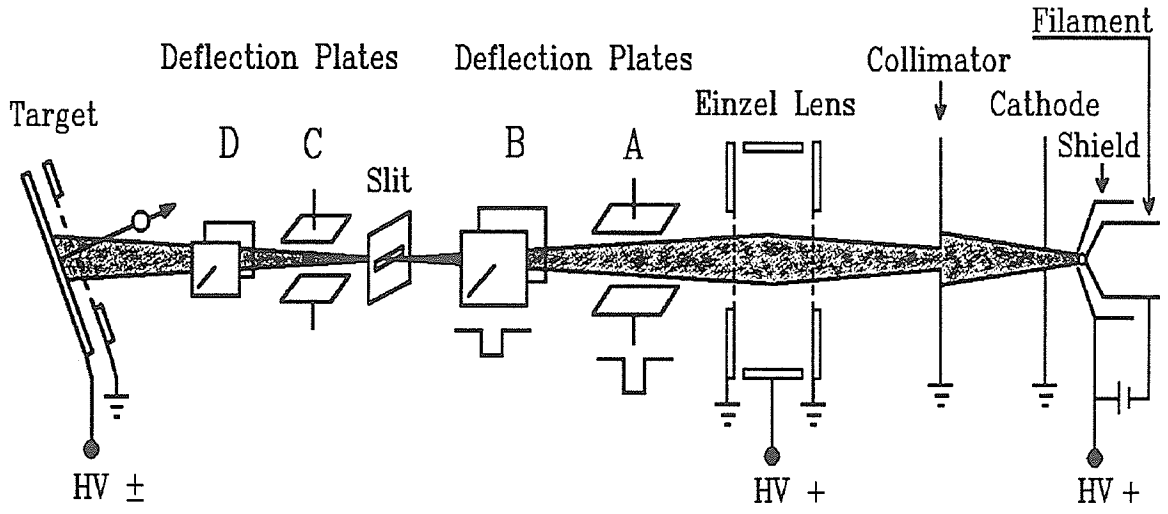

Figure 2.12 Schematic diagram of the pulsed ion gun (not to scale).

grid (at ground) and arrives at the target surface (at high voltage) with a decreased or increased ion energy. The final energy of the primary ions when they strike the target at perpendicular incidence is the primary ion accelerating energy minus (for positive target voltage) or plus (for negative target voltage) the secondary ion accelerating energy. Two additional sets of deflection plates C and D after the slit were added to allow the beam to be moved around on the target.

In the previous design [130], the shield and filament were fixed, and the position of the cathode aperture could be adjusted in the plane perpendicular to the ion beam axis to provide accurate alignment of the extracted beam. In the new gun, the cathode and the shield are aligned and fixed, but the position of the filament can be adjusted externally in three dimensions to provide the optimum extraction of the primary ions. The advantage of this modification is that the output of the primary ion beam can be optimized "on line" from time to time, and the primary ion beam axis remains unchanged.

The size of the primary ion beam spot on the target may depend on the size of the cesium aluminosilicate bead on the filament (or the size of the cesium source) and the beam focusing condition, but the spot is usually $\leq$3 mm in diameter, and can be measured by scanning the pulsed primary beam across a strip of CsI on the target using the deflection plates C and D.

For various purposes, the primary ion flux at the target may be set to a suitable value by varying the dc ion-beam current; this is done by adjustment of the filament current, (hence the temperature of the filament) to change the emission rate of the Cs^+ ions. Under various operating conditions, the dc current at the plane of the slit has ranged from a few nA to a few hundred nA. Normally the beam is adjusted so that ~100 to ~2000 ions per pulse pass through the slit and hit the target at a repetition rate of 2-5

kHz, corresponding to an average ion current of ~0.1 to ~1pA. Since the target beam spot has a diameter of ~3 mm, the average ion current density on the beam spot is ~1-14 pA/cm^2.

The continuous extraction of primary ions from the source may cause undesirable effects if a large number of primary ions per pulse is needed at the target. The high target current density for a given pulse duration requires high dc ion beam at the slit and hence high filament current. This results in short lifetimes of the source (a few hours to a few days depending on the size and shape of the filament bead) and the slit, and requires high pumping speed for the source in order to prevent it from sparking due to the discharging of the shield or filament (both at 18-25 kV) to ground. However, the problem can be easily solved by operating the source in a pulsed extraction mode. This is done by applying a proper timed pulse (with an amplitude of ~400 V) to the anode shield surrounding the filament source, so that the ions emitted continuously from the filament are trapped and accumulated inside the shield and pulse out for a few microseconds in each cycle; this creates a "bunching" effect. For the same filament current as in the continuous extraction, the primary ion flux at the target could be increased by a factor of up to 10 by setting proper timing of the pulse and adjusting the filament position. So for a given primary ion current density at the target, the filament and slit currents can be much lower and the lifetimes of the filament source and slit are much longer. Also a lower pumping speed at the source could be satisfactory in the pulsed extraction mode than in the in continuous extraction mode. The most important feature of the pulsed extraction is its effectiveness in reducing background resulting from primary ion leakage from the slit between the pulses [131]. So the ion gun on the reflecting instrument has been employed mostly in the pulsed extraction mode to obtain the advantages mentioned

above.

2.4 SAMPLE PREPARATION AND TARGET INSERTION

As mention briefly in the previous chapter, sample preparation is a critical step in mass spectrometric analysis of organic compounds by particle or laser desorption methods, in particular when biomolecular samples are considered. Glycerol and analogs have been successfully used as liquid matrices in the FAB, or liquid SIMS method, however they usually produce significant chemical noise and normally require relatively large amount of sample. Furthermore, the high vapour pressure they produce is likely to cause problems, such as high voltage breakdown, and the surface renewal observed in FAB is not likely to be produced by the small primary currents used in the TOF spectrometer.

In TOF-SIMS or PDMS methods, the sample is usually prepared by depositing and drying an appropriate sample solution on a solid surface because the solid targets are more compatible with the high electric fields and open source geometry normally used in a TOF mass spectrometer. Three types of sample preparation techniques have mainly been used for analysis of biomolecules, particularly peptides, using the reflecting instrument.

2.4.1 The Electrospray Deposition

The first technique used is depositing the sample on a metal substrate by the

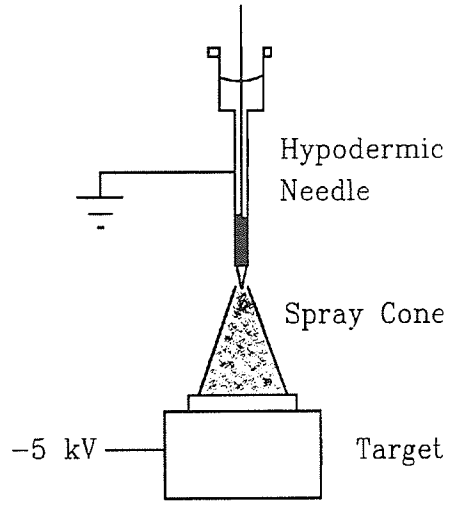

Figure 2.13 Simple electrospray device used for target preparations.

electrospray method, which was first adopted in ^{252}Cf PDMS [166]. The simple device used for electrospray is shown in Fig. 2.13. Here a hypodermic needle at ground potential is positioned with its tip several mm to a few cm above a metal substrate at a negative potential of several kilovolts. A solution containing the sample is placed into the reservoir of the needle, and a regulated flow of the solution is obtained by inserting a thin stainless steel wire into the needle. The drop that forms at the end of the needle is charged by the electric field and dispersed by Coulomb forces into a fine spray of charged droplets onto the metal substrate. The droplets should be small enough so that most solvent evaporates and the solute residue hits the substrate without visibly wetting it. The desired spray quality and spot size can be obtained if the flow rate, the distance, and the potential between the needle and the substrate are chosen properly.

A typical concentration of sample solution is 1μg/μ*L*, and methanol, acetone, and acetic acid are the most common solvents used in electrospray because they have low surface tension and high volatility and are easy to spray. If a sample is not soluble in these solvents but soluble in water, then it is usually dissolved in a small amount of water and diluted with one of these solvents in order to reduce the surface tension of the solution. The metal substrate used for the electrospray deposition is usually aluminium, either as a film on a polyester backing or as a solid foil, because it is easily stretched to obtain a planar surface and is inexpensive.

Apart from the limited number of solvents useful for spraying, the electrospray deposition requires relative large amount of sample and the surface formed is rather undefined, consisting of inhomogeneous layers of small (μm dimension) sample clumps. Thus the desorption of ions from the sample film prepared by electrospray method occurs primarily from bulk material. This is not very efficient if one likes to exploit the true sensitivity of a surface technique like SIMS.

2.4.2 Direct Deposition on an Etched Silver Foil

The second technique used is the direct deposition of a sample solution onto a etched silver substrate [167,168]. A silver foil is normally cut into small (~1 cm diameter) disks and then placed into a warmed nitric acid solution (ca. 50°C, 2N) until the silver surface loses its sheen and becomes dull white. The process usually takes a few minutes and can be accelerated by using more concentrated nitric acid or increasing the temperature of the solution.

The etching process produces a very rough, hydrophilic surface that causes a drop of solution to spread out rapidly over the surface and dry quickly; thus a uniform layer can be formed on the surface. Depending on the amount and concentration of the deposited solution, this preparation results in submonolayers, monolayers, or multilayers of the sample molecules on the substrate surface, or at least their equivalents. Benninghoven has estimated for some small molecules (MW ~a few hundred u) that a single monolayer corresponds to 1μ*L* of 10^{-3} mol/*L* solution (containing about 6×10^{14} molecules or 1 nanomole) deposited on 1 cm^2 of an etched silver surface, and only when the sample amount exceeds one monolayer equivalent, does a multilayer and crystallite

formation on the substrate start [116].

In organic SIMS it has been found that, up to a monolayer equivalent, the molecular ion yields increase linearly with the surface concentration of the sample molecules [116]. Desorption of a multilayer of sample molecules may not give higher yields because the effective target size is perhaps limited to the top monolayer by radiation damage.

The deposition of sample molecules on the etched silver substrate produces good mass spectra for a very small amount (picomole) of peptide molecules, thereby gives higher sensitivity than the electrospray method. For a surface coverage of a monolayer or less, strong silver adduct quasimolecular ions of the sample are observed due to the strong interaction between the sample molecules and the surface. This is an advantage if one wants to study the decay pattern of these particular ions [169].

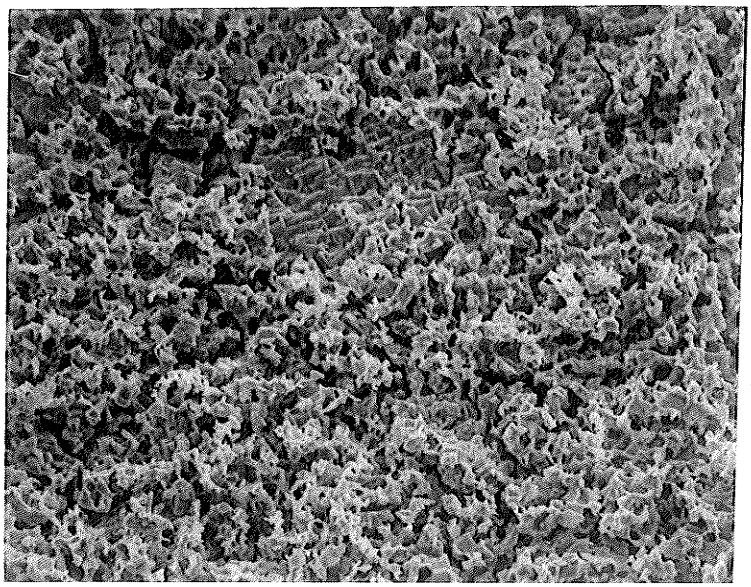

Figure 2.14 Electron microscope photograph of a typical etched silver surface. Magnification × 1000.

It is not well understood how the etched silver surface interacts with sample molecules to produce good molecular ion yields; however, the increased surface area caused by the extremely rough texture of the etched surface as shown in Fig. 2.14, and formation of monolayers of sample molecules, rather than bulk material on the surface, due to the hydrophillic nature of the surface may be partly responsible for good spectra. A decrease in fragmentation, as well as an increase in secondary ionization efficiency, has been observed by comparing the mass spectra obtained from organic compounds adsorbed as monolayers on a solid substrate with those obtained from corresponding pure compounds as bulk materials on the surface [32].

Sample deposition using an etched silver substrate is also much simpler and has less contamination problems compared with the electrospray method. A target is usually prepared by dropping one, or a few μL, of an appropriate sample solution onto the cleaned, etched silver surface and waiting until the solvent evaporates. A silver disk can usually be etched several times. The etched silver substrate offers improved sensitivity and good spectra can be obtained for a large number of biomolecules. However, using low energy ion bombardment, the mass range of organic molecules by this preparation method is limited to about 3000 u, as in electrospray preparation [170]. The silver adduct ions in the spectra are often useful but can also sometimes complicate the interpretation of the spectra.

2.4.3 Direct Deposition on a Nitrocellulose Substrate

The third and also the most common technique used here for biomolecular sample preparation now is the use of a nitrocellulose (NC) substrate as a backing to adsorb the

sample molecules.

The use of non-metallic sample backings for analysis of peptides and proteins was first studied in ^{252}Cf fission fragment desorption mass spectrometry. Jordan et al [171] have found an improved protonated molecule yield and low metastable ion population for polypeptides adsorbed on Nafion (a perfluorinated cation exchange polymer) instead of deposited on a metal foil by electrospray. Jonsson and coworkers [96], using nitrocellulose (NC) as sample backing, have demonstrated even more dramatic enhancements in quasimolecular ion yields and improvements in the quality of the mass spectra of peptides and small proteins. Their results indicated that protonated polypeptides desorbed from NC undergo substantially less fragmentation than polypeptides desorbed from bulk material. A strong enhancement of the desorption yield of multiply charged (protonated) intact molecule species was also observed from NC. Alai et al [172] also reported improvement of mass spectra of samples prepared by electrospraying polypeptides dissolved in solutions containing glutathione (functioning as a matrix).

Encouraged by the works of Jonsson et al, the NC substrate was introduced in our laboratory for the analysis of biomolecules, particularly polypeptides, bombarded by low energy (keV) primary ions. Improvements of the mass spectra similar to those observed in PDMS were obtained in our SIMS method, and differences in relative quasimolecular ion yields between fission fragment and keV Cs^+ ion bombardment were reduced significantly by the use of the NC bound peptide samples rather than electrospray samples. For the first time, intact protonated molecules of an organic compound as large as bovine insulin were observed by keV energy particle bombardment of solid samples [97], although it had been produced fairly readily by MeV fission fragment bombardment even with electrospray sample deposition [15], or by keV bombardment of a sample in

glycerol. Thus NC extends the useful mass range that can be studied with low energy ions to proteins with molecular weights up to ~10,000 u [173].

Like samples deposited on the etched silver substrate, sample molecules are adsorbed onto the NC substrate probably as a monolayer, but the molecules seem to be more weakly bound to NC than to the molecular solids or to an etched silver surface. This may possibly be the reason for increased quasimolecular ion yield and decreased fragmentation for the molecules desorbed from NC compared with the etched silver surfaces. The reduction of the binding energy of the sample molecule to the surface presumably lowers the energy required for sample desorption. Ions could then be desorbed at increased distances from the point of primary ion impact, where less energy is available for equilibration among the vibrational and translational degrees of freedom of the desorbed molecule. Since the annular area for desorption increases in size at these larger distances, more quasimolecular ions could be desorbed with less internal energy of excitation resulting in an increased quasimolecular ion yield, decreased fragmentation, and higher mass range [97,171-176].

The sample preparation procedure with a NC substrate is as follows: A white NC membrane is first dissolved in acetone to make a solution at a concentration of 1-5 μg/μL. The NC substrate is then prepared by electrospraying the solution onto a metal backing (i.e. aluminium, silver or stainless steel) to yield a coverage of about 20-200 μg/cm^2 of NC. A thick NC film gives a better yield of molecular ions (perhaps its rougher surface has more area for sample molecule adsorption), but a thin NC film produced cleaner spectra (less background), probably because of less surface charging. The satisfactory thickness (~50-100 μg/cm$^{2)}$ can be judged visually during the spray. Electron microscope photographs of the NC surfaces are shown in Fig. 2.15. The NC substrates were washed

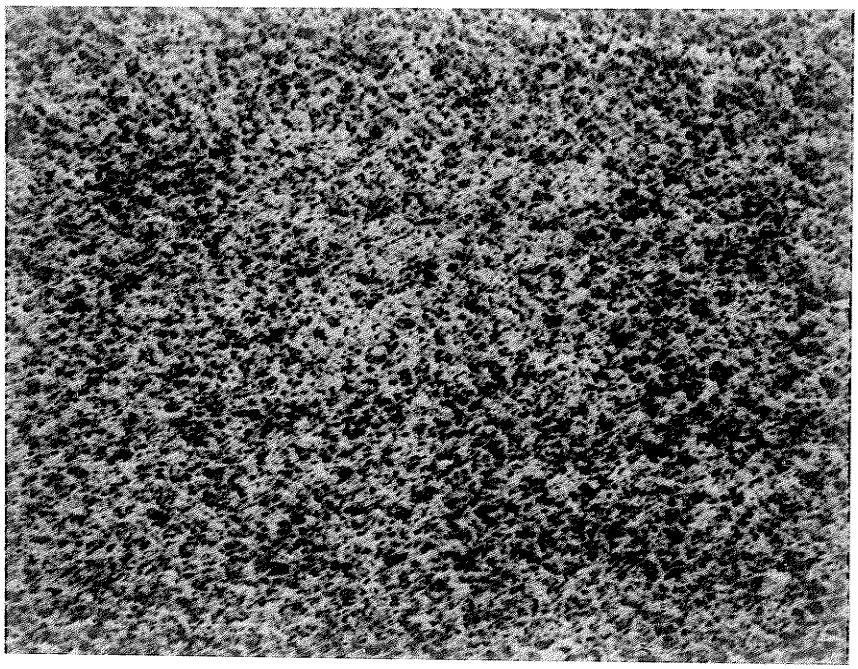

(a)

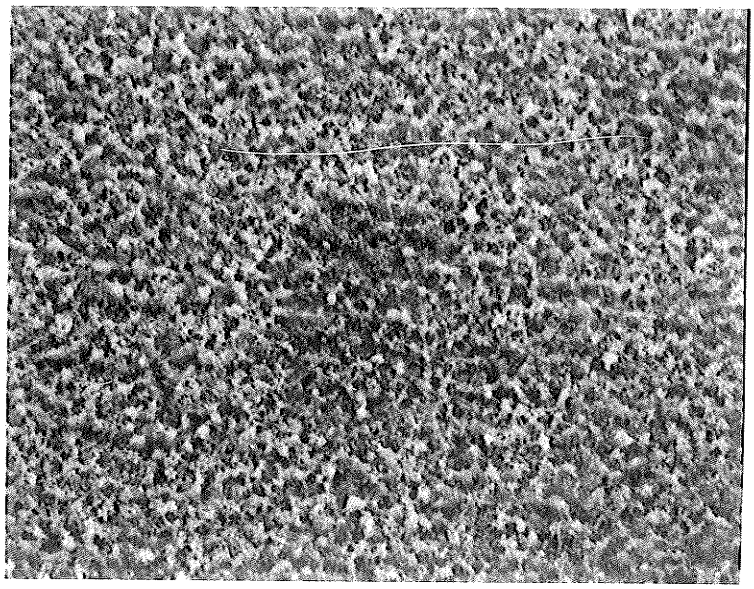

(b)

Figure 2.15 Electron microscope photographs of nitrocellulose surfaces prepared by electrospraying of (a) 1 μg/μL solution and (b) 5 μg/μL solution on silver surfaces. The respective surface concentration is (a) ~50 μg/cm^2 and (b) ~150 μg/cm^2. Magnification is 1000 in both photographs.

with 40-80 μ*L* of 0.1% aqueous trifluoroacetic acid (TFA) solution to remove possible salt contamination prior to sample deposition. The sample was usually dissolved in 0.1-10% aqueous TFA at a concentration of ≤1 μg/μ*L*. A 0.5-5 μ*L* amount of sample solution was applied to the NC film, and distribution of the droplet on a large area of the NC substrate may be achieved by blowing the solution over the area. The target was introduced into the mass spectrometer after the solvent evaporated. The use of a NC substrate allows selective adsorption of peptides and proteins from solutions, and buffers and salts necessary to keep the protein in solution can be removed by washing the target with 0.1% TFA after the sample deposition. This washing procedure has been found useful to improve the peak shape and increase the abundance of protonated molecules in the spectra [97], because cations, such as Na^{+}, in the salts can "quench" the formation of molecular ions, and the impurities may cause more background. However, small peptides, which do not adhere to the NC as well as larger peptides, may also be washed away partly or completely in this washing procedure. Salt contamination has not been a serious problem in our case with NC substrates if precautions are taken in the sample preparation process, such as washing the NC substrate prior to sample deposition and using washed plastic vials and pipette tips for sample mixing and transportation. Thus for the present measurements, the targets were not usually washed after sample deposition.

2.4.4 Target Insertion

There were three types of target holders used for different purposes. The aluminized polyester or thin aluminium foils were stretched over a 12 mm diameter stainless steel ring with a tightly fitting outer ring [Fig.2.16 (a)] . Thick metal foils such

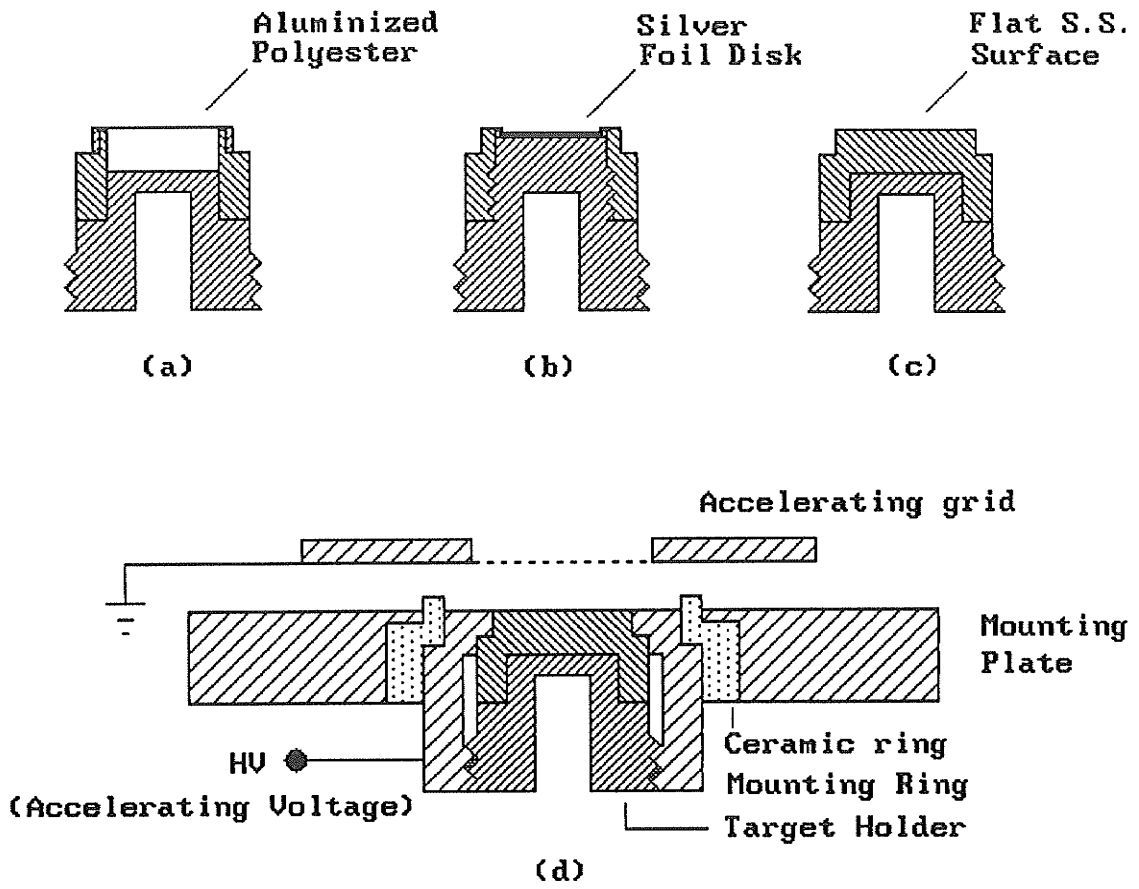

Figure 2.16 Cross-section view of (a-c) the target holders; and (d) target and accelerating grid assembly.

as silver, stainless steel, or aluminium were cut into 12 mm diameter disks and put on a stainless steel cylinder and fixed by a screw retainer [Fig.2.16 (b)]. The samples or nitrocellulose can also be directly deposited onto the stainless steel surface of the third target holder [Fig.2.16 (c)]. This target holder was made to maintain the flattest possible surface. The target is inserted into the system by a stainless steel rod through a vacuum lock. After the target is screwed in position [Fig.2.16 (d)], the rod is pulled out of the system, so that the vacuum in the system can recover quickly. Usually it takes about 5-10 minutes to change a target and for the system to get back to the operating pressure.

2.5 ION TRANSMISSION AND DETECTION

2.5.1 The Detectors

Usually microchannel plates are used to detect the ions at the end of the flight path in TOF mass spectrometers because of their large active area and good time resolution. A chevron microchannel electron multiplier, illustrated in Fig. 2.17 (a) was used for both top and bottom detectors in the reflecting instrument. For each detector, two microchannel plates (with 4 cm diameter effective area) are separated by a 250 μm stainless steel ring and mounted 1 mm from a stainless steel collector. The front surface of the first plate is usually at ground, a typical potential difference of 1 kV was applied to each plate and 200 V is placed between the second plate and the collector. The voltages were supplied by a voltage divider mounted outside the vacuum chamber. An electron gain of ~10^7 is achieved in this configuration and the output pulse has a rise time of ~0.5 ns and a pulse width of 1.5 ns [131,177].

The plates consists of an array of continuous dynode electron multipliers (12~15 μm diameter) at a small angle (~5°) to the plate normal, and the open area ratio is typically 50%. The bias angle increases the probability that an incoming ion strikes the channel surface, but this may produce a time spread due to some ions hitting the channel surface near the entrance and others deep inside. This spread may be significant in a high resolution measurement. Also, as the microchannel plates are of non-imaging quality, their surfaces are not always perfectly flat nor uniformly sensitive. So an electron converter was constructed and used in the bottom detector assembly with the hope of improving the

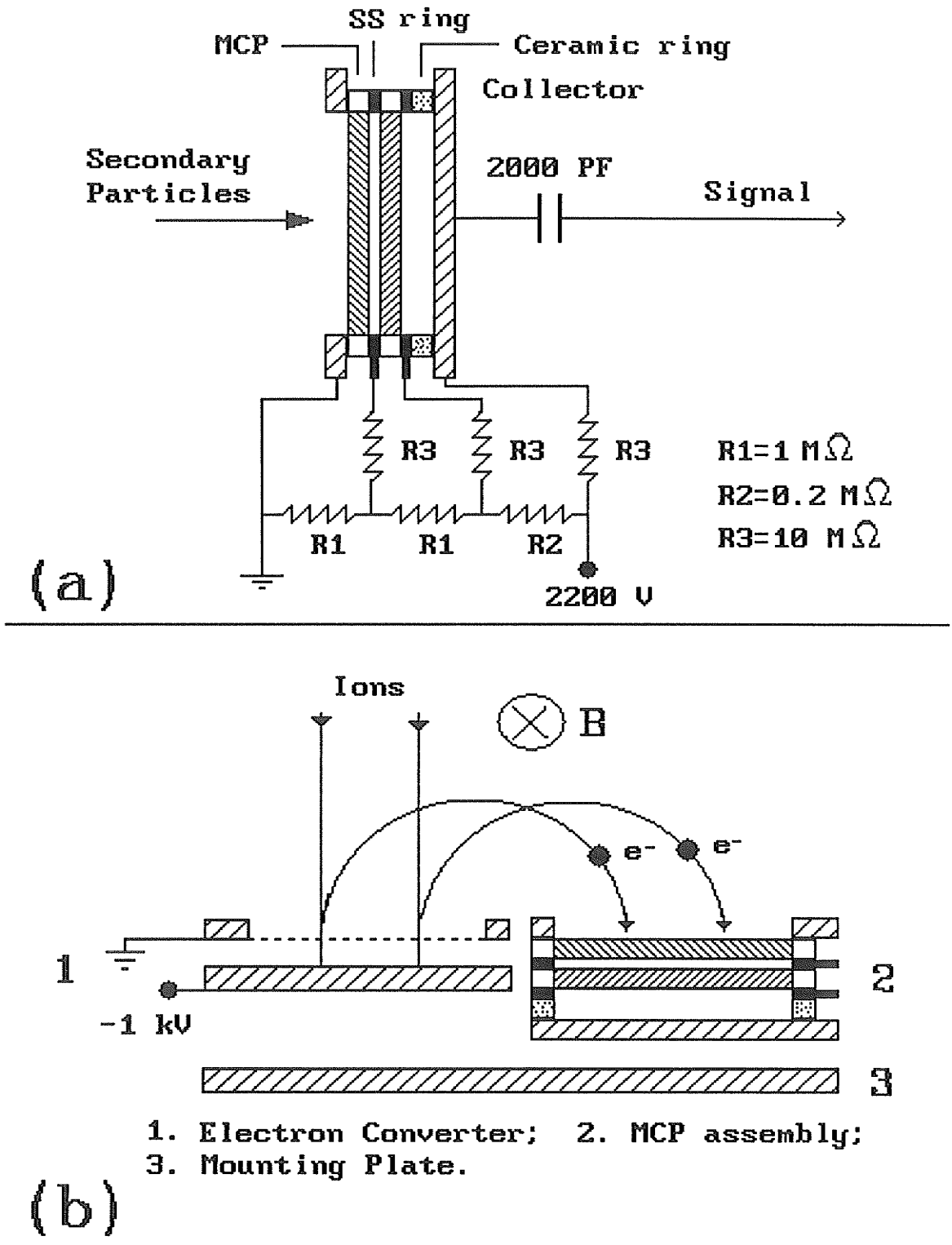

Figure 2.17 Cross section view of the detectors: (a) chevron microchannel electron multiplier, (b) electron converter detector assembly.

mass resolution and sensitivity.

The bottom detector assembly is illustrated in Fig. 2.17 (b). Here the secondary electrons are produced on a plane surface of the conversion dynode by an incoming ion. As in similar devices [144,178-180], the electrons are accelerated and bent by a uniform magnetic field into the electron multiplier mounted beside the converter. The transport is isochronous. Since the electrons are much lighter, they are accelerated to much higher velocity compared with the incident ions, so the time spread due to the bias channel or uneven surface of a microchannel plate is no longer significant.

The conversion dynode consists of a flat aluminium plate, 4 mm thick and with a circular effective area 4 cm in diameter. The plate is coated with a thin film of CsI by vacuum evaporation. The CsI coating may have an enhanced electron conversion efficiency due to the low work function [181]. The conversion dynode is maintained at a high negative potential and a 90% transmission grid is at ground potential to provide for post-acceleration of positive ions into the dynode and the acceleration of the secondary electrons away from the dynode. The distance from the grid to the dynode is 2 mm, and a typical negative voltage of 1-1.5 kV was placed on the dynode for the detection of positive ions. For detecting negative ions, a lower negative voltage (ca. -500V) was usually applied to the dynode to decrease the deceleration of the incoming negative ions. The converter and the detector were mounted on a common base plate which can be tilted by three micrometer screws for optimal mass resolution.

The magnetic field for bending the electrons is produced by a pair of rectangular coils separated by 11 cm apart and mounted outside the vacuum chamber. The center-to-center separation of the conversion dynode and the microchannel plate is 6 cm, so the electrons travel through a semicircular path with a radius of 3 cm. For a 1 keV electron

this corresponds to a magnetic field strength of ~36 gauss. The variation of the magnetic field in the volume (10×4×3 cm^3) containing the electron path was measured to be less than 10% (by a Hall probe). The field strength is adjusted by varying the current in the coils to produce optimal counting rate in the detector.

2.5.2 Ion Detection Efficiency

As in most other types of mass spectrometer, TOF mass spectrometers use secondary electron emission followed by electron multiplication as the means for detection. Ion detection efficiency becomes an important matter when dealing with high-mass secondary ions because of their low velocity. The interaction which follows the impact of ions on a surface and results in the ejection of an electron or electrons is complex and is not well understood. The number of electrons or the probability of an electron being ejected following the impact of an ion may depend on many parameters, which include the velocity and number of atoms in the incident ion, and the properties of the detecting surfaces. Using high molecular weight water clusters (up to ~60 000 u), Beuhler and Friedman have measured the detection efficiency of water cluster molecular ions as a function of their velocities and suggested a threshold velocity of ~18 000 m/s for the incident ion exists for efficient electron ejection from copper surfaces [182]. They later reported secondary electron emission from aluminium oxide surfaces when the ion velocity was as low as 10 000 m/s [183]. The detection efficiency of biomolecules has been studied subsequently. Hedin and coworkers have suggested an ion threshold velocity similar to that for the detection of water clusters also exists at about 18 000 m/s for the detection of bovine insulin molecular ions incident on copper surfaces [184]. However,

detection of larger molecular ions from both organic and inorganic material with velocities below the "threshold" is not uncommon. Detection of protein molecular ions from glucose isomerase (m/z=172 400) with velocity as low as 4 800 m/s has been reported recently [79]. It is not clear what the detection efficiency of ions with velocities below the "threshold" is, but considerable improvement can be achieved by post acceleration to increase ion velocities. For example, an improvement in signal-to-noise ratio by about a factor of 50 has been observed [78] for 3 keV porcine trypsin molecular ions (m/z=23 450), by increasing the post-acceleration potential from 6 kV (corresponding ion velocity of 13 000 m/s) to 20 kV (corresponding ion velocity of 13 000 m/s).

Recently Geno and Macfarlane [185] have studied the detection efficiency for a series of amino acids and peptides using direct detection with microchannel plates. They found that secondary electron coefficients γ vary exponentially with velocity between 15,000 and 32,000 m/s, and linearly with mass from m/z 86 to m/z 1059, where the average probability P for detecting an ion is related to γ by $P=1-e^{\gamma}$. In their studies, the detection efficiency of 100%, i.e. the probability of detection P=1 was observed for 3 keV lysine molecular ions (MW=146.1) and for 10 keV bradykinin molecular ions (MW=1059.3). The molecular ions of amino acids and peptides at velocities clearly below the "threshold" were also detected. The detection probability of bovine insulin $(M+H)^+$ ion as a function of ion velocity is illustrated in Fig. 2.18.

In our case the typical energy of parent ions incident on the CsI surfaces on bottom detector is ~14 keV; this is satisfactory for most compounds studied here with masses below ~3000 u (velocity above 30 000 m/s). However it is clear from Fig. 2.18 that for high mass molecules, a higher total energy of ions is still desirable to increase the detection efficiency. For example, for molecular ions from bovine insulin, the

detection efficiency will be increased from ~0.2 for a total ion energy of ~13 keV (velocity≈20 900 m/s) to ~0.5 for a total ion energy of ~20 keV (velocity≈26 000 m/s).

Although a direct comparison of the detection efficiency of the electron converter detector with that of a chevron microchannel plate (CMCP) has not been made here, generally the amplititude of the signal pulses from the electron converter detector is much higher than that from the CMCP detector. In the electron converter detector, the average number of secondary electrons per incident ion may perhaps be higher because of the low work function of CsI surface, and the probability that these electrons will lead to a cascade at the surface of the microchannel plate is higher since these electrons are

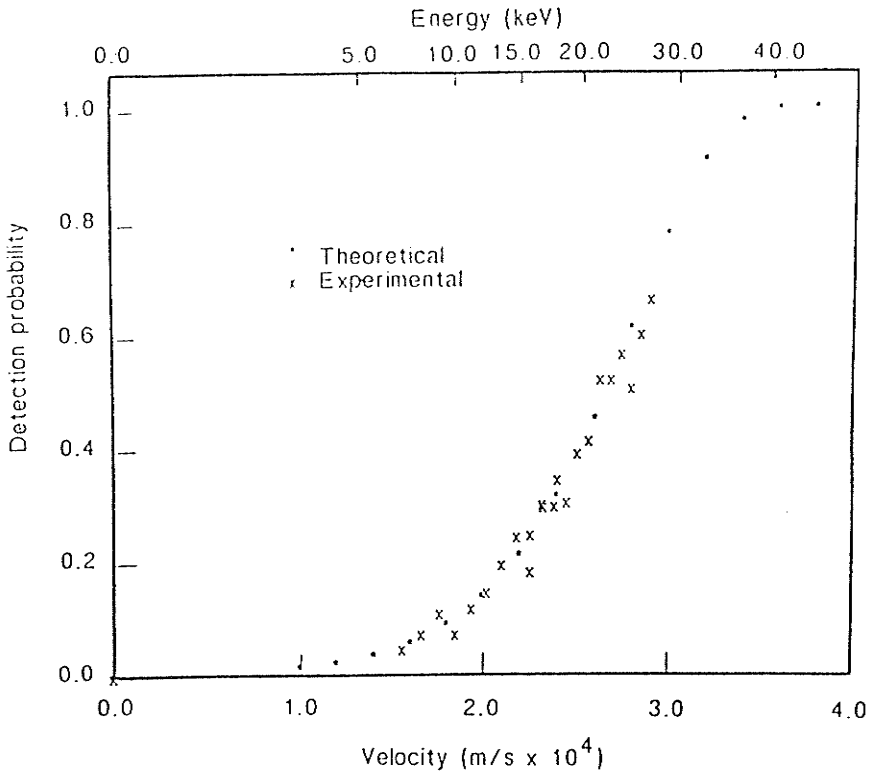

Figure 2.18 Detection probability of the bovine insulin $[M+H]^+$ ion as a function of corrected ion velocity. Taken from ref. 185.

accelerated to ~1 keV before they strike it. The high signal amplititude may result in an improved signal-to-noise ratio by using higher discriminator threshold, thereby better detection efficiency for heavy and slow ions as observed by Danigel et al [144].

2.5.3 Ion Transmission

The instrument transmission is an important factor in determining the sensitivity of a mass spectrometer. A TOF mass spectrometer usually has high transmission since no slits are needed for mass analysis and also because of its simple open target geometry. In the reflecting TOF instrument, the number of secondary ions that reach the detector is partly determined by the angular spread of the beam resulting from the radial velocity distribution and the size of the detector, but also by the number and transparency of the grids used to define the electric fields.

For a spectrometer with a relatively short flight path, a 4 cm diameter detector may be large enough to cover most of the beam. For instance, for a flight path of 1.6 m >90% of secondary alanine ions at 10 keV will hit the 4 cm detector [131]. For Manitoba TOF II, the effective flight path is ~2.5 m, so some loss in beam intensity was found in early measurements. For a stable species, such as Na^+, the intensity is typically reduced by a factor of ~2 in the reflected spectrum (from the bottom detector) compared with the direct spectrum (from the top detector). The ions hitting the bottom detector have to go through one more 90% transmission grid in the electron converter than the ions hitting the top detector, but most of the ions lost are believed to be those which have too high a transverse velocity to hit the bottom detector after reflection. It is convenient to define two parameters here $E_r=mv_r^2/2$ and $E_z=mv_z^2/2$, where v_r and v_z are the radial and axial

velocity of an ion. For ions that are able to hit a detector, the maximum radial velocity they can have can be calculated from the simple formula $E_r=(r/L)^2E_z$, where r is the radius of the detector, L is the flight path. The bottom detector has a radius of 2 cm, for ions with E_z=10 keV, and generated in a 3 mm spot centred on the target to hit the detector, the maximum radial velocity they can have corresponds to $E_r\approx$0.55 eV. Assuming the ions ejected from the surface with a cosine angular distribution consistent with our observations [241], about 55% of the 1 eV ions and 28% of the 2 eV ions desorbed from surface are ejected into a detectable angle. An electrostatic lens was therefore inserted to reduce the ion loss due to the radial velocity distribution.

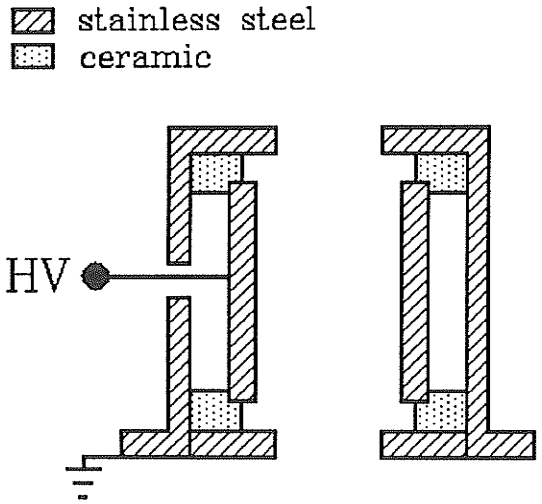

Figure 2.19 Cross section view of the three-electrode gridless Einzel lens.

The lens shown in Fig. 2.19 is a three-electrode gridless Einzel lens, with ground potential on the entry and exit sides and a high potential on the central electrode. The lens, with an overall length of ~4 cm, was mounted about 12 cm above the target on top of the secondary ion deflection plate assembly because this is a convenient place to insert it. Since the effective flight path to the bottom detector is ~2.5 m, the lens has a magnification of ~20, which is close to the ratio of the size of the detector (4 cm) to the size of the beam spot on the target (<3 mm). The lens has big apertures (12 mm diameter) on both sides; ions with E_z=10 keV will go through these apertures if they have E_r less than ~8 ev when the lens is "off" or less than 14 eV when

the lens is "on". Thus it will not block the beam. The voltage placed on the central electrode for optimum counting rate of the bottom detector is about one third of the ion acceleration voltage. The leaking field from these apertures was shielded to prevent the reflected beam from being deflected. The lens has been tested for transport of Cs^+ secondary ions from a CsI target. For 10 keV Cs^+ ions, the intensity in a reflected spectrum is ~59% of that in the direct spectrum without placing voltage on the lens; by turning on the lens, the intensity in the reflected spectrum increased to ~90% of that in the direct spectrum. This means that apart from the loss in passing through the grid there is no ion loss in the mirror, so the transmission of the mirror is close to the total grid transparency, i.e. ~80%. When both direct and reflected spectra were taken with the lens turned on, then the intensity in the reflected spectrum was 75% of that in the direct spectrum, which is very close to what is expected, so the lens seems to be working properly. When the lens was on, there was also an improvement of transmission to the top detector since the intensity in the direct spectrum without using the lens was ~82 % of that using the lens, this is probably because the radial velocity distribution of metal atomic ions such as Cs^+ is larger than that of organic molecular ions. Each spectrum was taken for a period during which the same amount of charge was accumulated on the slit of the ion gun, since the number of primary ions hitting the target is proportional to the number of primary ions hitting the slit. Thus the spectra were taken for the same primary ion dose on the target. The variations of the secondary Cs^+ ion intensity from spectrum to spectrum with the "same" primary ion dose were measured within 7% from the top detector.

2.6 DATA SYSTEM AND ELECTRONICS

The data system for time-of-flight measurements was developed in this laboratory and has been described in the literature [148,149]. A schematic diagram of the data system and related electronics is shown in Fig. 2.20. Here a clock signal with a frequency of up to 5 kHz provides a trigger signal for the ion gun and a "start" signal for the time-to-digital converter (TDC). A pulse is sent to the anode shield allowing the beam to be extracted for several microseconds. The bunch of primary ions extracted is then pulsed using the deflection plates A and B triggered by the delayed pulses to produce a ~2 ns ion burst for desorption. The corresponding "stop" signal comes from the detectors. The detector output pulse is amplified by a fast preamplifier and passed into a constant fraction discriminator; the NIM output pulse from the discriminator is then used as the "stop" pulse for a TDC. The TDC generates a digital measurement of the flight time of that ion or neutral and stores the number in a memory buffer. The TDC used is a LeCroy 4208 which has a common start and up to 8 separate stop inputs, a dead time between stops specified as 3 ns, and a time resolution of 1 ns. For daughter ion measurements, it is configured to use only 2 inputs, each of which can accept up to 4 stops for each start. Before the next start pulse arrives, i.e. within 250 μs for a typical frequency of 4 kHz, the numbers of the flight time are transferred to the front-end-processor (INCAA Capro 68k, a fast computer based on the Motorola MC 68000 chip). Various logical operations can then be carried out before the data are stored in one or more histograms in the 0.5 Mbyte memory of the Capro. The histograms of data are then transferred to the main computer where the histograms can be displayed, and stored permanently on disks. A DEC LSI 11/23 was initially used as the main controller computer, but it was subsequently replaced

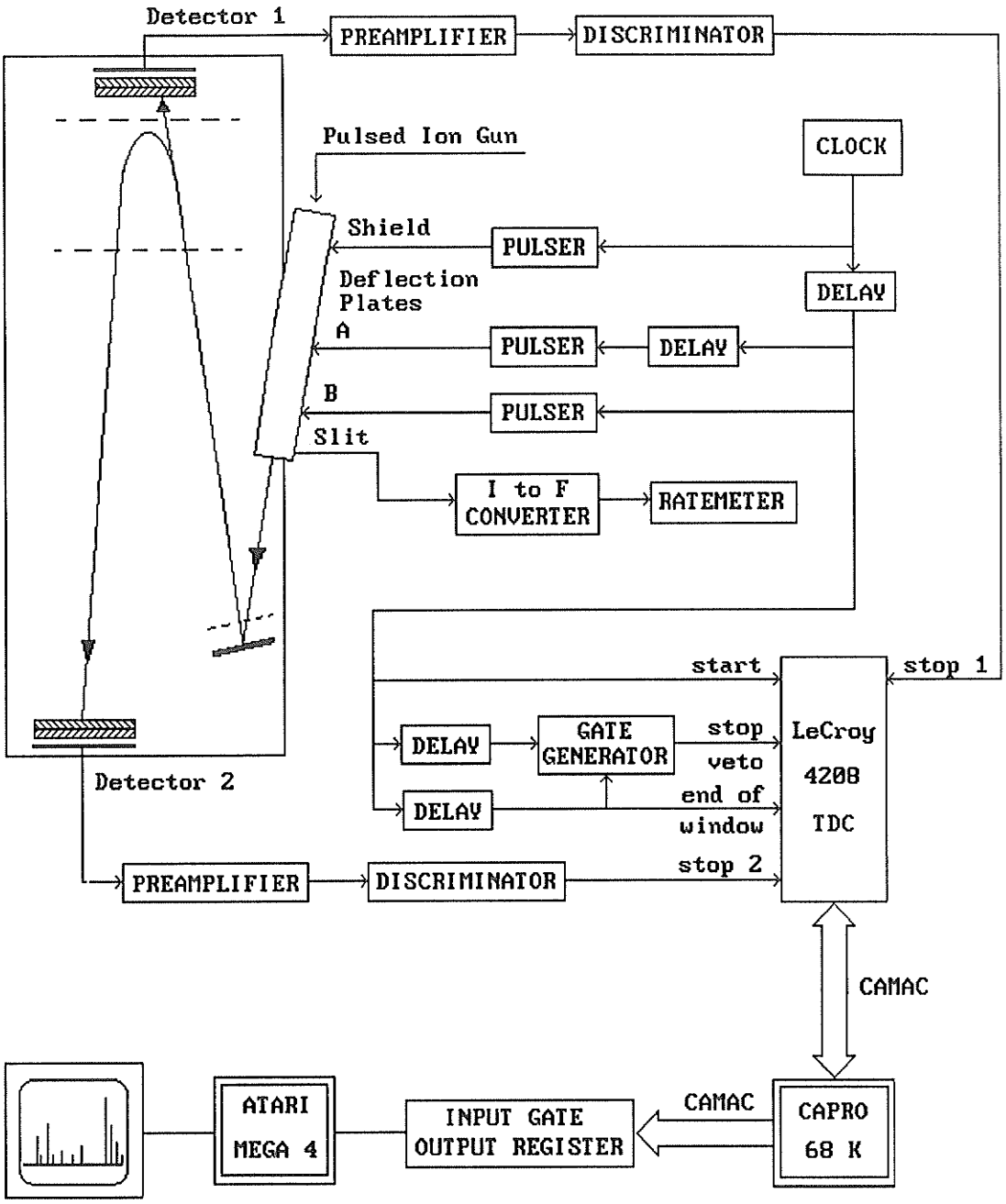

Figure 2.20 Schematic diagram of the electronic timing circuits and data system used for the reflecting TOF mass spectrometer.

by an Atari Mega 4 computer (based on a 68000 processor running at 8 MHz). The Atari Mega 4 has 4 Mbytes of directly addressable RAM, which can be important when handling large spectra. The Capro 68k CAMAC controller is then used to read the TDC and transfer the data to the Atari through a Kinetic System 3063 IGOR (input-gate output register).

With this data system, a maximum of 8 events can be recorded in each observation period, and spectra can be accumulated at a total counting rate up to ~20,000 counts/s; this corresponds to an average of 5 events per cycle at a repetition frequency of 4 kHz. This is not a serious limitation when the secondary ions are produced by low energy (keV) primary ion bombardment, as in our case, since very few such primary ions produce more than one secondary ion [186]. The primary beam has merely to be reduced to an intensity which produces an average of ≤5 secondary ion per primary pulse.

Although a hard-wired data system may be faster, the system described above has adequate speed for most of the applications. A major advantage is its control by software, which provides much greater flexibility than a hard-wired system. For example, it is fairly simple to introduce programs to search for correlations between particles within a given observation period (ca. ≤120 μs) or to measure the multiplicity (the number of secondary ions per individual primary ion). The Capro or Atari is fast enough to carry out these operations while the TDC is collecting data from the next period, so no time is wasted.

During data acquisition, preliminary analysis such as rough mass calibration and simple intergrals between selected points, may be performed; when sufficient data have been collected, whole or any portion of a spectrum, with a selected bin width may be saved onto a disk for permanent storage. The data analysis program provides more detailed analysis of the stored spectra. For example, peak centroids can now be calculated

to yield more accurate flight times of the ions and give better mass calibration; background may be subtracted from a selected part of the spectrum to improve the accuracy of the centroid calculation or for display purposes, or spectra subtraction can be performed to yield a difference spectrum which is useful particularly in the analysis of correlated spectra or daughter ion spectra.

In the last year, a new data system using an Orsay TDC (which has 256 stop inputs and 0.5 ns time resolution) and Atari Mega 4 computer was assembled in our laboratory. This new data system can accommodate a relatively large number of secondary ions per pulse and has better precision for time measurements. It has been used for laser desorption experiments performed on the linear instrument and for sequencing an "unknown" peptide using the reflecting instrument. Apart from the "unknown" peptide spectrum, all the data reported here were obtained from the reflecting instrument using the data system with the LeCroy 4208 TDC.

CHAPTER 3

PERFORMANCE

3.1 MASS RANGE

In other types of mass spectrometer, measurement of high mass ions may be difficult or expensive. In contrast, TOF measurements simply require a timer of sufficiently large range, e.g. ~100 μs for a 10 keV ion of mass 20,000 u in an instrument with a flight path of 1 m. In principle, a TOF mass analyzer has unlimited mass range; the practical upper mass limit of a TOF mass spectrometer is determined by the efficiency of the desorption method and the detection efficiency of the detector. Fig. 3.1 shows the spectrum of CsI, which illustrate the mass range of the reflecting instrument for this inorganic compound. The CsI spectrum was taken with 12.5 kV acceleration voltage, 1 kV post acceleration on the bottom detector, 12.5 keV primary ion energy and with 196 μs time window and 4 ns bin width. The CsI thin film was coated on a metal substrate by vacuum evaporation, and the target was irradiated with a ~6 nA dc primary ion beam for ~5 min before taking the spectrum. The irradiation was used here because it increased the abundance of CsI cluster ions in the spectrum [131]. In Fig. 3.1, the peaks labelled n include both the nth parent cluster ions and daughter cluster ions; the daughter ions are

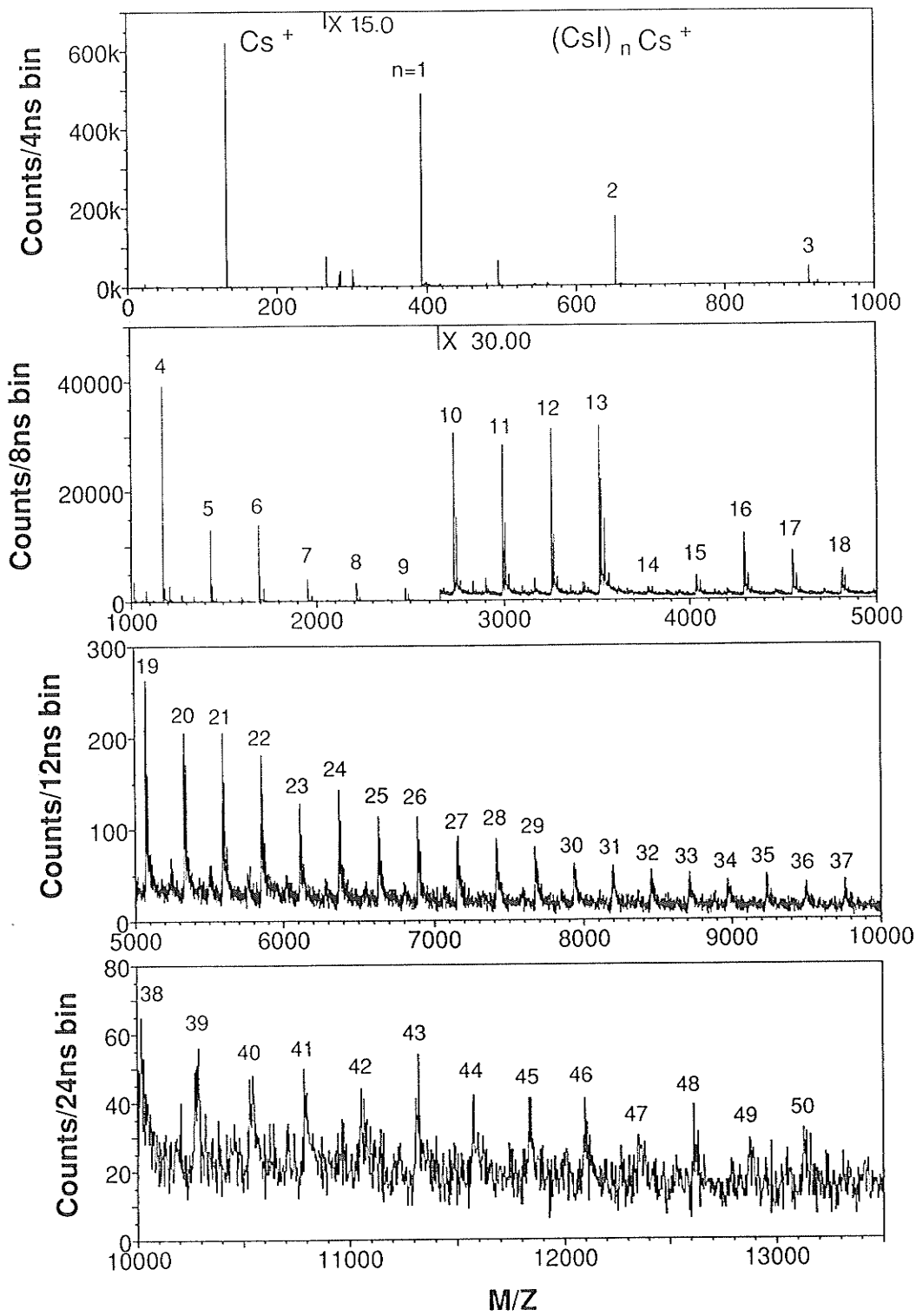

Figure 3.1 Reflected time-of-flight mass spectrum of positive CsI cluster ions $(CsI)_nCs^+$, the group of peaks under the label n, includes both nth parent and daughter cluster ions, see §5.2 for detail.

from metastable decomposition of the clusters of higher mass, e.g. from n+1, or n+2 parent cluster ions. More about the metastable decays of CsI cluster ions will be discussed in Chapter 5. Fig. 3.1 indicates that CsI cluster ions up to n=50 have been produced and detected, or an upper mass limit of above 13,000 is achieved under the experimental conditions.

For organic compounds, the ionization efficiency depends not only on the properties of the primary ion, but also strongly on the sample preparation. Using nitrocellulose (NC) substrate to adsorb sample molecules, the mass range of organic compounds by low energy ion bombardment was extended to ~10,000 u [97,138,173]. As an example of the high mass organic compounds analyzed here, Fig. 3.2 shows the reflected spectrum of bovine insulin with mass 5733 u. The sample was dissolved in 0.1%

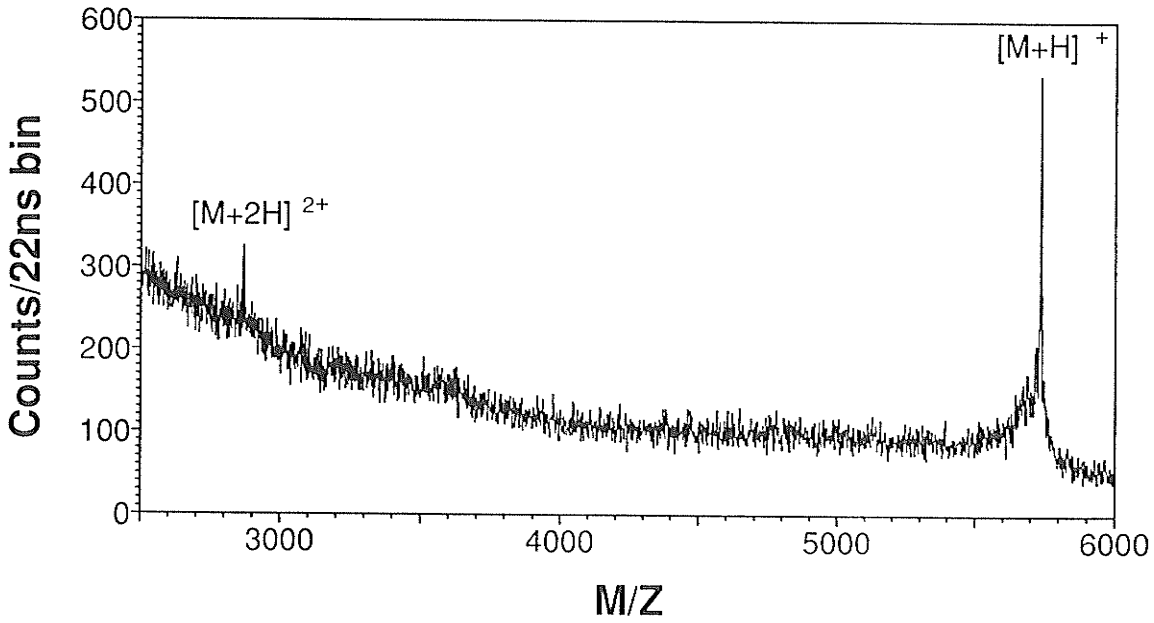

Figure 3.2 Reflected positive ion spectrum from bovine insulin (5733 u) deposited on a nitrocellulose substrate, produced by bombardment with 12.5 keV Cs^+ ions.

TFA, and a few μL of 1μg/μL sample solution was deposited on NC substrate that was electrosprayed on a metallic backing. The spectrum was taken with the same primary ion and secondary ion energy as in the CsI spectrum shown above. Since the detection efficiency falls off rapidly for large and slow ions, e.g. the detection efficiency is only ~0.2 for 13 keV bovine insulin ions [185], using higher acceleration and post acceleration voltages is desirable for improving the detection efficiency of these large molecules. However, the current mass range seems limited largely by the efficiency of desorption by the Cs^+ ions used. As discussed in chapter 1, the mass range of a TOF spectrometer can be extended significantly by using more efficient desorption methods such as the recently emerged matrix-assisted laser desorption.

3.2 BACKGROUND

The detection of the metastable decay products in the flight tube of a linear TOF mass spectrometer may increase the parent ion detection efficiency and enable measurement on a short time scale. However, the signal-to-background ratio and the resolution deteriorate due to the increasing background resulting from metastable decomposition. The background in Manitoba TOF I, the linear instrument, is mainly caused by metastable decomposition of parent ions during acceleration and in free flight since the background due to the primary ion leakage can be largely reduced by using pulsed extraction [131]. As in the linear instrument, the main background in the reflecting instrument is also caused by metastable decomposition but it is reduced considerably compared with background in the linear instrument. Neutral fragments from unimolecular

decay before reflection will go through the mirror since they are not affected by the electric field in the mirror, while charged fragments are moved to a lower mass spectral region away from the parent ion since they have less energy and therefore spend less time than their parents in the mirror. Thus sharp peaks arising from undissociated ions may be observed with less of the underlying broad distribution caused by metastable decay. Thus, the ion mirror not only improves the resolution but also increases the signal-to-background ratio of a mass spectrum.

Fig. 3.3 shows an example of the reduction of background in reflected spectrum

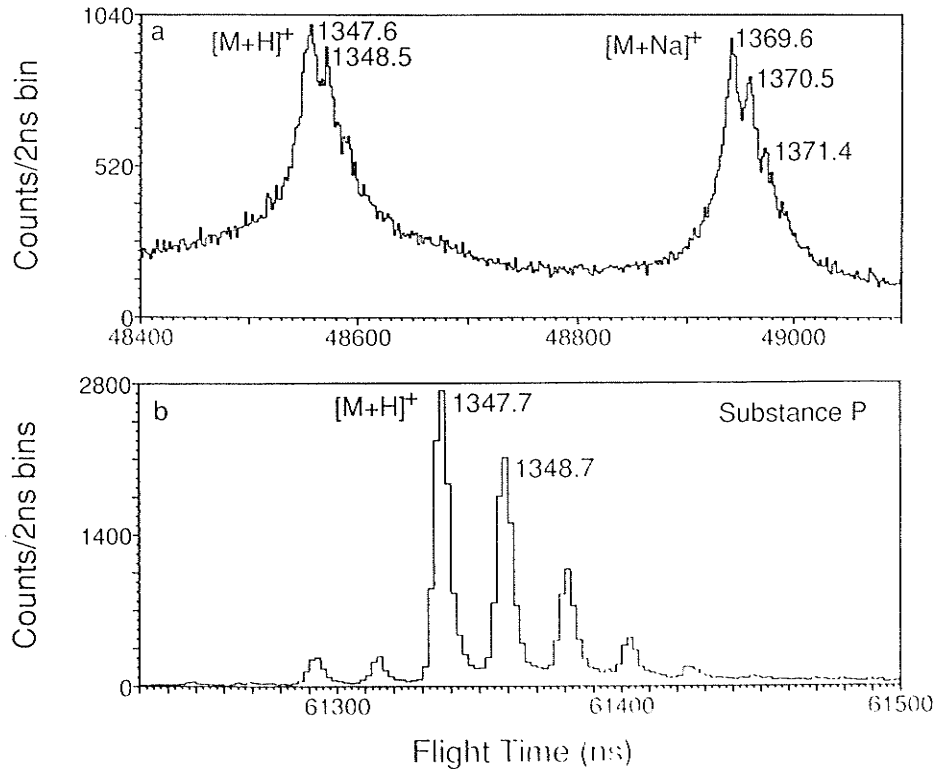

Figure 3.3 TOF spectra of the peptide substance P: (a) with the linear spectrometer (electrospray), showing the $[M+H]^+$ and $[M+Na]^+$ ions, and (b) with the reflecting spectrometer (NC substrate), showing only the $[M+H]^+$ isotopic distribution; in (b) the scale is expanded, so $[M+Na]^+$ ions are outside the range of the figure.

of substance P compared with the spectrum of the same compound taken by the linear instrument. The improvements in signal-to-background can also be seen in the spectra of larger molecules, Fig. 3.4(a) & (b) show the molecular ion region of the direct and reflected spectra of ACTH 1-17 and bovine insulin. Clearly, the backgrounds due to metastable decay are reduced considerably in all cases, and sharp or well resolved molecular ion peaks can be seen only in the reflected spectra.

3.3 MASS RESOLUTION

The flight time in a reflecting time-of-flight mass spectrometer is proportional to $\sqrt{m/q}$ as in a linear TOF instrument. The flight time for an ion desorbed with zero initial velocity is

$$t=\frac{2(L+2d)}{\sqrt{2U_0}}\sqrt{\frac{m}{q}} \tag{3-1}$$

so the mass resolution is related to time resolution by

$$\frac{\Delta m}{m}=\frac{2\Delta t}{t} \tag{3-2}$$

Generally, ions are desorbed with an initial energy distribution. Under the normal mirror voltage setting, i.e. if the mirror voltage is chosen according to Eq. (2-17), the time spread produced after acceleration due to the initial energy distribution is compensated by the mirror, but the time spread in the acceleration gap will contribute to the peak width Δt. As discussed in §2.2, the time spread induced in the acceleration region can also be reduced by setting the mirror voltage to a lower value than that specified in Eq. (2-17).

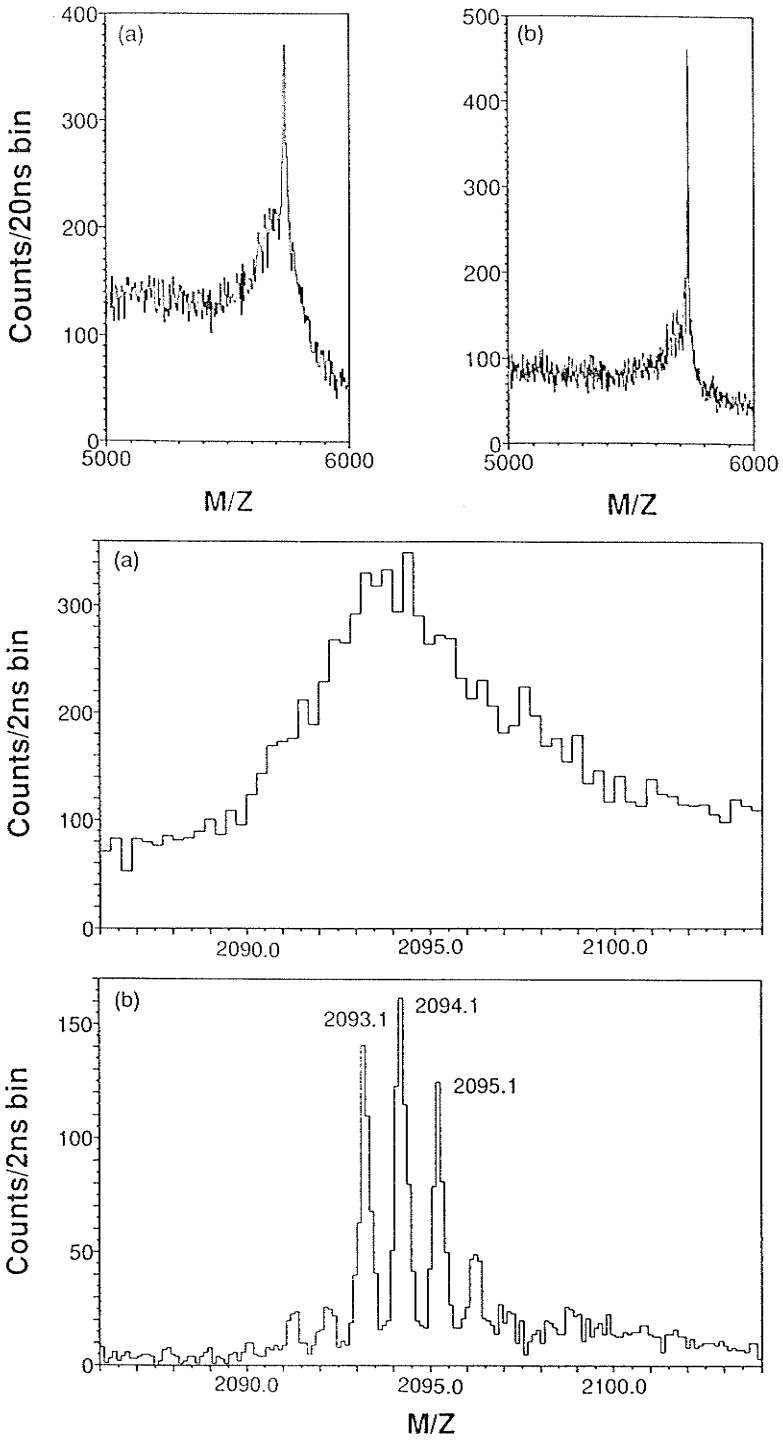

Figure 3.4 Molecular ion regions of positive ion spectra from bovine insulin (5733 u) and ACTH 1-17, deposited on a nitrocellulose substrate, produced by bombardment with 12.5 keV Cs^+ ions. (a) Direct spectra measured in the upper detector with the mirror off; (b) the reflected spectra observed in the lower detector.

however, there are other factors contributing to the peak width and limit the mass resolution, some of these factors are discussed below.

3.3.1 Factors Affecting the Resolution

For high resolution measurements, electric and mechanical tolerances are obviously tighter than at low resolution. The parameters of the spectrometer must remain constant in time, at least for the duration of an individual measurement. They must also be constant over the region traversed by the charged particles. In our case, this region has a diameter of ≤3 mm at the target (the size of the primary ion beam spot) and ≤4 cm at the detector (its diameter), so the region is ≤2 cm in diameter at the back of the mirror. Errors from various sources will combine, but an idea of the required tolerances may be obtained by calculating the errors in various parameters which individually give a mass error, Δm, such that $\Delta m/m=10^{-4}$ (i.e. mass resolving power $m/\Delta m$=10,000). Since $\Delta m/m=2\Delta v/v=2\Delta t/t$, this corresponds to a timing error, Δt, such that $\Delta t/t=5\times10^{-5}$. Some of the sources of error can be listed as follows:

3.3.1.1 Sources of initial time spread

In §2.2, for convenience and clarity, we have calculated the behaviour of the secondary ions *after* they leave the reference plane (after acceleration) and the corrections if the acceleration region is included. From this point of view, the time and velocity spreads of the ion distribution on the reference (object) plane can be taken as the initial conditions for the analysis. Under the normal mirror voltage setting, the velocity spread

is compensated by the mirror, but the time spread will appear also at the detector; it has several causes.

a). A time spread approximately independent of mass is caused by the finite duration of the primary beam pulse at the target, transit time variations in the detection electronics, and the finite resolution (1 ns) of the time digitizer and data system. An upper limit on these effects is provided by the width of the peak corresponding to secondary electrons ejected from the target by the primary beam pulse; transit time spreads within the spectrometer are not very large for the electrons because of their high velocity. Fig. 3.5 shows the electron peak, which has a width of ~2 ns. For this width and an accelerating voltage of 10 kV, the

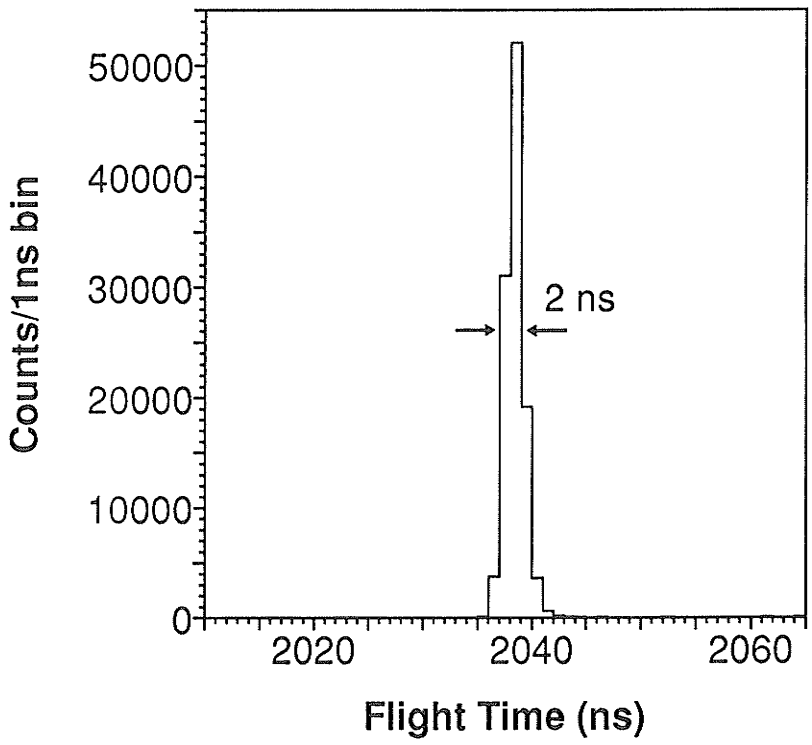

Figure 3.5 Peak due to secondary electrons ejected from the target by the primary ion pulse, as observed in the reflecting TOF spectrometer (top detector).

suggested tolerance is attained for masses ≥493 u and the spread becomes progressively less important as the mass increases. High-resolution measurements for light ions would require a decrease in the accelerating voltage (although this would make the energy spread more important).

b). A time spread at the reference (object) plane stems from the finite angle (1.43°) between it and the target. Since the beam spot is ≤3 mm in diameter, the spread in path length is ≤3(sin1.43°)≈0.075 mm. For a total spectrometer path length of 2.5 m, $\Delta t/t \leq 3(\sin 1.43°)/2500 \approx 3\times10^{-5}$. This is acceptable, but for cases where the beam spot must be larger (e.g. for fission fragment bombardment), it may be worthwhile to go to the Orsay geometry [145-147] where the angle θ=0°.

c). An additional time spread is introduced due to the initial energy distribution as the ion traverses the ~4 mm distance between the target and the object plane during acceleration. These are not well compensated by the mirror if its field is determined by Eq. (2-17) with $k=U_{i0}/U_0$, where U_{i0} is the average or peak value of initial energy distribution. In organic and cluster SIMS application, the initial energy distributions (FWHM) usually fall into a range between about 0.25 to 2.25 eV [160]. The worst case corresponds to an initial energy distribution of 1.25±1 eV; the corresponding time spread it produced can be calculated from Eq. 5 to 7 in Appendix A (as has been shown in Fig. 2.7), and this gives an over all (across 2.5 m effective flight path) time spread $\Delta t/t$ of ~4.4×10^{-5} for 5 kV acceleration voltage or ~3.1×10^{-5} for 10 kV acceleration voltage. These values are still acceptable, but in the case where the initial energy distribution is large, the mirror field may be reduced to obtain more compensation for the additional time spread induced in the acceleration region as discussed in §2.2.3.2.

3.3.1.2 The requirement of the electric and mechanical tolerances

a). Under normal mirror voltage setting, the stability of the accelerating voltage, V, is not critical because the mirror corrects for such variations to first order. The required stability can be calculated from Eq. 2 to 4 in Appendix A, or can be estimated from Eq. (2-4), $\Delta t/t=5\times10^{-5}$ corresponds to $(\delta/v_0)^2\approx10^{-4}$, so $(\Delta V)/V\leq0.02$, a rather trivial requirement.

b). The required stability of the mirror voltage, V_m, is much more difficult to attain; here the proposed tolerance corresponds to $\Delta V_m/V_m\leq10^{-4}$, a restriction both on stability during the whole period of measurement and on short-term fluctuations (i.e. ripple). However, power supplies that meet these specifications for stability and ripple are available commercially.

c). In our mirror, As remarked above, the region traversed by ions which can enter the detector has a diameter ≤2 cm at the back of the mirror, ≤6 cm at the front. It is therefore important to keep the field sufficiently uniform in this region. From the analysis in §2.2.4, the variation of the field in the region is only $\Delta E_z/E_z\approx8.2\times10^{-7}$, much better than the valued required to maintain the specified tolerance.

d). There may also be variations in the electric field within the mirror caused by mechanical defects. To maintain the suggested tolerance, the electric field should be constant to 1 part in 10^4. Thus, the front and back plates of the mirror (~35 cm apart) should be flat and parallel to $350/10^4$=0.035 mm over the 2 cm diameter of the sensitive region.

e). The face of the charged particle detector must be plane and perpendicular to

the *spectrometer axis* to keep L_2 constant (see Fig. 2.3). In our case, the detector has a diameter of 4 cm, so the suggested tolerance requires the angle, α, between the spectrometer axis and the normal to the detector to be limited to a value given by $40(\sin \alpha)/2500=5\times10^{-5}$, or $\alpha\leq0.18°$. To allow for small mechanical errors, the bottom detector in the reflecting instrument can be aligned by three micrometer screws.

As discussed in section 2.5.1, the channels in the chevron microchannel electron multiplies used for detectors gives a spread in L_2 because some particles hit the electron-emitting surface near the channel entrance and others farther in. For a channel angle of 5° and a channel diameter 15 μm, the resulting spread in path length is $\Delta L_2\approx170$ μm, given $\Delta t/t\approx9\times10^{-5}$. It appeared that this effect might be a significant limitation on the resolution, so a electron convertor detector has been used to eliminate this spread. Since the secondary ions only hit the conversion dynode surface which is flat, and the resulting electrons are accelerated to a much higher velocity compared with the incident ions and transported isochronously to the chevron microchannel electron multipliers, the effect is no longer significant.

3.3.1.3 Effect of the grids

In the simple linear TOF instrument, the axial velocity of the ion may be changed by scattering from the accelerating grid, thus producing a spread in flight time [187,188]. In a reflecting instrument, however, the mirror compensates the velocity spread which

exists at the reference plane *after* deflection by this grid and small changes in velocity before that have little effect [see Sect. 1(c) above]. Therefore, the mirror corrects for the effects of scattering from the accelerating grid.

On the other hand, the mirror is unable to compensate for scattering from its own entrance grid when the ion enters or leaves. Expressions have been derived for the scattering from grids in electrostatic lenses [189-191] and for plane parallel geometry [191]. In the latter case, the maximum scattering angle, μ_{max}, for paraxial rays is given by Verster [191].

$$\tan\mu_{max} \approx \frac{D(\overline{E}_2 - \overline{E}_1)}{8V}$$

assuming $D(\overline{E}_2 - \overline{E}_1) \ll V$ and grid wires of zero radius, where D is the spacing between grid wires; $\overline{E}_1$ *and* $\overline{E}_2$ are the average electric fields above and below the grid.

Verster has also reported calculations of actual ion trajectories using a ray tracer (analogue computer) [191]. Electrostatic field values were obtained from electrolytic tank measurements on grids with wires of various radii. Within the square aperture between adjacent grid wires, the scattering is ≤30% higher than the paraxial result near the mid-points of the sides and ≤30% lower than the paraxial result near the corners. Thus, it appears that the paraxial expression is a fairly good approximation.

In our reflecting spectrometer, $D \approx 0.36$ mm, $\overline{E}_2 = 0$, and $\overline{E}_1 \approx 10/350$ kV mm^{-1} for V=10kV. The maximum scattering angle for paraxial rays from the equation above is $\mu_{max} \approx 0.0074°$. The corresponding change in average velocity, Δv_z, is given by $\Delta v_z/v_z \approx \mu_{max}\sin\mu_{max} \approx 1.7\times10^{-8}$, so the effect is not significant in our case. The grid does, however, produce some loss in intensity; since its transmission is 90% and the ion pass through it twice the net transmission is ~80%.

3.3.2 Experimental Results

3.3.2.1 Performance of the mirror.

In order to compare the properties of the mirror with the predictions of Eqs. (2-15)-(2-18) and Eq. 2 to 4 in appendix A, a variation in velocity v_z has been produced by changing the accelerating voltage V, while keeping the mirror voltage fixed. Fig. 3.6 shows a comparison between the experimental measurements of Cs^+ peak and the flight time variations calculated from Eq. 2 to 4 in appendix A. Since the exact average initial energy of the Cs^+ ions under our condition is not known, a zero average initial energy is

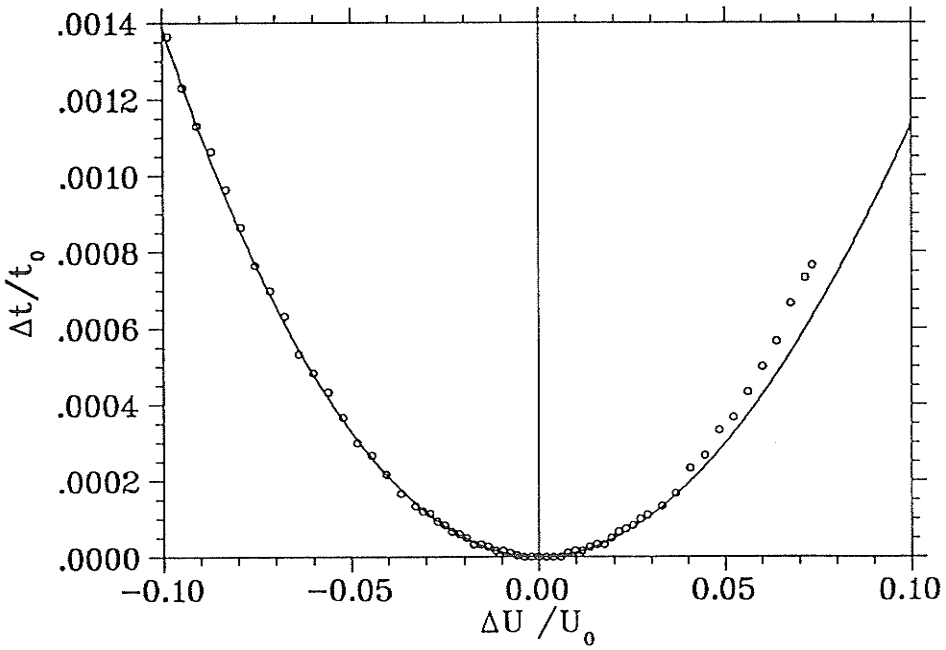

Figure 3.6 Time variations, $\Delta t/t$, as the accelerating voltage, $V=U/cos^2\theta$ is varied about its optimum position ($V_0 \approx 5$ kV). The solid line is calculated from Eq. (2-17) with $U_i=0$, and the circles is from the experimental data.

assumed in the calculations. This should be a very good approximation since the average Cs^+ ion initial energy is expected to be a very small percentage ($\ll$1%) of the total ion kinetic energy (~5 keV) in the experiment, as remarked in §2.2.3.1, the effect of the initial energy is negligible in this case. Although there are some deviations for large values of $\Delta U/U_0$, or $\Delta V/V_0$, the overall agreement is good. The practical range of voltage variation is much smaller than the total variation shown in Fig. 3.6. For example, a ±80 V changes in accelerating voltage from optimum ~5 kV, produced time variation of only 1 ns from the minimum of ~30000 ns or $(\Delta t/t)=3.33\times10^{-5}$, which is in good agreement with the calculated value of 3.16 or 3.25×10^{-5} for corresponding +1.6% or -1.6% variations in accelerating voltage. Thus, the mirror appears to be working properly. The deviations appeared at larger accelerating voltages ($\Delta U/U_0>0.04$) indicate the electric field at the end of the mirror is weaker than it supposed to be, This is probably due to the mechanical defects of the mirror in that region, such as the accuracy (thickness) of the rings and position of the end grid.

3.3.2.2 Operation under the reduced mirror voltage.

The performance of the mirror under the normal mirror voltage setting has been described above. In §2.2.3.2, we have also discussed the effect of the acceleration region and the time spread in the case of an ion initial energy distribution. As pointed out there, a possible solution for reducing the time spread is to reduce the mirror voltage from the normal setting specified by Eq. (2-17). The predicted behaviour and the practical solution are depicted in Fig. 2.7 and 2.8, these have also been observed in the experiments. When the accelerating voltage is at the optimum value (minimum flight time in Fig. 3.6) of ~5

kV, the Cs^+ peak is wider than the $(CsI)_2Cs^+$ peak although the flight time of the Cs^+ peak is only about half of the $(CsI)_2Cs^+$ peak. The Cs^+ peak became narrower while the $(CsI)_2Cs^+$ peak width (Fig. 3.8) remained about the same as the accelerating voltage was increased above the optimum value. The Cs^+ peak width was reduced by ~1 ns when the accelerating voltage exceeded the optimum by 500 V. Fig. 3.7(a) and (b) shows the Cs^+ peaks taken at optimum accelerating voltage and 500 V above the optimum respectively. The mirror voltage corresponded to the normal setting for 5 kV accelerating voltage and was kept the same in the experiment. These observations are consistent with the predictions. Under the normal mirror voltage setting [Eq. (2-17)], the time spread induced in the acceleration region is not compensated by the mirror, as a result, the total time spread of an ion packet at the detector is still dependent on the ion initial energy

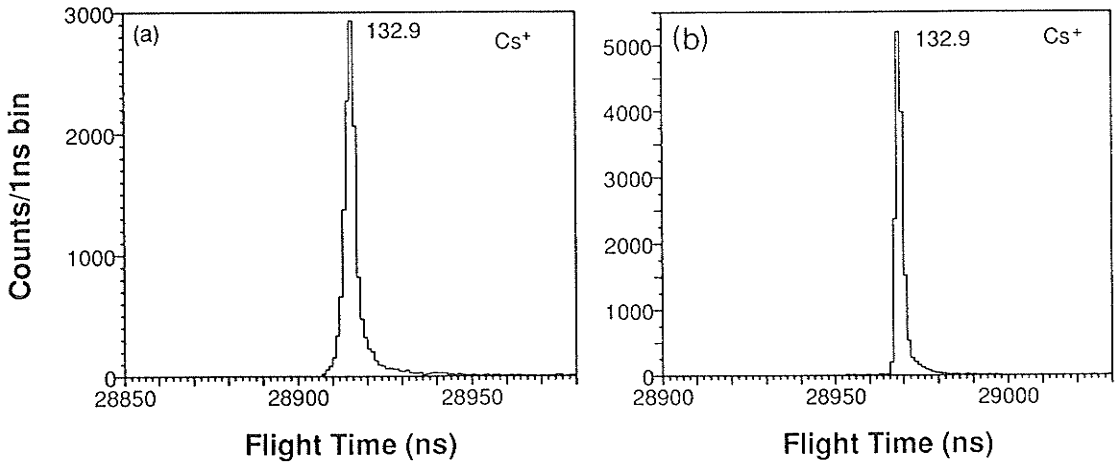

Figure 3.7 Cs^+ peaks from the positive reflected spectra of CsI. (a) The spectrum recorded at optimum accelerating voltage ($V_0 \approx 5$ kV, the minimum in Fig. 3.6), and normal mirror voltage setting determined by Eq. (2-17). (b) The spectrum recorded at an accelerating voltage ~10% higher than that in (a) (i.e. equivalent to a reduction in mirror voltage by ~9%).

distribution. The time spread is larger for ions with a larger energy spread and a lower average initial energy, i.e. a larger relative energy spread $\Delta U_i/U_{i0}$, as depicted in Fig. 2.7. The experimental results under the normal mirror voltage setting suggested that Cs^+ ions may have larger relative initial energy spread than the second cluster ions. When the accelerating voltage is increased by ~10% above the optimum value, this is equivalent to the reduction of the mirror voltage by ~9% (the mirror was longer than the minimum length required) from the focusing value required for the new accelerating voltage as specified by Eq. (2-17). As depicted in Fig. 2.8, under the reduced mirror field, the mirror can provide more compensation for the time spread induced in the acceleration region for a given initial energy distribution. Thus the time spread of the Cs^+ is reduced. For the second cluster ions, probably the relative initial energy spread is small and the time spread in the acceleration region is not significant even under the normal mirror voltage setting, as a result, its peak width remained about same when the acceleration voltage increases. So a single stage mirror may also accommodate larger relative initial energy spread providing the mirror is operated under the reduced field. The optimum reduction in mirror field would however be different for an ion with a different energy distribution.

3.3.2.3 Resolution for inorganic compounds

A mass resolving power $M/\Delta M_{FWHM} \approx 13{,}000$ (Fig. 3.8) is achieved with this reflecting TOF mass spectrometer. Thus, the resolution is improved by more than a factor of 4 compared with the linear spectrometer. The measured resolution (FWHM) of $(CsI)_2Cs^+$ at m/z 652.5 with accelerating voltage $V \approx 5$ kV, and normal mirror voltage setting, is ≈1/13,000, see Fig. 3.8(a), which is very close to what is expected through the

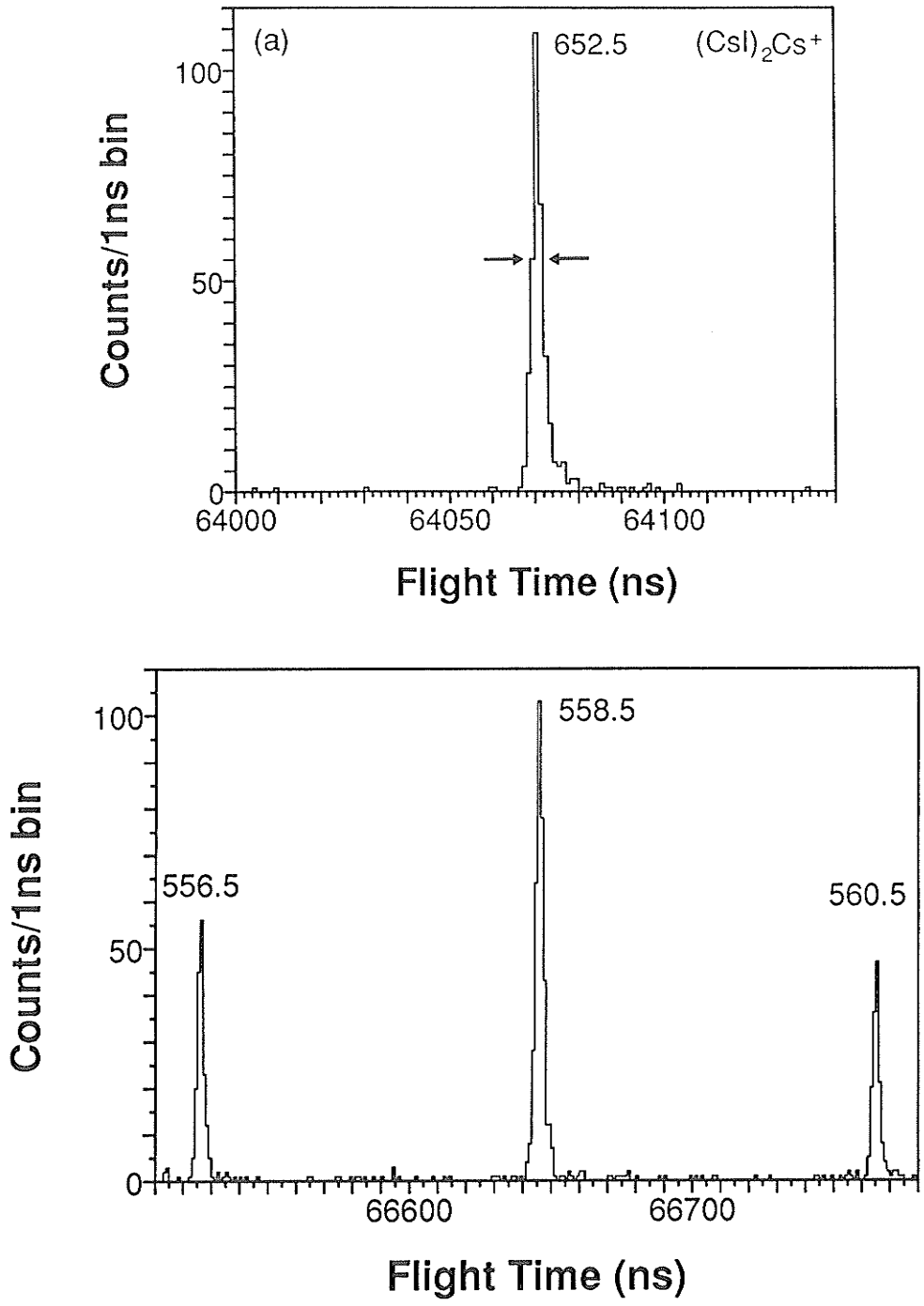

Figure 3.8 Positive ion TOF spectra observed in the reflecting mass spectrometer (Manitoba TOF II). Primary ion energy ~18 keV, secondary accelerating voltage ~5 kV. (a) The second cluster ion $(CsI)_2Cs^+$ in the spectrum of CsI. $\Delta t_{FWHM}/t \approx 1/26000$ so $m/\Delta m_{FWHM} \approx 13000$. (b) The distribution of isotopic peaks of the second cluster ions $(CsBr)_2Cs^+$ in the spectrum of CsBr.

analysis in §3.2.1. The resolution obtained here is also similar to what has been reported on a two-stage mirror TOF-SIMS instrument [120], and again, we note that the two-stage mirror is unnecessary under our conditions. For further improvement in resolution, the time spreads and the residual defects in the spectrometer, such as those discussed in §3.4.1 become important, and have to be reduced in order to obtain even higher resolution. A resolving power of $m/\Delta m_{FWHM} \approx 13{,}000$ can thus be obtained with a *single* stage mirror, providing the ion optical source is sufficiently well defined in position.

Fig. 3.8(b) shows good separation of the triplet of molecular ion region of $(CsBr)_2Cs^+$ at mass ~558.5, resolution similar to that shown in Fig. 3.8(a) is obtained.

3.3.2.4 Resolution for organic compounds

Fig. 3.9 shows the sample spectra in the molecular ion region of γ-endorphin and mellitin obtained with nitrocellulose substrate; a mass resolving power of 7000 is achieved for the molecular ion peaks from γ-endorphin. The resolution obtained for big peptide molecules is not as good as inorganic molecules. This may be partly because some of the peptide molecules have relatively long lifetime and they may decay in the second field free path after being reflected. This will result in peak broadening due to the energy release during the metastable decompositions. Some of the peak broadening may also be due to uncompensated time spread arising in the acceleration region if the large organic molecular ions have larger relative initial energy spread than the inorganic molecular ions. Nevertheless, clearly separated isotopic peaks are obtained for peptides of mass up to several thousands mass unit with our reflecting instrument. A mass resolution of 7000 should be good enough to separate the isotopic peaks of even larger

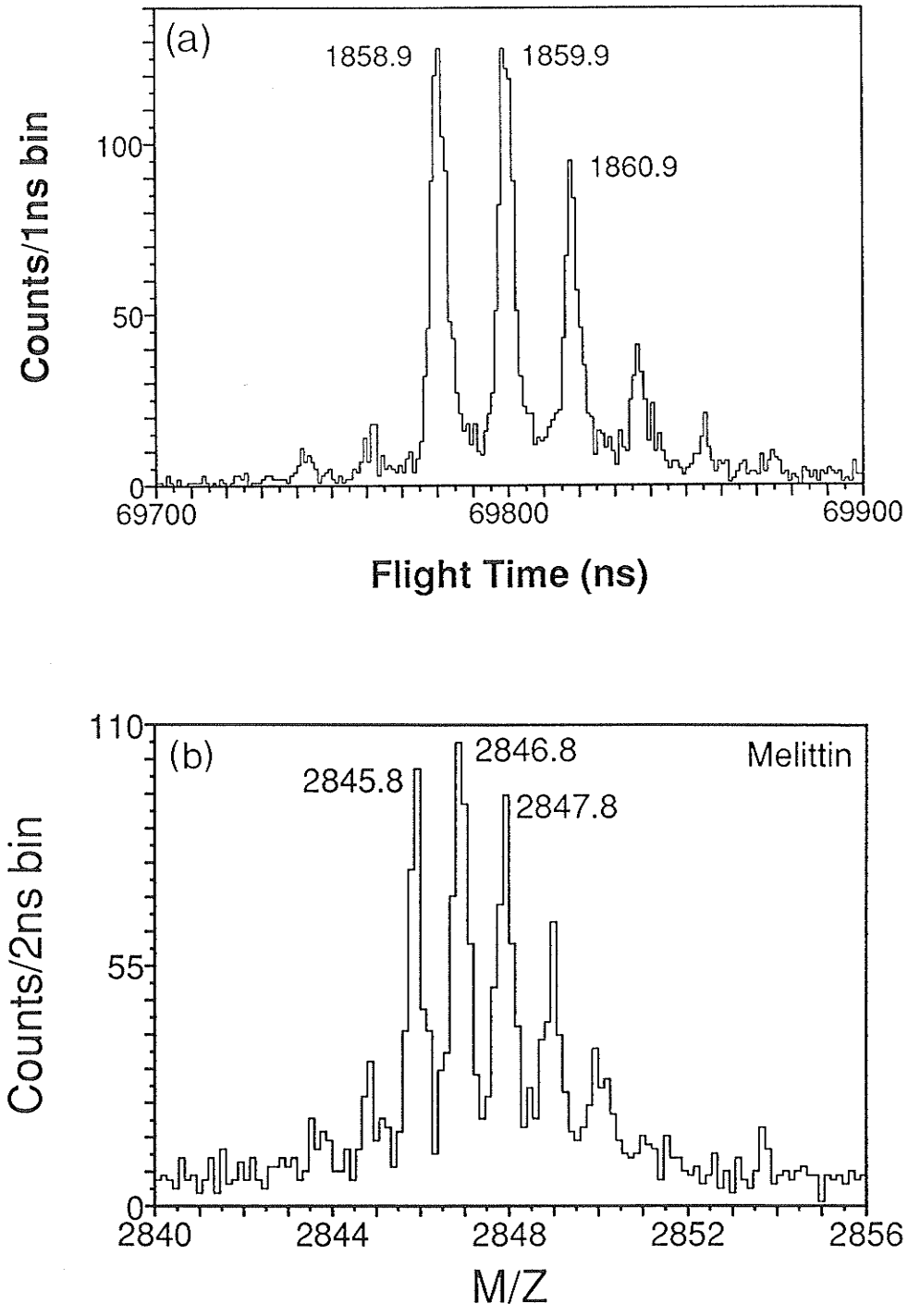

Figure 3.9 Reflected mass spectra of the $[M+H]^+$ ions from the peptides. (a) γ-endorphin ($m/z \approx 1859$), $m/\Delta m_{FWHM} = t/2\Delta t_{FWHM} \approx 7000$. (b) melittin ($m/z \approx 2846$).

organic molecular ions such as bovine insulin (MW=5733), but the difficulty encountered in the experiment is that under the static SIMS condition, as the mass of sample molecules increases, the molecular ion yield is too low to obtain reasonable statistics in a reasonable period of time (ca few hours), and the peak broadening due to metastable decompositions after reflection becomes progressively more serious as it can be seen from Fig. 3.9.

3.4 MASS CALIBRATION

Mass accuracy is important in the mass spectrometric method. An accurate mass determination can ease the peak assignment and help interpretation of the spectra considerably. In many applications, an accurate mass determination (±0.1 u) is required to derive or confirm the composition of a molecular ion such as in sequencing of a peptide molecule.

Since the flight time is proportional to $\sqrt{m/q}$ in a TOF instrument, there is a simple relation between mass and apparent flight time

$$t=c\sqrt{m/q}+t_0 \tag{3-3}$$

where c is a constant if the ion mean initial energy is the same for all species or independent of mass, and t_0 is a constant time difference between the time zero of the TDC and the time that ions take off the target. In our case, the TDC "start" signal is the same as the ion gun deflection plate trigger signal, so the t_0 here is the time of the primary ions spent in travel between the deflection plates and the target. The mass can

be calculated from the flight time by

$$m/q=c'(t-t_0)^2 \tag{3-4}$$

because of the simultaneous detection of all masses in a TOF mass spectrometer, peaks with known masses in a spectrum can be used for mass calibration, i.e. to determine the two parameters c' and t_0. therefore, the calibration procedure is simpler compared with that in conventional mass spectrometers, no special calibration standards and peak matching methods are necessary.

Normally, the mean initial energy distribution is not the same for all species and masses, The corresponding time deviations can be quite large in a linear TOF instrument. This is often the major source of error in mass determination. In the reflecting instrument, the time deviation due to difference in initial energy distribution has been reduced significantly by velocity focusing, resulting in a better mass determination accuracy.

In practice, usually two peaks in low mass region are selected as calibration peaks. These include hydrocarbon molecular ions and atomic ions such as H^+, CH_3^+, $C_3H_3^+$, $C_4H_9^+$, Na^+ etc., because these peaks are present in almost any positive SIMS spectrum, and can be identified easily.

The accuracy of mass determination was evaluated for a number of peptides and CsI spectra up to mass ~3000 u. Most of the peptide samples were prepared with the nitrocellulose substrate, and the spectra were taken under the normal mirror voltage setting with a 2ns time bin width. For each peptide, the mass of the $[M+H]^+$ ions in 5 spectra of independent preparations were obtained by calibrating the spectra with low mass ions H^+, CH_3^+, $C_3H_3^+$, and Na^+; $C_4H_9^+$ peak was not used in the calibrations because of interferences from ions with very close mass from the nitrocellulose substrate. The

TABLE 3.1 Mass Deviations $\Delta m = m_{exptl} - m_{calcd}$ Obtained for $[M+H]^+$ ions of Peptides from 5 Independent Measurements

		Calibration ions			
Sample		H^+, $C_3H_3^+$	H^+, Na^+	CH_3^+, $C_3H_3^+$	Na^+, $C_3H_3^+$
Bradykinin	1	0.012	-0.951	0.224	2.085
$C_{50}H_{74}N_{15}O_{11}$	2	0.035	-0.571	0.176	1.368
$[M+H]^+$	Δm 3	0.049	-0.248	0.234	0.719
1060.569	4	0.024	-0.786	0.233	1.881
	5	0.016	-0.071	0.240	0.245
$<\Delta m>\pm\sigma_{n-1}$		0.027±0.015	-0.525±0.366	0.221±0.026	1.260±0.775
$(<\Delta m>\pm\sigma_{n-1})/m$		25.4±14.1 ppm	-495±345 ppm	208±24.5 ppm	1188±731ppm
Substance P	1	-0.050	-0.327	0.355	0.684
$C_{63}H_{99}N_{18}O_{13}S$	2	-0.003	-0.426	0.215	0.618
$[M+H]^+$	Δm 3	0.082	-0.439	0.313	1.015
1347.734	[a]4	0.047	-0.354	0.247	1.029
	[a,b]5	-0.071	-0.548	-0.165	1.102
$<\Delta m>\pm\sigma_{n-1}$		0.001±0.064	-0.425±0.077	0.193±0.207	0.890±0.226
$(<\Delta m>\pm\sigma_{n-1})/m$		0.7±47.4 ppm	-315±57.1 ppm	143±154 ppm	660±168 ppm
γ-endorphin	1	-0.040	-0.705	0.361	1.570
$C_{83}H_{131}N_{19}O_{27}S$	2	-0.016	-0.575	0.405	1.276
$[M+H]^+$	Δm 3	0.010	-0.275	0.285	0.696
1858.926	4	0.025	-0.569	0.213	1.392
	5	-0.058	-0.502	0.187	0.971
$<\Delta m>\pm\sigma_{n-1}$		-0.016±0.034	-0.525±0.158	0.290±0.093	1.181±0.348
$(<\Delta m>\pm\sigma_{n-1})/m$		-8.4±18.2 ppm	-284±84.9 ppm	156±50 ppm	635±187 ppm
ACTH 1-17	1	-0.003	-0.468	0.473	1.045
$C_{95}H_{145}N_{29}O_{23}S$	2	-0.052	-0.687	0.424	1.161
$[M+H]^+$	Δm 3	-0.002	-0.146	0.498	0.391
2093.086	4	-0.011	-0.571	0.512	1.209
	5	-0.016	-0.399	0.305	0.811
$<\Delta m>\pm\sigma_{n-1}$		-0.017±0.021	-0.454±0.204	0.442±0.084	0.923±0.335
$(<\Delta m>\pm\sigma_{n-1})/m$		-8±10 ppm	-217±97.4 ppm	211±40.1 ppm	441±160 ppm

[a] Sample was deposited on silver substrate.
[b] Spectrum was taken with 1ns time bin width.

results are shown in table 3.1.

The data presented in Table 3.1 show that the H^+, $C_3H_3^+$ pair gives consistently good results, and an accuracy $\Delta m/m$ of less than 50 ppm was obtained for these compounds by using only two low mass peaks in calibration. The Na^+, $C_3H_3^+$ group, on the other hand, produces the biggest deviation. One reason might be that the mass separation is different for these groups; the former has the biggest separation while the latter has the least separation. Some of the mass deviations may also caused by the error in peak centroid determinations due to the 2ns time bin width used here or low statistics of the peaks. However, the mass deviations are not random. For example, the H^+, Na^+ group produces a negative average deviation of few hundred ppm, while the CH_3^+, $C_3H_3^+$ and Na^+, $C_3H_3^+$ yield the positive average deviations of few hundred and several hundred to a thousand respectively. This is apparently related to the ions used in calibrations. From Fig. 2.7, we know that under the normal mirror voltage setting, there is some residual time spread produced in the acceleration region due to ion initial energy distribution, as a result, the time of flight of a peak is still dependent on the mean ion initial energy. This may be largely responsible for these large deviations between different groups of calibration ions. The ion initial energy distribution is influenced by various experiment parameters including primary ion parameters and sample preparation. The different sample preparations, e.g. using different substrate could result in different binding energy between the sample molecules and the substrate and surface charging effect which will affect the initial energy distribution [160,192]. The mean initial energy of H^+ may differ from that of high mass molecular ions, however, the combination of H^+ and $C_3H_3^+$ makes a good choice for the calibration of the peptide molecules. The residual effect of ion initial energy distribution on mass calibration can be reduced considerably

if the mirror is operated under the reduced field as discussed in §2.2.3.2. This has been confirmed by performing calibrations on the CsI spectra mentioned in the previous section. The calibrations show that for the spectrum taken under normal mirror voltage setting, a differences of ~113±5 ppm in the masses of the cluster ions are produced due to using different groups of calibration ions, i.e. (H^+,$C_3H_3^+$) and (Na^+,Cs^+); for the spectrum taken under the 10% increase of the acceleration voltage over the first spectrum while the mirror voltage is kept the same, (this is equivalent to the reduction of the mirror voltage by ~9%), the two groups of calibration ions above give almost the same results on the masses of the cluster ions or only a differences of a few ppm. Although the peptide samples have not been measured under the reduced mirror field yet, improvement over the dependence on ion initial energy is expected, combining with the use of a narrower time bin width (e.g. 0.5 ns is now available in our lab), a mass accuracy better than that in Table 3.1 can be expected with the reflecting instrument.

3.5 SENSITIVITY

High sensitivity is important in mass spectrometry, particularly when dealing with trace material or biomolecules, since many of them are available only in very small quantities. The sensitivity of a mass spectrometer depends on the product of the desorption efficiency and the spectrometer efficiency, where spectrometer efficiency is defined here as the ratio of the number of ions recorded in the spectrum to the number of ions ejected from the target. A TOF mass spectrometer has higher efficiency than most other types of mass spectrometer, which is the result of two factors. First, the transmission

is high since no slits are needed. For the reflecting instrument, as estimated in section 2.5.3, an overall transmission of 37-55% can be expected with an accelerating grid of 60-90% transmission, which is much better than a quadrupole instrument where a typical transmission is only 10^{-4}. Second the whole mass spectrum can be recorded for each primary event, in principle all ions giving pulses in the detector are integrated to form the final spectrum. For a TOF mass spectrometer with an overall transmission of 10%, The combined factors increase the TOF efficiency by a factor ~10^5 compared to a typical quadrupole mass spectrometer [116].

Sensitivity measurements in TOF spectrometers have reported low resolution "molecular" ion peaks from 50 femtomoles of bradykinin (1060 u) on Au [194] and from 20 femtomoles of arginine vasopressin (1083 u) on nitrocellulose [195]. Such sensitivity measurements have also been performed on the reflecting instrument here for peptide samples desorbed by ~10 keV Cs^+ ion bombardment [196]. By using the deflection plates C and D added recently in the ion gun [196], the primary ion beam can be positioned on the target. Since the beam spot on the target is mostly contained with a circle of diameter of 2 mm, the samples were deposited on an area ~3 mm^2 instead of the previous area ~50 mm^2, with a corresponding increase in sensitivity.

A series of peptides with molecular weight range 500-6000 on nitrocellulose substrates have been examined. The substrates were prepared by electrospraying a 5 μg/μL nitrocellulose solution on to an aluminium foil disk covered by another disk with a 2mm aperture to make a 2mm diameter nitrocellulose film on the foil to adsorb the sample molecules. The peptide samples were weighed on an Fisher electronic microbalance with an accuracy of 10 μg. A sample amount of ~200-500 μg was weighed in order to reduce the error in weighting. In order to determine the detection limit, the weighed samples

were first dissolved in 0.1% aqueous TFA to make a 1 μg/μL sample solution; less concentrated sample solutions were then prepared by serial dilution using 0.1% aqueous TFA. A target was prepared by depositing 0.5 microliter of peptide solution on the nitrocellulose spot. Targets were inserted into the spectrometer after the solution dried. The spectra were usually accumulated with a repetition frequency of 4 kHz until ~100 counts/2ns bin were obtained for the most abundant isotope peak in the molecular ion region. For Bradykinin, this corresponds to the accumulation times of ~1-120 min for a sample concentration of 1 μg/μL to 10 pg/μL. For bigger peptides, it took longer than for smaller ones since the yield of bigger peptides is lower than the smaller ones.

Well resolved $[M+H]^+$ ion peaks were obtained from 5 to 35 femtomoles of peptides of masses up to ~3000 u. The amount of sample indicated here and below is the total amount that applied on the target, the actual amount consumed in the measurement is expected to be much less since the yield of molecular ions did not go down very much after the spectra were taken. As for the examples, the molecular ion regions of a 10 femtomole sample of bradykinin and a 27 femtomole sample of γ-endorphin are shown in Fig. 3.10. Reflected spectra have not only better resolution but also a better signal/background ratio than direct spectra, a factor of importance when dealing with small amounts of sample. In Fig. 3.10(a) the signal/background ratio is ~10. Fig. 3.11 shows the direct and reflected spectra from 50 femtomoles of bradykinin. The spectrum indicates the improved signal/background ratio obtained for larger samples.

The relative yield of the molecular ions of bradykinin versus the amount of sample on target is shown in Fig. 3.12, in which the yield of the molecular ion is normalized to CH_3^+, assumed to represent the background. It can be seen from the curve that, up to the sample amount of ~50 ng or ~47 picomoles, the molecular ion yield increases with the

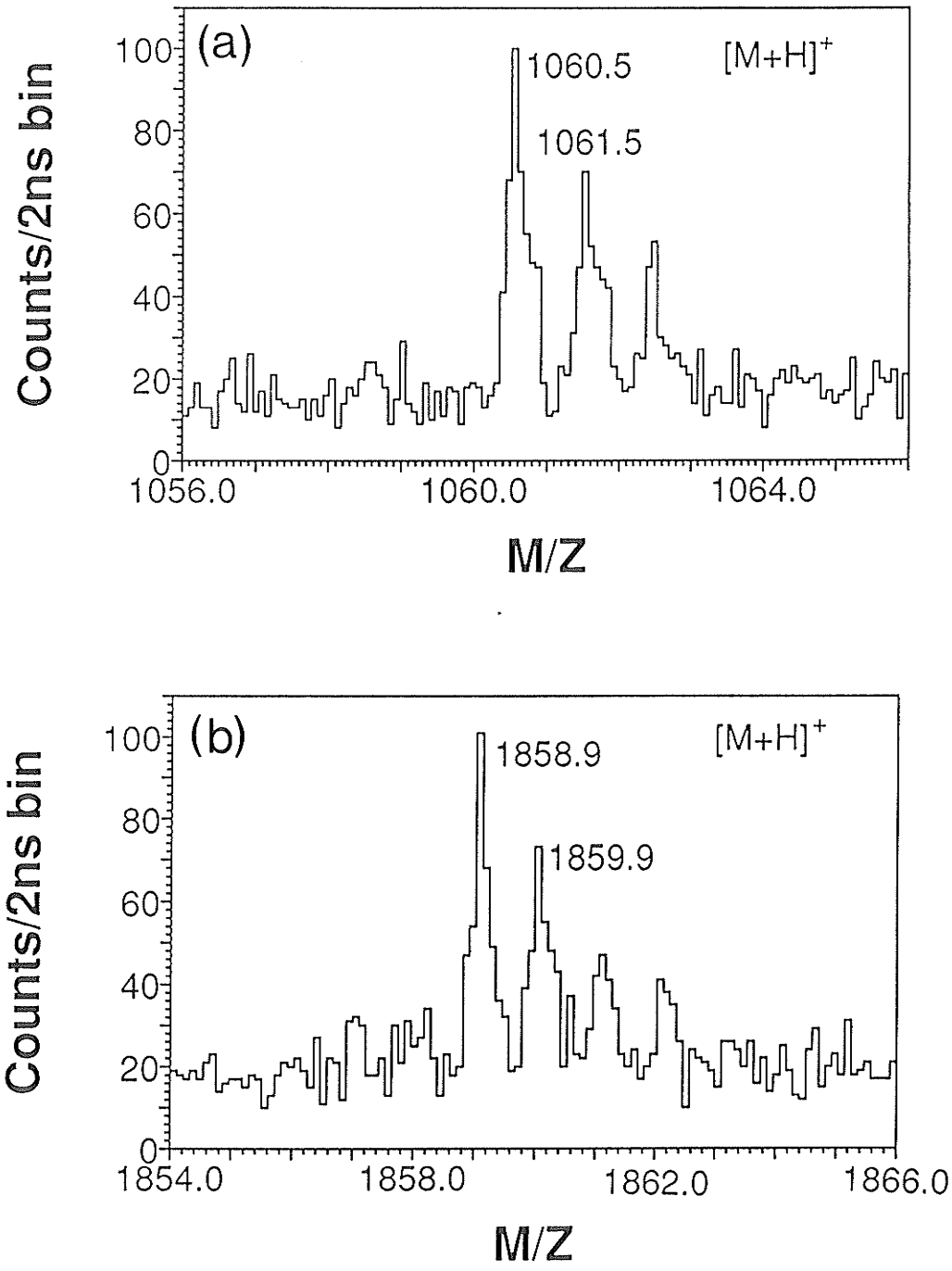

Figure 3.10 Molecular ion region of the peptide mass spectra obtained with (a) 10 femtomoles bradykinin and (b) 27 femtomoles γ-endorphin applied on the targets.

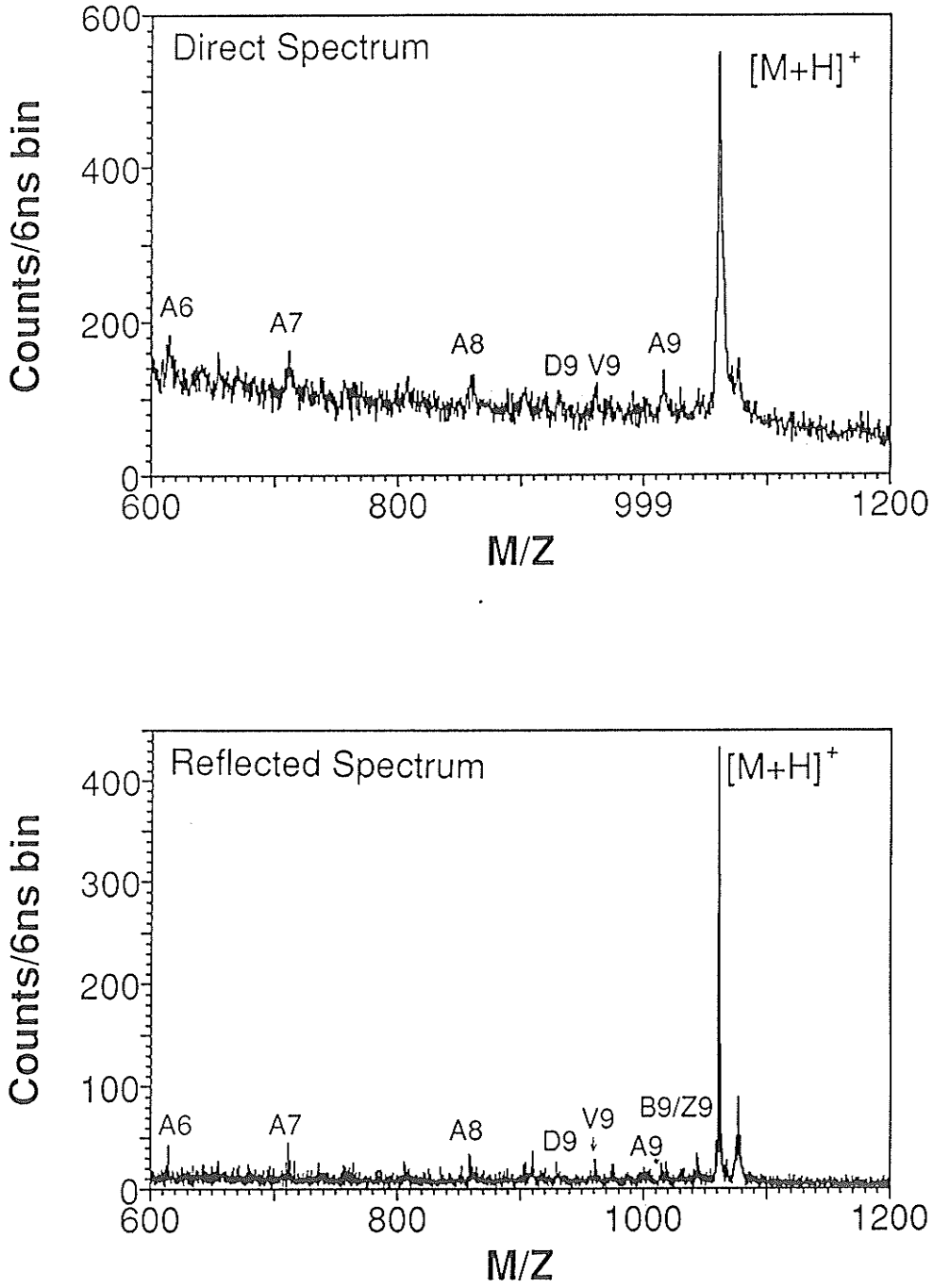

Figure 3.11 Direct and reflected mass spectra obtained with 50 femtomoles bradykinin on target.

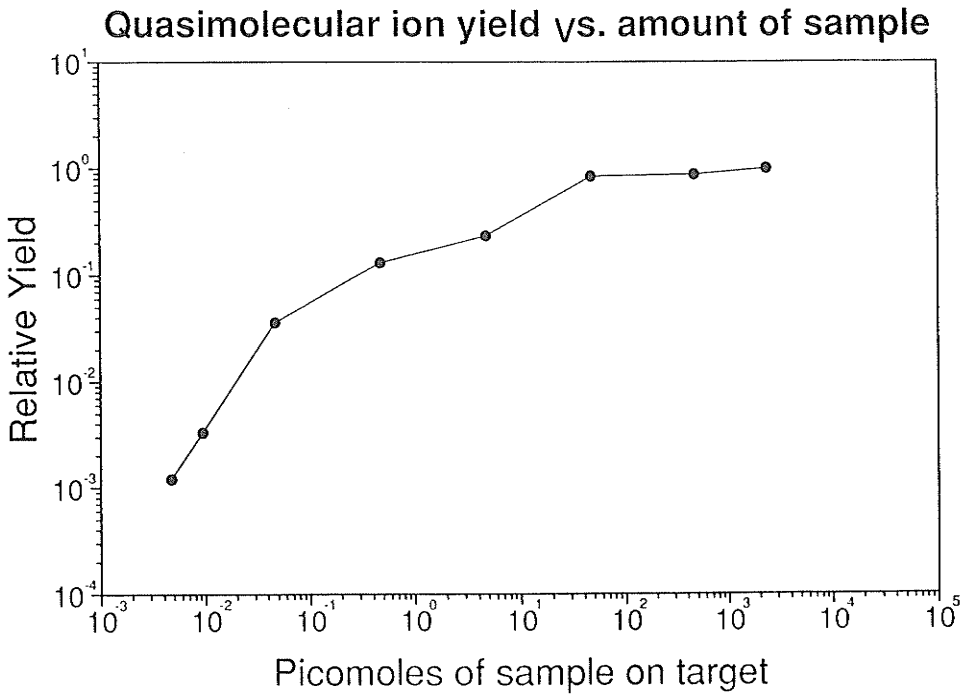

Figure 3.12 The relative yield of the molecular ions, $Y([M+H]^+)/Y(CH_3^+)$, of bradykinin verses the amount of sample applied on target.

amount of sample on the target and the yield remains about constant for sample amount exceeding ~50 ng. This agrees with the observation of Benninghoven et al [116], since 47 picomoles sample on ~2mm spot corresponds to a surface concentration of ~1.5 nanomoles/cm^2 which is approximately equal to a single monolayer of molecules on the surface (a monolayer of molecules corresponds to a surface concentration of ~1 nanomole/cm^2 [116]).

CHAPTER 4

DAUGHTER ION MEASUREMENTS-MS/MS

4.1 INTRODUCTION

Many studies have been carried out on the daughter ions formed in mass spectrometers by unimolecular decay, collision-induced dissociation, or photodissociation. Measurement of the daughter ion mass spectrum of a given parent ion provides useful structural information about the parent [40]. Such measurement are carried out by various methods, often referred to as tandem mass spectrometry (MS/MS) [150,151]. Tandem mass spectrometry is a powerful tool for obtaining structure information on large molecules and for analysis of mixtures [150,151]. True tandem instruments use two separate mass resolving systems with a decomposition region between them; the first selects a given parent ion while the second measures the spectrum of its decomposition products. The commonly used tandem mass spectrometers are multiple sector instruments, (various combinations of electric and magnetic sectors), triple quadrupoles, or hybrid instruments. Although these instruments can provide very high resolution for both parent and daughter, their efficiency is greatly reduced by the necessity of selecting a single parent ion in the first spectrometer and scanning the daughter-ion mass spectrum in the

second mass spectrometer; i.e. only one parent/daughter pair is examined at a time, so the instrument must often operate at lower resolution to provide an adequate data rate. This has spurred the recent development of detector arrays that measure simultaneously a range of daughter-ion masses in the second spectrometer [197,198].

Alternatively, daughter-ion mass spectra may be examined in a type of mass spectrometer that does not require scanning. In particular, a reflecting time-of-flight instrument is able to examine the full mass range for *both* parent and daughter at the same time [121,137,146,186]. Thus it may yield information similar to that provided by true tandem instruments, but with higher efficiency [199-202].

4.2 THE REFLECTING TOF MASS SPECTROMETER AS A TANDEM INSTRUMENT

A reflecting TOF mass spectrometer in the configuration of Fig. 2.1 possesses some of the characteristics of a tandem instrument. A parent ion that decays in the region between the target and the mirror normally gives rise to one neutral and one charged daughter, both of which have approximately the same velocity as the parent. When the mirror voltage is turned on, the neutral fragment still continues on into detector 1, its time-of-flight identifying the parent ion. Thus detector 1 and the flight path between it and the target constitute a linear TOF spectrometer (MS-1) that measures the mass of the parent. The charged product is reflected by the mirror into detector 2, and its mass is determined by the total flight time, if the mass of the parent is known. Detector 2, together with the mirror and the overall flight path, constitute a reflecting TOF

spectrometer (MS-2) that measures the mass of the charged product ion.

In this description, the two "spectrometers" MS-1 and MS-2 have elements in common and the decay region is part of both. Thus, the analogy with normal tandem instruments is not perfect, but it may be useful for comparison with other varieties. The principle of operation and properties of MS-1 and MS-2 are described below.

4.2.1 The Parent Ion Spectrometer MS-1

Fig. 4.1 shows secondary ion mass spectra observed in detector 1 from bombardment of the tripeptide glycyl-glycyl-phenylalanine (GGF) by ~10 keV Cs^+ ions. The direct spectrum (a) is taken with the mirror voltage off, so the peaks include undissociated parent ions as well as charged and neutral daughters. The neutral spectrum (b) is taken with the mirror voltage on, so the peaks include only the neutral fragments. These peaks are wider, but their centroids coincide with the peak positions in the direct spectrum, as expected. Thus the flight time of a neutral fragment identifies its parent ion.

The effective resolution in MS-1 is determined by the velocity spread of the neutral daughters, i.e. by the energy released in the decay. Table 4.1 lists measured resolving powers $M/\Delta M_{FWHM}$ in MS-1 for various parent ions from several peptides, which vary from 50 to 200 [199]. So clearly, MS-1 is not a high resolution device. However, the resolution is usually sufficient to distinguish between different cationized species [see Fig. 4.1(b)] for peptides of mass upto ~2000 u, or between different components of simple mixtures.

Although the resolution in MS-1 is modest, the instrument has useful features. The masses of all parent ions whose neutral daughters detected are measured at the same time;

TABLE 4.1 Resolving Power $M/\Delta M_{FWHM}$ in MS-1

	$[M+H]^+$	$[M+Na]^+$	$[M+K]^+$	$[M+Ag]^+$
GGF	90	280		60
Leu-Enkephalin	75	190	75	55
Met-Enkephalin	75	180	80	50
Substance P (1-9)	130			

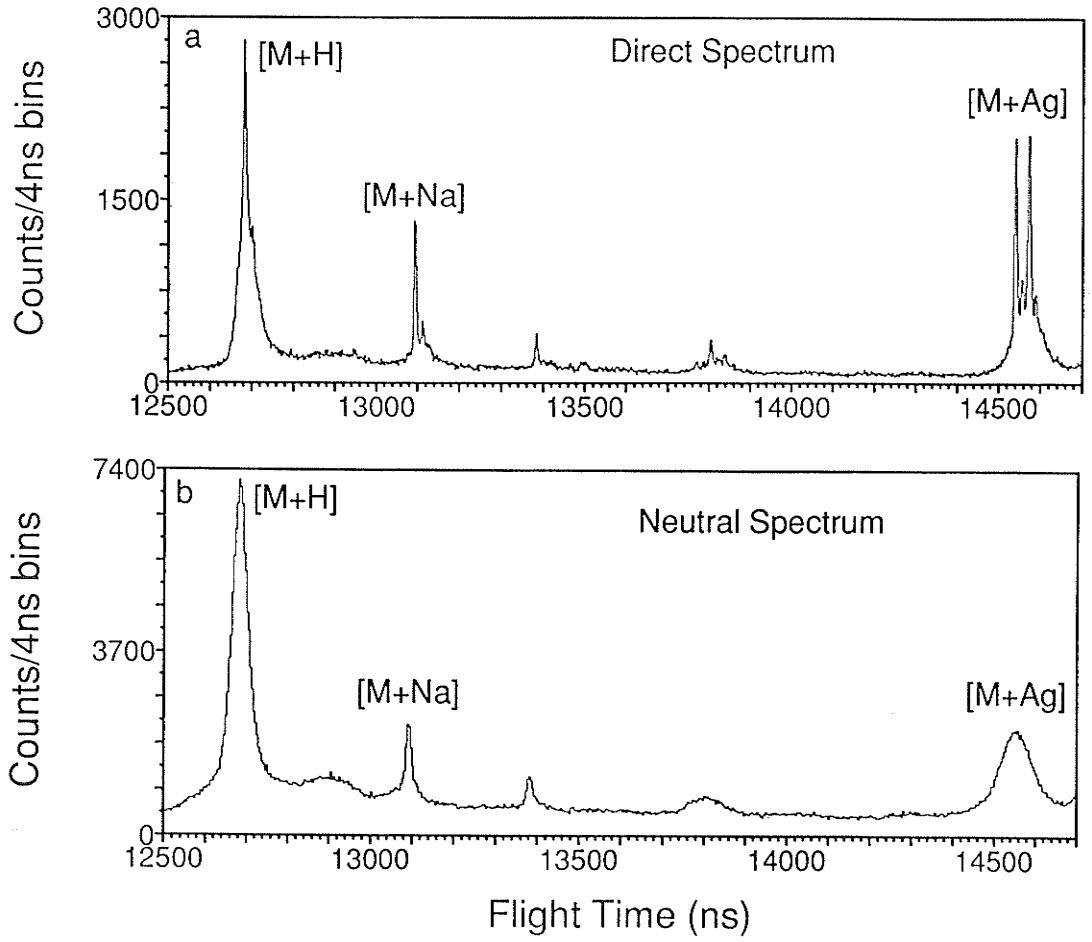

Figure 4.1 TOF secondary ion mass spectra from GGF (MW≈279) in detector 1 (a) with the mirror voltage off, and (b) with the mirror voltage on. The spectrum (b) was recorded for a time about three times as long as the spectrum (a). In (a) the peak labeled $[M+H]^+$ includes parent ions as well as charged and neutral decay products, but in (b) the peak labeled $[M+H]^+$ includes only the neutral products from decay of the $[M+H]^+$ parent; a similar relation holds for the other peaks shown.

no scanning is necessary. MS-1 also serves to identify those parent ions that decompose between the target and the mirror, since these are the only ones that can give a neutral fragment in detector 1.

4.2.2 The Daughter Ion Spectrometer MS-2

Fig. 4.2(a) shows a portion of the overall reflected spectrum of GGF measured in detector 2. The spectrum includes parent ions of every mass together with the charged daughters resulting from their decomposition. As discussed in §2.2, in the spectrometer utilizing a single-stage mirror, there is a simple linear relation between the mass ratio m′/m and the corresponding flight time ratio t^*/t of the daughter ion to its parent. The relation is derived in Eq. (2-7) for a typical case, that is

$$2\frac{t^*}{t}=\frac{m'}{m}+1$$

The flight time of a daughter ion depends on the mass of its parent as well as its own mass. Although this complicates the spectrum, it is useful for separating the daughter ions arising from decay in free flight from ions of the same mass produced directly at the target. For example, the peak at ≈23,500 ns in Fig. 4.2(a) corresponds to a daughter ion of mass≈166 u from decay of the $[M+H]^+$ ion, while an ion of the same mass produced at the target appears at ≈22,800 ns.

It has been shown in §3.3, the mirror produces a considerable improvement in resolution for the parent ions. A smaller improvement is seen in the daughter ion peaks, particularly at low mass, because the daughters do not spend a long enough time in the

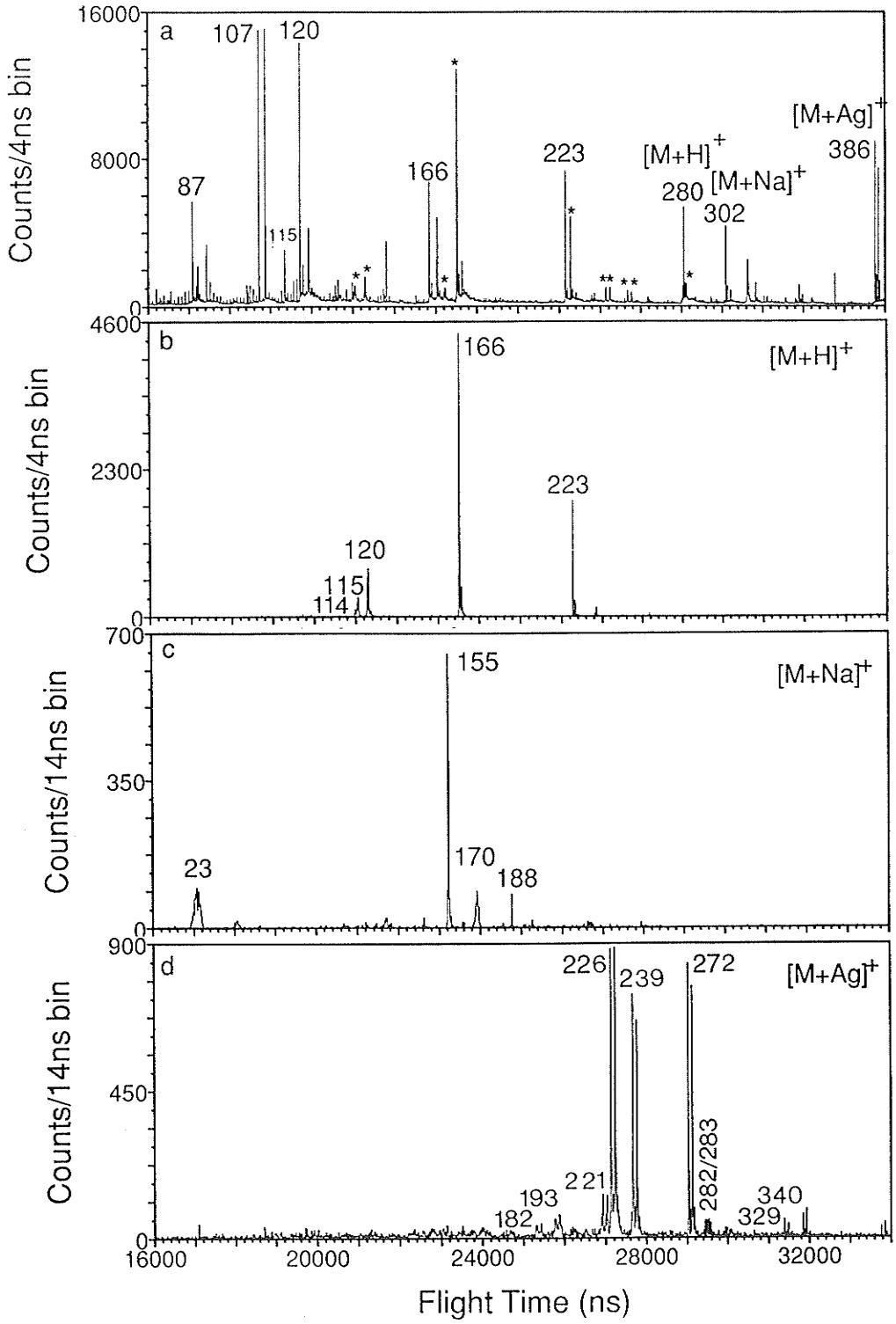

Figure 4.2 TOF spectra in detector 2; (a) total spectrum; peaks shown with asterisks correspond to daughter ions; (b) spectrum correlated with $[M+H]^+$ neutral; (c) spectrum correlated with $[M+Na]^+$ neutral; (d) spectrum correlated with $[M+Ag]^+$ neutral.

mirror to provide full compensation for their velocity spread [121,137].

4.3 CORRELATED MASS MEASUREMENTS

4.3.1 Principle of correlated mass measurement

The spectrometer is operated as a tandem instrument by measuring the daughter ions in MS-2 that are correlated with a given neutral fragment in MS-1. In order to avoid false correlations caused by random events, a low primary beam current is used, so that on average only about one secondary ion decay is observed for each primary ion pulse. During the observation period (typically ~100 μs) following the arrival of a given primary ion pulse at the target, the flight times of neutrals and ions are both digitized and stored in a memory buffer in the time digitizer (TDC). At the end of the observation period these numbers are transferred to computer, which examines the spectrum of the neutral fragments to see whether one has arrived within a set of preselected time windows [148,149]. For example, in the GGF neutral spectrum of Fig.4.2(b) the computer first searches the region between 12,640 and 12,750 ns for a neutral event corresponding to an $[M+H]^+$ decay; if such an event is found, the flight times of any charged particles detected in that observation period are recorded in a dedicated section of computer memory. The computer then searches between 13,050 and 13,120 ns for a neutral event corresponding to an $[M+Na]^+$ decay; if one is found, the computer stores the daughter ion flight times in a second section of memory. The process is repeated for the $[M+Ag]^+$ parent and for any other parent ions of interest. The calculations are carried out while the

time digitizer is gathering data during the next observation period, so usually no time is lost [148,149].

After many observation periods, daughter ion spectra arising from the decays of the selected parent ions have been accumulated in computer memory. The daughter ion spectra corresponding to the decays of $[M+H]^+$, $[M+Na]^+$ and $[M+Ag]^+$ ions of GGF are shown in Fig. 4.2(b), 4.2(c) and 4.2(d). It can be seen from Fig. 4.2(a) that although the resolution in the reflected spectrum is better and the background signals are smaller than for the direct spectrum; the reflected spectrum is more complicated. The time scale calibration for daughter ions from metastable decompositions differs from the parent ion time calibration [see Eq. (2-7)], producing, in effect, several superimposed mass spectra. In the high-mass part of the reflected mass spectrum, the cationized molecules $[M+H]^+$, $[M+Na]^+$ and $[M+Ag]^+$ are prominent. Although daughter ions are also present in this spectrum, they are not usually readily distinguished from other fragments because their intensities are quite low. However, they are readily observed in the correlated (i.e. daughter ion) spectra. It is clear that this method is fairly efficient at separating useful events from background; for example, the peak corresponding to the 155 u decay ion is prominent in the correlated spectrum of Fig. 4.2(c), but is barely visible in Fig. 4.2(a). Since the daughter ion spectra are much simpler than the overall reflected spectrum of Fig. 4.2(a), unambiguous assignment of decay pathways can often be made.

Although the option has not yet been utilized very often, it is also possible to generate "parent ion" mass spectra of selected daughter ions. This is obvious from the principle described above. In this case, a time window is selected for detection of a given daughter ion in detector 2, and the correlated neutral fragments detected in detector 1 are recorded. The recorded neutrals, which have approximately the same flight time as their

parent ions, thus correspond to a parent ion spectrum. As remarked in §4.2.1, the recorded neutral peaks are broadened by kinetic energy released upon fragmentation. In general this will not be a serious problem, because such spectra normally contain very few peaks, and high resolution is not necessary to resolve them or to measure their time centroids, at least for a simple mixture.

4.3.2 Efficiency of the Correlated Measurement

The correlated data can also be used to estimate the probability of detecting a decay event. For a given decay, the number of events when both neutral and charged fragments are detected, (i.e. the number of "coincidences" [N_{coin}]) is measured by the number of counts in that peak in the correlated spectra [Fig. 4.2(b), 4.2(c) and 4.2(d)]. The total number of daughter ions detected from this decay (N_+) is measured by the number of counts in the corresponding peak in the overall reflected spectrum [Fig. 4.2(a)]. The ratio N_{coin}/N_+ is therefore a direct measure of the probability of detecting a neutral fragment when the corresponding daughter ion has been detected, i.e. the efficiency ε_n for detection of the neutral fragment. Fig. 4.3(a) shows the ratio N_{coin}/N_+ for $[M+H]^+$ decays in GGF and leu-enkephalin. As might be expected, the ratio decreases as the energy E_n of the neutral fragment becomes smaller —— from ε_n~50% at E_n=6 keV to ε_n~20% at E_n=1 keV.

The total number of neutrals detected from decay of a given parent ion is given by the number of counts in that peak in the neutral spectrum [Fig. 4.1(b)]. By an argument similar to the one above, the ratio of N_{coin} (for all peaks) to the total number of neutrals detected gives the average efficiency $\varepsilon_+$for detecting charged daughters from

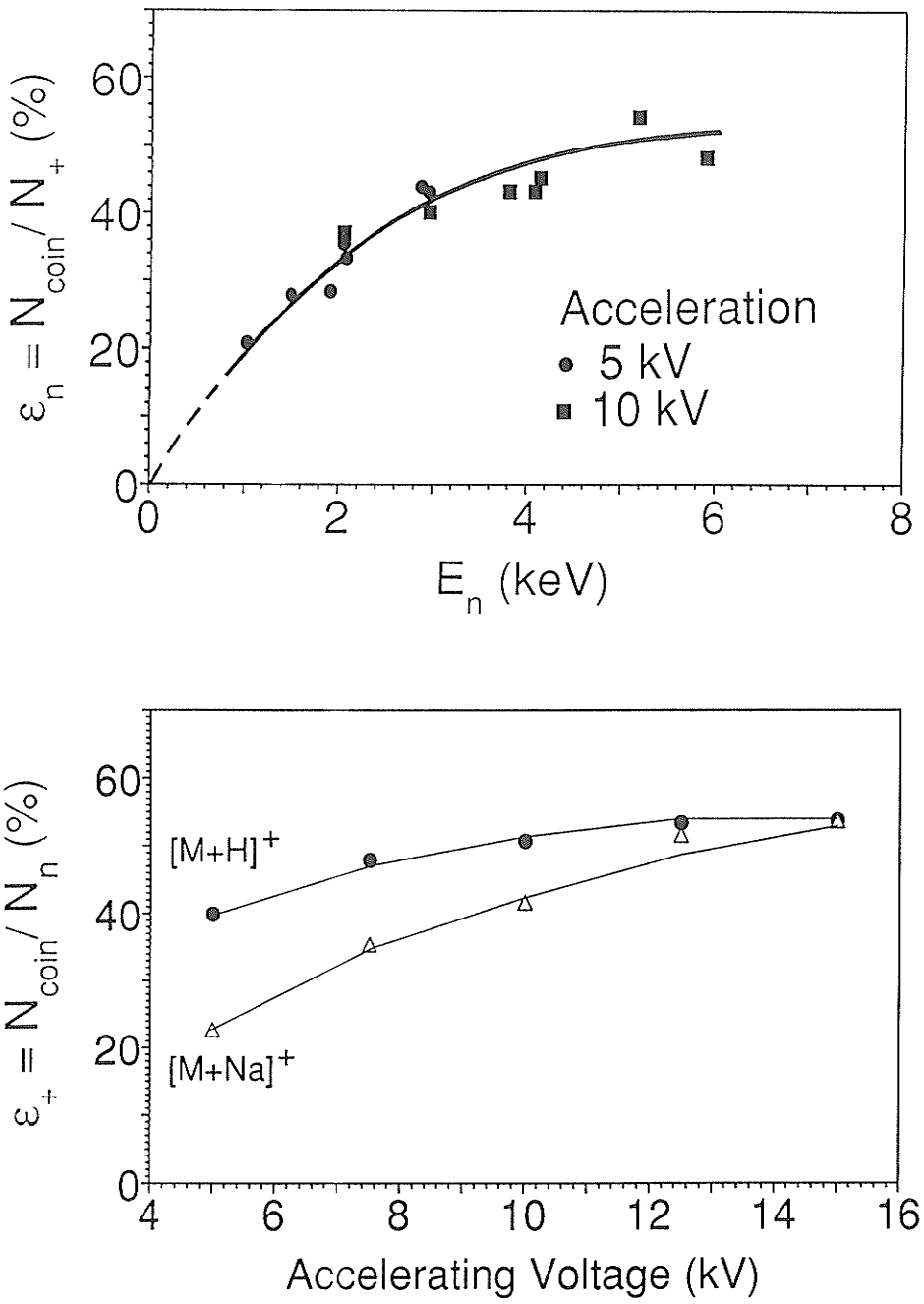

Figure 4.3 (a) Neutral fragment detection efficiency; (b) charged daughter average detection efficiency.

the decay of a given parent when the corresponding neutral fragment has been observed, although in this case the efficiency for individual daughter ions cannot be determined. Fig. 4.3(b) shows the average efficiency ε_+ for detecting charged daughters as a function of secondary ion acceleration voltage for $[M+H]^+$ and $[M+Na]^+$ decay in GGF. The large difference in ε_+ between the $[M+H]^+$ and $[M+Na]^+$ daughters at 5 kV arises because of the different decay patterns; a substantial fraction of the $[M+Na]^+$ ions decay by emission of Na^+, which has a small detection efficiency because of its low energy. No information is available on the variation of efficiency with daughter ion mass, but the effect is expected to be much smaller than with the neutrals, because the positive ions are accelerated across 1 kV before striking the detector.

It should be noted that these efficiencies are overall figures. they take into account all losses in the spectrometer and in the detection system, such as attenuation in the mirror grids, particles that miss the detectors, and particles that strike detectors but are not recorded. It is clear from Fig. 4.3 that strong correlations exist between ion and neutral efficiencies as a function of m′/m. These effects are included in the measured ε_n and ε_+. If we assume that other correlations are small, we may estimate the efficiency of detecting *both* charged and neutral fragments from any decay as the product $(\varepsilon_n\varepsilon_+)$, or ~25% for a typical decay where m′=m/2. This efficiency is obtained simultaneously for all parent ions.

Since our earlier reports on daughter ion measurements [169,199], we have enlarged the front aperture of the ion mirror and increased the accelerating voltage; these improvements have given an increase in the overall efficiency $(\varepsilon_n\varepsilon_+)$ by an order of magnitude [200-202]. They have also enabled observation of additional decay channels, as shown in Fig. 4.2c. The efficiencies may be compared with those observed in other

types of tandem instrument. In these spectrometers, stable ions may be lost at the entrance slit of MS-1 or en route through the spectrometer, while metastable parents may decay before reaching the decomposition region. If more than one parent ion is to be examined, the efficiency of MS-1 is reduced correspondingly. Similar effects occur in MS-2, where scanning produces large losses unless an array detector is used.

4.4 DAUGHTER ION RESOLUTION AND SENSITIVITY

4.4.1 Daughter Ion Mass Resolution

Unit mass resolution is obtained for parent ions of peptides of masses up to several thousand u by the use of the reflector, as illustrated in §3.3.2 However, as remarked above, daughter ions do not spend enough time in the mirror to reap full benefit from its effect, so the resolution for daughter ions deteriorates significantly as m′/m decreases. Fig. 4.4(a) illustrates this effect for the mass 278/279 u daughter ion doublet from leucine enkephalin [169]; the two components are not resolved in the normal daughter ion spectrum from $[M+H]^+$ decay. For the same reason the Na^+ daughter ion peak in Fig. 4.3(c) is very wide. The problem is accentuated for peptides of larger mass, since in this case there may be many daughter ions with small m'/m, so their peaks merge. Fig 4.5(a) shows a section of the low mass spectrum from unimolecular decay of the $[M+H]^+$ ion of the peptide α-neoendorphin (m/z 1227) [200]; again the daughters are completely unresolved. This is a serious difficulty because the lower portion of the daughter-ion mass spectrum is often extremely important for proper interpretation of the

peptide structure, as pointed out by Sato et al [203].

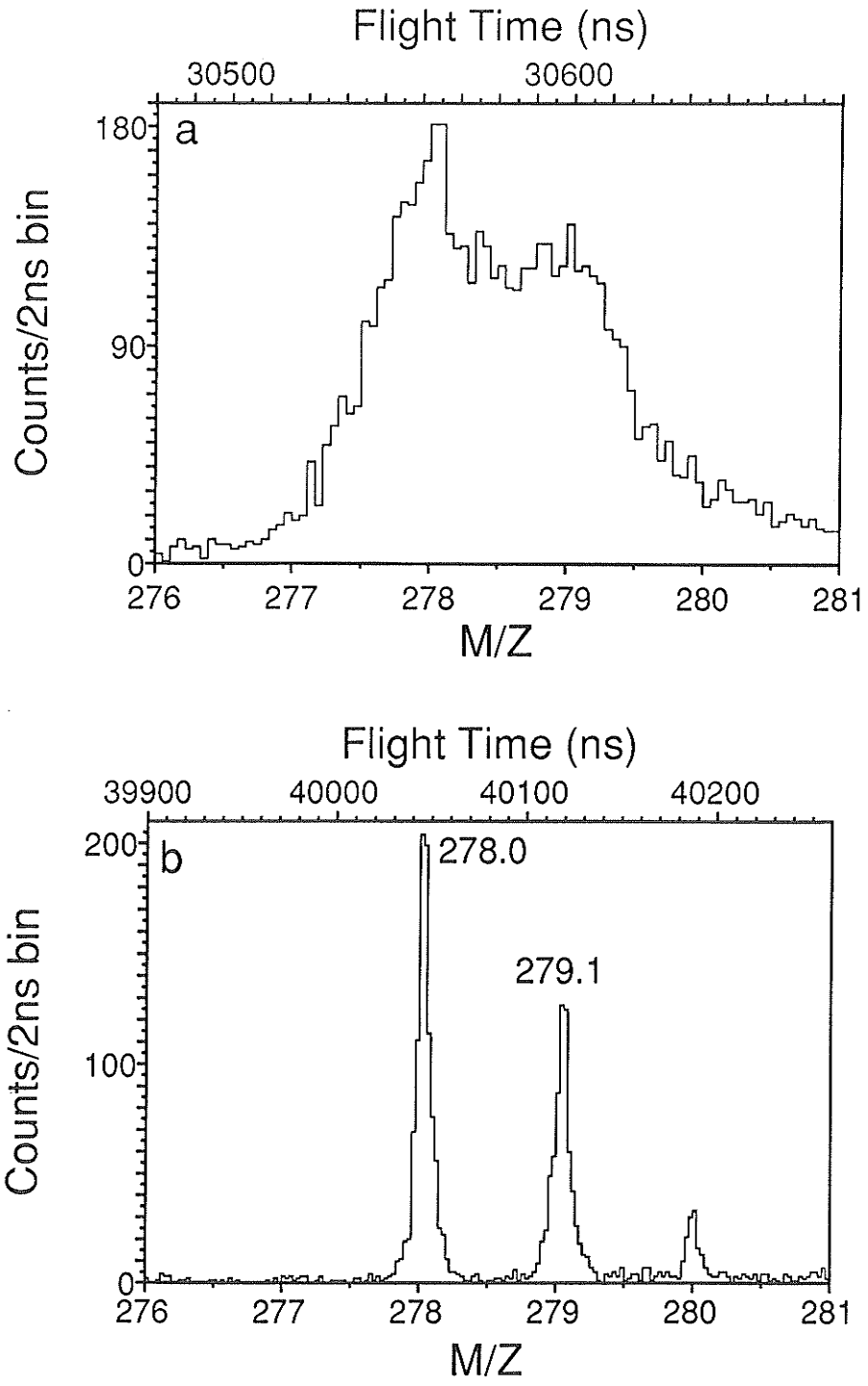

Figure 4.4 Daughter ion doublet from the $[M+H]^+$ parent ion of leucine enkephalin (MW≈555 u) with the mirror optimized (a) for the parent ion and (b) for the daughter.

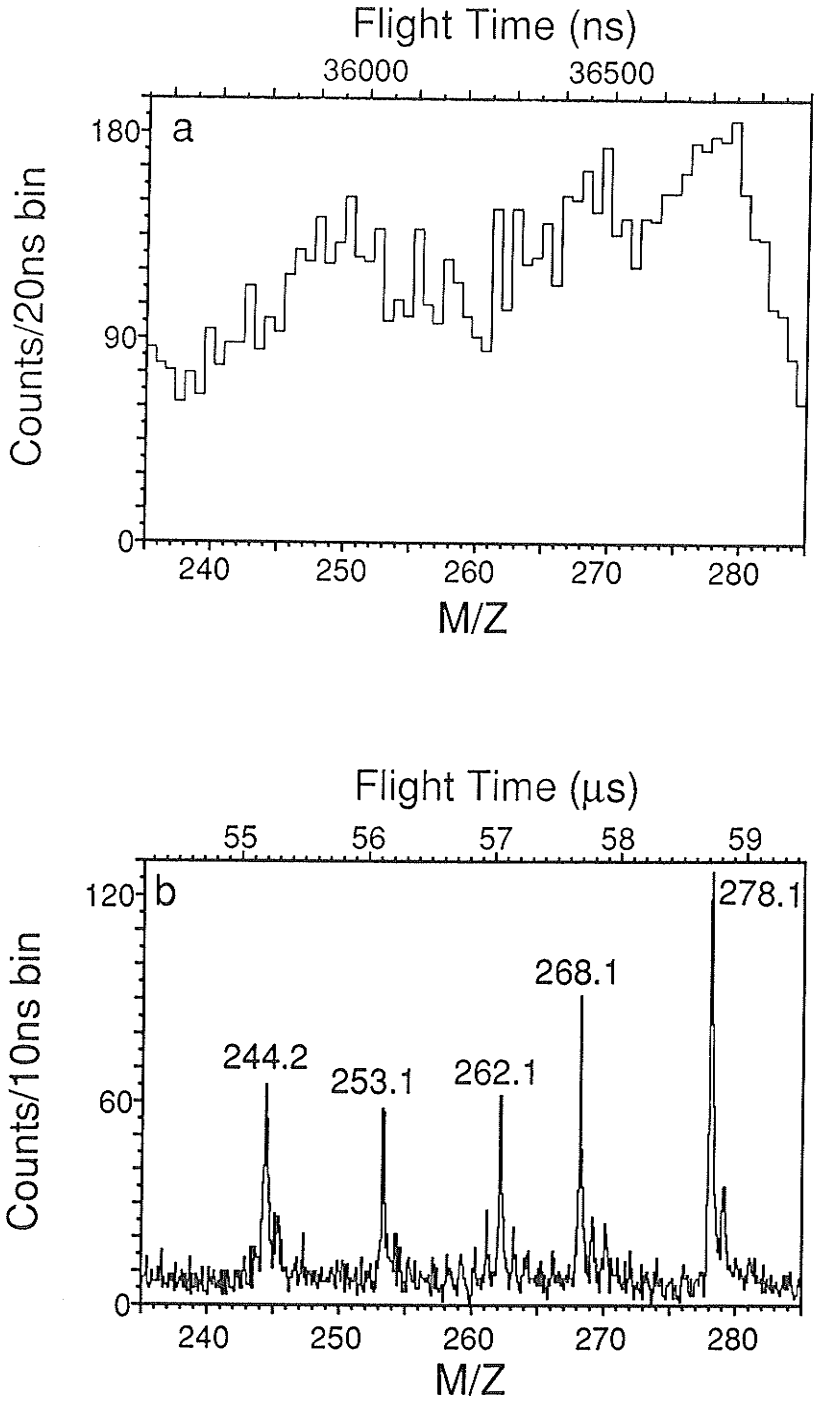

Figure 4.5 Portion of the daughter ion spectrum from $[M+H]^+$ decay of α-neoendorphin with the mirror optimized (a) for the parent ion and (b) for the daughter ion of mass 278 u.

peptide structure, as pointed out by Sato et al [203].

Fortunately there is a simple solution to this problem. As discussed in §2.2.2, it is possible to optimize the reflector for examination of a particular daughter ion of mass m' by reducing the electric field in the mirror to a value that gives the same flight time t for the daughter as previously obtained for the parent ion. This requires the reduction of the mirror voltage to a fraction m'/m of its previous value. The mass m'' of another daughter ion can then be determined from its flight time t^{**} by an equation similar to Eq.(2-7).

$$2\frac{t^{**}}{t} = \frac{m''}{m'} + 1 \qquad (4\text{-}1)$$

Under this condition, the parent ions and daughters of mass appreciably greater than m' pass through the reflector, so only part of the overall daughter ion spectrum can be examined at one time. The results of this technique are clearly indicated in Fig. 4.4(b) where reduction of the mirror voltage to optimize the resolution for mass 279 u yields a well-resolved doublet [200,202]. The improvement is even more dramatic when examining daughters from parent ions of large mass. Fig. 4.5(b) shows a same portion of the daughter ion spectrum (~240 to 280 u) as in Fig. 4.5(a), with the mirror voltage optimized for mass 278 u, the completely unresolved daughter ions in Fig. 4.5(a) are well separated now. Of course, this procedure requires examination of the daughter ion spectrum in several segments, so the efficiency is reduced, but it would appear that the extra measuring time can usually be justified by the improvement in resolution and the additional information produced.

4.4.2 Daughter Ion Sensitivity

High sensitivity in femtomole range is achieved for parent ions in the reflecting TOF mass spectrometer as shown in §3.5. In principle, a high sensitivity for daughter ions is also expected because of the high efficiency of the correlated daughter ion measurement as illustrated in §4.3. In practice, measurements of daughter ion spectra by our technique depend on various additional factors such as the rate of the metastable decay of the parent ion, the detection efficiency for the neutral fragment and the daughter ion transmission. Comparing with parent ions, there are two additional factors affecting the daughter ion transmission.

First of all, daughter ions may have a larger radial velocity distribution because of the kinetic energy released in metastable decomposition. As shown in §2.5.3, the transmission of parent ions can be improved by reducing the angular spread of the beam with the electrostatic lens. However, this is not feasible for daughter ions. It has been observed that when the lens is turned on, a daughter ion peak is split into two peaks, so the resolution and the ratio of signal-to-background deteriorated in spite of the increase in counts. The doublet appears because some parent ions decay before the lens, others decay after the lens. The daughter ions from the parents that decomposed before the lens spend some time passing through the lens while those from parents that decompose after the lens do not. The additional angular spread of the daughter ion may be significant, although the average kinetic energy release in metastable decay is usually <100 meV [204].

Secondly, there is a lateral or radial displacement between a parent ion and its daughter (see Fig. 2.1) in the plane of the ion trajectory. This is caused by the non-

perpendicular reflection and different penetration depths between parents and daughters in mirror. In our case, the incident angle is ~1.5°, and the effective mirror depth for a parent ion is ~62.5 cm, the maximum displacement is ~3 cm between daughter ions of mass close to zero and those close to the parent. This spread cannot be reduced by the lens. It seems necessary to increase the size of the detector 2 to improve the transmission of the daughter ions. However, if the daughter ion spectrum is measured in several sections as described above, then the lateral spread is not a serious problem since only the daughter ions whose flight paths are close to their parent are important in each section.

Although the daughter ion sensitivity is affected by many additional factors such as those mentioned above, almost complete daughter ion spectra from leu-enkephalin, met-enkephalin and bradykinin have been observed with samples of ~200 femtomoles [196]. Fig. 4.6 shows the daughter ion spectrum from 200 femtomoles of bradykinin. In the three sections illustrated, the mirror voltages were set to optimize the resolutions of parent (1064 u), daughter (527 u) and daughter (302 u) respectively. Considerable structural information can be extracted from such daughter ion spectra. Fig. 4.7 shows the upper section of the daughter ion spectrum from both 100 and 50 femtomoles of bradykinin. These spectra were taken under the same conditions as those in Fig. 4.6.

4.5 DAUGHTER ION MASS CALIBRATION AND ACCURACY

The mass of a daughter ion can be determined by optimizing the mirror for the given daughter, as described in Eqs. (2-11) and (2-12). This has been used to determine

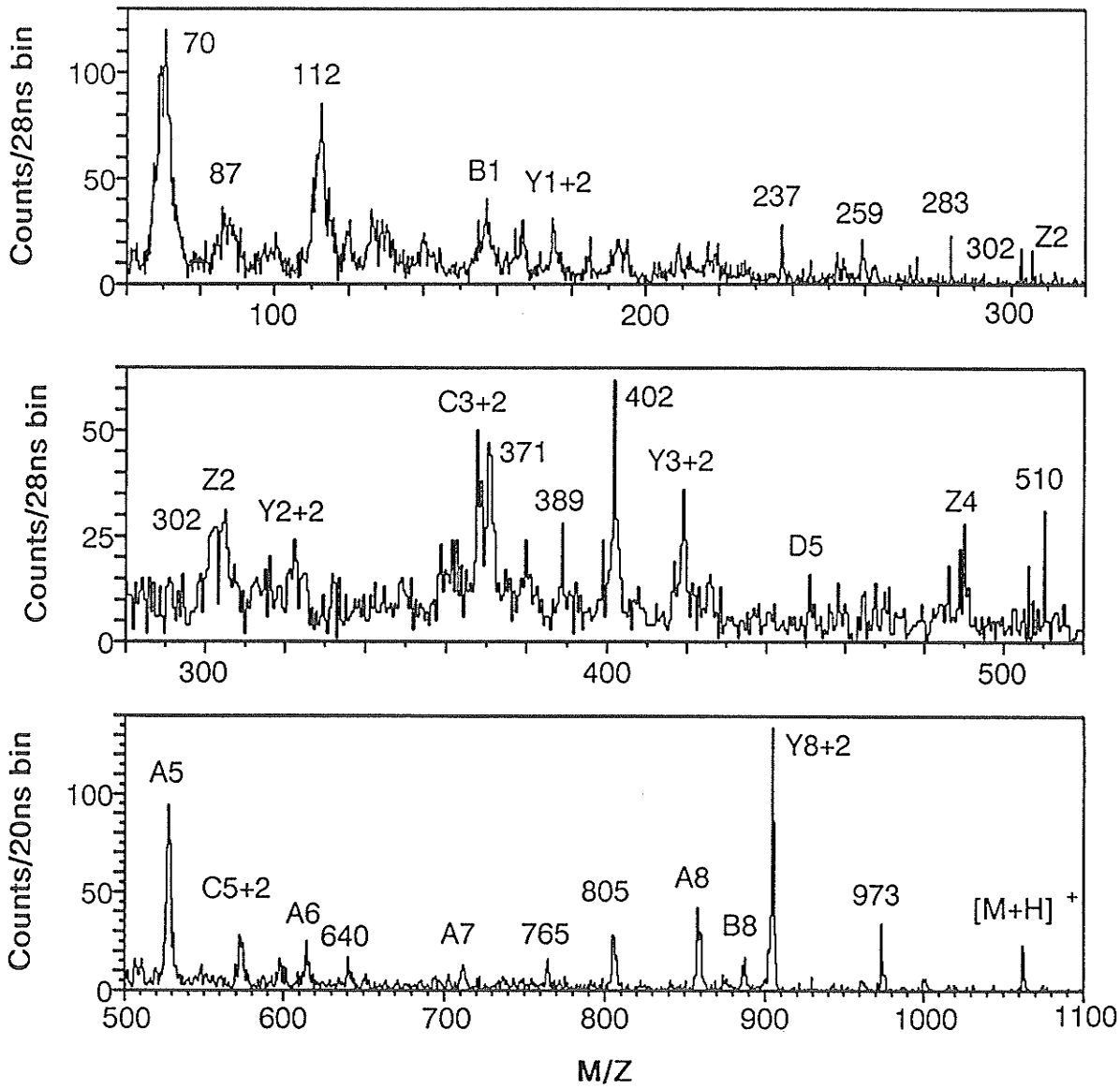

Figure 4.6 Daughter ion spectrum obtained with 200 femtomoles of bradykinin applied on target.

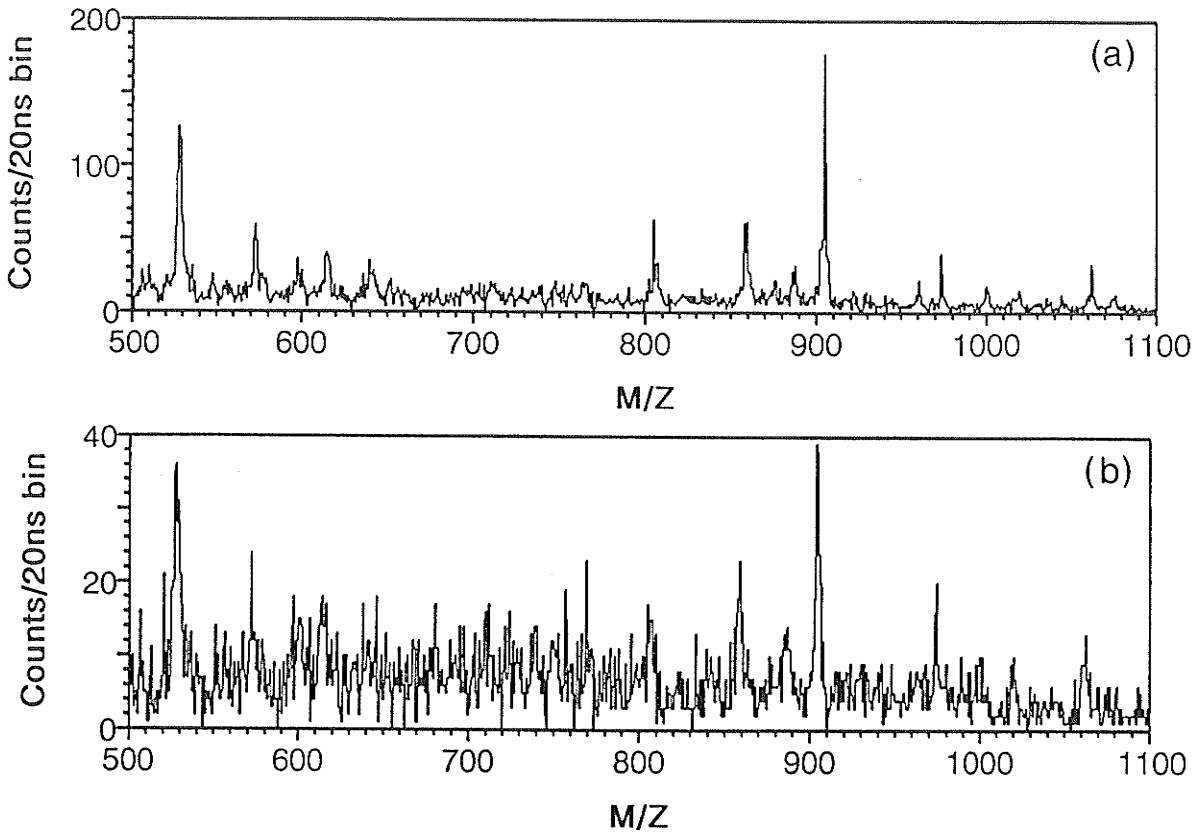

Figure 4.7 The upper sections of the daughter ion spectrum (a) obtained with 100 femtomoles of bradykinin on target, (b) obtained with 50 femtomoles of bradykinin on target. see Fig.4.6 for peak assignments.

the masses of daughter ions for several compounds. The mirror voltages V'_m and V_m, corresponding to the respective optimal values for daughter and parent ions were measured with a high voltage probe and a digital voltmeter. If the mass of the parent ion is known, then the daughter ion masses can be calculated from Eq. (2-12), i.e.

$$m'=m\frac{E'}{E}=m\frac{V'_m}{V_m}$$

Table 4.2 shows the measured and calculated masses of daughter ions from decompositions of $[M+H]^+$ of leucine-enkephalin. It can be seen that most measured

TABLE 4.2 Daughter Ions From Leucine-Enkephalin $[M+H]^+$

Daughter Ion Mass m′		
Experimental	Calculated	$\Delta m=m'_{expl}-m'_{calc}$
443.20	443.19	0.01
425.15	425.18	-0.03
397.14	397.19	-0.05
336.17	336.19	-0.02
279.16	279.17	-0.01
278.06	278.11	-0.05
262.11	262.12	-0.01
221.08	221.09	-0.01
205.09	205.10	-0.01
177.10	177.10	0.00
136.09	136.07	0.02
120.08	120.08	0.00

Parent Ion Mass 556.28

masses agree with calculated masses very well. The maximum experimental error of $\Delta m'/m'$ is only $\sim 1.8\times10^{-4}$ at m′=278.11 u, this is probably caused largely by the accuracy of the digital voltmeter used in the experiment. The maximum error could be induced due to the accuracy of the voltmeter is

$$\frac{\Delta m'}{m'}=\Delta V\left(\frac{1}{V'}+\frac{1}{V}\right)$$

where ΔV is the accuracy of the meter which is 5×10^{-4} volt, and V′ and V is the readings of the meter corresponding to V'_m and V_m respectively. For the daughter ion of m′=278.11 u, this gives maximum possible error of $\Delta m'/m'\approx1.1\times10^{-4}$.

The procedure described above gives improved resolution and yields an accurate value for the mass of a given daughter ion as shown in last section and Table 4.2, but is

rather tedious. Normally however, the daughter ion masses are determined from Eq. (2-7), with the mirror at its voltage settings optimum for the parent ion [Eq. (2-17)], or from Eq. (4-1), in case the daughter ion spectrum is measured in more than one section. As mentioned in §2.2.3.3, considering the changes of the optimum mirror voltage setting due to the effect of the initial energy distribution in the acceleration region and possible defects in the mirror, some small correction may be needed for Eq. (2-7). Fig. 4.8 shows a comparison of measured [i.e. calculated from measured flight times using Eq. (2-7)] and known masses for daughter ions from the decay of CsI cluster. Since the correction to Eq. (2-7) is very small for an ion initial energy of several eV, a large part of the deviations are probably caused by non-linearities in the potential distribution within the mirror as

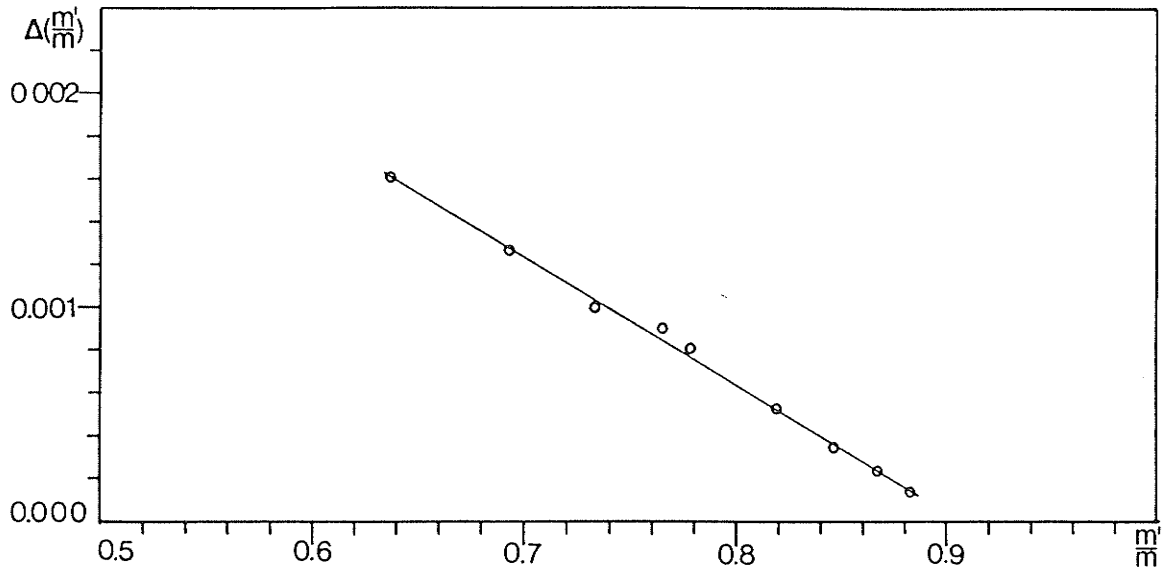

Figure 4.8 Differences in the ratio m'/m as measured [i.e. calculated from measured flight times using Eq. (2-7)] and the known mass ratio for daughter ions from the decay of CsI clusters.

shown in §3.3.2. The maximum difference in the m'/m ratio is $\sim 2\times10^{-3}$, but the points lie on a smooth curve with scatter $\leq 10^{-4}$. If this is used as a calibration curve, it appears that daughter ion masses can be determined to a small fraction of a mass unit for parent ions of masses up to several thousand units. The results for daughter ion measurements of peptides shown in chapter 5 support this conclusion. As will be seen, the errors in daughter ion mass determination arise mainly from the inaccuracy in determining the peak centroid due to low resolution, low signal-to-background ratio or low statistics. Sometimes several calibration compounds may be needed to cover a wider daughter ion mass range. Peptide compounds such as leucine-enkephalin have also been used as calibration compounds since the daughter ion masses have been measured and determined already.

CHAPTER 5

ANALYTICAL APPLICATIONS OF THE REFLECTING TOF MASS SPECTROMETER

5.1 INTRODUCTION

The unique capabilities of a time-of-flight mass spectrometer, such as high sensitivity, high mass range, and fast and simultaneous recording of all masses, have made it attractive in many applications. The installation of an ion mirror in a TOF mass spectrometer not only improves the resolution and the ratio of signal to background, but also enables measurement of daughter ion masses from a parent that decomposes in the first leg of the flight path. The latter feature of the reflecting instrument has given considerable advantages in molecular stability studies, molecular chemical structure and mixture analysis. Many samples, inorganic and organic (mostly peptides), have been analysed with the reflecting instrument, and particularly by the MS/MS method described in the preceding chapter. Some of the results obtained with the reflecting instrument are presented below; they also illustrate the analytical capability of the instrument. To identify the ionic fragments of peptides, a symbolism suggested by Roepstorff and Fohlman [205], and subsequently endorsed in slightly modified form by Biemann and Martin [40], has

been adopted in this thesis. A detailed explanation is given in Appendix B.

5.2 MEASUREMENTS OF DAUGHTER ION SPECTRA OF CsI CLUSTERS

The importance and the development of cluster studies are well documented [206,207]. Clusters, finite aggregates containing 2-10^4 particles, commonly play the very fundamental role of bridging the gap from atoms and molecules to the bulk. Studies of their properties provide ways and means to explore and understand the gradual transition from molecular to condensed matter systems; they are valuable in many areas of physics, material science and industry.

Secondary ion mass spectrometry with keV primary particles is a means of generating cluster ions and studying their relative stability [207]. Cluster ions formed by particle bombardment represent a sensitive probe for the investigation and elucidation of the sputtering and ionization mechanisms, which may also contribute to the understanding of the desorption process of involatile organic molecules.

The reflecting TOF instrument with correlated mass measurement provides a useful tool for studying the structure and stability of cluster ions. CsI is a good test case for metastable ion analysis because of its simple structure. Measurements of CsI clusters may also be useful in studies of more complex organic molecules for purposes such as daughter ion mass calibration shown in §4.5. The stability of CsI clusters has been investigated in our laboratory by using the linear TOF instrument with retarding grids, and clusters with n>7 were found to be metastable [133]. With the reflecting instrument and the MS/MS method discussed in the preceding chapter, such studies can be carried out

more easily and with much better resolution and accuracy.

The CsI targets were prepared by vacuum deposition, and they were irradiated with a several nA d.c. primary ion beam for ~5 min before taking the spectra. The target irradiation was performed here to increase the yields for big cluster ions [131]. The primary ion energy used in the experiments was 10 keV, and the secondary ions were accelerated to 12.5 keV. The post-accelerating voltage applied to the electron converter detector was 1 keV. An example of the reflected spectrum of CsI is shown in Fig. 3.1. Daughter ion spectra from metastable decays of the $(CsI)_nCs^+$ parent ions up to n=24 have also been taken; four daughter ion spectra from four parents were taken at a time, because of the limitations of the computer memory. The daughter ion spectra of the parent ions of n=9 to 16 along with the respective reflected spectra are shown in Fig. 5.1. Although intensity of the parent ion peaks goes down dramatically after $n \geq 10$ [see Fig.5.1(a)], daughter ion peaks remain intense. For this simple inorganic sample, the reflected spectrum shows most of the daughter ions and their relative probability for each ejected cluster. The daughter ion spectra are used to identify the decay paths of their parents. A daughter ion spectrum has the advantage of separating the useful events from background. This is particularly useful in dealing with daughters of low relative abundance. Fig. 5.2 shows the daughter ion spectra of parents of n=1 to 4 along with the reflected spectrum. The decay paths $(CsI)Cs^+ \rightarrow Cs^+ + CsI$ and $(CsI)_2Cs^+ \rightarrow Cs^+ + (CsI)_2$ cannot been seen in the reflected spectrum, but are clearly visible in the daughter ion spectra; similar results have been obtained for other decay channels, such as $(CsI)_5Cs^+ \rightarrow (CsI)Cs^+ + (CsI)_4$. Some decay paths, such as $(CsI)_2Cs^+ \rightarrow (CsI)Cs^+ + CsI$, are not very obvious from the reflected spectrum but are clearly visible in the daughter ion spectra. These daughter ions could not be seen in our early investigation [136,137] due to their low intensity; the present result is a direct

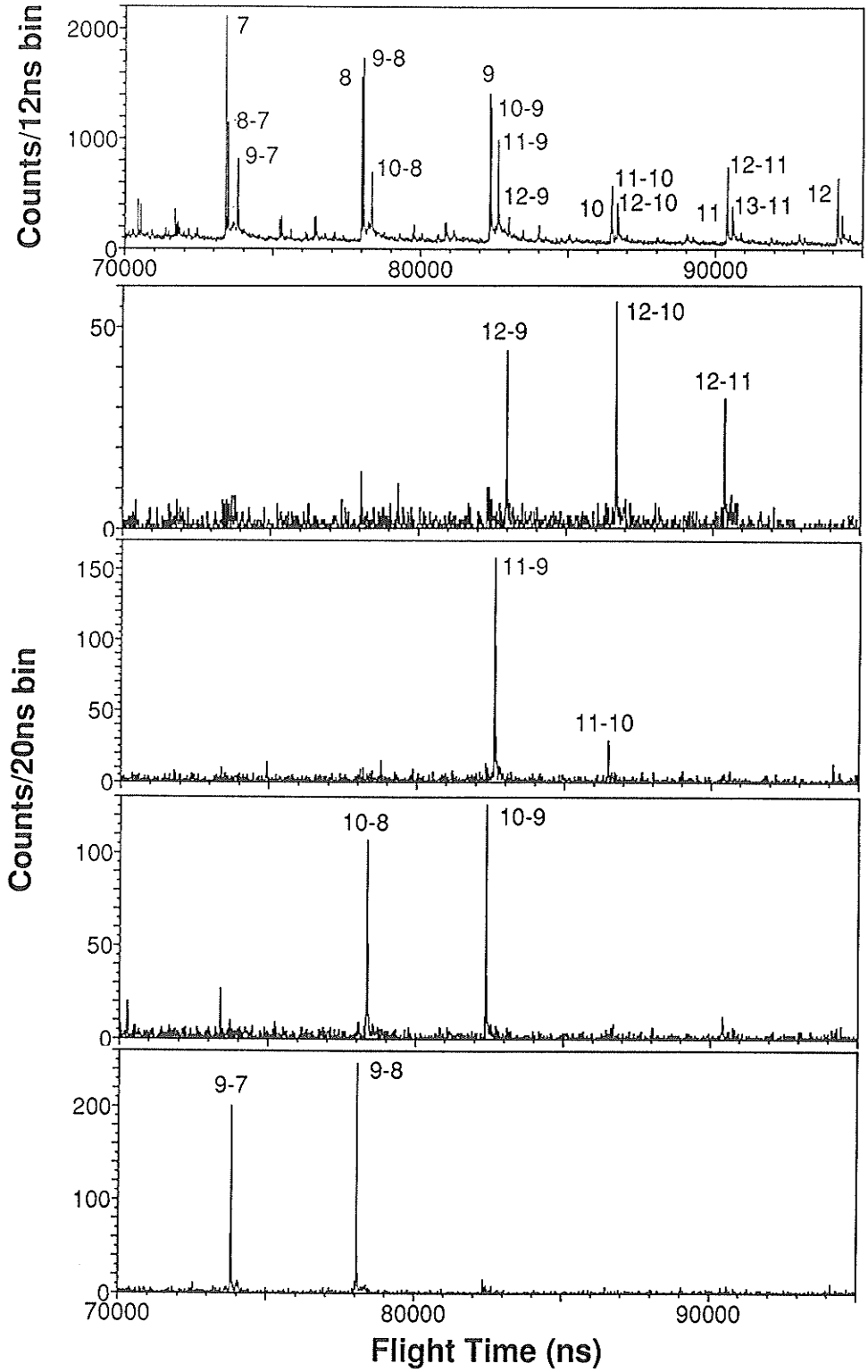

Figure 5.1 (a) TOF mass spectra of CsI: partial reflected spectrum (top) and daughter ion spectra of $(CsI)_nCs^+$ with n=9-12.

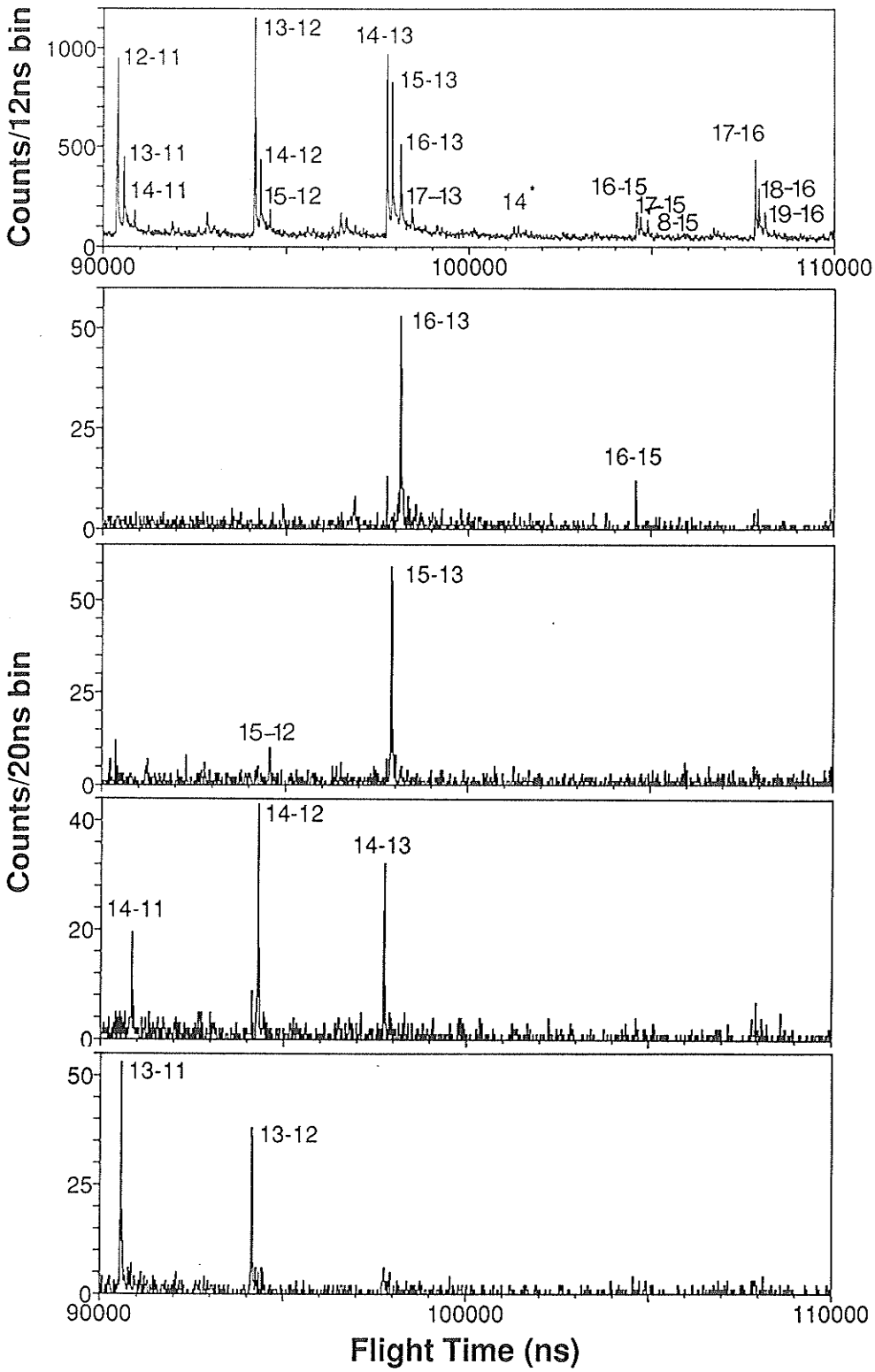

Figure 5.1 (b) TOF mass spectra of CsI: partial reflected spectrum (top) and daughter ion spectra of (CsI)nCs+ with n=13-16; the peaks labelled 14^{*} include n=14 daughters mainly from decay of parents with n=15 and 16.

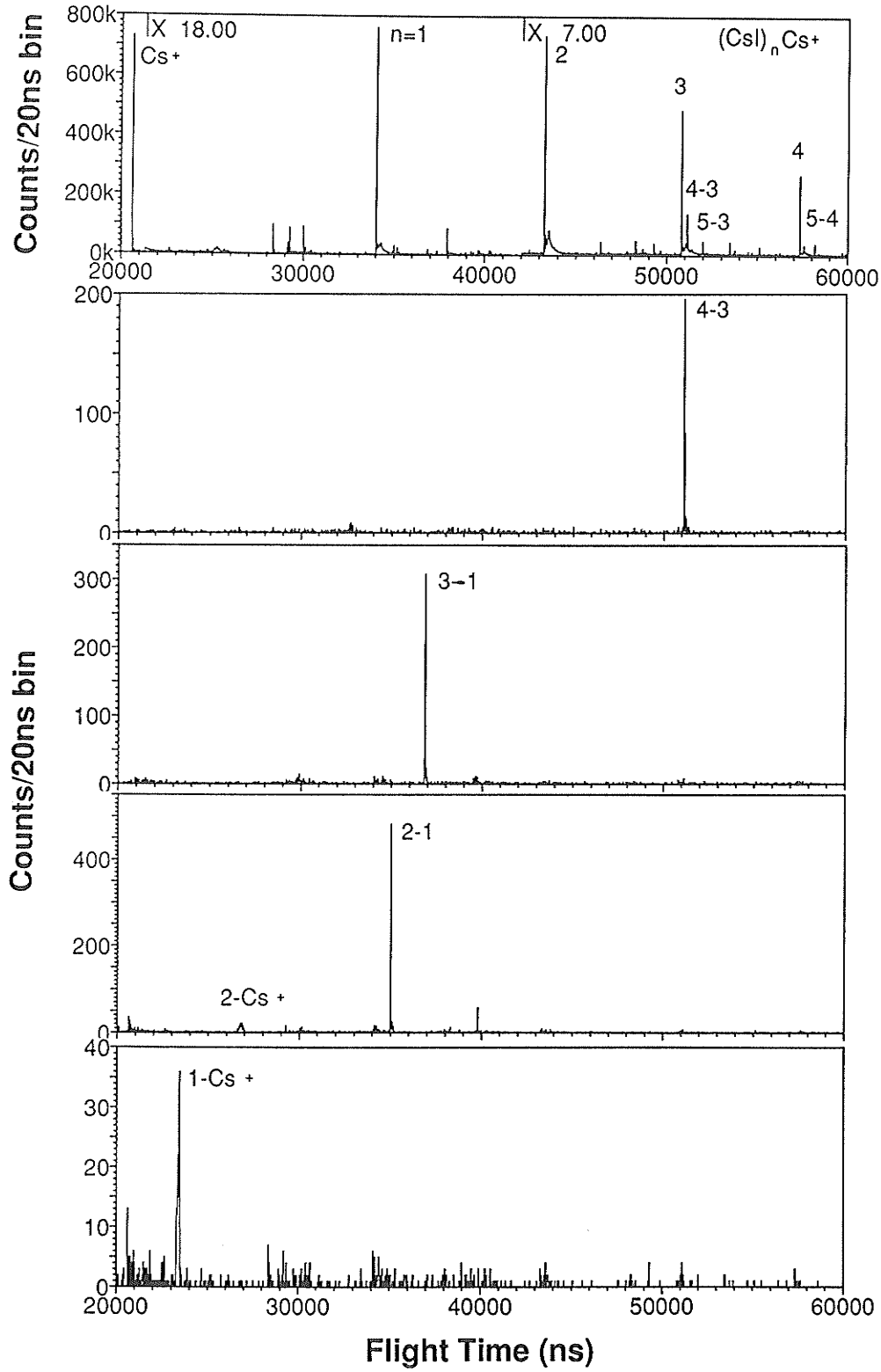

Figure 5.2 TOF mass spectra of CsI: partial reflected spectrum (top) and daughter ion spectra of $(CsI)_nCs^+$ with n=1-4.

Table 5.1 Major Decay Paths Observed for $(CsI)_nCs^+$ with n=1-16

P (n)	1	2	3	4	5	6	7	8	9	10	11	12	13	14	15	16
D (n)	Cs^+	Cs^+	1	3	1	4	5	6	7	8	9	9	11	11	12	13
		1			3	5	6	7	8	9	10	10	12	12	13	15
					4							11		13		

P (n)= Parent Ions Cluster Number n; D (n)=Daughter Ions Cluster Number n.

consequence of the improved efficiency of the correlated measurement [200] as discussed in §.4.3.2. Most of the daughter ions are formed by losing 1 or 2 neutral CsI groups; however, 3 or 4 CsI losses have also been observed. The major decay paths observed for $(CsI)_nCs^+$ parents with n=1-16 are listed in Table 5.1.

The relative stability of the clusters can be obtained from a reflected spectrum. Since this is equivalent to measuring the spectrum ≥10 μs after the ion emission (~10 μs for the first cluster parent ions), the cluster distribution reflected by the mirror is somewhat similar to that obtained in a sector field instrument (Fig. 5.3 [133-135]). For this plot, all the peaks corresponding to a product cluster at n are integrated, e.g. for n=7, the peaks labelled 7, 8→7 and 9→7 are integrated. For n>10, this corresponds to a distribution of daughter ions since very few parents are detected. As expected, n=13 is heavily favoured as a daughter ion while n=14 and 15 daughter ions are suppressed. Ejected cluster ions with n=13 [see Fig.5.1(b)] do not exhibit anomalous stability. This is consistent with the observations and conclusions made by Ens et al with the linear TOF instrument [133], since the charged alkali-halide clusters with a high degree of cubic symmetry, e.g., 3×3×3 at n=13, are expected to be particularly stable, and the addition of CsI molecules to these structures should have low binding energies.

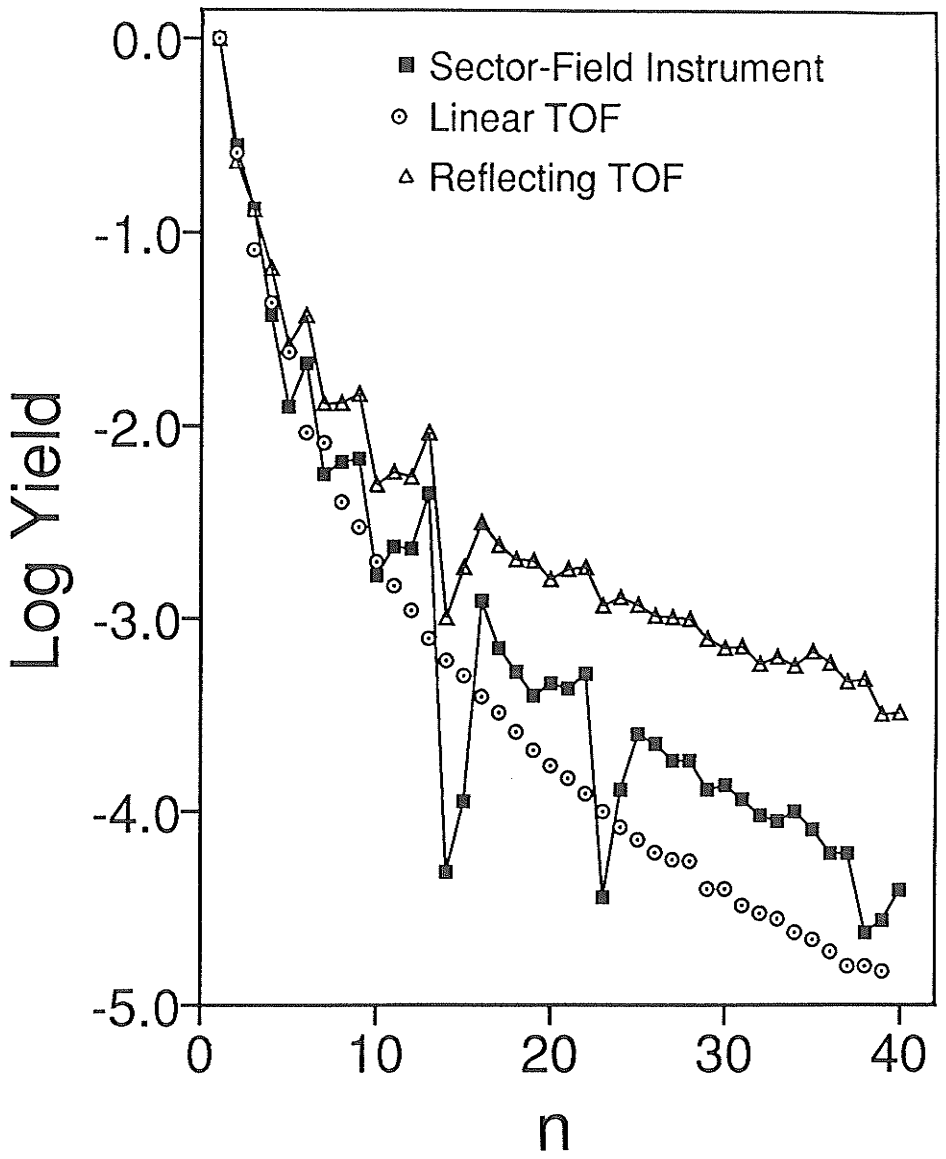

Figure 5.3 Relative yields of $(CsI)_nCs^+$ clusters measured in the reflecting TOF, in a linear TOF [133] and in a sector instrument [135], all normalized to n=1.

5.3 DAUGHTER ION SPECTRA AS A PROBE OF MOLECULAR STRUCTURE AND REACTION PATHWAYS FOR THREE SMALL PEPTIDES

5.3.1 Introduction

The advantages of daughter ion mass spectra for structure and reaction pathway analysis of ions have been well documented [40,42,150,151]. The use of the reflecting TOF mass spectrometer to analyze daughter ion mass spectra of metastable ions has been described in chapter 4. Some representative spectra have been presented for the decomposition of cationized molecules of glyycylglycylphenylalanine (GGF); similar results have been obtained from leucine-enkephalin and methionine-enkephalin. Since our early reports on these compounds [169,186], more decay paths have been observed and better signal-to-background ratios have been obtained for the daughter ion spectra; again this is because of the improved efficiency of the correlated measurement [200]. The daughter ion spectra, which can be analyzed with greater simplicity and less ambiguity than "direct" spectra, are strongly influenced by the identity of the bound cation (H^+, Na^+, K^+, or Ag^+). Many of the daughter ions are formed by known reactions, yielding structural and sequence information. In addition, the $[M+Na]^+$ and $[M+Ag]^+$ ions decompose by a previously unreported pathway [169], namely, rearrangement of a C-terminal carboxyl oxygen (as OH) onto the daughter ion containing the N terminal. This is, in fact, the main channel for $[M+Na]^+$ decay and accounts for large fraction of $[M+Ag]^+$ decompositions. This assignment is supported by ^{18}O-labelling studies of the C terminal of GGF. The spectra also illustrate the performance and capabilities of the instrument. It is interesting that, after our paper was submitted for publication, and after

the publication of the paper [169], several other groups drew similar conclusions about the oxygen migration from the C terminus in FABMS using conventional tandem instruments [208-212], and it was claimed as a useful "novel" reaction pathway in two recent publications [211,212].

5.3.2 Experimental

The peptide samples (Sigma Chemical Co.) were used as supplied. Labelling of the C terminus of GGF with ^{18}O was based on a method described in the literature [213].*1 To about 0.1 mg of peptide were added ca. 20 μL of $H_2{}^{18}O$ (97 atom % ^{18}O; Merck, Sharp and Dohme (Canada) Ltd.) and ca. 1 μL of 3 M HCl in a sealed vial. After 16 h at 42.5 °C volatiles were removed by evaporation and the residuel was analysed in the reflecting TOF mass spectrometer. This analysis indicated ca. 50% incorporation of ^{18}O into the peptide. For mass spectrometric study, a few micrograms of each sample, at a solute concentration of ca. 1 mg/mL in methanol, was either electrosprayed onto the metal surface of aluminized Mylar film, or deposited from methanol or 0.1% aqueous TFA solution to give a thin solid deposit on 12-50 mm^2 of an etched silver or nitrocellulose surface. The spectra of ^{18}O labelled GGF was reported earlier [169]; the other spectra of these three peptides presented in this thesis are spectra updated from the earlier version [169]. For these spectra, the samples were dissolved in 0.1% aqueous TFA instead of methanol, and the sample solutions were deposited on etched silver surfaces for GGF and leucine-enkephalin, and on nitrocellulose surfaces for methionine-enkephalin.

---

*1The labelling was done by Dr. Westmore in the Chemistry department of the University of Manitoba.

The secondary ions were accelerated to ~13 keV in these experiments instead of ~5 keV as in the early experiments [169], to improve the efficiency of the correlated measurements.

5.3.3 Results and Discussion

5.3.3.1 Glycylglycylphenylalanine (GGF)

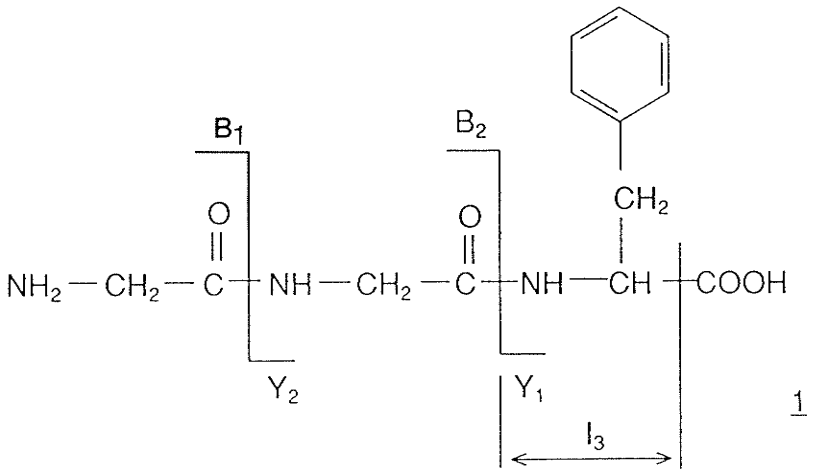

1

The spectra of GGF were shown in Fig. 4.2 and 4.3 in chapter 4, as an illustration of the principle of the correlated MS/MS measurement. A comparison between the peaks labelled $[M+H]^+$ and $[M+Na]^+$ in the direct and neutral spectra (Fig. 4.2a) and the daughter ion spectra for decomposition of $[M+H]^+$ and $[M+Na]^+$, presented in parts b and c of Fig. 4.2, respectively, shows that $[M+Na]^+$ ions undergo significantly less extensive decomposition. This indicates that $[M+Na]^+$ ions surviving the acceleration period (ca. 10^{-7}s) are significantly more stable than corresponding surviving $[M+H]^+$ ions. The results are summarized in Table 5.2. Two points can be made immediately. First,

TABLE 5.2 Daughter Ion Spectra of Cationized Molecules of GGF

Parent ion mass exptl (calcd)	Daughter ion mass exptl (calcd)	Assignment[a,b] (Positive ions)	Mass difference (exptl-calcd)
$[M+H]^+$	223.13 (223.11)	Y_2+2	0.02
280.15 (280.13)	166.08 (166.09)	Y_1+2	-0.01
	120.08 (120.08)	I_3+1	0.00
	115.07 (115.05)	B_2	0.02
	114.07 (114.04)	$(B_2Y_3)_2$	0.03
$[M+Na]^+$	188.03 (188.07)	Y_1+1+Na	-0.04
302.10 (302.12)	169.96 (170.06)	Y_1+1+Na-H_2O	0.10
	155.02 (155.05)	B_2+17+Na	-0.03
	22.98 (22.99)	Na	-0.01
$[M+^{107}Ag]^+$	339.97 (340.02)	A_3-1+Ag	-0.05
386.00 (386.03)	328.94 (329.00)	Y_2+1+Ag	-0.06
	281.88	?	
	282.97	?	
	271.95 (271.99)	Y_1+1+Ag	-0.04
	238.94 (238.96)	B_2+17+Ag	-0.02
	225.96 (225.98)	I_3+Ag	-0.02
	220.86 (220.95)	B_2-1+Ag	-0.09
	193.03 (192.95)	A_2-1+Ag	0.08
	181.90 (181.94)	B_1+17+Ag	-0.04

[a] $I_3=C_8H_9N$; $B_2=C_4H_7N_2O_2$; $Y_1=C_9H_{10}NO_2$; $Y_2=C_{11}H_{13}N_2O_3$. [b] Assumes 1=H; 2=2H.
see Appendix B for the notations used in the assignments.

considerable variation in the stabilities and decomposition pathways of the different cationized molecules is apparent. Second, information about ion decomposition can be extracted from the reflected and daughter ion mass spectra with greater simplicity and less ambiguity than from a direct mass spectrum. The second point is particularly important because matrix effects and the presence of impurities in the sample are minimized. In this respect the advantages of the present technique are similar to those of daughter ion studies made by other methods. As will be shown later, structural information for other small

peptides can also be readily obtained.

Before discussing the structural detail that can be derived from the daughter ion spectra, it is appropriate to assess the confidence that can be placed on the measured masses by comparing experimental and calculated masses (most abundant isotopes) based on the assignments given. As shown in Table 5.2, the calculated masses of parent and daughter ions are consistently within 0.1 u of the experimental masses. The largest differences are associated with small peaks. For such peaks, poor counting statistics mean that centroid determination is imprecise. The small errors of the error for known ions means that, for all ions, the nominal masses are not in doubt, and the assignments are expected to be quite accurate. (For the relatively low mass ions studied here the concept of nominal mass is still meaningful.)

The formation of some daughter ions can be explained by bond fissions accompanied by incorporation of up to two extra hydrogen atoms or a metal cation to give ion structures expected to be stable. Specifically, these are B_2, Y_1+2, Y_2+2, and I_3+1 (see Appendix B for the notations), which are known fragmentations [40], together with the silver analogues Y_1+1+Ag, Y_2+1+Ag and I_3+Ag etc (see Table 5.2). Sequence information can be obtained directly from some of these.

A significant new finding is the appearance in these spectra of abundant B_2+17+Na and B_2+17+Ag daughter ions. These represent a major channel of decay from $[M+Na]^+$ and $[M+Ag]^+$, respectively, and have no analogue among the daughter ions from $[M+H]^+$. These ions are *not* analogues of C_n+2, i.e. C_n+1+Na/Ag, that have been reported in peptide mass spectra [40]. The latter ions would correspond to B_2+16+Na/Ag. At the same time, when Na^+ or Ag^+ is bound to the peptide molecule, the fragmentations leading to B_2 and Y_2+2 (or their Na or Ag analogues) are suppressed. This implies that the metal

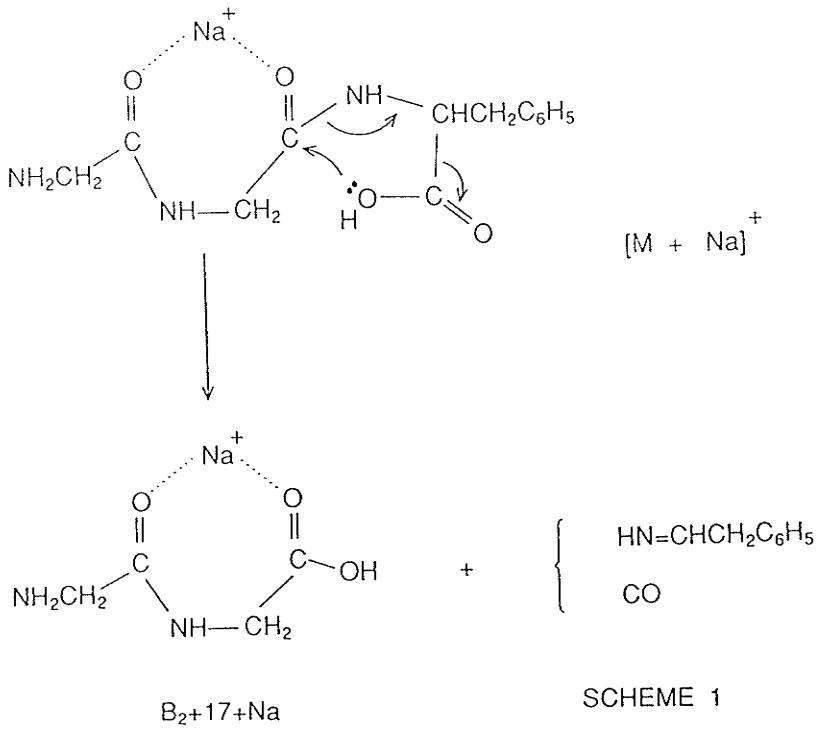

B_2+17+Na

SCHEME 1

ions are bound to the peptide in such a way that peptide bond fission is prevented. Chelation of the peptide to the metal ions offers an attractive mechanism for reducing the number of decomposition channels and diverting the fragmentation along alternative pathways. It is known that, in solution, Na^+ binds preferentially to peptide carbonyls [214]. If this is also true in the gas phase, then the decomposing form of $[M+Na]^+$ may be as depicted in Scheme I. Although Na^+ attachment to the carbonyl oxygen increases the double bond character of the amide CN bond, it also makes the carbon atom more susceptible to nucleophilic attack. (The *net* result of these competing effects may be quite sensitive to the actual cation that is bound.) The hydroxyl of the terminal carboxyl group is suitably placed for just such attack and thereby to trigger the rearrangement shown, which leads also to stable neutral species. Thus, B+17+Na/Ag is assigned as B+OH+Na/Ag. This even-electron species is to be preferred over an alternative

assignment such as the odd-electron species B+NH_3+Na/Ag. The alternative assignment has several problems: it is not apparent where to place the two rearranged hydrogens, even-electron parent ions tend to decompose to even-electron rather than odd-electron daughters, and it is difficult to conceive of stable neutral species that could be eliminated. Support for the mechanism proposed in Scheme I is provided by ^{18}O-labelling studies to be described later.

The nature of the binding of Ag^+ to the peptide is not well documented. If we assume, from the well-known complexing of Ag^+ by amines, that Ag^+ binds preferentially

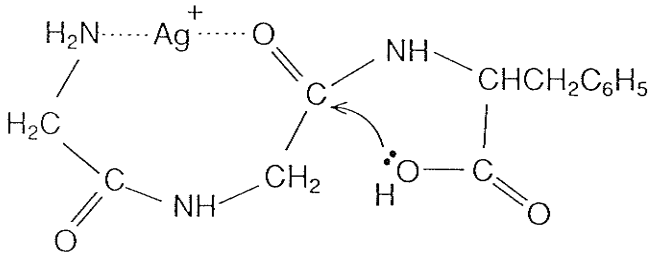

$[M + Ag]^+$

to the primary amino group and note that Ag^+ has a strong tendency to form collinear bonds, then it is geometrically possible for Ag^+ to also bind to the second peptide carbonyl removed form the peptide N terminus, as shown in the structure. (Note that this is not possible for the peptide carbonyl first removed from the N terminus.) Such a structure could undergo a decomposition similar to that depicted in Scheme I for $[M+Na]^+$.

5.3.3.2 Leucine-enkephalin and methionine-enkephalin.

Fig. 5.4 shows daughter ion spectra for the various cationized molecules of Leu-enkephalin [215] deposited on an etched silver surface. Fig. 5.5 shows a partial reflected

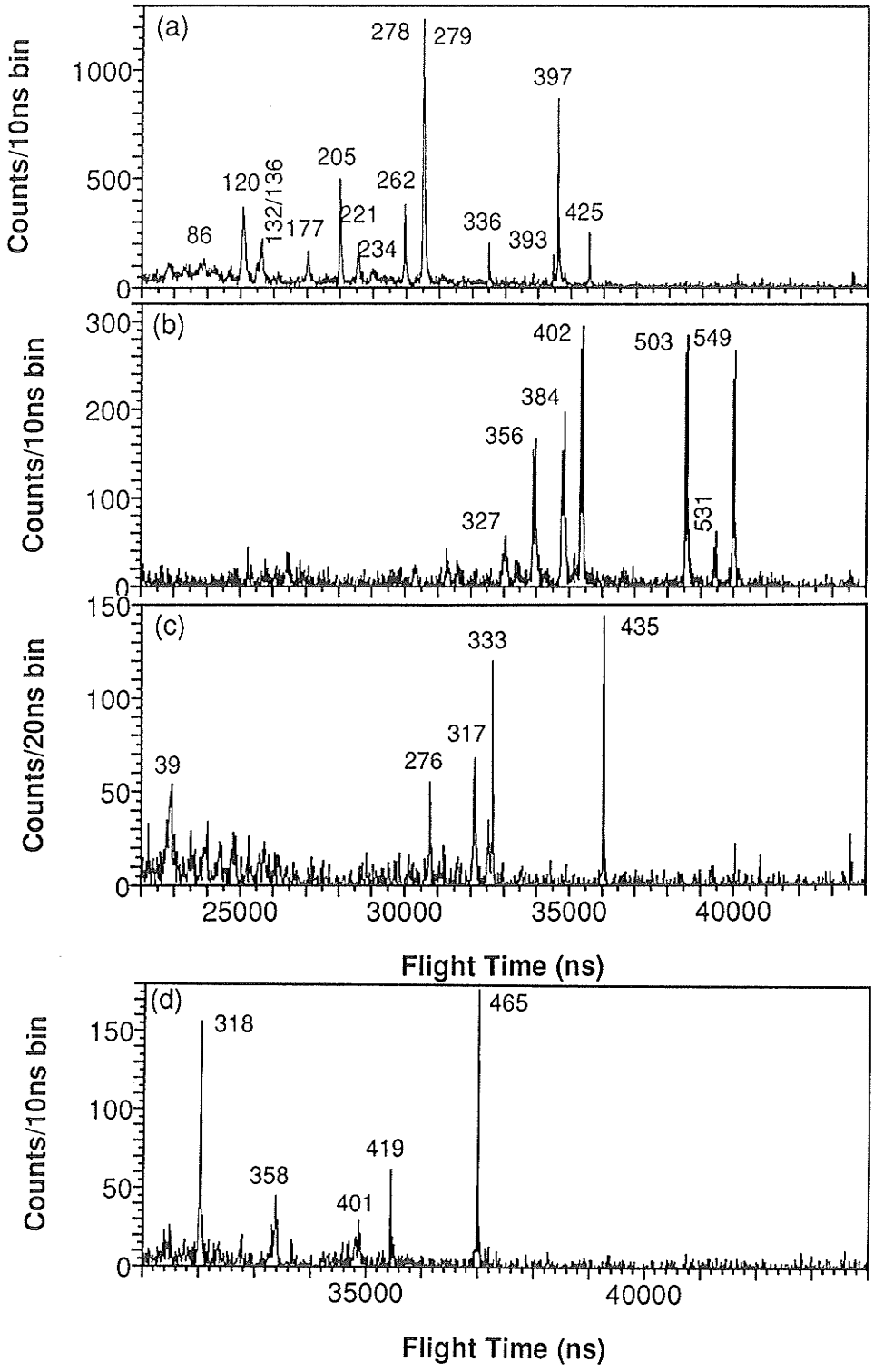

Figure 5.4 Daughter ion mass spectra of parent ions from Leu-enkephalin deposited on etched silver: (a) $[M+H]^+$, (b) $[M+Ag]^+$, (c) $[M+K]^+$, (d) $[M+Na]^+$. Nominal masses of daughter ions are shown.

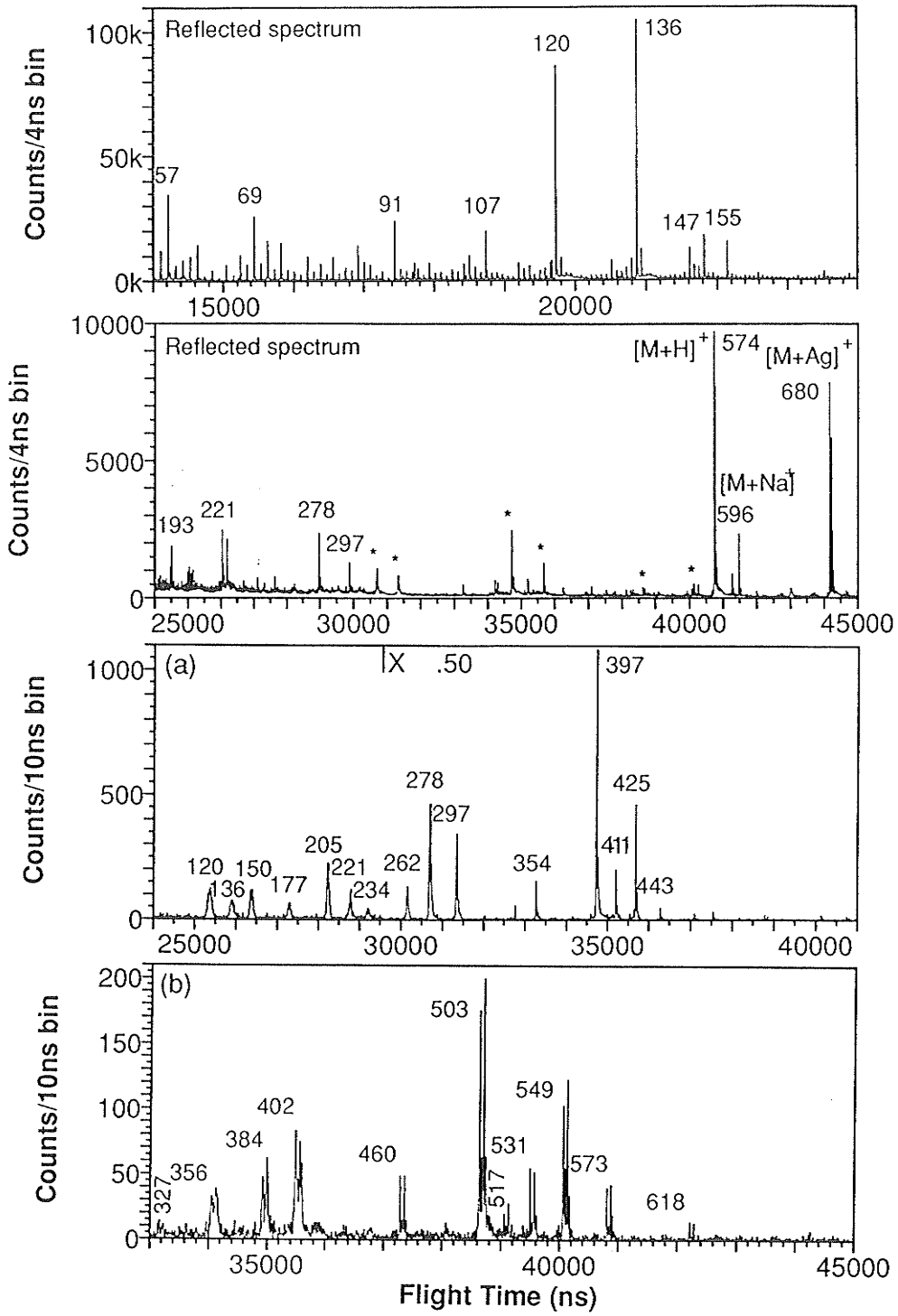

Figure 5.5 Reflected and daughter ion mass spectra from Met-enkephalin deposited on nitrocellulose electrosprayed onto a silver backing: (top) partial reflected spectrum; nominal masses of stable ions are shown. Peaks denoted by an asterisk correspond to daughter ions. (bottom) daughter ion spectra of (a) $[M+H]^+$, (b) $[M+Ag]^+$. Nominal masses of daughter ions are shown.

ion spectrum and daughter ion spectra of $[M+H]^+$ and $[M+Ag]^+$ for Met-enkephalin [216] deposited on a nitrocellulose surface; some peaks labelled with asterisks in the reflected spectrum result from daughters of metastable parent ions. It is interesting that for methionine enkephalin, strong silver adducted molecular ions have been observed even when the sample solution (dissolved in 0.1% aqueous TFA) was deposited on a nitrocellulose surface, which had been electrosprayed on a silver foil backing, and the foil was thought to be fully covered with nitrocellulose. It can be seen from the reflected spectrum that the $[M+Ag]^+$ doublet is intense and there are no Ag^+ peaks in the spectrum. The m/z 107 peak is a fragment from tyrosine, not from silver, because silver ions would appear as a doublet, m/z 107 and m/z 109 u, with respective relative abundances of 51.83% and 48.17%. This phenomenon has not been observed for GGF and leucine-enkephalin deposited on the nitrocellulose surface. Tables 5.3 and 5.4 summarize the

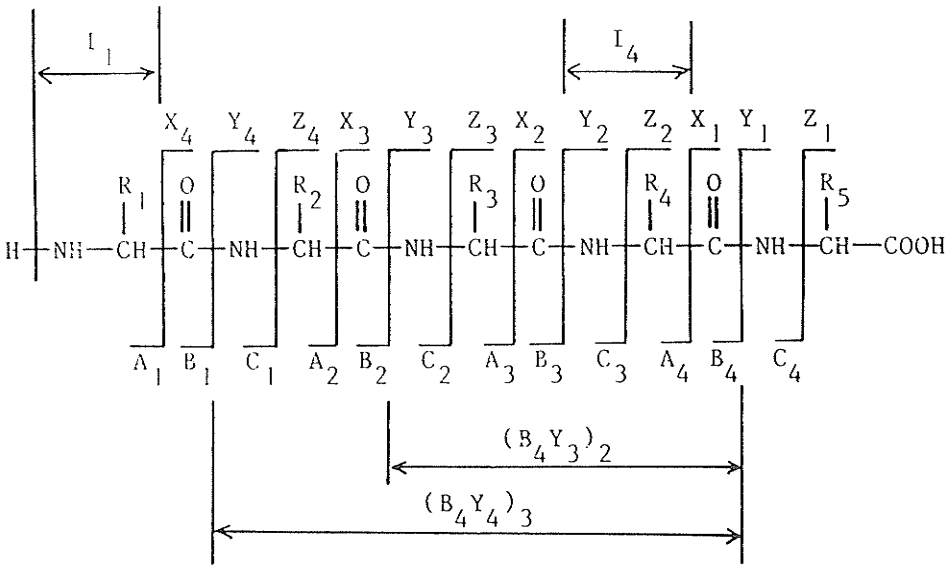

2 and 3: $R_1 = CH_2C_6H_4OH$; $R_2 = R_3 = H$; $R_4 = CH_2C_6H_5$

2: $R_5 = CH_2CH(CH_3)_2$ (leu); 3: $R_5 = CH_2CH_2SCH_3$ (met)

TABLE 5.3. Daughter Ion Spectra of Cationized Molecules of Leu-Enkephalin

Parent ion Mass exptl (calcd)	Daughter ion mass exptl (calcd)	Assignment[a,b] (positive ion)	mass difference (exptl-calcd)
$[M+H]^+$ $C_{28}H_{38}N_5O_7$	425.22 (425.18)	B_4	0.04
556.31 (556.29)	397.20 (397.19)	A_4	0.01
	393.18 (393.21)	Y_4+2	-0.03
	336.19 (336.19)	Y_3+2	0.00
	279.08 (279.17)	Y_2+2	-0.09
	278.16 (278.11)	B_3	0.05
	262.28 (262.12)	$(B_4Y_4)_3$+1	0.16
	234.38 (234.12)	$(A_4Y_4)_3$+1	0.26
	221.06 (221.09)	B_2	-0.03
	205.19 (205.10)	$(B_4Y_3)_2$+1	0.09
	177.05 (177.10)	$(A_4Y_3)_2$+1	-0.05
	136.04 (136.07)	I_1+1	-0.03
	132.17 (132.10)	Y_1+2	0.07
	120.22 (120.08)	I_4+1	0.14
$[M+Na]^+$	465.13 (465.17)	B_4+17+Na	-0.04
$C_{28}H_{37}N_5O_7Na$	419.13 (419.17)	A_4-1+Na	-0.04
578.28 (578.26)	358.19 (358.17)	Y_3+1+Na	0.02
	318.11 (318.11)	B_3+17+Na	0.00
$[M+K]^+$	435.14 (435.14)	A_4-1+K	0.00
$C_{28}H_{37}N_5O_7K$	333.19 (333.10)	C_3+1+K	0.09
594.23 (594.20)	316.95 (317.13)	Y_3+1+K	-0.02
	276.21 (276.07)	C_2+1+K	0.14
	38.62 (38.96)	K	-0.03
$[M+^{107}Ag]^+$	549.02 (549.09)	B_4+17+Ag	-0.07
$C_{28}H_{37}N_5O_7Ag$	531.04 (531.08)	B_4-1+Ag	-0.04
662.17 (662.17)	503.05 (503.08)	A_4-1+Ag	-0.03
	442.07 (442.09)	Y_3+1+Ag	-0.02
	401.99 (402.02)	B_3+17+Ag	-0.03
	384.01 (384.01)	B_3-1+Ag	0.00
	356.07 (356.02)	A_3-1+Ag	0.05
	326.67 (326.99)	B_2-1+Ag	-0.32
*$[M+2Na-H]^+$	493.09 (493.19)	Q-$CH_2C_6H_4OH$	-0.10
$C_{28}H_{36}N_5O_7Na_2$	436.93 (437.18)	Y_4+2Na	-0.25
600.22 (600.24)	418.90 (419.17)	A_4-1+Na	-0.27
$C_{28}H_{36}N_5O_7Na$=Q	379.99 (380.16)	Y_3+2Na	-0.17
	338.86 (339.10)	C_3+2Na	-0.24
	322.99 (323.13)	Y_2+2Na	-0.14
	281.92 (282.08)	C_2+2Na	-0.16
	225.29 (225.06)	C_1+2Na	0.23
	175.94 (176.07)	Y_1+2Na	-0.13

[b]Assumes 1=H; 2=2H; 16=NH_2; 17=OH.
*Earlier results [169].

TABLE 5.4. Daughter Ion Spectra of Cationized Molecules of Met-Enkephalin

Parent ion Mass exptl (calcd)	Daughter ion mass exptl (calcd)	Assignment[a,b] (positive ion)	mass difference (exptl-calcd)
$[M+H]^+$	443.20 (443.19)	B_4+17+H	0.01
$C_{27}H_{36}N_5O_7S$	425.25 (425.18)	B_4	0.07
574.27 (574.23)	411.17 (411.17)	Y_4+2	0.00
	397.24 (397.19)	A_4	0.05
	354.15 (354.15)	Y_3+2	0.00
	297.23 (297.13)	Y_2+2	0.10
	278.20 (278.11)	B_3	0.09
	262.10 (262.12)	$(B_4Y_4)_3$+1	-0.02
	233.83 (234.12)	$(A_4Y_4)_3$+1	-0.29
	220.96 (221.09)	B_2	-0.13
	205.01 (205.10)	$(B_4Y_3)_2$+1	-0.09
	177.09 (177.10)	$(A_4Y_3)_2$+1	-0.01
	150.03 (150.06)	Y_1+2	-0.03
	135.77 (136.07)	I_1+1	-0.30
	119.88 (120.08)	I_4+1	-0.20
$[M+Na]^+$	465.21 (465.17)	B_4+17+Na	0.04
$C_{27}H_{36}N_5O_7SNa$	419.13 (419.17)	A_4-1+Na	-0.04
596.24 (596.22)	358.19 (358.17)	Y_3+1+Na	0.02
	318.11 (318.11)	B_3+17+Na	0.00
*$[M+K]^+$	434.98 (435.14)	A_4-1+K	-0.16
$C_{27}H_{36}N_5O_7SK$	333.08 (333.10)	C_3+1+K	-0.02
612.20 (612.19)	317.11 (317.13)	Y_3+1+K	-0.02
	276.22 (276.07)	C_2+1+K	0.15
$[M+^{107}Ag]^+$	618.11	?	
$C_{27}H_{36}N_5O_7SAg$	573.18	?	
680.15 (680.13)	549.16 (549.09)	B_4+17+Ag	0.07
	531.13 (531.08)	B_4-1+Ag	0.05
	517.08 (517.07)	Y_4+1+Ag	0.01
	503.16 (503.08)	A_4-1+Ag	0.08
	460.11 (460.04)	Y_3+1+Ag	0.07
	402.30 (402.02)	B_3+17+Ag	0.28
	384.03 (384.01)	B_3-1+Ag	0.02
	355.96 (356.02)	A_3-1+Ag	-0.06
	326.90 (326.99)	B_2-1+Ag	-0.09

[b]Assumes 1=H; 2=2H; 16=NH_2; 17=OH.
*Earlier results [169].

daughter ions obtained from cationized molecules of Leu-enkephalin and Met-enkephalin, respectively, which differ only in the C-terminal amino acid. Since methionine has a molecular mass 18 u greater than that of leucine, it is easily possible to identify those ions containing the C-terminal amino acid residue. In addition to proton and sodium ion attachment, potassium ion attachment is observed for these molecules. Although the abundance of $[M+K]^+$ in the spectra is never large, this species is less stable than $[M+Na]^+$ and yields a daughter ion spectrum of reasonable quality for both molecules. As can be seen, the reflected spectrum can be very complex due to daughter ions from the metastable decompositions of various parents, but the daughter ion spectra obtained is much "cleaner".

An attempt to generate $[M+Cs]^+$ ions of Leu-enkephalin by spiking the sample with cesium iodide resulted instead in the detection of Cs^+, without any evidence in the spectrum for $[M+Cs]^+$ (or any Cs-containing fragment ions). Attachment of Na^+ ions was greatly enhanced probably because of the Na^+ impurity in the CsI sample, producing a significant yield of $[M+2Na-H]^+$ ions. (Since water was not rigorously excluded during sample preparation, it may compete with the peptide for binding of alkali-metal ions. It has been pointed out [219] that, when water is excluded, Cs^+ bonds very strongly to oxygen in ether linkages to form stable $[M+Cs]^+$ ions.) The number and yield of daughter ions produced by decomposition of $[M+2Na-H]^+$, listed in Table 5.3 indicate it to be less stable than $[M+Na]^+$.

As before, several of the ions in Tables 5.3 and 5.4 can be directly explained by a simple bond fission, together with the incorporation of hydrogen or metal atoms, if necessary. From these, sequence information can readily be deduced but will not be elaborated upon here, since this is self-evident from the tables. Furthermore, the daughter

ions from unimolecular decomposition of $[M+H]^+$ are similar to those reported by others [215-218] for collisionally induced decompositions. Instead, some other noteworthy features of the daughter ion spectra are now discussed.

The hydroxyl transfer mechanism proposed in Scheme I for the decomposition of $[M+Na]^+$ and $[M+Ag]^+$ ions of GGF can be invoked to explain the formation of B_4+17+(Na/Ag) and B_3+17+Na/Ag) daughter ions from the enkephalins. For B_4+17+(Na/Ag) this would be analogous to that proposed for GGF in Scheme I. The B_4+17+(Na/Ag) ion can be regarded as the $[M+(Na/Ag)]^+$ ion of a tetrapeptide and after reorganization of the metal-peptide bonds could decompose to B_3+17+(Na/Ag), again by the mechanism of Scheme I. Scheme II depicts an alternative mechanism for the formation of B_3+17+(Na/Ag) from $[M+Ag]^+$. The presence of B_4+17+H as a daughter ion

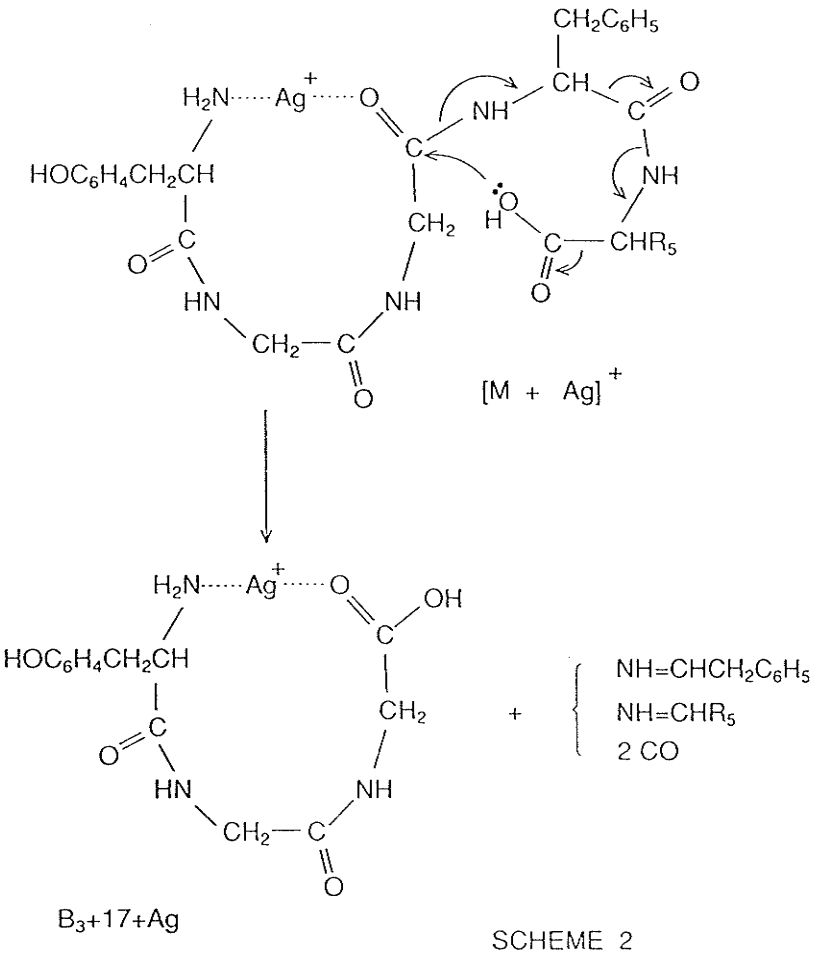

SCHEME 2

of $[M+H]^+$ of Met-enkephalin is an indication that an analogous decomposition reaction *can* occur for protonated molecules, though less readily. Furthermore, the decomposition reaction has not been observed for $[M+K]^+$ of either molecule, suggesting perhaps, that the carbonyl carbon is less susceptible to nucleophilic attack when K^+ rather than Na^+ or Ag^+ is bound to carbonyl oxygen.

In the case of the Ag-containing ions, further ions are observed 18 and 46 u lower than B_n+17+Ag. These have been assigned as B_n-1+Ag and A_n-1+Ag, respectively. They could be analogues of known B_n and A_n species that are formed directly from $[M+Ag]^+$ but might be formed from B_n+17+Ag, by simple losses of H_2O or HCOOH, respectively.

The *m/z* 262, 205, 234 and 177 ions are interior fragments. The first two have previously been assigned an acylium ion structure [40], consistent with B-type ions as their immediate precursors. They can be represented by a two-letter code, based on that originally suggested [205], as $(B_4Y_4)_3$+1 and $(B_4Y_3)_2$+1, respectively. In these codes the first letter indicates the first bond cleaved (perhaps not implied in the original proposal), and the last subscript denotes the number of amino acid residues contained in the ion fragment. (Note that this value, when subtracted from the sum of the subscripts within the parentheses, gives the number of amino acid residues in the intact peptide.) However, if

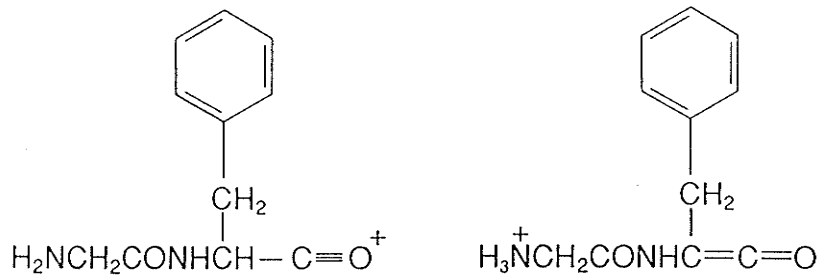

m/z 205

Y_3+2 and Y_4+2 are their precursors, then an ammonium ion structure seems more probable. The isomeric ion structures for *m/z* 205 are as shown. Experimental confirmation of the actual precursors has not been achieved because the correlated spectra for decomposition of these putative precursor ions are too weak.

$[M+K]^+$ ions, upon fragmentation, yield a number of sequence-related daughter ions. Interestingly, these differ from the sequences of daughter ions from $[M+H]^+$.

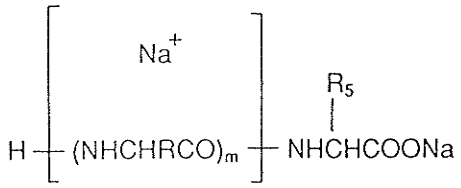

Y_n+2Na (m = 0 - 3)

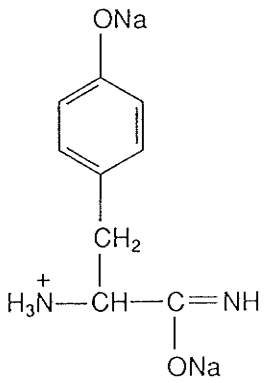

C_1+2Na

Most of the daughter ions from $[M+2Na-1]^+$ retain two sodium atoms. Those in the Y_n+2Na series likely have structures based on that shown. The prominence of C_1+2Na in the C_n+2Na sequence suggests the involvement of the phenolic group of tyrosine, as shown. However, the phenolic group is not essential because even phenylalanine can form an $[M+2Na-1]^+$ ion [220].

5.3.3.3 ^{18}O-Labelling studies.

Labelling studies with ^{18}O fulfilled two purposes: (a) to provide support for the mechanism proposed in Scheme I and (b) to evaluate the current capability of the instrument in selecting specifically labelled parent ions for daughter ion analysis. This

technique, of course, is well-known when double (or higher) sector, triple quadrupole, or FT mass spectrometers are used, but has not been used frequently with TOF instruments [169,236].

Labelling of the C-terminal COOH group of peptides with ^{18}O is achieved under acidic conditions that may also promote hydrolysis of the peptide. We did succeed, however, in achieving sufficient ^{18}O incorporation into GGF for these studies. The extent of incorporation was determined from the areas of the peaks in the $[M+H]^+$, and $[M+Ag]^+$ regions of the reflected spectrum [169]. The P/(P+2)/(P+4) ratios were 33.9:43.7:22.4 and 44.5:40.3:15.2 for $[M+H]^+$ and $[M+Na]^+$, respectively, and 23.4:46.3:25.3:4.9 for P/(P+2)/(P+4)/(P+6) of $[M+Ag]^+$. (P represents the isotopic ion of lowest *m/z* value in the natural abundance ion group corresponding to the indicated ion type.) These ratios lead to calculated incorporations of 43.7, 40.3, and 48.2% for a single ^{18}O and 22.4, 15.2, and 5.0% for two ^{18}O atoms, respectively. The $[M+Na]^+$ ratios are probably the most reliable owing to the greater signal/background ratio.

To study decompositions of isotopically-labelled parent ions it is necessary to record daughter ions in detector 2 that correspond to arrival of the associated neutral species in detector 1. In principle, a time window should be selected such that only events corresponding to a specific isotopically labelled species are used. In practice, the success of this strategy depends upon the width of the peak corresponding to the arrival of the neutral species. The results described here illustrate three different situations.

For decomposition of $[M+H]^+$ ions the neutral species peaks observed in detector 1 with the mirror on are relatively broad. Consequently, a relatively wide time window was selected to include all isotopically labelled components of $[M+H]^+$. The daughter ion spectrum [169] confirmed, as expected, that the ^{18}O label is located on the C terminal.

The measured P/(P+2)/(P+4) ratios for the C terminal Y_1+2 (*m/z* 166/168/170) and Y_2+2 (223/225/227) fragments were 47.5:44.8:7.7 and 51.6:48.4:0, respectively, i.e. close to the values above for ^{18}O incorporation into the intact molecule. Incorporation of ^{18}O into the B_2 ion (*m/z*115) was not detected, but the signal involved was, admittedly, very small. Thus, within experimental error, all of the ^{18}O is located at the C terminal.

To study decomposition of $[M+Na]^+$, it is possible to open a narrow time window that selects individual isotopically labelled parent ions. The neutral species peak profile is shown in Fig. 5.6a. When a narrow time window centred on 18.56 μs is used to select the *m/z* 302 parent (unlabelled), the B_2+17+Na daughter is observed unshifted at *m/z* 155, as expected [169]. (Actually, ca. 5% of the ^{18}O-labelled daughter is recorded at *m/z* 157 because some neutrals from ^{18}O parents fall within the time window for neutrals from ^{16}O parents.) When a narrow time window centred on 18.64 μs is used to select the neutral from *m/z* 304 labelled parent (Fig. 5.6a), the daughter ions are recorded at *m/z* 155 and

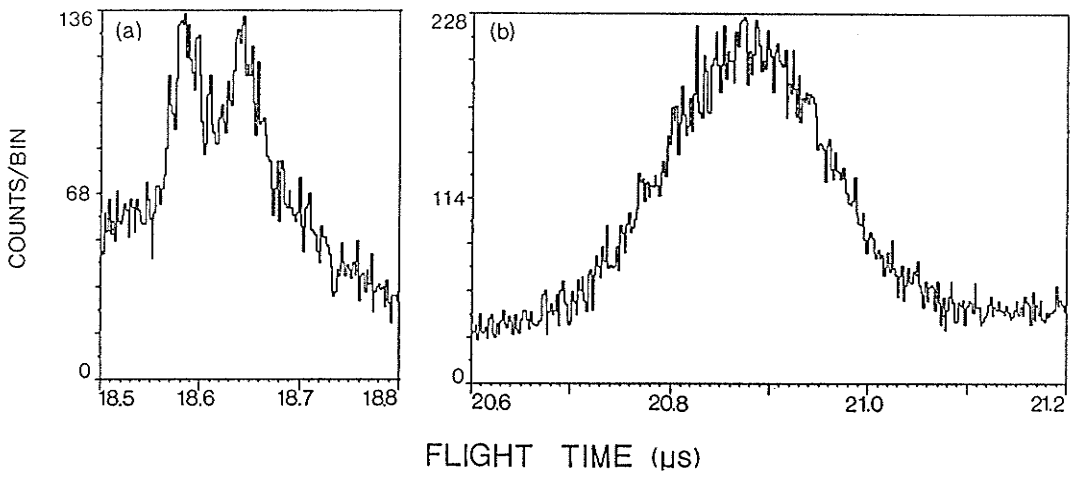

Figure 5.6 Neutral species peak profile for decompositions of ions from ^{18}O-labelled GGF; (a) $[M+Na]^+$, (b) $[M+Ag]^+$. (Time bins of 2 ns are used in both cases). In (a) the flight times of neutral decay products from labelled and unlabeled ions are partially resolved.

157 in the ratio 55:45 [169]. Ideally, this ratio should be 50:50 for incorporation of one of the two COOH oxygens into the N-terminal daughter. The deviation is ascribed to imperfect selection of the neutral from the *m/z* 304 parent by the time window; i.e. some neutrals from *m/z* 302 parents are included within it. Only an oxygen transfer to the N-terminal ion fragment, such as that proposed in Scheme I, can account for this result.

To study decomposition of $[M+Ag]^+$ ions, it was not possible to adjust the time window to select a neutral from a specifically labelled parent ion. The neutral species peak profile from $[M+Ag]^+$ decompositions, shown in Fig. 5.6(b), is virtually structureless. Adjusting the time window served only to change the isotopic percentages in the daughter ions. Nevertheless, the extent of ^{18}O incorporation into B_2+17+Ag can be estimated. The *m/z* 226/228 ratio of 51.2:48.8 gives the ratio of Ag isotopes in the I_3+Ag ion. Assuming that this ratio is maintained in other daughter ions, the *m/z* 272/274/276 ratio of 22.0:51.4:26.6 for Y_1+1+Ag then yields a ratio of 42.0:58.0:0 for $^{16}O_2$:$^{16}O^{18}O$:$^{18}O_2$. Similarly, the *m/z* 239/241/243 ratio of 34.0:48.9:17.0 yields a ratio of 65.7:31.7:2.6 for $^{16}O_2$:$^{16}O^{18}O$:$^{18}O_2$ in B_2+17+Ag. Thus, it incorporates ca. 55% of the ^{18}O available in the parent $[M+Ag]^+$ ion. This is very close to the value of 50% required to support the mechanism of Scheme I.

These results can be compared to two recent studies of decomposition of cationized peptide molecules. In the first study, in which a reflecting TOF mass spectrometer was used, $[M+Na]^+$ ions of Leu-enkephalin and Met-enkephalin were reported to give daughter ions of *m/z* 317 and 464 [221]. These were assigned as C_n-type fragments (with Na^+ addition) but probably correspond to the ions we observe at *m/z* 318 and 465 (Tables 5.3 and 5.4) formed by oxygen transfer from the C terminal. The second study recorded the decompositions of cationized molecules of hippurylhistidylleucine in

a triple sector (EBE) mass spectrometer [217]. The daughter ion spectra of collisionally activated $[M+H]^+$ and $[M+Na]^+$ ions, produced by xenon atom bombardment of the sample in a thioglycerol/glycerol matrix spiked with the alkali-metal chloride salt, were quite different from each other, in agreement with the present observations. Of particular interest to our study is a daughter ion of $[M+Na]^+$ at *m/z* 338±1 that could correspond to B_3+17+Na (in the current symbolism), for which *m/z* 339 is required.

We may also compare a secondary ion mass spectrum of 2-Ala-5-Leu-enkephalin on etched silver, recently measured in an ion cyclotron mass spectrometer [222]. Ions were observed at *m/z* 332 and 479 and assigned as inner fragments; however, these are, in fact, the values predicted for B_3+17+Na and B_4+17+Na, respectively. The corresponding doublets for Ag addition also appear in the spectra, although they are not listed in the tables.

It therefore appears likely that the type of rearrangement discussed above has been observed previously but was unrecognized because of instrumental limitations. The present technique has provided identification of the parent ion decaying into a given daughter, as well as accurate measurement of the daughter ion mass, *both* of which are necessary for determination of the decay pathways. Similar conclusions, or evidence supporting the rearrangement, have been reported recently by several groups using conventional tandem mass spectrometers [208-212].

Qualitatively, the daughter ion spectra observed in the reflecting TOF mass spectrometer are similar to those generated by collisional activation in other types of instruments. For instance, the daughter ion spectrum of Leucine-enkephalin (Fig. 5.4 a) observed here is almost identical to that produced by collisionally activated decomposition in a hybrid tandem mass spectrometer with EBqQ or BEqQ configuration [218]. Our

ability to observe daughter ion spectra without resorting to collisional activation is a consequence of different internal energy excitation of secondary ions due to different matrices used (solid matrix used in our studies, liquid matrix used in other types of instruments). Also important are the earlier observational time frame for decompositions in a TOF instrument (10^{-7}-10^{-6}s) compared to that of sector-field (10^{-5}-10^{-4}s), triple quadrupole (10^{-4}-10^{-3}s), or FT-ICR (10^{-2}-10^{0}s) instruments, as well as our ability to observe fragmentations that occur anywhere within the first leg of the flight path of the reflecting TOF instrument.

5.4 PEPTIDE SEQUENCING

5.4.1 Introduction

Considerable effort have been made in the development and application of mass spectrometric methods for analysis of involatile and thermolabile biomolecules, such as peptides and nucleotides, in particular, for sequence determination of peptides. The application of mass spectrometry to obtain sequence information for a small peptide was first reported thirty years ago [223]. Such measurements required chemical derivatization to enhance sample volatility, but the advent of methods to produce desorbed ions directly from a liquid or solid substrate has enabled the derivatization step to be avoided. Mass spectra of involatile non-derivatized peptides can now be obtained by bombarding the sample with energetic ions, or photons [40,224] as discussed in chapter 1.

In spite of these advances, it is frequently difficult to extract much structural

information from the normal FAB mass spectrum obtained in conventional mass spectrometers. The peptide $[M+H]^+$ ions often exhibit little fragmentation and the fragment ions observed are difficult to distinguish from artifacts, such as background ions from a liquid matrix. These difficulties have stimulated the application of tandem mass spectrometry [150,151] to peptide analysis, using instruments of various configurations. As discussed in chapter 4, daughter ion mass spectra may be examined in a reflecting TOF spectrometer with higher efficiency. Daughter ion mass spectra from unimolecular decay of various parent ions in several small peptides of molecular mass ≤600 have been presented in chapter 4 and §5.3; extensions of these measurements to a number of larger peptides of mass up to ~2000 u are presented below. As remarked in §5.3, daughter ion mass spectra from metastable decompositions are affected by the measuring time scale of the instrument and the amount of internal energy excitation of secondary ions. These factors affect also the normal mass spectra. In some cases the reflected TOF mass spectra may provide more structural information than normal FAB spectra. Examples of using reflected TOF mass spectra in peptide sequencing will now be described. Unless otherwise indicated, the samples used in the measurements below were obtained from Sigma Chemical Company (St. Louis, MO, USA) and were used as supplied. The detailed sample preparation procedures can be found in §2.4 of this thesis.

5.4.2 Peptides of Molecular Weight ≥1000 u

Several peptides with molecular weight ≥1000 has been studied here with the reflecting instrument, and the daughter ion mass spectra from the metastable decompositions of the $[M+H]^+$ ions were recorded. These include bradykinin (MW=1060,

see §4.4.2 [196]), Phe^2-Ala^6-LHRH (MW=1223), adrenocorticotropic hormone (ACTH) 1-10 (MW=1299), tyrothricin (a mixture of cyclic decapeptides of masses ~1300 u) [225], α-neoendorphin (MW=1228) [200] and substance P (MW=1347) [226]. Many daughter ions have been observed for each of these compounds, and considerable structure information can be extracted from both the reflected and daughter ion spectra. The results for Substance P and α-neoendorphin are given below.

5.4.2.1 Substance P

The sample was dissolved in 0.1% aqueous TFA. A drop of this solution was deposited, either on etched silver or on a thin film of nitrocellulose, electrosprayed onto a conducting backing. In general, nitrocellulose substrates gave higher abundances for

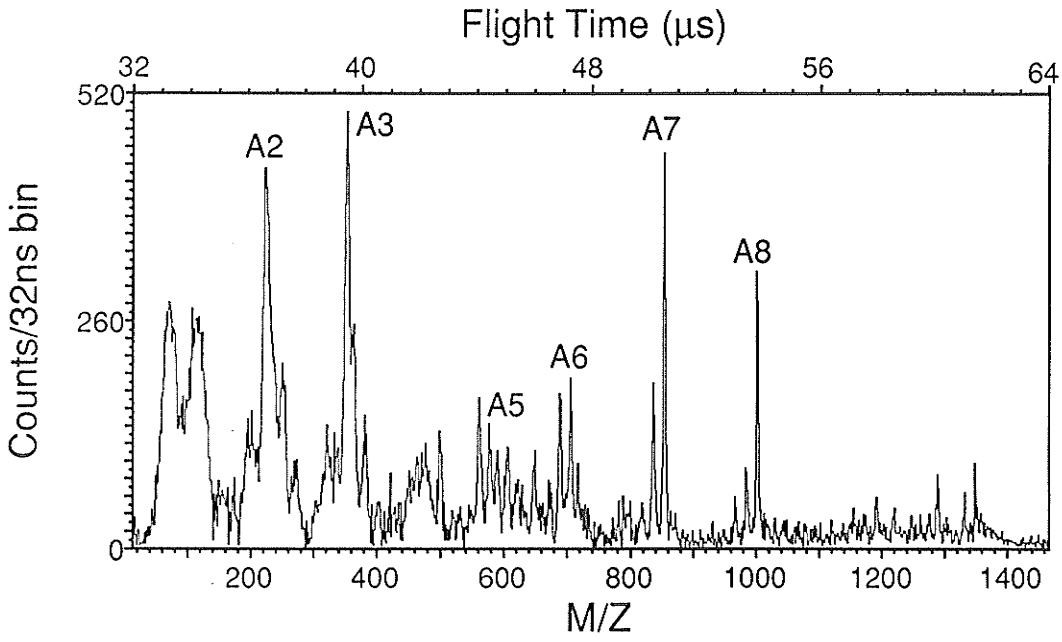

Figure 5.7 Daughter ion spectrum from decomposition of $[M+H]^+$ ions of Substance P (on NC) with the mirror voltage optimized for the parent ion.

parent ions and high-mass daughter ions, while silver gave more metastable-ion decays to low-mass daughter ions. The substrate used is indicated by (Ag) or (NC) in the Figure captions. Fig. 5.7 Shows the daughter-ion spectrum from unimolecular decay of the $[M+H]^+$ ion of the peptide with the mirror voltage optimized for the parent ion. Many daughter ions are visible, but in the lower mass range only the most prominent ones can be identified because of the deterioration of the resolution as m'/m decreases. As described in §4.4, significant improvement can be obtained by measuring the spectra in several segments, with the resolution optimized for successively lower mass values. Several such segments are shown in Fig. 5.8 (a-e). In each case only the upper mass region of the observed daughter ion mass spectrum (flight times ~47 μs to 64 μs) is shown, but the region from 32 to 47 μs flight time is also available for examination of the lower-mass region at poorer resolution. The spectral regions displayed in Fig. 5.8 (a-e) have been chosen to be large enough to give some overlap between segments. An example of the effects of optimizing the voltage at different values is seen by comparing the A_2 peak in Fig. 5.8 (c,d); the isotopic peak at m/z 227 is separated only in the latter spectrum.

No particular effort was expended in these experiments to minimize the amount of sample used or to measure it accurately. For each target, it is estimated that ~0.5 nmol was deposited on a spot ~1 cm in diameter. The primary ion beam was ≤3 mm diameter so the amount of sample struck by the beam was ~50 pmol. The large target area was necessary at the time the experiment was performed, because of uncertainty in the point of impact of the primary beam. The measurements shown in Fig. 5.8 (b-e) were all taken on the same target. No large diminution in the intensity was observed, so it seems likely that most of the sample could be recovered, if necessary.

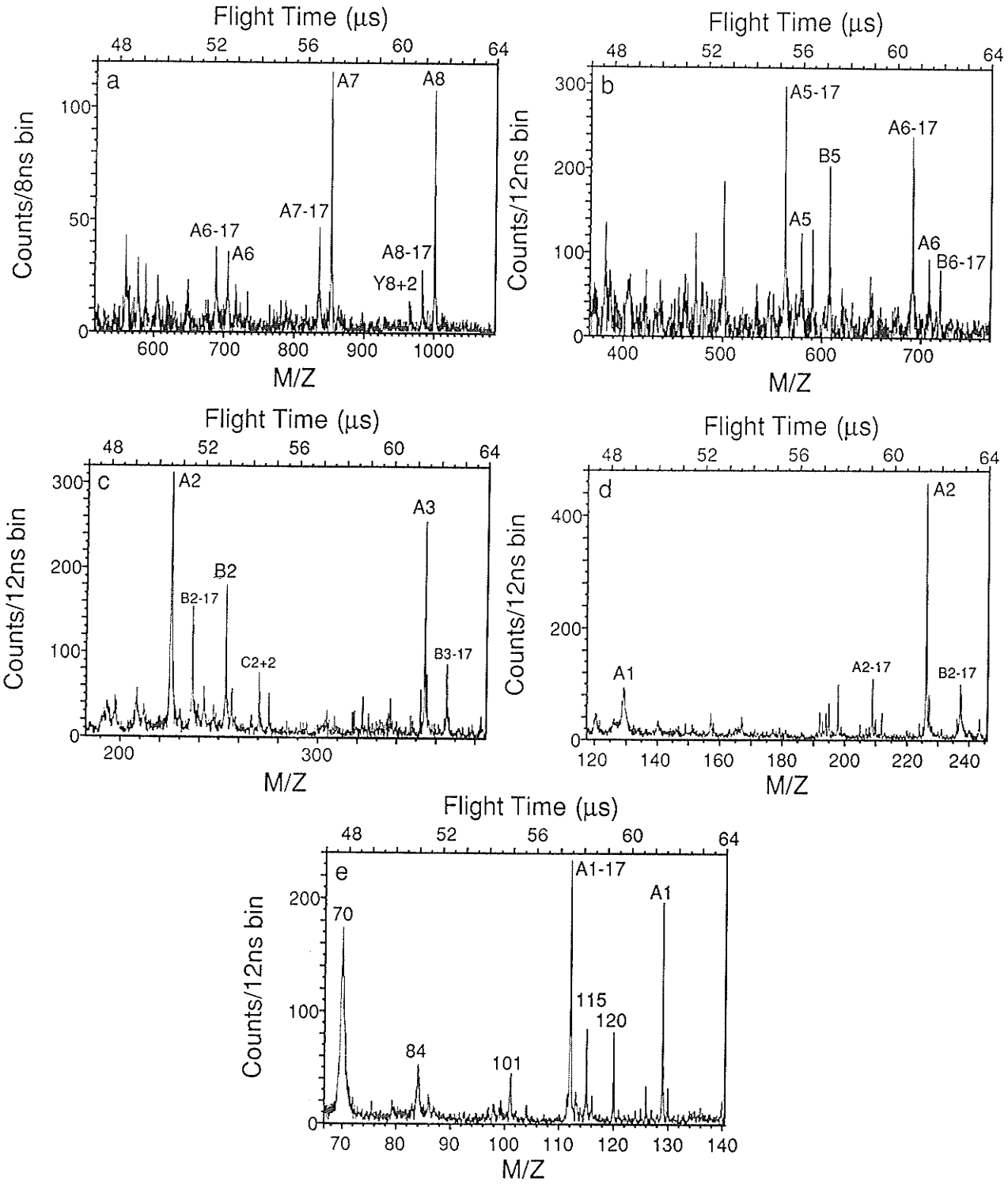

Figure 5.8 Segments of the daughter-ion spectra from decomposition of $[M+H]^+$ parent ions of Substance P with the mirror voltage optimized for successively lower values of daughter ion mass : (a) A_8 (*m/z* 1001) (on NC) (b) A_6 (*m/z* 707) (on Ag) (c) A_3 (*m/z* 354) (on Ag) (d) A_2 (*m/z* 226) (on Ag) (e) A_1 (*m/z* 129) (on Ag).

Six overlapping spectra (Fig. 5.7 & 5.8 (a-e)) along with the reflected spectrum were used for the Substance P measurements. This number may be compared with the 48 segments required in the array detector measurements of Hill et al [198], performed in a four sector tandem mass spectrometer. As remarked above, the six spectra (Fig. 5.7 & 5.8 (a-e)) and the reflected spectrum were obtained from two targets, so sample consumption was not excessive, but the time required was six times as long as the time to take a single spectrum. Since each measurement requires ~1h (with 4 kHz repetition rate) this may be a significant disadvantage in some cases. Some improvement can be achieved by increasing the data acquisition rate so as to decrease the required measuring time.

The major ions observed in the Substance P daughter ion spectrum are listed in Table 5.5, together with the assignments and their calculated values. Errors are found to be <0.3 u in most cases for ions of reasonable abundance, so their assignments are expected to be fairly reliable. Similar results have been obtained for the other peptides (MW≥1000 u) mentioned earlier. In each case a large improvement in daughter ion resolution was obtained by measuring the spectrum in several segments, with the mirror voltage optimized for the particular segment observed.

It is interesting to compare the results for Substance P with normal FAB and FAB collision-induced decomposition (CID) spectra for the same compound measured in the four-sector tandem mass spectrometer at the Massachusetts Institute of Technology (MIT) [198,227]. For the latter instrument (Fig. 5.9a), an almost complete set of A_n ions was observed (n=1-10) together with several D_n ions (n=3,5,6,10), B_2 and C_2+2 in the CID daughter ion spectrum. The D_n ions and several A_n ions are missing from our daughter ion spectra but a variety of others, including prominent A_n-17 and B_n-17 ions are present.

TABLE 5.5 Daughter-ion spectra from unimolecular decay of $[M+H]^+$ (*m/z* 1347.7) ions of Substance P (Arg-Pro-Lys-Pro-Gln-Gln-Phe-Phe-Gly-Leu-Met-NH2)

Observed *m/z*[a]	Assignment	Calculated *m/z*[a]	Obs.-Calcd. *m/z*[a]
1332.1	B_{11}	1331.6	0.5
1288.7	MH-$(NH_2)_2$C+NH	1289.6	-0.9
1002.1	A_8	1001.6	0.5
984.2	A_8-17	984.5	-0.3
966.5	Y_8+2	966.5	0
854.6	A_7	854.5	0.1
837.6	A_7-17	837.5	0.1
735.6	B_6	735.4	0.2
718.7	B_6-17	718.4	0.3
707.3	A_6	707.4	-0.1
690.7	A_6-17	690.4	0.3
607.2	B_5	607.4	-0.2
590.2	B_5-17	590.3	-0.1
579.2	A_5	579.4	-0.2
562.2	A_5-17	562.3	-0.1
501.1	B_7Y_8+1 (Pro.Gln.Gln.Phe+1)	501.2	-0.1
473.1	B_7X_8+1 (Pro.Gln.Gln.Phe+1-CO)	473.2	-0.1
365.8	B_3-17	365.2	0.6
354.2	A_3	354.3	-0.1
276.2	B_7Y_6+1 (Gln.Phe+1)	276.1	0.1
271.2	C_2+2	271.2	0
257.2	B_6Y_7+1 (Gln.Gln+1)	257.1	0.1
254.2	B_2	254.2	0
243.2	$B_{11}Y_2$-1 (Leu.Met-1)	243.1	0.1
237.1	B_2-17	237.1	0
226.1	A_2/B_4Y_9+1 (Lys.Pro+1)	226.2	-0.1
209.1	A_2-17	209.1	0
198.1	B_4X_9+1 (Lys.Pro+1-CO)	198.2	-0.1
128.9	A_1=R(Arg)[b]	129.1	-0.2
126.1	(Gln-2)[c]?	126.0	0.1
120.3	F(Phe)[b]	120.1	0.2
115.3	(Leu+2)[c]?	115.1	0.2
112.4	A_1-17	112.1	0.3
101.4	K(Lys)[b]/Q(Gln)[b]	101.1	0.3
84.3	$C_6H_6N_3$	84.1	0.2
70.4	P(Pro)[b]	70.1	0.3

[a]The first two measurements determine the centroid of the isotopic distribution, so these are compared with the calculated chemical mass. The remainder determine the principal mass.
[b]Immonium ion derived from the indicated amino acid residue.
[c]Amino acid residue=NHCHRCO.

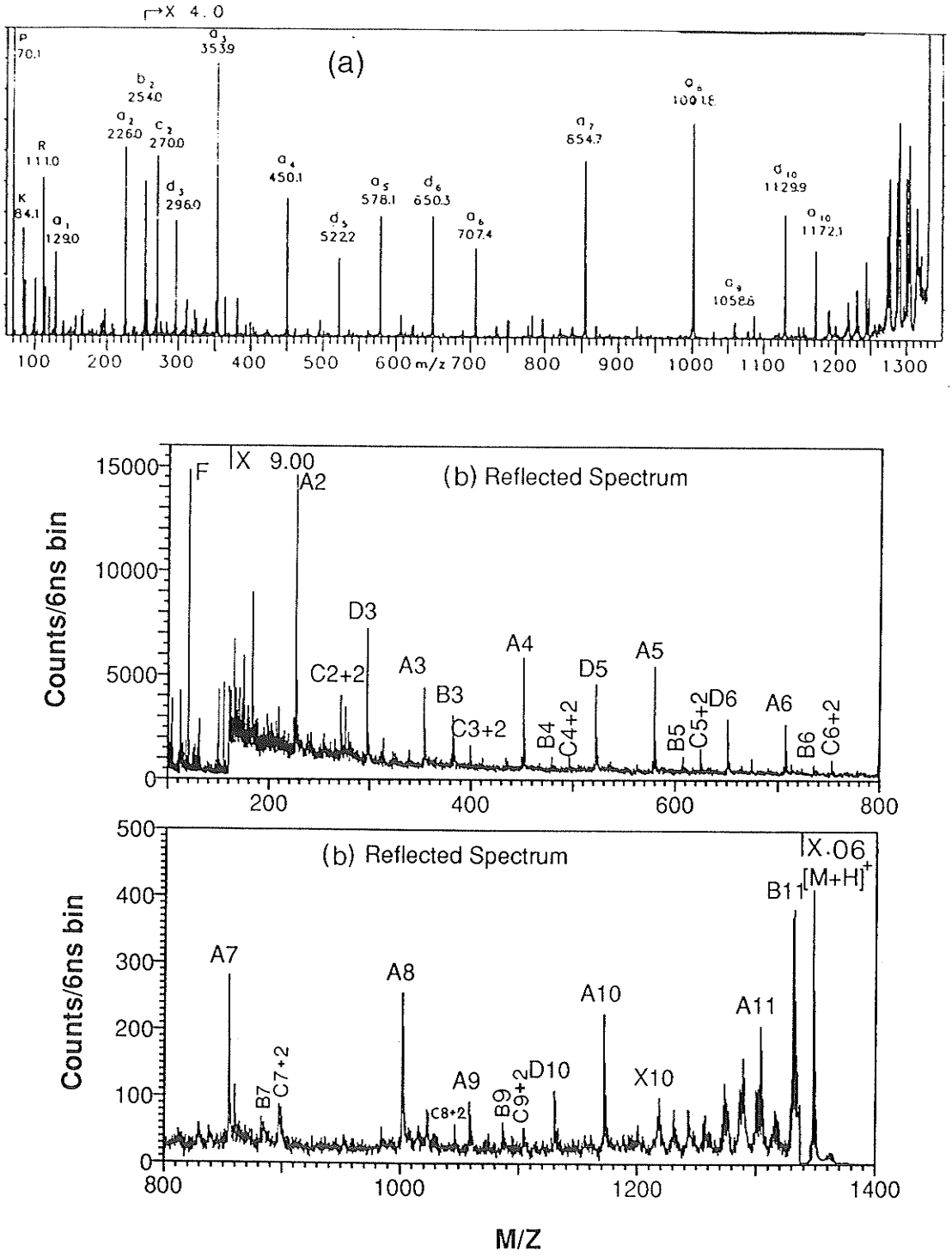

Figure 5.9 (a) FAB CID daughter ion mass spectrum of Substance P measured in a four-sector tandem mass spectrometer equipped with a array detector at MIT [198]. (b) SIMS reflected mass spectrum of Substance P measured in the reflecting TOF mass spectrometer in Manitoba.

These extend down to n=1, so apparently they arise from NH_3 loss from the N-terminal arginine. Such ions have been reported previously from low-energy (~100 eV) CID of $[M+H]^+$ ions of arginine-containing peptides [210,228], and from high-energy (keV) CID of A_n parent ions from Substance P [227]. Our metastable decay daughter ion spectra differ from the MIT FAB CID daughter ion spectra, and our reflected spectrum differs from their normal FAB spectrum [227]. However, it is interesting to note that, apart from some differences in relative abundance, our reflected spectrum (Fig. 5.9b) is remarkably similar to their daughter ion spectrum. Almost all the sequence ions observed in their CID daughter ion spectrum are present as major fragment ions in our reflected spectrum. In contrast, their normal FAB spectrum of Substance P shows a few weak, fragment ion signals necessary for sequencing the peptide. In the FAB spectrum, the low mass range (m/z<500) is dominated by cluster ions of glycerol, the matrix. At higher mass, some N-terminal ions of type C_n and C-terminal ions of type Y_n are observable above the background ions [227]. In our case, for this compound, the reflected spectrum provides more complete sequence information than do the metastable decay daughter ion spectra, in contrast to the FAB experiments for which the daughter ion spectra are more informative than the normal spectrum.

We may suggest two possible explanations for the differences, namely the internal energy excitation and the time scale of the measurement. (i) The secondary ion production takes place in a solid in our case and in a liquid matrix at MIT. Greater fragmentation may be expected in the solid because of the increased binding. (ii) Our experiments examine the decomposition of $[M+H]^+$ ions produced by Cs^+ ion bombardment of a solid sample, where as the MIT measurements rely on excitation of the parent ions by collisions in the gas phase. Thus, we measure the decay of parent ions of lifetimes

between ~0.2 μs (the acceleration time) and ~15 μs, with a correspondingly large range of internal excitation energies and decay pathways. On the other hand, the parent ions studied at MIT are probably relatively homogeneous in internal energy, since ions surviving passage through the first spectrometer have a low internal-energy content (life-times ≥50 μs) and the amount of energy gained by collision is small. Ions resulting from prompt decompositions, i.e. decompositions during acceleration (at times ≤0.2 μs) are not observed as *daughters* of $[M+H]^+$ in our measurements, but no such limitation exists in the MIT experiments for decays **after** collisional activation. We note that this restriction applies to our present metastable-ion decay experiments, but not to experiments in which parent ions are photodissociated after acceleration [225].

5.4.2.2 α-neoendorphin

This sample was also dissolved in 0.1% aqueous TFA solution and then deposited on the nitrocellulose substrate. The full daughter ion spectrum, with the mirror optimized for the $[M+H]^+$ ions, is shown in Fig. 5.10, Although the daughter ions in the upper part of the spectrum can be distinguished clearly, it becomes progressively more difficult to identify the daughters of lower mass as a result of the worsening resolution. As in the case of substance P, a considerable improvement is again obtained by measuring the daughter ion spectrum in several sections. Daughter ion spectra have been recorded for several values of the mirror voltage, with the resolution optimized for successively lower values of the daughter ion mass. Fig. 5.11 shows a portion of each segment of such spectra. The results are listed in Table 5.6. A nearly complete set of N-terminal ions is observed, along with some C-terminal ions and some internal fragments. Considerable

sequence information can be extracted from the daughter ion spectra. These spectra may also be compared with the reflected spectrum of this compound shown in Fig. 5.12. Although similar sequence ions are observed in the higher mass range (≥660), there is little sequence information in the lower mass range of the reflected spectrum, and the few fragment ions are also of insufficient relative abundance to make them clearly distinguishable from background ions. So for α-neoendorphin the metastable decay daughter ion spectrum provides more structural information and less confusion than does the reflected spectrum, since the sample peaks are well separated from the background. It can be seen from the examples of substance P and α-neoendorphin that, in peptide sequencing, the metastable decay daughter ion spectrum and the reflected spectrum may provide complementary information, provided the sample is pure in the case of the reflected spectrum. The choices among the two types of spectra may well be compound dependent.

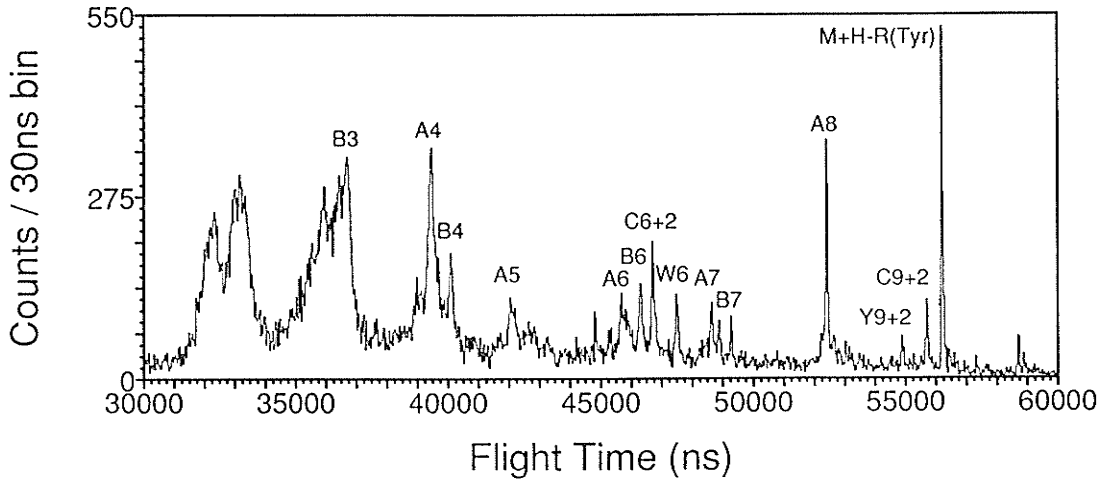

Figure 5.10 Daughter ions from unimolecular decay of $[M+H]^+$ of α-neoendorphin deposited on nitrocellulose substrate, mirror optimized for parent ions.

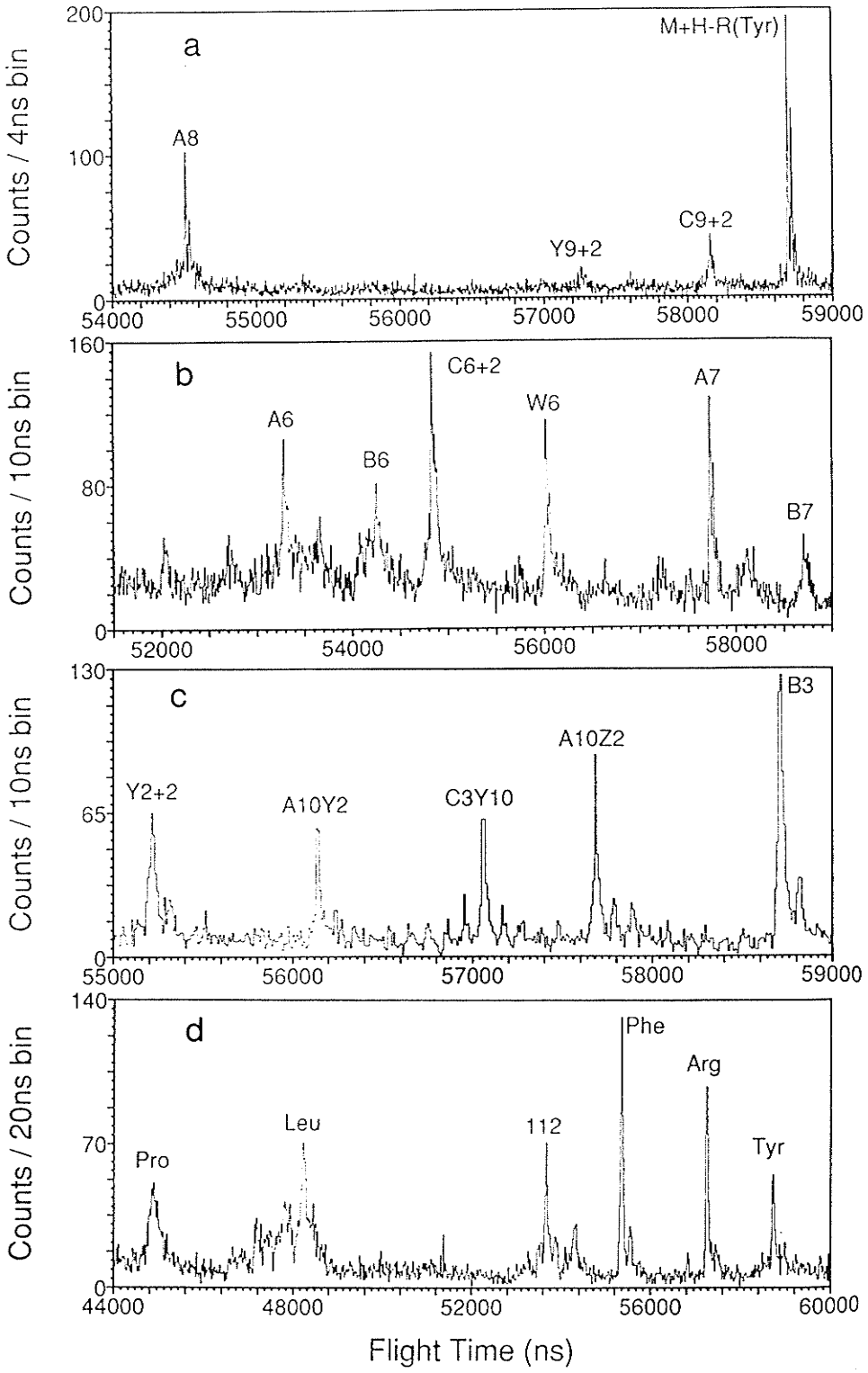

Figure 5.11 Daughter ions from $[M+H]^+$ of α-neoendorphin as in Fig. 5.10 but with mirror optimized for (a) ~1120 u, (b) 820 u, (c) ~280 u, (d) ~140 u.

TABLE 5.6 Daughter ion spectra from unimolecular decay of $[M+H]^+$ (*m/z*=1228.7) of α-neoendorphin (H-Tyr-Gly-Gly-Phe-Leu-Arg-Lys-Tyr-Pro-Lys-OH)

Observed *m/z*	Assignment	Calculated *m/z*	(Obs.-Calcd.) *m/z*
1121.5	$[M+H-R_{Tyr}]$	1121.6	-0.1
1100.1	C_9+2	1099.6	0.5
1065.4	Y_9+2	1065.6	-0.2
957.4	A_8	957.5	-0.1
822.5	B_7	822.5	0.0
804.7	Y_6+2	804.5	0.2
794.4	A_7	794.5	-0.1
745.2	W_6	745.4	-0.2
711.2	$_C6+2$	711.4	-0.2
694.4	B_6	694.4	0.0
666.5	A_6	666.4	0.1
510.7	A_5	510.3	0.4
425.2	B_4	425.2	0.0
397.2	A_4	397.2	0.0
278.1	B_3	278.1	0.0
268.0	$A_{10}Z_2$ (Pro.Lys)	268.1	-0.1
261.9	C_3Y_{10} (Tyr.Gly.Gly)	262.1	-0.2
253.2	$A_{10}Y_2$ (Pro.Lys)	253.1	0.1
244.1	Y_2+2	244.2	-0.1
136.1	A_1 or I_1, I_8 (Tyr)	136.1	0.0
129.0	I_6 (Arg)	129.1	-0.1
120.0	I_4 (Phe)	120.1	-0.1
112.1	I_6-NH_3	112.0	0.1
86.0	I_5 (Leu)	86.1	-0.1
84.2	$NH_2(C_3H_4N_2)^+$	84.1	0.1
70.1	I_9 (Pro)	70.1	0.0
59.8	$(NH_2)_2C=NH_2^+$	60.1	0.3

5.4.3 Peptides of Molecular Weight ~2000 u

Some peptides with molecular weight around 2000 u have also been examined here by the correlated method. Considerable structure and sequence information can be obtained from daughter ion spectra in some cases, but generally the signal-to-noise ratio

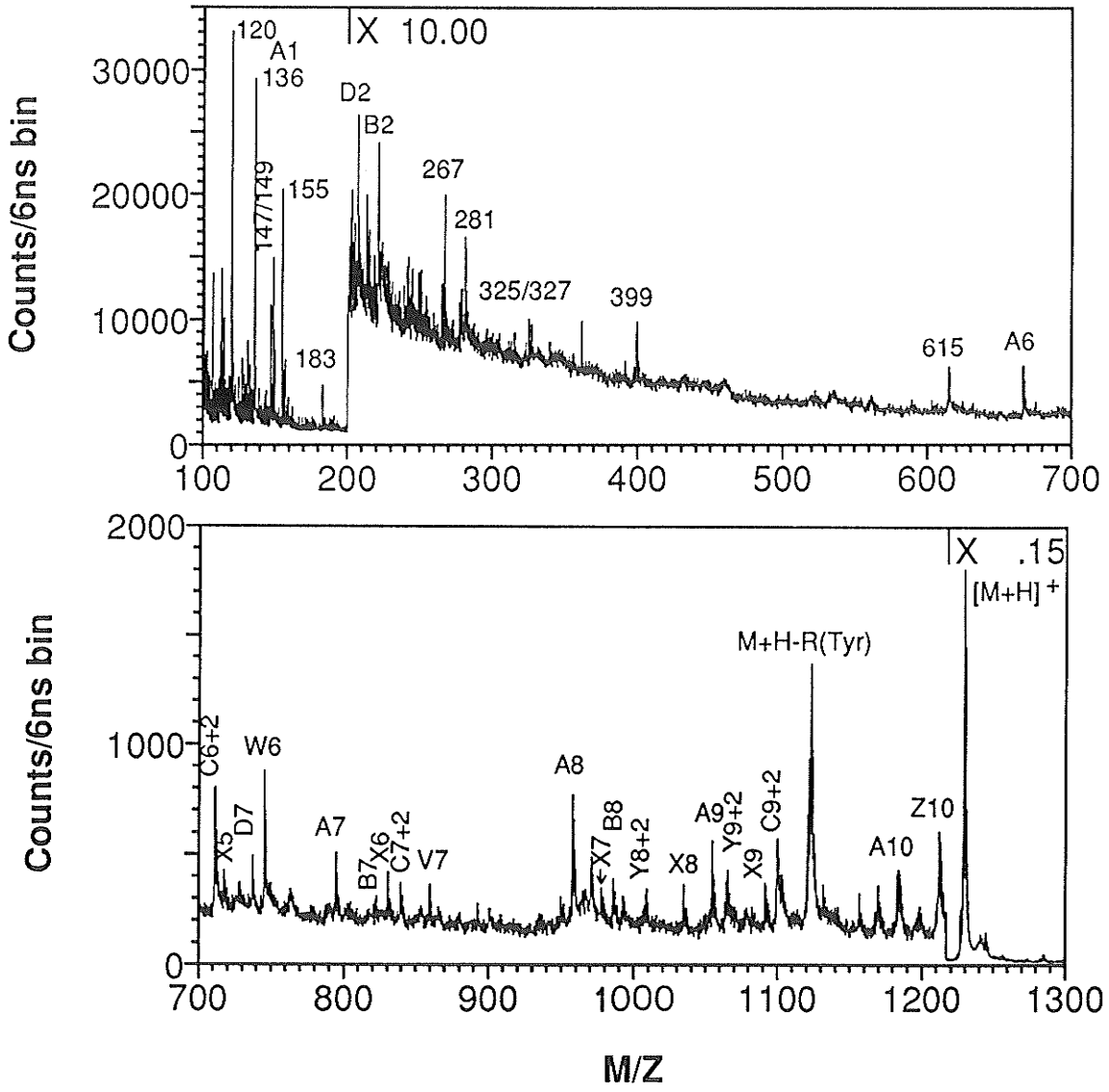

Figure 5.12 Partial reflected mass spectrum of α-neoendorphin deposited on nitrocellulose; the sequence ions are labelled as described in Appendix B.

of the daughter ion spectra decreases with increasing mass. Some of the causes will be discussed in the next section. For the results presented below, the peptide samples were usually dissolved in 0.1-1% TFA/water solvent to make a ~1 μg/μL solution. The targets were then prepared by dropping a few μL of the peptide solution onto the nitrocellulose substrate, which had been electrosprayed onto a metal backing.

5.4.3.1 α-endorphin and γ-endorphin

a) α-*endorphin* (β-endorphin 1-16) (MW 1744.8)

H-Tyr-Gly-Gly-Phe-Met-Thr-Ser-Glu-Lys-Ser-Gln-Thr-Pro-Leu-Val-Thr-OH

The reflected TOF mass spectrum of α-endorphin is shown in Fig. 5.13. Although this normal TOF spectrum exhibits little fragmentation, many daughter ions are observed in the correlated metastable decay daughter ion spectrum (Fig. 5.14) [202]. The daughter ion spectrum contains peaks mainly due to a series of N-terminal B fragments and/or C-terminal Y+2 fragments. Some peaks are dual-labelled because the masses of these B fragments are very close to those of the Y+2 fragments (the mass difference is ~1 u) for this compound. Since the $[M+H]^+$ parent ions selected here contain full isotopic distribution, these B and Y+2 ions cannot be distinguished here. These results may be compared with the FAB and FAB metastable decay daughter ion spectra of the same compound measured in a two sector instrument (VG Micromass ZAB-2HF of reverse, i.e. BE, geometry), where six peptides, including four β-endorphins and two adrenocorticotropic hormone (ACTH) peptides, were studied [230]. As above, the FAB spectrum is quite different from our reflected spectrum. There is a series of Y_n+2 fragment ions, n=4-12, in the FAB spectrum, although the intensities of most of the Y+2 ions are low. They are almost absent in the reflected spectrum. The metastable daughter ion spectra are qualitatively similar although there are some differences: the B_{15} ion is the most intense peak in the FAB metastable daughter ion spectrum, but is of low intensity in our correlated metastable daughter ion spectrum. It is possible that the low intensity of the B_{15} peak in our spectrum is a result of the low detection efficiency for the corresponding small neutral fragments resulting from the decay $[M+H]^+ \rightarrow B_{15}^+ + 119$.

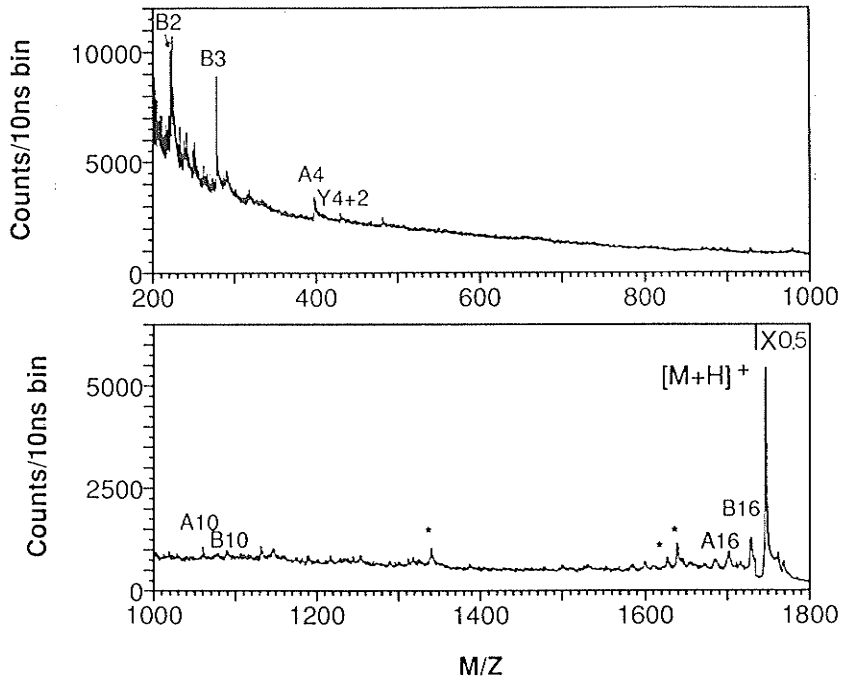

Figure 5.13 Reflected mass spectrum of α-endorphin deposited on nitrocellulose. Peaks denoted by an asterisk correspond to daughter ions of B_{12} (1318 u), B_{15} (1627 u) and V_{16} (1638 u).

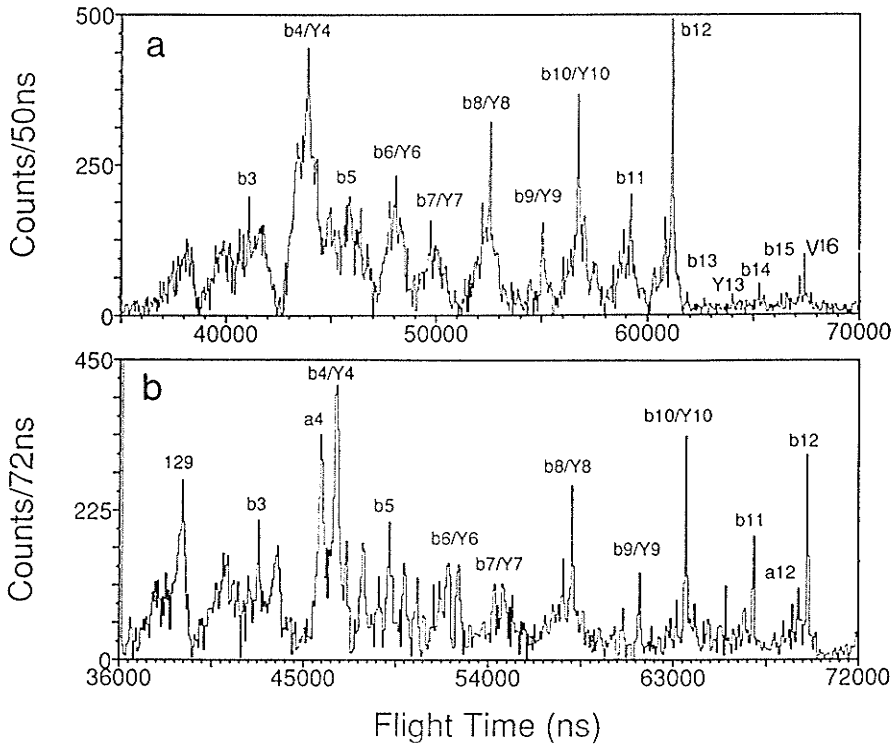

Figure 5.14 Daughter ion mass spectra of α-endorphin with mirror optimized for: (a) the parent ion (1746 u), and (b) B_{12} (1318 u).

The energy of the neutral fragment (119 u) is only about 6.8% (~850 eV) of the parent (~12.5 keV), and the neutral detection efficiency N_{coin}/N_+ (see §4.3.2) for mass 119 neutral is ~0.17, about a factor of 3 lower than for mass 428 (energy ~3 keV) neutral resulting from $[M+H]^+ \rightarrow B_{12}+428$ decay. A low correlated detection efficiency is thus expected for $[M+H]^+ \rightarrow B_{15}+119$ decay. This can be seen from the reflected spectrum; the three peaks labelled with an asterisk are daughter ions corresponding to B_{12}, B_{15} and V_{16}, and the intensity ratio of B_{15}/B_{12} is higher than that in the correlated daughter ion spectrum. This is even more apparent on comparing the intensity ratio V_{16}/B_{12} in the two spectra. Another difference is that our daughter ion spectrum exhibits more fragment ions, especially at the lower mass range where the daughter ions still give intense peaks down to a mass of ~100 u. In contrast, in the FAB metastable ion spectrum, the daughter ions can only be seen down to B_6 or Y_6+2 (m/z ~658 u, or energy ~3 keV). This is partly due to the lower detection efficiency in the FAB measurements, since the parent ions have only 8 keV energy, whereas in our case, the energy of the parent ions right after acceleration is 12.5 keV, so the velocity of the parent and daughter ions is higher than that in the FAB experiments. There is also 1 kV post-acceleration placed on the electron converter detector, so the energy of the daughter ions of mass 658 is ~5.7 keV when they strike the detector. Apart from the explanations discussed above, the other causes of these observed differences are perhaps largely due to differences in the time scale of the measurement and to the amount of energy dissipation in the desorption process, as mentioned earlier.

b) γ-*endorphin* (β-endorphin 1-17) (MW 1857.9)

H-Tyr-Gly-Gly-Phe-Met-Thr-Ser-Glu-Lys-Ser-Gln-Thr-Pro-Leu-Val-Thr-Leu-OH

γ-endorphin has also been analysed. It has one more amino acid (leucine) than

α-endorphin, and its spectrum helps to remove the ambiguity of some B and Y+2 fragment assignments encountered in the analysis of α-endorphin. An accelerating voltage of 15 keV was used in the measurements (12.5 kV was used for the α-endorphin measurements) in order to improve the detecting efficiency. The patterns of the spectra and the fragment ions detected are similar to those observed from α-endorphin. There is also little fragmentation in the reflected spectrum but many sequence fragment ions in the metastable daughter ion spectrum. Fig. 5.15 shows the daughter ion spectrum with the mirror optimized on $[M+H]^+$ parent ions; again the resolution for the lower mass daughter ions can be improved by measuring the daughter ion spectrum in several segments with the mirror optimized for successively lower mass values. The upper mass regions of 5 such segments are shown in Fig. 5.16 (a-e). An almost complete series of N-terminal B fragment ions are observed, along with many C-terminal Y+2 fragment ions. Some other types of sequence ions and internal fragments have also been observed. A comparison

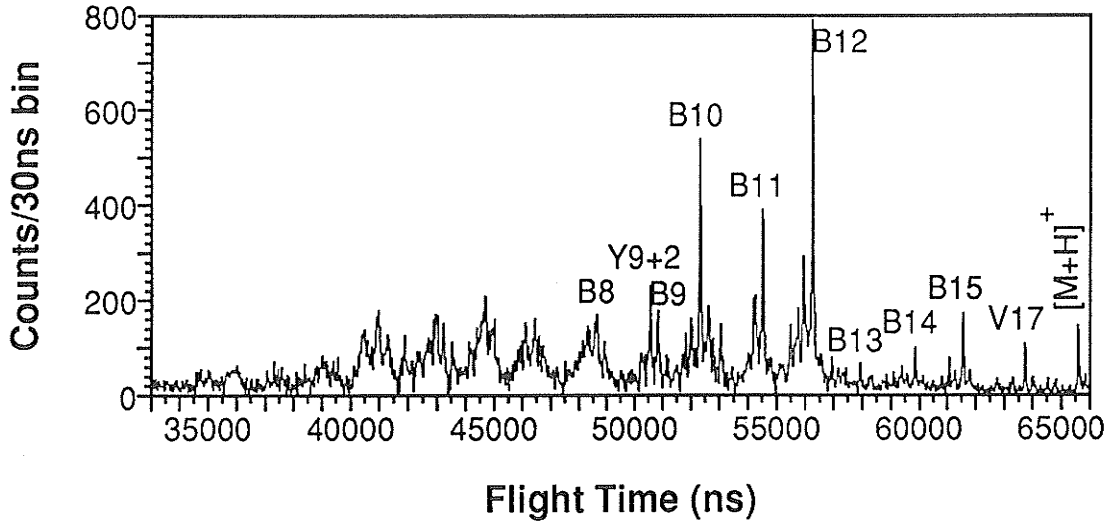

Figure 5.15 Daughter ion mass spectrum of γ-endorphin deposited on nitrocellulose, with mirror optimized for parent ion (1859 u).

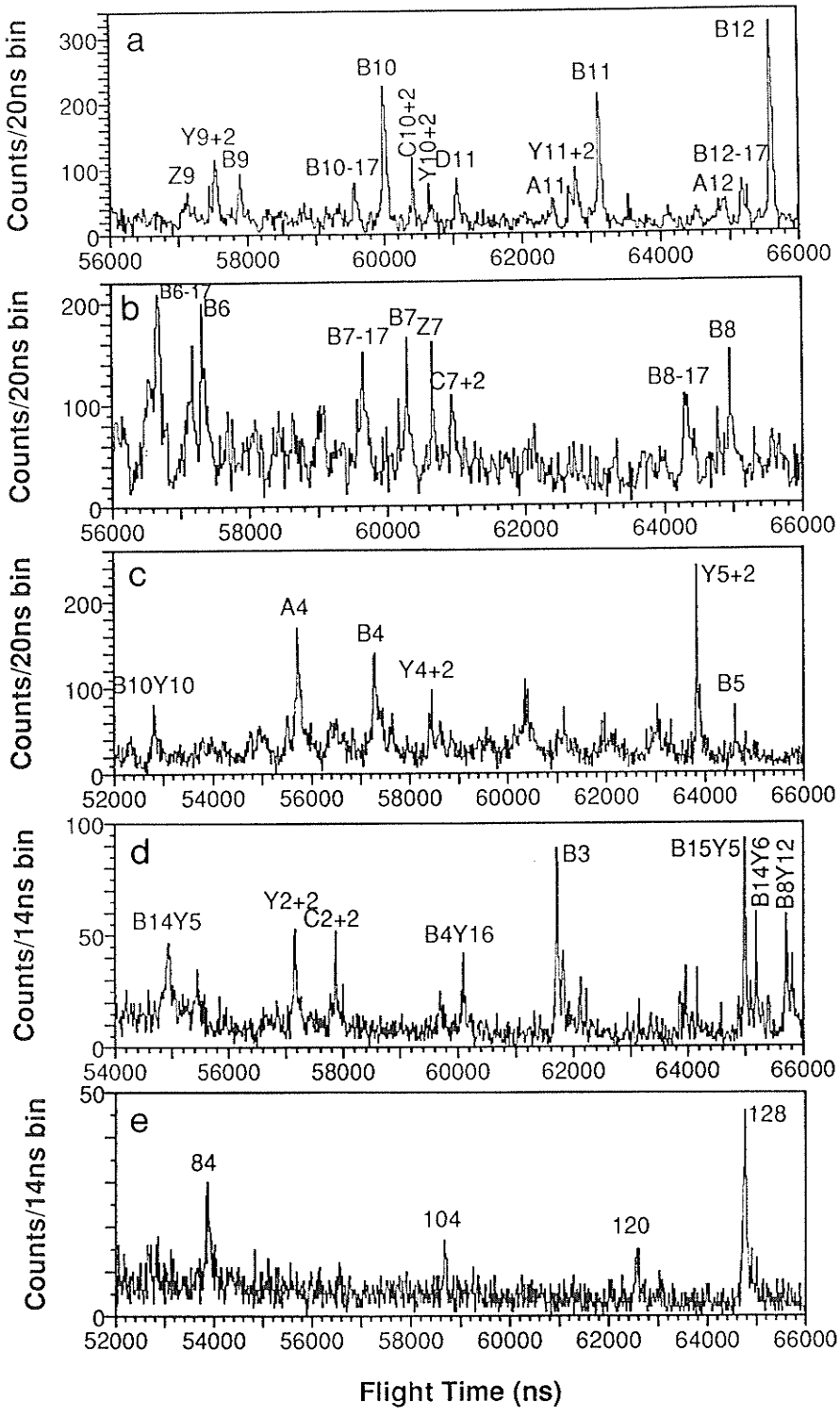

Figure 5.16 Daughter ion spectra from $[M+H]^+$ of γ-endorphin as in Fig. 5.15 but with mirror optimized for (a) B_{12} (1318 u), (b) C_8+2 (890 u), (c) C_5+2 (573 u), (d) Z_3 (315 u), (e) Y_1+2 (132 u).

between the metastable daughter ions of γ-endorphin observed here and those observed in FAB sector instruments [230] shows them to be very similar, as has been noted above for α-endorphin. In the high mass region, the spectra obtained in the two cases are more or less similar, but in the lower mass region (<858 u or Y_8+2), no daughter ions were observed in the FAB case [230], but there are plenty of daughter ions, extending down to *m/z* 84 in our case.

5.4.3.2 ACTH 1-17 (MW 2092.1) and an unknown peptide

a) *Adrenocorticotropic hormone (ACTH) 1-17* (MW 2092.1)

H-Ser-Tyr-Ser-Met-Glu-His-Phe-Arg-Trp-Gly-Lys-Pro-Val-Gly-Lys-Lys-Arg-OH

The reflected mass spectrum is shown in Fig. 5.17. Unlike the reflected spectra of the endorphin peptides presented above, this spectrum shows many fragment ions. It also appears to be different from a FAB spectrum of ACTH 1-16-NH_2, presented as a "typical" FAB spectrum of the ACTH peptides [230], where only a few fragments were observed. The major fragment ions of ACTH 1-17 observed here include many N-terminal fragment ions of type A_n (n=2,5,8-17) and C_n+2 (n=4,8,10,15,16), many C-terminal fragment ions of type X_n (n=1-12,16) and Y_n+2 (n=2-4,7-9,16), and a variety of side chain loss fragment ions of type D_n (n=6,9,11,17), V_n (n=4,5,7,8) and W_n (n=2,3,5,7). Thus there is much structural information available in the reflected spectrum. In addition to the observation of a strong, singly-charged protonated molecule peak in both cases, a common feature of our reflected spectrum of ACTH 1-17 and the FAB spectrum of ACTH 1-16-NH_2, is the observation of doubly-protonated molecules, which have not been seen in the endorphin peptides. There are also many fragment ions in our daughter ion

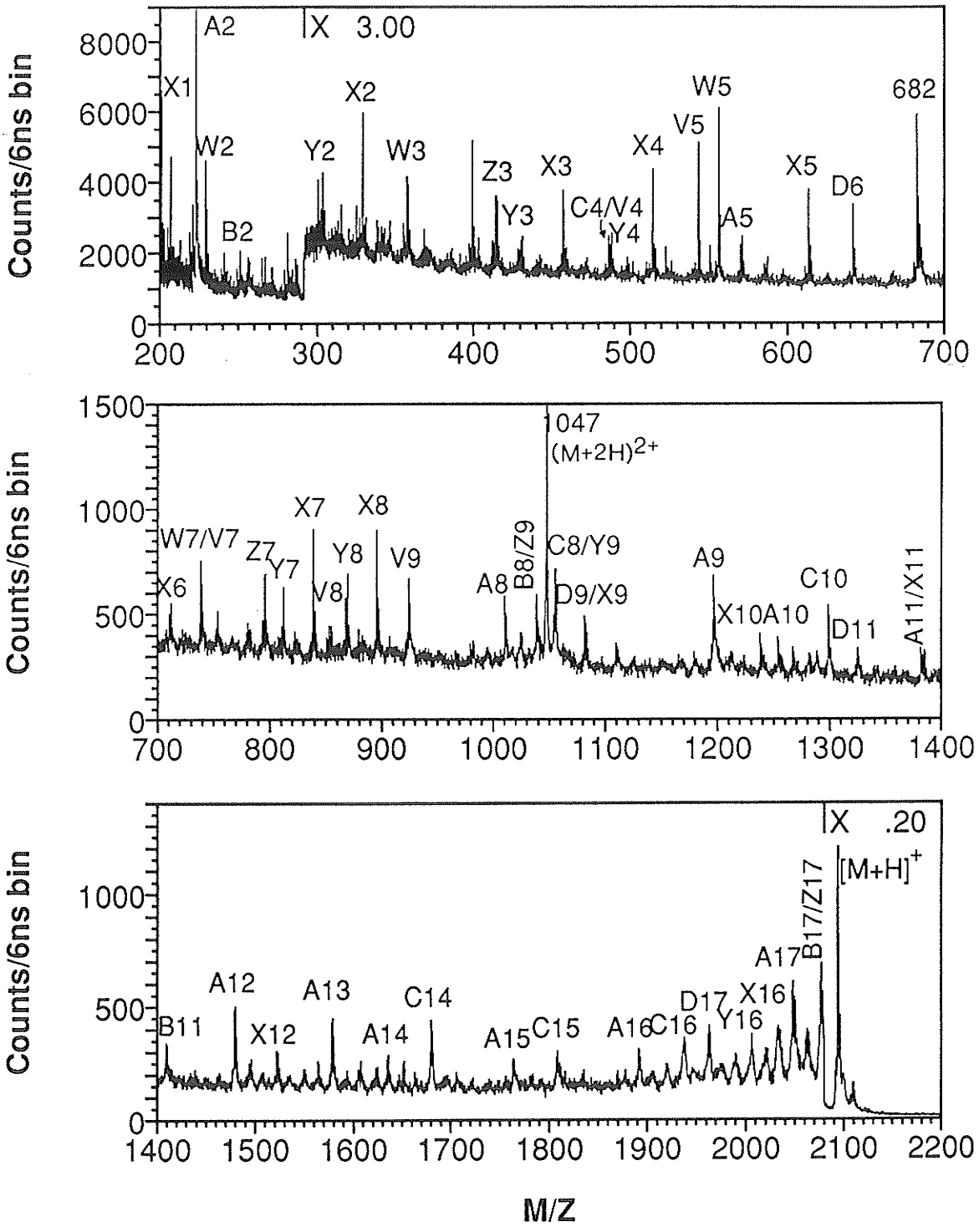

Figure 5.17 Reflected positive ion mass spectrum of ACTH 1-17 (MW=2092.08) deposited on nitrocellulose.

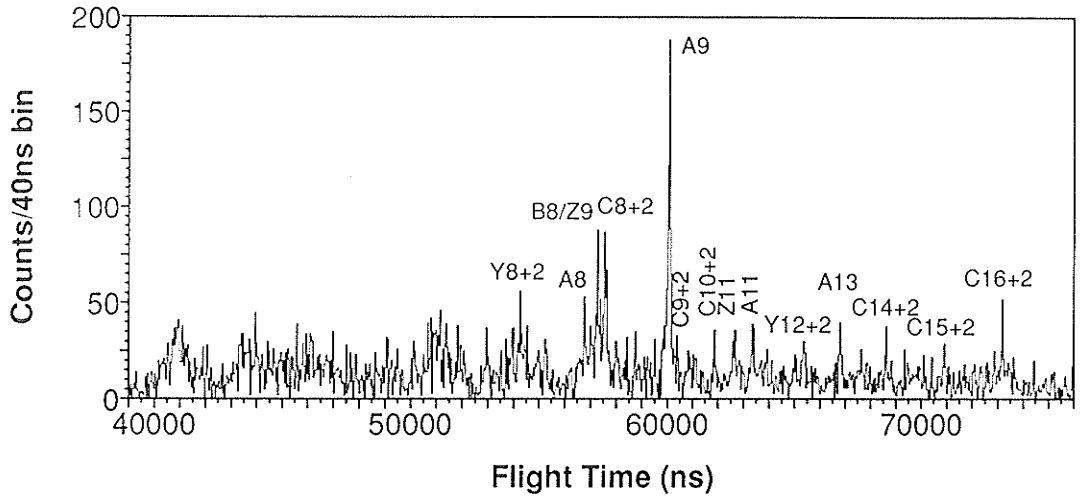

Figure 5.18 Daughter ion spectrum from unimolecular decay of $[M+H]^+$ (2093 u) from ACTH 1-17 on nitrocellulose substrate (mirror optimized for parent ions).

spectrum (Fig. 5.18); however, the abundances of most of them are too low to be distinguished clearly from the background, apart from the A_9 fragment (m/z=1196.5) in the middle of the spectrum. This might be expected, since the number of possible decay channels increases with the size of a peptide, and the molecular ion yield and the correlated measurement efficiency decrease with an increase of mass. Much lower daughter ion abundances were also observed for ACTH 1-16-NH_2 than for the endorphin peptides in the FAB metastable daughter ion spectrum [230]. Thus, the $[M+H]^+$ ions of the ACTH peptides produced appear to be more stable than those of the endorphin peptides, so, apart from other factors that may affect the fragmentation of a peptide, the extent of fragmentation of a peptide again appears to be compound-dependent.

b) *An unknown peptide*

An *unknown* peptide has also been analysed here by the reflecting instrument. A 1.5 μg sample of this peptide was obtained from the organizers of a workshop of the 38th American Society for Mass Spectrometry (ASMS) Conference. Some 40 laboratories

requested a sample of this peptide (one of the two unknowns), but our lab was the only one to present results on this unknown at the conference held in Tucson, Arizona. At the workshop it was announced that the peptide was dynorphin A (MW=2146.2 u), whose sequence is:

H-Tyr-Gly-Gly-Phe-Leu-Arg-Arg-Ile-Arg-Pro-Lys-Leu-Lys-Trp-Asp-Asn-Gln-OH

Our experiments further demonstrate the capabilities of the reflecting TOF instrument, particularly, its high sensitivity. The detailed analysis of this peptide has been reported elsewhere [231]. Fig. 5.19 shows a partial reflected spectrum of this compound.

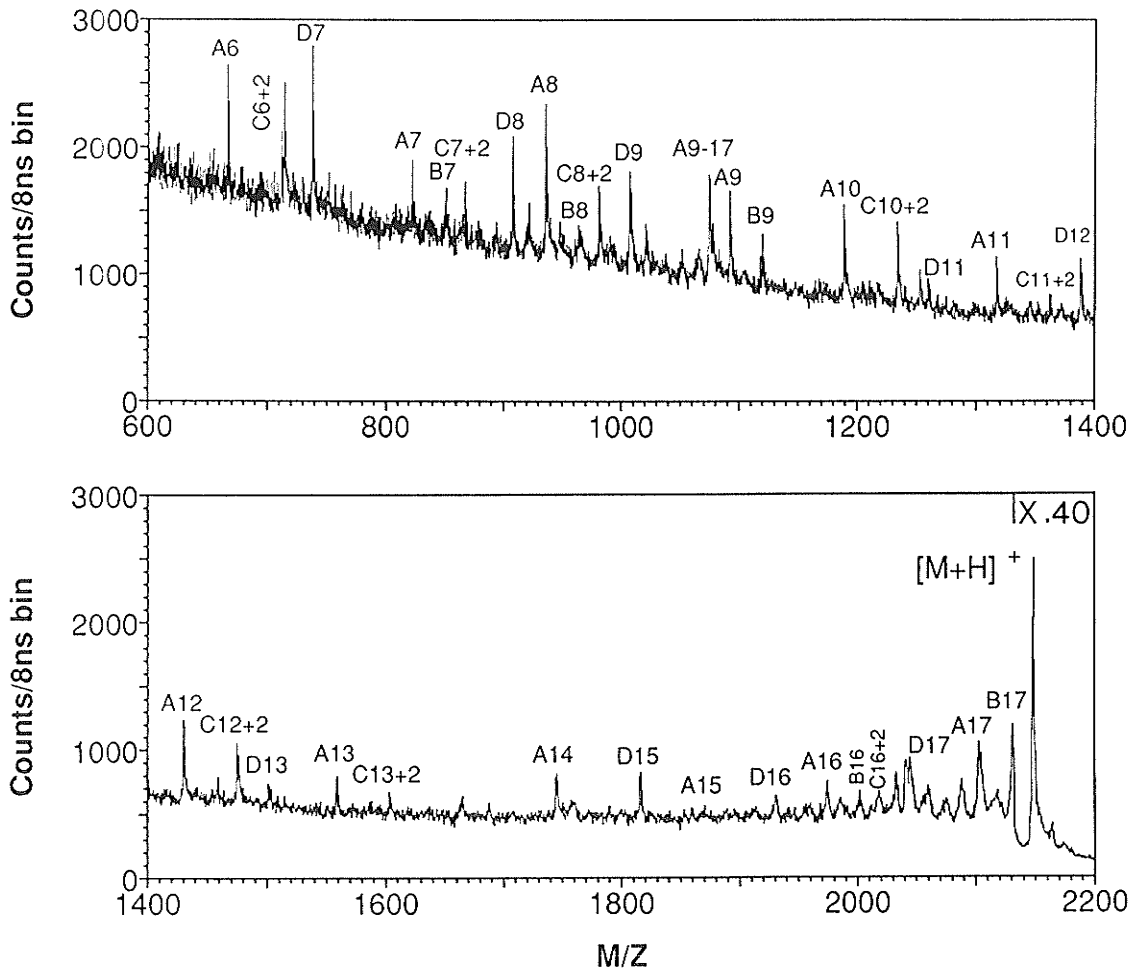

Figure 5.19 Partial reflected positive ion mass spectrum of Dynorphin A (MW=2146.2).

1 μL (0.2 μg/μL) sample solution was deposited on an ~ 2mm diameter nitrocellulose spot, and reflected and daughter ion mass spectra were accumulated simultaneously for a few hours until spectra with reasonable statistics were obtained. Since our SIMS method is nondestructive, no large diminution in signal intensity was observed after 9 hours of measurement. Although only a few fragment ions were reliably observed in the daughter ion spectrum, however, we were able to obtain more than half of the sequence and an accurate mass of the "unknown" peptide [231], based on the many fragment and molecular ions observed in the reflected spectrum (Fig. 5.19).

From the examples of peptide analysis presented above, it can be seen that, both the metastable daughter ion spectrum and the reflected TOF spectrum are useful in peptide sequencing, provided the sample is pure in latter case, and the choice of spectrum used appears to be compound-dependent.

5.5 PEPTIDE DIGESTION AND MIXTURE ANALYSIS

5.5.1 Peptide Digestion on Target

There is increasing difficulty in obtaining sequence information of peptides from daughter ion spectra as the mass of the parent ion increases. Most FAB collision induced dissociation (CID) daughter ion mass spectra (MS/MS analysis) of biomolecules are limited to $m/z<2000$ u [232,233]. The limitations can be attributed to at least three factors: (i) the yield of parent ions decreases as their masses increase; hence the number of parent ions available to produce daughter ions decreases. (ii) the possible decay paths or the

degrees of vibrational freedom of the molecular ions increase, so the average energy imparted per vibrational mode by collision or by the desorption process in the case of metastable decay studies, may be insufficient for fragmentation. In the case of CID, the energy transfer between the low molecular weight collision gases and target ions is also inefficient [232-234]. The average abundance of the daughter ions also decreases since more decay channels are available for fewer parent ions. (iii) The average detection efficiency for daughter ions decreases because both the velocity and average energy of the daughter ions decrease as the mass of the parent ion increases. In addition, the detection efficiency of neutrals also decreases in our case, thus resulting in a low correlated (or daughter ion) measurement efficiency.

As can be seen from the peptide spectra presented in the last 2 sections, the fragmentation abundance, or the signal-to-background, in daughter ion spectra is reduced considerably as the mass of the peptide increases from ~500 to ~2000 u. One way to overcome this difficulty is to reduce the size of the molecules in a predictable manner. Perhaps the simplest method for achieving a reduction in peptide length is to cleave a peptide at specific amino acid residues by using enzymatic digests. The mixture of smaller peptide products of enzymatic cleavage can then be separated and analysed by MS/MS methods. A variety of enzymes such as trypsin, chymotrypsin or Staphylococcus aureus V8 protease, can be used to cleave proteins or peptides, the choice of enzyme being dependent upon the amino acid residue in the protein or peptide where cleavage is desired. For example, trypsin cleaves peptides on the C-terminal side of the basic amino acid residues arginine and lysine unless the next residue is proline, whereas chymotrypsin cleaves peptides on the C-terminal side of tyrosine, tryptophan, phenylalanine, leucine and methionine unless the next amino acid residue is proline. Specific cleavage by enzymatic

digests can also be used to confirm a certain amino acid sequence, as found in the sequencing of the unknown peptide [231] described in the last section.

Most reported enzymatic reactions have been performed in solution, the reaction products separated by liquid chromatography, and then analyzed by mass spectrometry. The enzymatic digestions here, however, were performed on surface-bound peptides directly on targets, as reported by Chait et al [235,236]. Since our SIMS analyses are practically nondestructive of sample, there is no need for additional sample material to be used for enzymatic reaction, so the mass spectra of the sample before and after digestion can be recorded from the same target. This is a particular advantage if only a limited amount of the sample is available for investigation. Partly because of its selectivity, trypsin is a good general choice for digestion of medium size polypeptides (MW 1000-3000 u) which usually contain a few arginine or lysine residues, Thus, a small number of cleavages can be achieved, and the large portions of the peptide that remain intact can be sequenced by our MS/MS method.

The peptide samples were dissolved in 0.1% aqueous TFA to form 0.1-1 μg/μL solutions, and several μL of the solution was placed on a nitrocellulose surface, which had been electrosprayed onto a metallic target backing. After recording all necessary mass spectra, the target was taken out of the spectrometer for enzymatic digestion. The digestions were performed on the samples by simply placing the enzyme solution (pH≈8) on the sample surface. For tryptic digestion, a typical reaction solution used here contained 0.05M NH_4HCO_3 and 3.3×10^{-6}M trypsin (pH≈8.3) as prescribed by Chait et al [236]. The temperature of the reactions ranged from ~22°C to 38°C, and the times ranged from ~1 to 30 minutes. After the reaction, 4-10 μL of 0.1% aqueous TFA was usually added to the sample, because in most cases, it increased the abundances of

reaction product ions and the molecular ions of unreacted starting peptide. The target was then reinserted into the mass spectrometer to record mass spectra.

Enzymatic digestion of several peptides, including γ-endorphin, ACTH 1-17, and dynorphin A (the unknown at the time of the experiments) has been tested. For each peptide, cleavages at the expected sites of the peptide chain were observed. The results for γ-endorphin are now discussed. It is a good example for tryptic digestion, because it contains only one lysine residue near the middle of the peptide chain. In this experiment, 4 μL of 1 μg/μL γ-endorphin solution was deposited on ~50 mm^2 area on the nitrocellulose surface of the target. The recorded mass spectrum is shown in Fig. 5.20 (a). The target was then taken out of the spectrometer, and 20 μl of reaction solution containing 0.05 M NH_4HCO_3 and 3.3×10^{-6}M trypsin at pH ~8 was dropped onto the sample surface. After a 12 minute reaction at ~24 °C (room temperature), the target was reinserted in the spectrometer. The spectrum recorded is shown in Fig. 5.20 (b). The new fragments A and B in the spectrum, with chemical masses of m/z=1020 and 859, indicate that the γ-endorphin was cleaved at C-terminal side of the lysine residue as expected. The expected sequences of the fragments A and B are:

Fragment A (MW=1018.44) H-Tyr-Gly-Gly-Phe-Met-Thr-Ser-Glu-Lys-OH

Fragment B (MW=857.49) H-Ser-Gln-Thr-Pro-Leu-Val-Thr-Leu-OH

The target was again removed, and 8 μL of 0.1% aqueous TFA solution was added to the sample. The effect of the addition of 0.1% TFA to the sample is shown in Fig. 5.20 (c). The relative intensity of the B fragment peak remains about same, the molecular ion peak increases by nearly a factor of ~2, but the fragment A peak increases dramatically, by about a factor of 6. The metastable decay daughter ion mass spectra of fragments A and B were then recorded along with the reflected spectrum (Fig. 5.20 (d)). Fig. 5.21 (a)

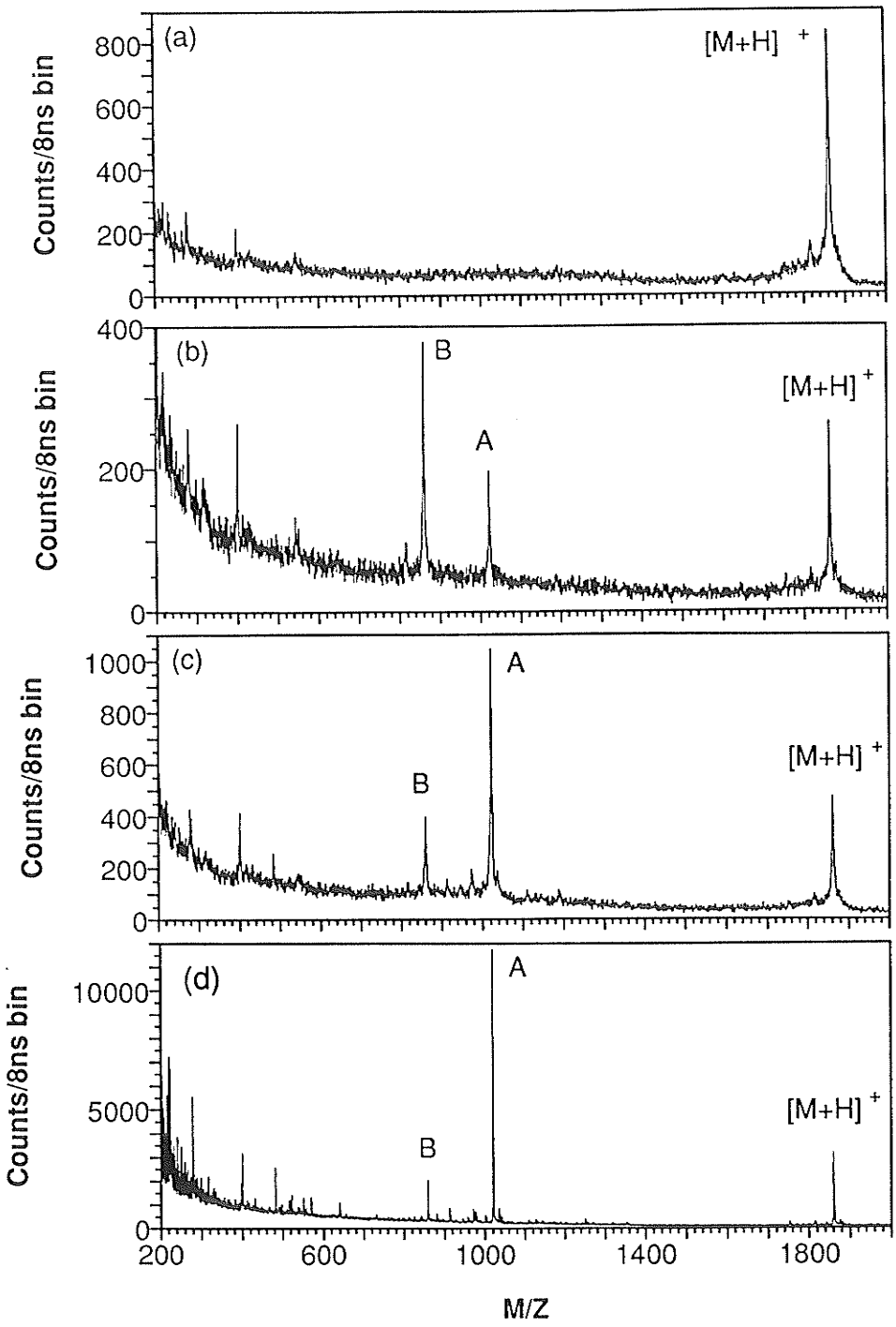

Figure 5.20 Positive ion TOF mass spectra of γ-endorphin, bound to a nitrocellulose surface. Direct spectrum (a) recorded prior to any reaction, (b) recorded after reaction with trypsin for 12 minutes at 24 ^{0}C, (c) recorded after (b) and after an addition of 8 μL 0.1% aqueous TFA to the target; (d) Reflected spectrum, target is same as in (c). The measured mass of fragment A is 1019.5 u and fragment B is 858.5 u.

& (b) show the respective daughter ion spectra of the fragments A and B. The labelled peaks correspond to the peptide sequences shown above. It can be seen that most daughter ions are related to the sequence of the corresponding peptide fragment and, compared to the daughter ion spectra of γ-endorphin presented in the last section, these spectra are of much better quality and signal-to-background ratio.

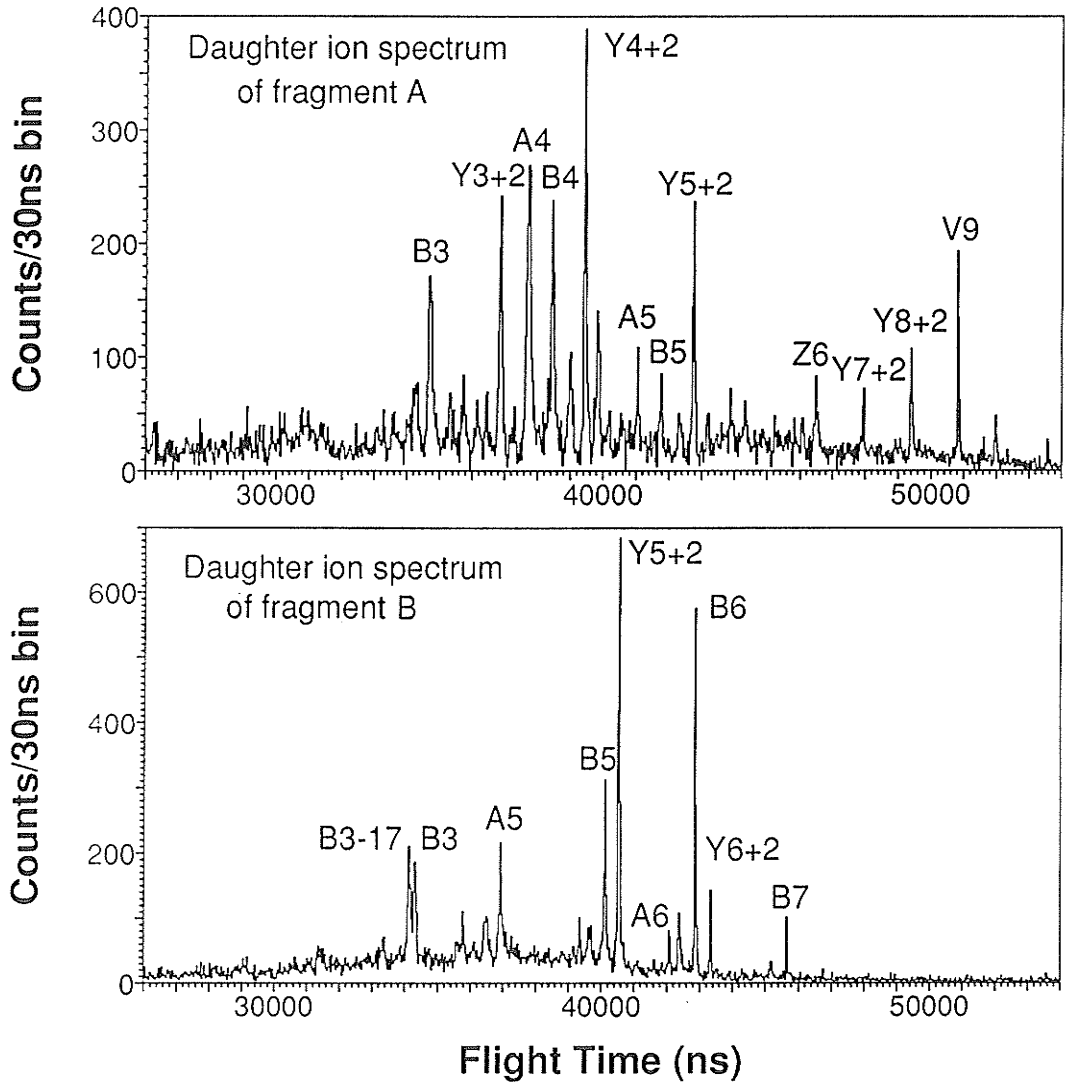

Figure 5.21 Daughter ion spectra of the reaction products A and B from tryptic digestion of γ-endorphin.

5.5.2 Peptide Mixture Analysis

Many biological samples exist as mixtures because of the presence of related compounds, or the presence of contaminants such as salts. In addition, interference from matrix ions may also be considered as a mixture analysis. Tandem mass spectrometry is a powerful tool in mixture analysis. By using MS/MS methods, the mixture can be analysed without resorting to pre-separation of the components of the mixture. The disadvantages of most commercial tandem instruments are low efficiency and high expense. In contrast, our MS/MS method can provide a high efficiency and economical approach to some mixture analysis problems. Our MS/MS analysis of the enzymatic digestion product of a peptide, demonstrated in the previous section is practically a real mixture analysis. Further examples of mixture analysis by our reflecting TOF MS/MS method are presented below.

5.5.2.1 Simple peptide mixture

Fig. 5.22 shows the direct and neutral mass spectra of a simple peptide mixture. The mixture was made by mixing 1μg/μL peptide solutions of glycylglycylphenylalanine, leucine-enkephalin, methionine-enkephalin and proenkephalin in the volume ratio 1:1:1:0.5. A few μL of this solution was deposited on the nitrocellulose surface of the target. The daughter ion spectra of $[M+H]^+$ ions of all four peptide components were recorded simultaneously and are presented in Figs. 5.23 (1-4). The structure of each parent ion can be analysed by using the mass of the parent ion and its daughter ion spectrum. If the daughter ion spectrum, or the metastable decay pattern of the parent from

the pure peptide is known, the parent can be identified by the daughter ion spectrum recorded from the mixture. By comparing some of the daughter ion spectra (shown in Chapter 4 and § 5.3) from the respective pure peptides, it is easy to identify these peaks in the mixture spectrum. For leucine-enkephalin, methionine-enkephalin and proenkephalin, the daughter ions of $[M+H]^+$ obtained from the mixture are same as those from their respective pure samples. These parents could be readily identified if they were present in an unknown mixture. Some extra peaks were observed in the daughter ion

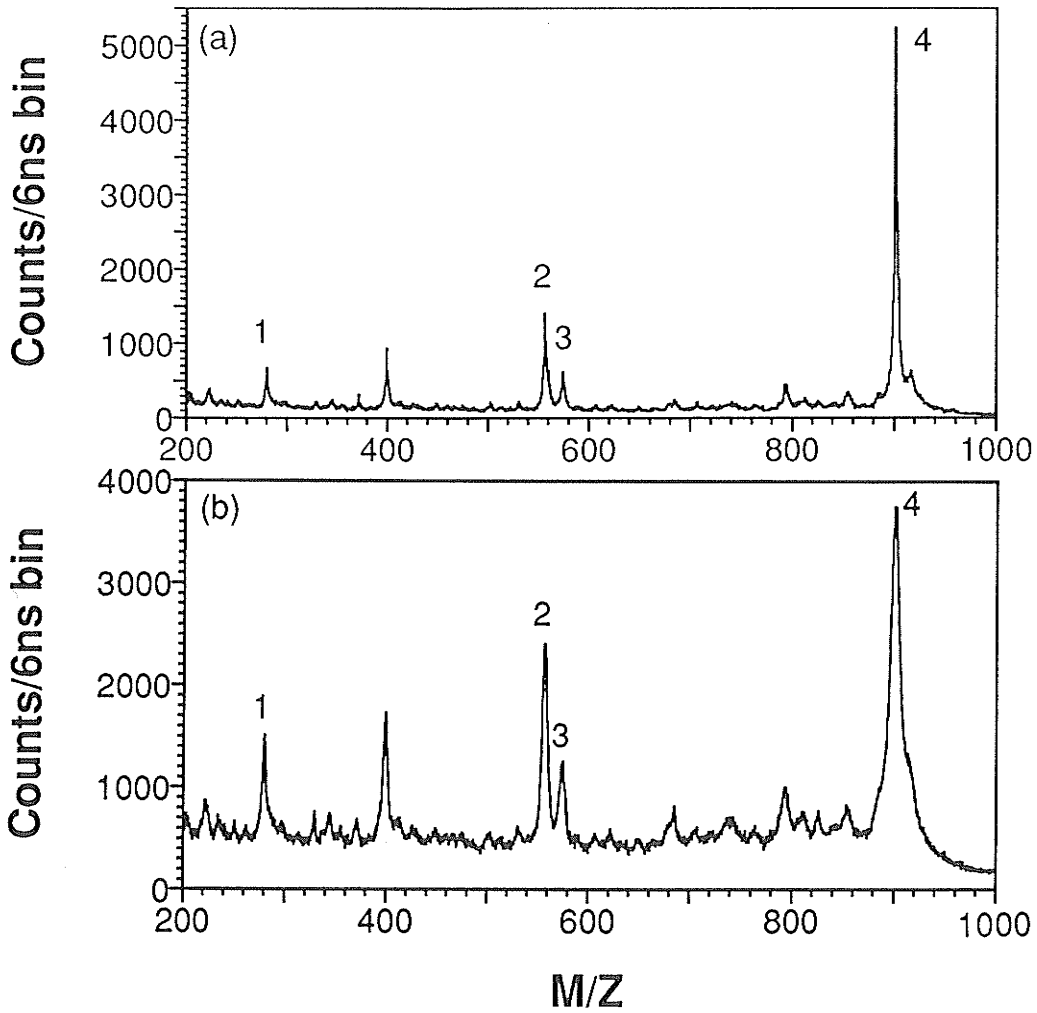

Figure 5.22 (a) Direct TOF mass spectrum of peptide mixture containing GGF, 280 u (peak 1*), Leu-enkephalin 556 u, (peak 2), Met-enkephalin 574 u, (peak 3) and proenkephalin 900 u,(peak 4); (b) neutral spectrum.

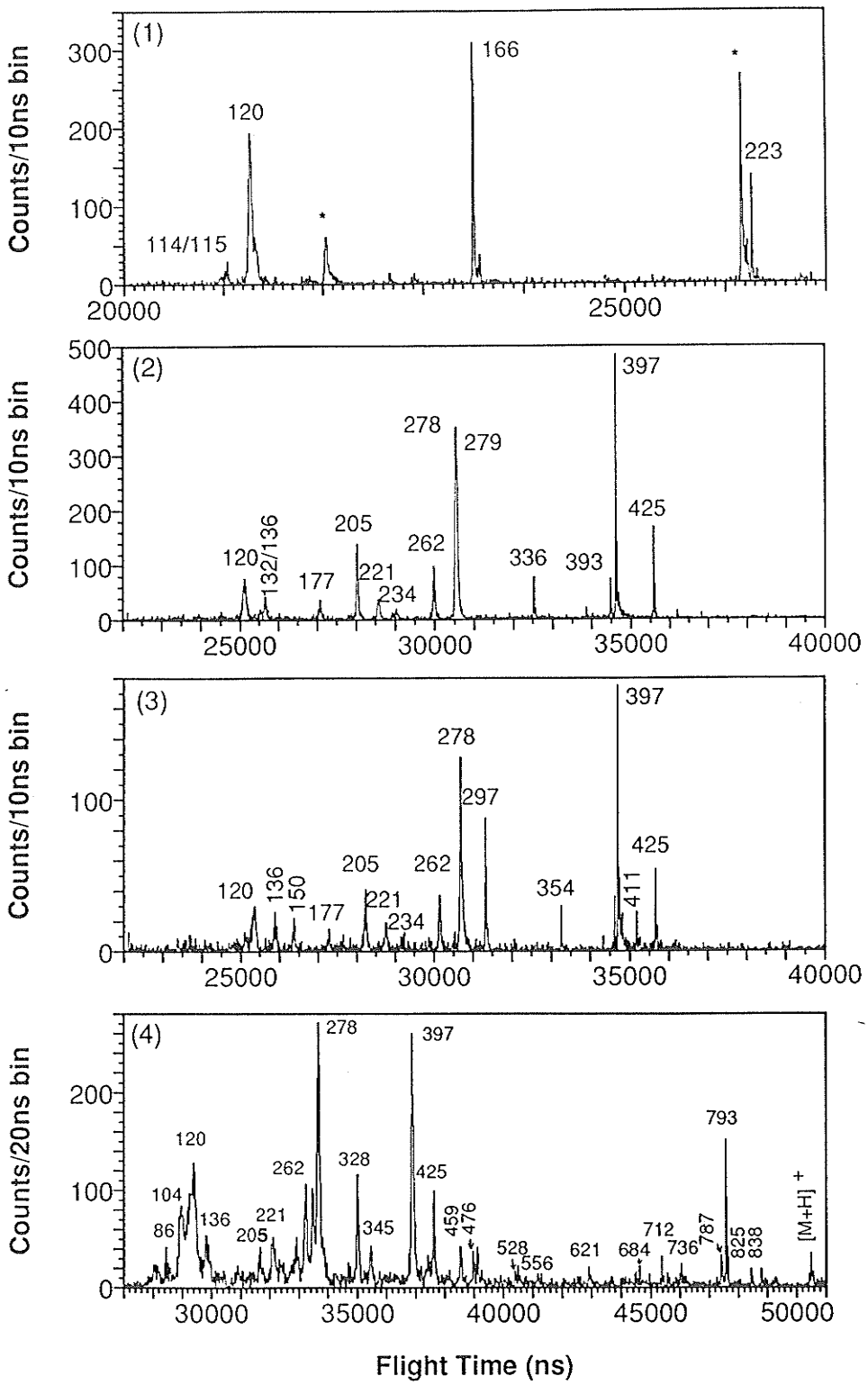

Figure 5.23 Daughter ion spectra correlated with neutral fragments from decay of component 1 (GGF), 2 (Leu-enkephalin), 3 (Met-enkephalin) and 4 (proenkephalin) in the mixture. The mirror is optimized for parent ions.

spectrum of $[M+H]^+$ from GGF in the mixture; two peaks (*m/z* 136, 221), denoted by an asterisk, are from parent ions of *m/z* 278, which is a common fragment (B_3) of the three other peptides, since all three contain the sequence Tyr-Gly-Gly-Phe-. The *m/z* 120 peak consists of two daughters, one from *m/z* 280, $[M+H]^+$ of GGF and the other from *m/z* 279, a fragment (Y_2+2) of leu-enkephalin. These complicat ions in the daughter ion spectrum of GGF rise because the GGF $[M+H]^+$ parent ion *m/z* 280 cannot be separated well from the other two parent peaks (*m/z* 278, 279) due to the limited resolution of the neutral spectrum (Fig. 5.22 (b)). For proenkephalin, many of the decays give nonresolved low mass daughters; hence, they cannot be identified in the daughter ion spectrum. However, as shown above, the problem is easily solved by recording the spectrum in several sections. Fig. 5.24 shows a low mass section of the daughter ion spectrum of proenkephalin in the mixture, for which the mirror voltage has been optimized on the daughter ion of mass ~ 221 u; it can be see that the broad humps in the Fig. 5.23 (4) spectrum are completely resolved in Fig. 5.24.

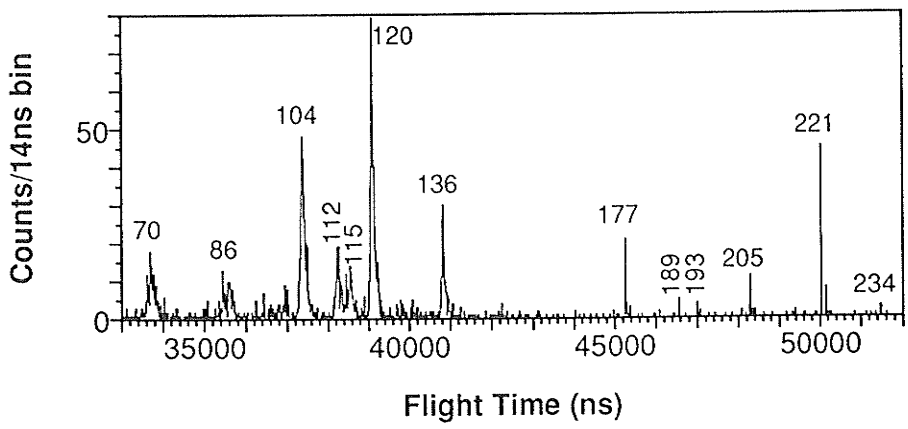

Figure 5.24 Section of daughter ion spectrum of proenkephalin in the mixture, with mirror optimized for the daughter of ~221 u.

5.5.2.2 Tyrothricin

The antimicrobial agent tyrothricin is a more complex sample; it exists as a mixture of cyclic decapeptides of masses ~1300 u. Fig. 5.25 shows a reflected spectrum of the molecular ion region of this compound. As reported by Barber et al [237], and in our early report [225], six minor components are visible in the mixture, in addition to the three well-known major constituents. The daughter ion spectra from tyrocidin A and B are shown in Figs. 5.26 (A) and (B). The two spectra have similar patterns but the latter is displaced by 39 u, since the mass of $[M+H]^+$ ions of tyrothricin A is 39 u higher than that of tyrothricin B, as shown in the reflected spectrum; this arises from replacement of phenylalanine by tryptophan. As remarked by Cody et al [238], the daughter ion spectra of such cyclic peptides are complicated, since a multiplicity of initial ring cleavages is possible. However, considerable structural information can be extracted from the daughter

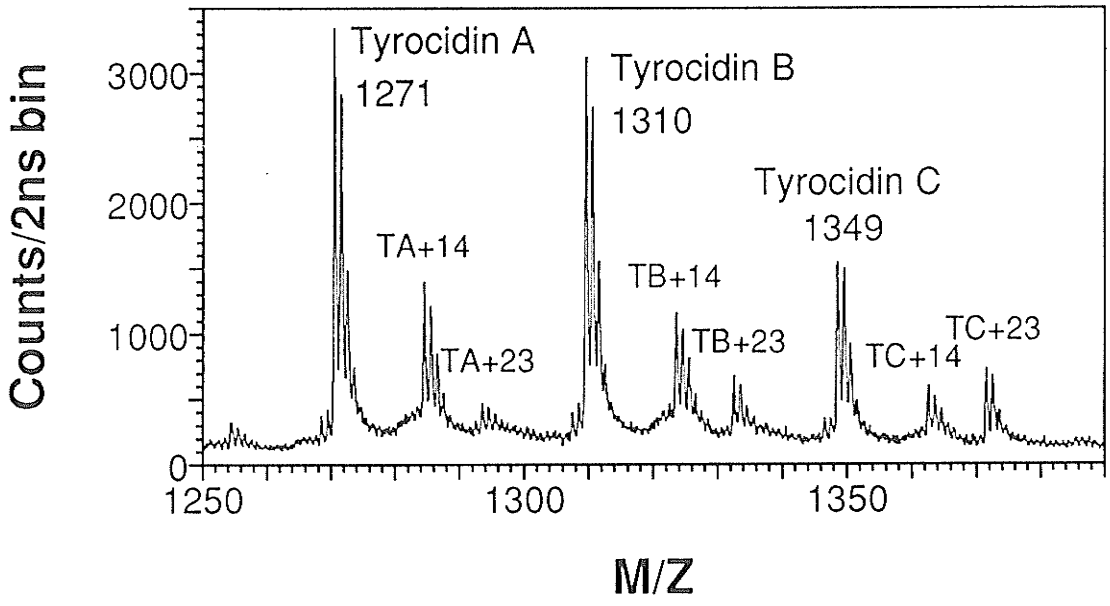

Figure 5.25 The molecular ion region of the reflected mass spectrum of tyrothricin.

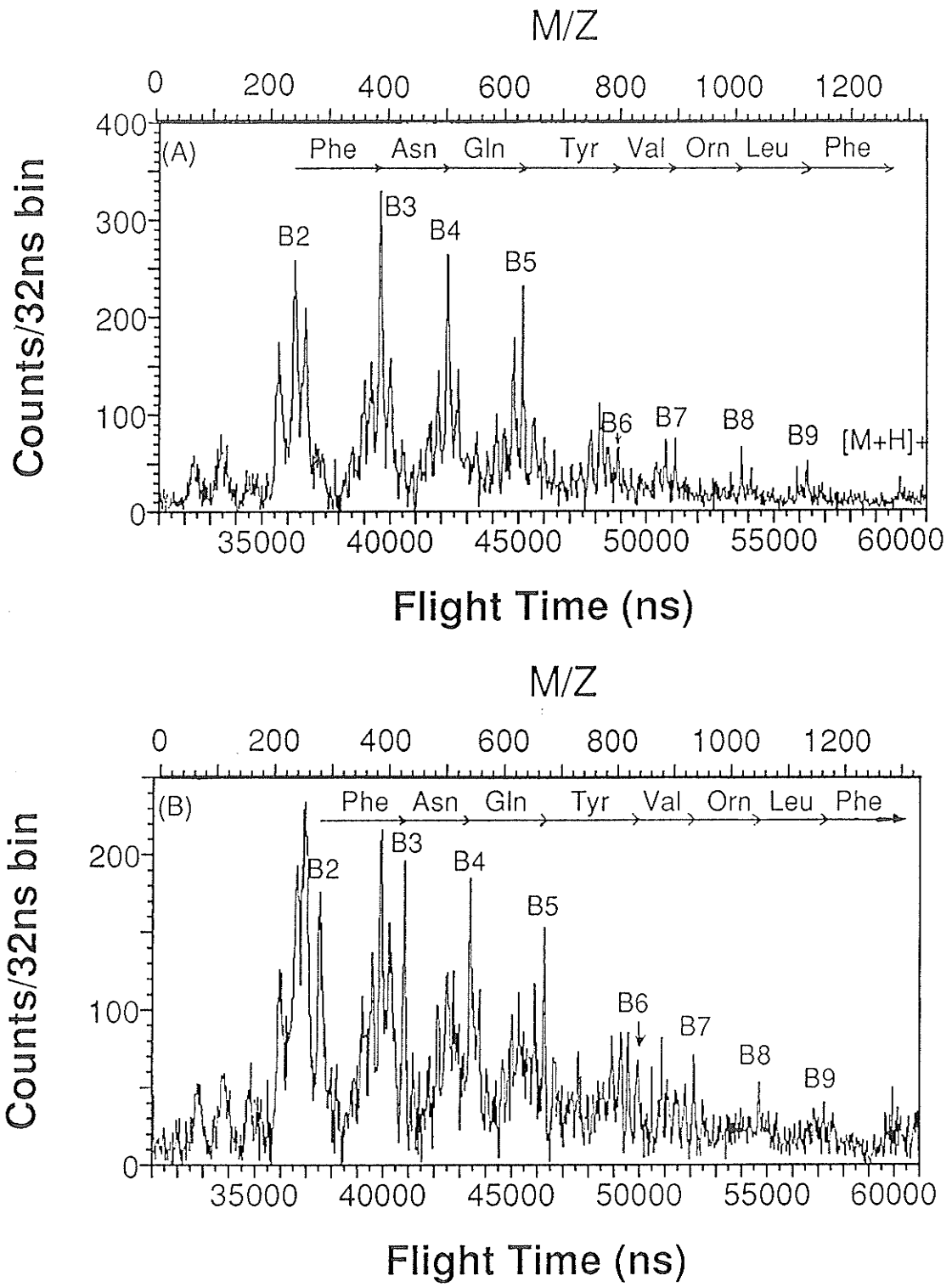

Figure 5.26 Daughter ion mass spectra from metastable decay of $[M+H]^+$ ions from (A) tyrocidin A, (B) tyrocidin B.

ion spectra, including the almost complete B ion sequence shown, which is consistent with the structure previously proposed [237].

5.6 NUCLEOTIDE ANALYSIS

Nucleotides represent another important category of biomolecules. The use of TOF-SIMS for characterization of unprotected and protected nucleotides has been investigated in our laboratory by recording and analysing the normal TOF mass spectra generated from samples deposited on an aluminium boehmite, AlO(OH), surface [239]. Recently both positive and negative, normal TOF and daughter ion mass spectra of two nucleotides have been obtained from samples on a nitrocellulose substrate. For peptide samples, positive ion spectra usually have higher molecular ion yields and more plentiful structure-related fragment ions. For nucleotides, the positive ion spectra also give good molecular ion peaks, but negative ion spectra usually provide more meaningful structure-related fragment ion information. Samples were dissolved in 0.1% aqueous TFA, as before, to give a concentration of ca 1μg/μL. A few μL of the solution were deposited on the nitrocellulose surface. For negative ion spectra, sample targets were bombarded by 35 keV Cs^+ primary ions, the negative secondary ions produced were accelerated to 12.5 keV, and they struck detector 2 (see Fig. 2.1) with an energy of 12 keV, since a voltage of -500 V was applied to the electron converter dynode to provide acceleration for secondary electrons. Negative ion spectra from two nucleotide samples are discussed below.

5.6.1 2-Isopropyl-TpT

2-Isopropyl-TpT is an unprotected dinucleotide, a sample of which was obtained from Dr. Hruska, of the Department of Chemistry, University of Manitoba. The negative reflected spectrum and the daughter ion spectrum from $[M-H]^-$, along with the molecular structure, are shown in Fig. 5.27. It can be seen from the reflected spectrum (Fig. 5.27(a)) that the molecular ions have good signal intensity for a sample on the nitrocellulose substrate; however, the weak structure-related fragment ions can hardly be distinguished from the intense background matrix ion peaks from nitrocellulose. The advantage of the MS/MS method is shown again clearly in this case. The "clean" daughter ion spectrum (Fig. 5.27 (b)) provides unambiguous fragment ion information, and allows full identification of this modified nucleotide.

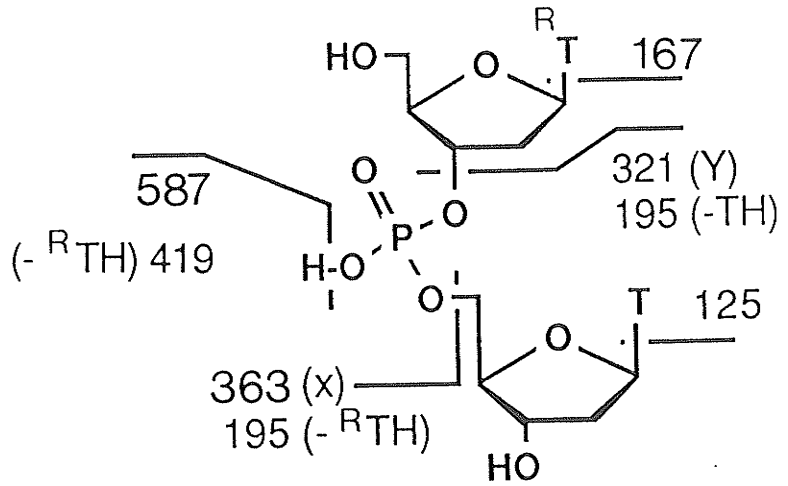

R=$CH(CH_3)_2$

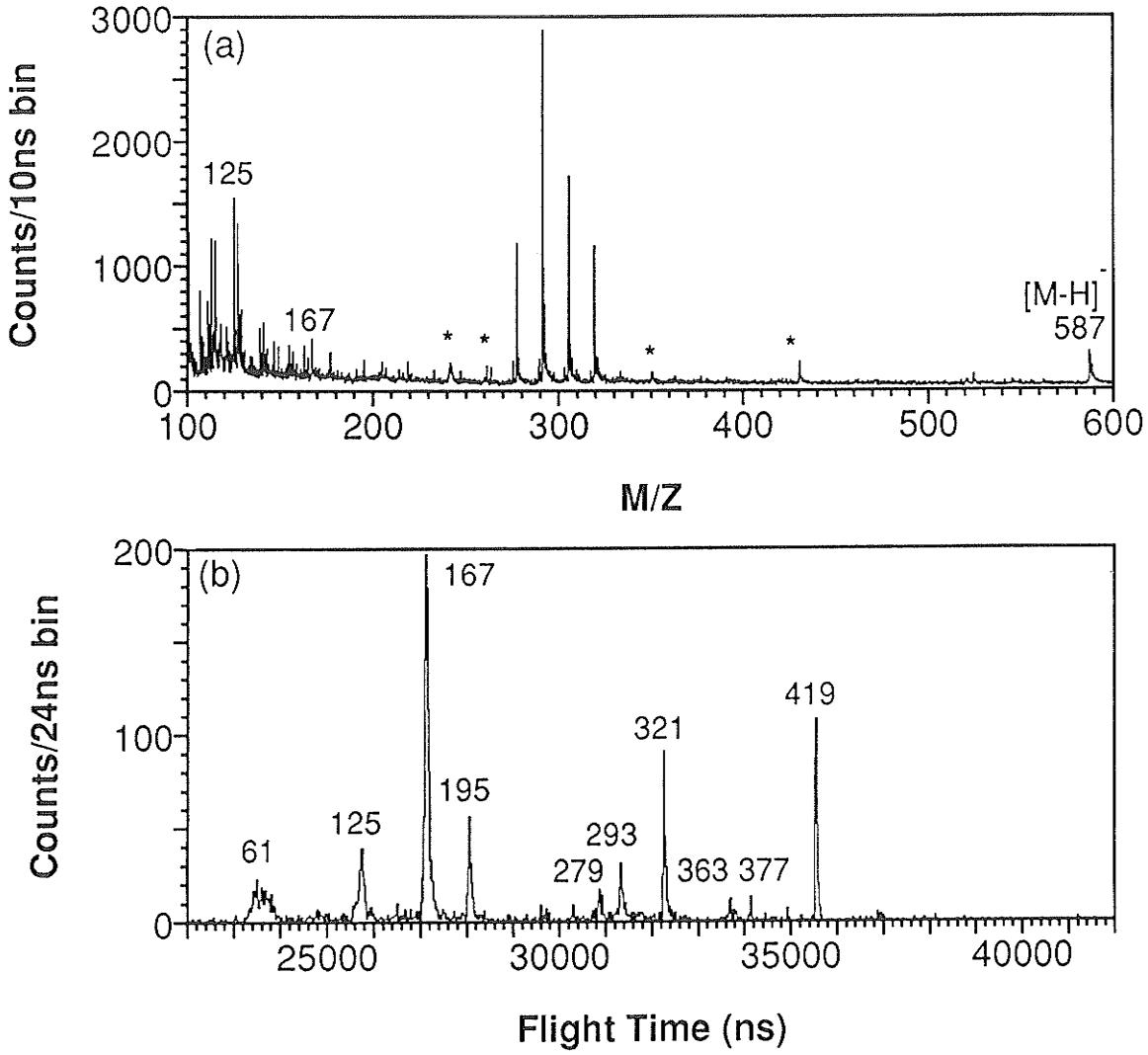

Figure 5.27 Negative ion TOF mass spectra of unprotected dinucleotide 2-isopropyl-TpT deposited on nitrocellulose: (a) reflected spectrum, peaks denoted with an asterisk are daughters of metastable ions, and the four unlabeled intense peaks around mass 300 u are from nitrocellulose. (b) daughter ion spectrum from metastable decay of $[M-H]^-$ from the dinucleotide, nominal masses are shown.

5.6.2 $_{Bz}G^{NPE}(2'p5'U)3'p5'U$ (GUU)

$_{Bz}G^{NPE}(2'p5'U)3'p5'U$ (GUU) is a protected trinucleotide (see the structure). This branched RNA fragment, synthesized at McGill University [240], contains an unusual feature, i.e. vicinal 2′-5′ and 3′-5′ phosphodiester linkages. The structure of this nucleotide and its normal TOF (direct) spectrum are shown in Fig. 5.28. As in the case of peptides,

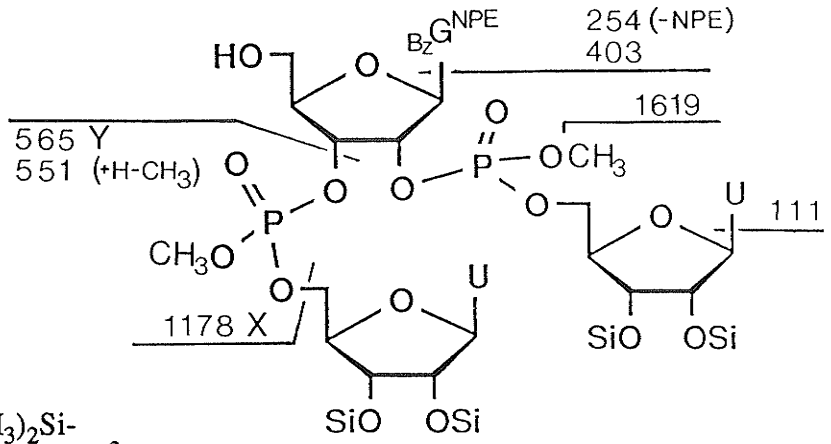

Si=t-Bu$(CH_3)_2$Si-
B_z=C_6H_5CO- (on N^2 of G)
NPE=p-$NO_2C_6H_4CH_2CH_2$- (on O^6 of G)

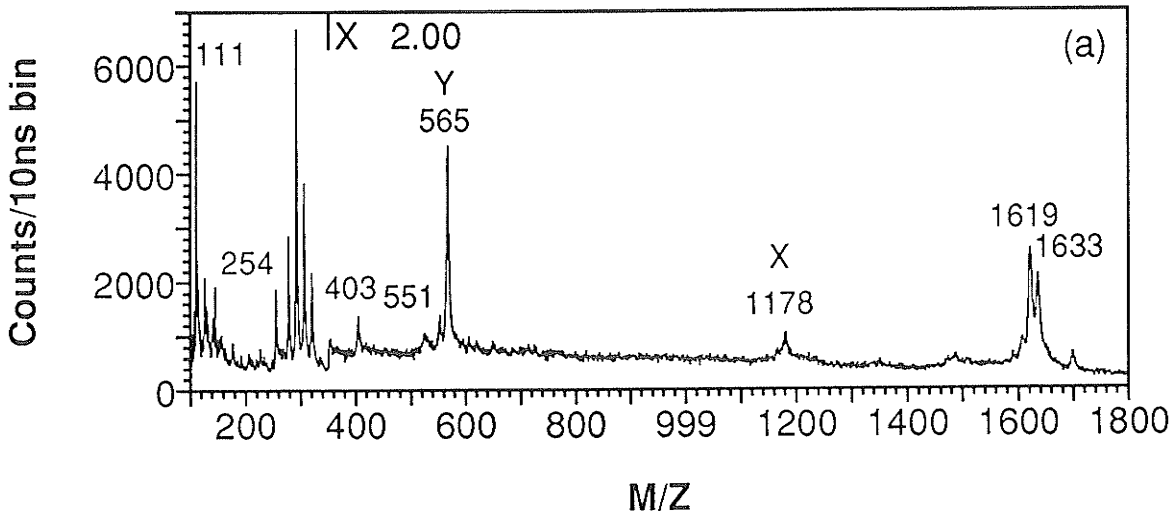

Figure 5.28 Negative ion TOF mass spectrum of protected trinucleotide GGU (see the structure) deposited on nitrocellulose, measured with mirror voltage off (direct spectrum).

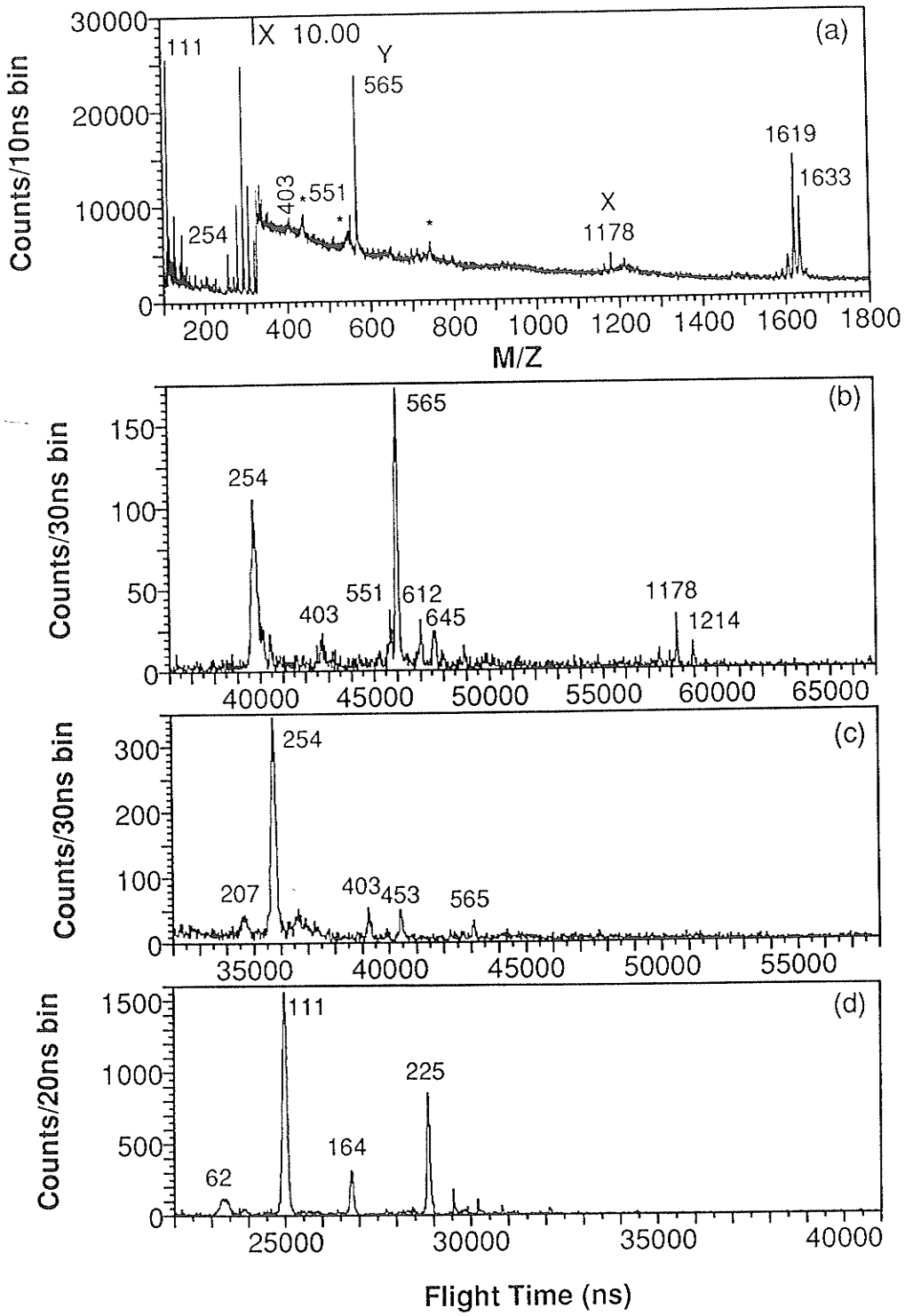

Figure 5.29 Negative ion TOF mass spectra of protected trinucleotide GGU (see the structure) deposited on nitrocellulose: (a) reflected spectrum, peaks denoted by an asterisk are daughters of metastable ions, and daughter ion spectra from (b) $[M-H]^-$ (1633 u), (c) X (1178 u), and (d) Y (565 u).

the molecular ion yield was also increased for this bigger nucleotide by using nitrocellulose rather than boehmite as a substrate. Apart from interference from matrix ions in the low mass region, some main fragment ions also have reasonable relative abundance; however, the daughter ion spectrum provides a better way to sort out the relationship between the fragment ions and the molecular ions, or between daughter ions and parent ions, particularly, when the molecular ion peak is not the only high mass peak in the region. Since several daughter ion mass spectra can be recorded simultaneously in our MS/MS method, the daughter ion spectra of the molecular ion and its three high mass fragment ions were recorded along with the reflected spectrum (Fig. 5.29 (a)). Figs. 5.29 (c-d) show the daughter ion spectra of $[M-H]^-$ (1633 u), fragment X (1178 u) and Y (565 u). The corresponding fragmentation pattern is shown in Fig. 5.28 and, again, unambiguous structural information can be extracted from the daughter ion spectra, thus allowing identification of the nucleotide.

5.7 CONCLUDING REMARKS (Personal and otherwise)

The construction of Manitoba TOF II, the reflecting time-of-flight mass spectrometer started in August 1985; the experimental work described in this thesis ended in the middle of 1990. Some preliminary results were obtained in early 1986 [136,137], but most of the results presented in this thesis were obtained in the last two years of measurements. Since the spectrometer was constructed, its performance, including the resolution, the spectrometer and correlated measurement efficiencies was improved gradually, as understanding of the problems improved; this resulted in better experimental

results and better quality spectra. A mass resolving power of $m/\Delta m_{FWHM}$ of ~13,000 has been achieved with the single-stage mirror in the case of secondary ions produced by primary ion bombardment; further improvement is still possible if the time spread in the acceleration region, along with the other factors (see chapter 3), is reduced. The effect of the initial energy distribution in the acceleration region has been studied only recently, so very limited experimental data were available for analysis. More systematic investigations need to be done, particularly on reduced mirror voltage operation to determine the feasibility of using a single-stage mirror in the case of a larger initial energy distribution, such as in a matrix-assisted laser desorption experiment.

The application of the nitrocellulose substrate in our laboratory [97,138] gave considerable improvement in measurement of peptide samples, which resulted in not only a higher mass range but also "cleaner" spectra, which are usually free of the sodium contamination problem and have better signal-to-background ratio. The reflecting TOF-SIMS spectrometer along with its MS/MS capability has been demonstrated to be a practically useful and sensitive technique in characterizing both inorganic and organic material; however, the mass range of organic molecules is still limited largely by the desorption efficiency. Since the mass range of a TOF analyzer is unlimited, employing a more efficient desorption method such as matrix-assisted laser desorption seems to be necessary and attractive.

Improvement of correlated measurement efficiency results in higher sensitivity and better daughter ion spectra. For larger molecules, the detection efficiency of the charged daughters can be improved further by increasing the acceleration and post-acceleration voltages, but the improvement of the neutral detection efficiency is expected to be more difficult; the neutral energy increases with accelerating voltage but neutral cannot be post-

accelerated; thus the efficiency of the correlated measurement is lower for decompositions that produce a large daughter ion and a small neutral. An alternative solution is to have some sort of physical selection of the parent ions, e.g. by a pair of deflection plates. The reflector could then be used as a high efficiency daughter ion mass analyzer or the second stage of a tandem mass spectrometer; in this case, the detection of a daughter ion spectrum is no longer affected by the detection of the neutrals. This might be useful if the matrix-assisted laser desorption method is employed; since a large number of secondary molecular ions are usually produced for each laser pulse, the coincidence method, which is based on single ion counting detection is no longer feasible. If the desorbed intact molecular ions are metastable, or if they can be dissociated with another laser, then the decomposition products of selected parent ions can be analyzed with the reflector. Since a time-of-flight analyzer is naturally suited for a pulsed ion source and also has high efficiency, such a daughter ion analysis appears to be attractive.

APPENDIX A

TIME VARIATIONS DUE TO CHANGES IN ACCELERATION VOLTAGE

A.1 The time variation due to changes in acceleration voltage can be calculated from Eq. (2-15) to (2-18). For convenience of discussion, the energy form of Eq. (2-16) is used in the following calculations.

The flight time [Eq. (2-16)] in terms of energy is

$$t=\frac{2m}{qE}\sqrt{\frac{2q}{m}(U+U_i)}+\frac{L}{\sqrt{\frac{2q}{m}(U+U_i)}}+\frac{2d}{\sqrt{\frac{2q}{m}(U+U_i)}+\sqrt{\frac{2q}{m}U_i}} \tag{1}$$

When the ion energy changes from qU_0 to $qU=q(U_0+\Delta U)$ due to changes in acceleration voltage, the flight time changes from t to $t+\Delta t$, the relative time variation can be written as

$$\frac{\Delta t}{t}=\frac{(\Delta t)_{reflex}}{t}+\frac{(\Delta t)_{accel}}{t} \tag{2}$$

where $(\Delta t)_{reflex}/t$ corresponds to the contributions of time variation in the mirror and in free flight, and $(\Delta t)_{accel}/t$ corresponds to the contribution in the acceleration region.

If the value of the mirror electric field is chosen according to Eq. (2-17), i.e. a focusing value for a given value of initial energy, then we have

$$\frac{(\Delta t)_{reflex}}{t} = \frac{\frac{1}{2}\left(\frac{\sqrt{1+w+k}}{p} + \frac{p}{\sqrt{1+w+k}} - 2\right) + \frac{d}{L}h^2\left(\sqrt{1+w+k} - 1\right)}{1+\frac{d}{L}(h+h^2)} \tag{3}$$

$$\frac{(\Delta t)_{accel}}{t} = \frac{\frac{d}{L}\left(\frac{p}{\sqrt{1+w+k}+\sqrt{k}} - h\right)}{1+\frac{d}{L}(h+h^2)} \tag{4}$$

where

$$p=\sqrt{1+k}; \quad h=\frac{\sqrt{1+k}}{\sqrt{1+k}+\sqrt{k}}; \quad k=\frac{U_i}{U_0}; \quad w=\frac{\Delta U}{U_0}$$

Equations 2 to 4 describe how, for a given value of initial energy, the flight time varies when the acceleration voltage changes under the first order focusing condition.

A.2 If ions with zero initial axial velocity are taken as reference ions, i.e. the value of the mirror electric field corresponding to the focusing condition of these ions is chosen, or we set $k=0$ in Eq. (2-17), then the time variation due to changes in both acceleration voltage and ion initial energy can be expressed as

$$\frac{\Delta t_{t0}}{t_0} = \frac{t+\Delta t-t_0}{t_0} = \frac{(\Delta t_{t0})_{reflex}}{t_0} + \frac{(\Delta t_{t0})_{accel}}{t_0} \tag{5}$$

$$\frac{(\Delta t_{t0})_{reflex}}{t_0} = \frac{\frac{1}{2}\left(\sqrt{1+w+k} + \frac{1}{\sqrt{1+w+k}} - 2\right) + \frac{d}{L}\left(\sqrt{1+w+k} - 1\right)}{1+\frac{2d}{L}} \tag{6}$$

$$\frac{(\Delta t_{t0})_{accel}}{t_0} = \frac{\frac{d}{L}\left(\frac{1}{\sqrt{1+w+k}+\sqrt{k}}-1\right)}{1+\frac{2d}{L}} \qquad (7)$$

where $t_0=2(L+2d)/v_0$ is the total flight time for ions with zero initial velocity.

APPENDIX B

PEPTIDE FRAGMENTATION AND ROEPSTORFF-FOHLMAN NOMENCLATURE

In SIMS/FAB, the fragment ions observed in a peptide spectrum are often characteristic of the peptide's structure. The fragment ions may be formed by breaking bonds along the peptide "backbone", with the addition of hydrogens, or by losing side chains. The fragment ions produced by breaking single bonds in a peptide backbone are of great interest since these ions give the best structure or sequence information of the peptide. To identify the ionic fragments of peptides, a symbolism has been adopted in this thesis. The symbolism is based on that suggested by Roepstorff and Fohlman [205] and subsequently endorsed in slightly modified form by Biemann and Martin [40]. The basic features of the symbolism are illustrated in Figure B.1. Ionic fragments that contain the N terminus result from backbone cleavages denoted by A, B, and C; those that contain the C terminus from backbone cleavages denoted by X, Y, and Z. In both cases, subscripts denote which bond is cleaved (i.e. the number of amino acid residues contained in the ion fragment) counting from the N terminus and C terminus, respectively. By extension, the letter I has been used here to denote immonium ions, with a subscript indicating the amino acid residue (numbered from the N terminal) from which it is derived. Examples of the interior fragment ion labeling are also given in Figure B.1, e.g. $(B_4Y_3)_2$, the subscript outside the bracket indicating the number of amino acid residues

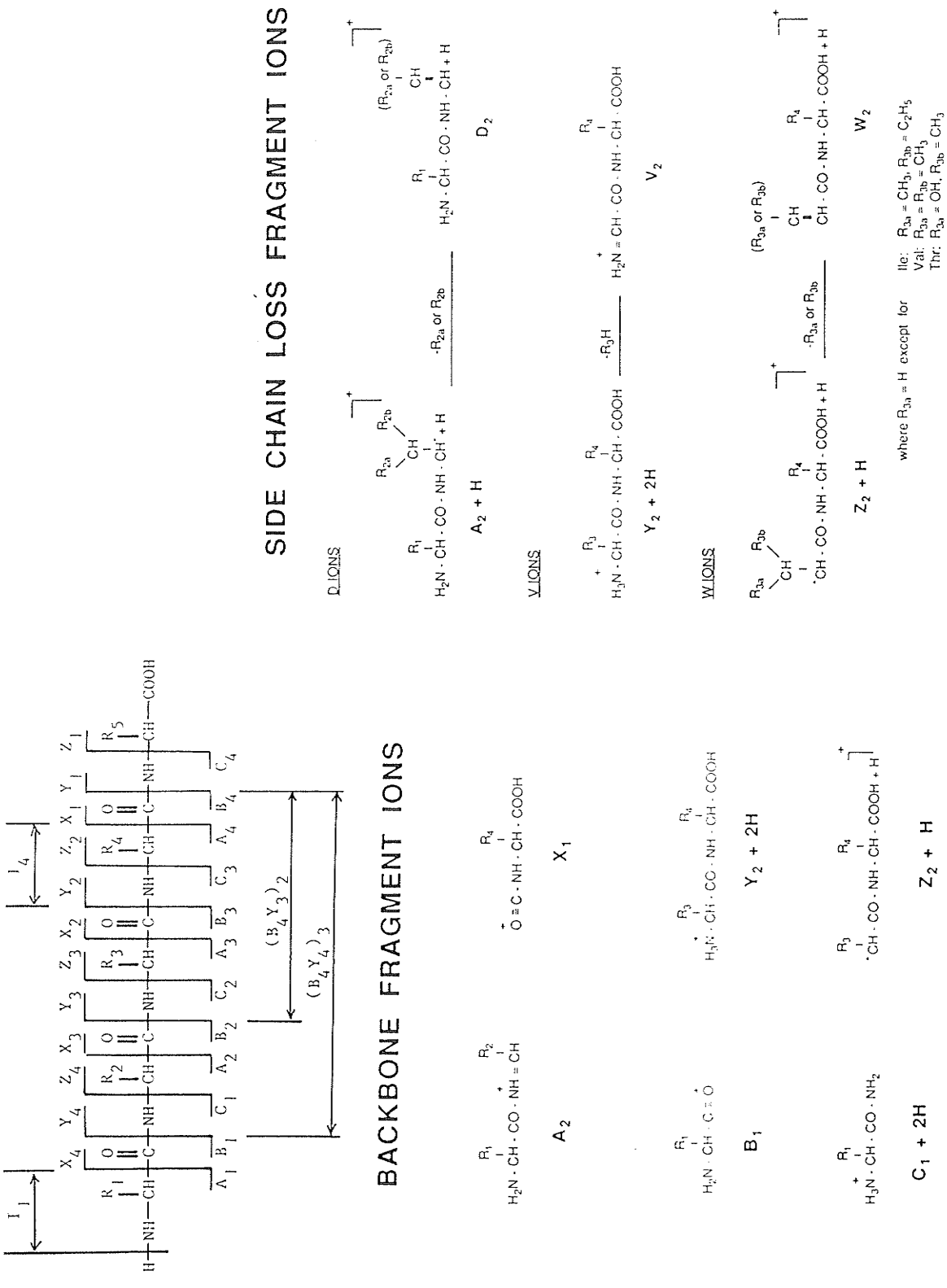

Figure B.1 Peptide Fragmentation. All backbone, side chain loss and interior fragmentation patterns are shown.

contained in the interior fragment. For the fragments with additional hydrogens or those containing metal ions (Na, Ag, K etc.) the integral mass value of hydrogen or chemical symbols of the metal elements have been added to the letter symbols to indicate the modified fragments rather than the primes and double primes of the original proposal [205]. Fragment ions may also be produced by losing amino acid side chains; these ions can also be useful in sequencing a peptide such as, for example, differentiating leucine from the isomeric isoleucine. [227]. The side chain loss fragment ions are labeled with D_n, V_n and W_n, which result from the side chain loss from the fragment ions A_n+H, Y_n+2H and Z_n+H respectively. The structures of the D_n, V_n and W_n ions are also illustrated in Figure B.1.

A recursive algorithm for generating the masses of these backbone and side chain loss fragment ions, as well as interior fragment ions is given in Table B.1.

TABLE B.1
A Recursive Procedure for Calculating the Masses of Peptide Fragment Ions

Type of ions	Mass calculation
N sequence ions	B=A+28 (CO) C=B+15 (NH) $D_n=C_m+28$ *$(CH=CH_2+H)$
C Sequence ions	Y=Z+15 (NH) X=Y+28 (CO) $W_m=Z_m+H-(R_m-CH_2)=Y_{m-1}+56$ *$(CH_2=CHCO+H)$ $V_m=Y_m+H-R_m=Y_{m-1}+57$ $(H_2N=CHCO)$
Interior sequence ions	$A_nX_m=C_nZ_m=B_nY_m$ $A_nY_m=B_nY_m+28$ (CO) $A_nZ_m=B_nY_m+43$ (CO+NH) $B_nX_m=B_nY_m-28$ (CO) $B_nZ_m=B_nY_m+15$ (NH) $C_nX_m=B_nY_m-43$ (CO+NH) $C_nY_m=B_nY_m-15$ (NH)

*(+ variants for isoleucine, threonine and Valine)

APPENDIX C

SYMBOLS, MASSES AND COMPOSITIONS OF AMINO ACID RESIDUES

The molecular weight of a peptide may be obtained by the addition of the masses of the appropriate amino acid residues and terminal groups shown in the following table.

TABLE C.1
Masses and Compositions of the Commonly Occurring Amino Acid Residues

Proper Name	Elemental Composition	Symbol	Monoisotopic Mass (u)	Average Mass (u)
Alanine	C_3H_5NO	Ala A	71.03711	71.0788
Arginine	$C_6H_{12}N_4O$	Arg R	156.10111	156.1875
Asparagine	$C_4H_6N_2O_2$	Asn N	114.04293	114.1038
Aspartic Acid	$C_4H_5NO_3$	Asp D	115.02694	115.0886
Cysteine	C_3H_5NOS	Cys C	103.00919	103.1388
Glutamic Acid	$C_5H_7NO_3$	Glu E	129.04259	129.1155
Glutamine	$C_5H_8N_2O_2$	Gln Q	128.05858	128.1307
Glycine	C_2H_3NO	Gly G	57.02146	57.0519
Histidine	$C_6H_7N_3O$	His H	137.05891	137.1411
Isoleucine	$C_6H_{11}NO$	Ile I	113.08406	113.1594
Leucine	$C_6H_{11}NO$	Leu L	113.08406	113.1594
Lysine	$C_6H_{12}N_2O$	Lys K	128.09496	128.1741
Methionine	C_5H_9NOS	Met M	131.04049	131.1926
Ornithine	$C_5H_{10}N_2O$	Orn O	114.07931	114.1472
Phenylalanine	C_9H_9NO	Phe F	147.06841	147.1766
Proline	C_5H_7NO	Pro P	97.05276	97.1167
Serine	$C_3H_5NO_2$	Ser S	87.03203	87.0782
Threonine	$C_4H_7NO_2$	Thr T	101.04768	101.1051
Tryptophan	$C_{11}H_{10}N_2O$	Trp W	186.07931	186.2132
Tyrosine	$C_9H_9NO_2$	Tyr Y	163.06333	163.1760
Valine	C_5H_9NO	Val V	99.06841	99.1326

REFERENCES

[1] J. J. Thomson, *Philos. Mag. VI*, **24**, 209, 668 (1912).

[2] A. J. Dempster, *Phys. Rev.* **11**, 316 (1918).

[3] F. W. Aston, *Philos. Mag.* **38**, 709 (1919).

[4] F. A. White and G.M. Wood, *Mass Spectrometry, Applications in Science and Engineering*, John Wiley & Sons, Chichester, England, (1986).

[5] A. Frigerio, *Essential Aspects of Mass Spectrometry*, Spctrum Publications Inc. Flushing, New York, (1974).

[6] M. S. B. Munson and F. H. Field, *J. Am. Chem. Soc.* **88**, 1621 (1962).

[7] M. G. Inghram and R.J. Gomer, *Chem. Phys.* **22**, 1279 (1954).

[8] H. D. Beckey, *Field Ionization Mass Spectrometry*, Pergamon, Oxford (1971).

[9] H. D. Beckey, *Int. J. Mass Spectrom. Ion Phys.* **2**, 500 (1969).

[10] D. F. Torgerson, R. P. Skowronski and R. D. Macfarlane, *Biochem. Biophys. Res. Commun.* **60**, 616 (1974).

[11] R. D. Macfarlame and D. F. Torgerson, *Science*, **191**, 920 (1976).

[12] D. Metta, H. Diamond, R. F. Barnes, J. Milsted, J. Jr. Gray, P. J. Henderson, C. M. Stenvenson, *J. Inorg. Nucl. Chem.* **27**, 33 (1965).

[13] H. W. Schmitt, W. E. kiker, C. W. Williams, *Phys. Rev.* **B 137**, 837 (1965).

[14] M. L. Vestal, *Mass Spectrom. Rev.* **2**, 447 (1983).

[15] B. Sundqvist and R. D. Macfarlane, *Mass Spectrom. Rev.* **4**, 421 (1985).

[16] G. Jonsson, A. Hedin, P. H & Kansson, B. Sundqvist, H. Bennich and P. Roepstorff. *Rapid Commun. Mass Spectrom.* **3**, 190 (1989).

[17] P. Dück, W. Treu, W. Galster, H. Frohlich and H. Voit, *Nucl. Instrum. Meth.*, **168**, 601 (1980).

[18] P. Håkansson, A. Johansson, I. Kamensky, B. Sunsquist, J. Fohlman and P. Peterson, *IEEE Trans, Nucl. Sci.* **28**, 1776 (1981).

[19] P. Håkansson, I. Kamensky and B. Sundqvist, *Nucl. Instrum. Meth.* **198**, 43 (1982).

[20] H. Voit, H. Fröhlich, P, Dück, B. Nees, E. Nieschler, W. Bischof and W. Tiereth, *IEEE Trans. Nucl. Sci.* **30**, 1759 (1983).

[21] R. D. Macfarlane, in *Ion Formation from Organic Solids*, Ed. by A. Benninghoven, Springer Series in Chem. Phys., **25**, 32 (1983).

[22] M. Salehpour, D. C Fishel and J. E. Hunt, *Phys. Rev.* **B38**, 12320 (1988).

[23] A. Benninghoven, F. G. Rüdenauer and H. W. Werner, *Secondary Ion Mass Spectrometry*, Chemical Analysis Vol. 86, John Wiley & Sons Inc. (1987).

[24] J. J. Thomson, *Philos. Mag.* **20**, 752 (1910).

[25] R. E. Honig, *J. Appl. Phy.* **29**, 549 (1958).

[26] R. E. Honig *Int. J. Mass Spectrom. Ion Proc.* **66**, 31 (1985).

[27] A. Benninghoven, D. Jaspers and W. Sichtermann, *Appl. Phys.* **11**, 35 (1976).

[28] A. Benninghoven, *Phys. Status Solid.* **34**, K 169 (1969).

[29] A. Benninghoven, *Surf. Sci.* **35**, 427 (1973).

[30] A. Benninghoven, *Z. Phys.* **230**, 403 (1970).

[31] A. Benninghoven, and W. K. Sichtermann, *Org. Mass Spectrom.* **12**, 595 (1977).

[32] A. Benninghoven, and W. K. Sichtermann, *Anal. Chem.* **50**, 1180 (1978).

[33] D.J. Surman and J.C. Vickerman, *J. C. S. Chem. Comm.* 324 (1981).

[34] M. Barber, R. J. Bordoli, R. D. Sedgwick, A. N. Tyler, *J. C. S. Chem. Comm.* 325 (1981).

[35] M. Barber, R. J. Bordoli, R. D. Sedgwick, A. N. Tyler, *Nature* **293**, 325 (1981).

[36] M. Barber, R. J. Bordoli, G. J. Elliott, R. D. Sedgwick, A. N. Tyler, *Anal. Chem.* **54**, 645A (1982).

[37] C. Fenselau, in *Ion Formation from Organic Solids, IFOS*, Ed. by A. Benninghoven, Springer Series in Chem. Phys., **25**, 99-100 (1983).

[38] H. N. Turner, B. I. Durnlap, R. J. Colton, *Anal. Chem.* **56**, 373 (1984).

[39] A. L. Burlingame, J. O. Whitney D. H. Russell, *Anal. Chem.* **56**, 373 (1984).

[40] K. Biemann and S. Martin, *Mass Spectrom. Rev.* **6**, 1 (1987).

[41] A. L. Burlingame, D. Maltby, D. H. Russell, P. T. Holland, *Anal. Chem.* **60**, 294A (1988).

[42] K. B. Tomer, *Mass Spectrom. Rev.* **6**, 445, 483 (1989).

[43] R. E. Honig and J. R. Woolston, *Appl. Phys. Lett.* **2**, 138, (1963).

[44] R. E. Honig, *Appl. Phys. Lett.* **3**, 8 (1963).

[45] F. J. Vastola and A. J. Pirone, in *Advances in Mass Spectrometry*, Ed. by E. E. Kendrick, Institute of Petrolem, London, Vol. 4, p. 107 (1968).

[46] R. O. Mumma, F. J. Vastola, *J. Org. Mass Spectrom.* **6**, 1373 (1972).

[47] E. Unsöld, F. Hillenkamp and R. Nitsche, *Analusis* **4**, 115 (1976).

[48] M. A. Posthumus, P. G. Kistemaker, H. C. C. Meuzelear and M. C. ten Noever de Brauw, *Anal. Chem.* **50**, 985 (1978).

[49] F. Heresch, ER, Schmid and J. F. K. Huber, *Anal. Chem.* **52**, 1803 (1980).

[50] R. J. Cotter, *Anal. Chem.*, **52**, 1760 (1980).

[51] E. D. Hardin and M. C. Vestal, *Anal. Chem.* **53**, 1492 (1981).

[52] R. Stall and F. W. Rollgen, *Org. Mass Spectrom.* **14**, 642 (1979).

[53] R. J. Conzemius and J. M. Capellen, *Int. J. Mass Spectrom. Ion Phys.* **34**, 197 (1980).

[54] R. Kaufmann, R. F. Hillenkamp, W. Wechsurg, H. J. Heinen, M. Schürmann, *Scanning Electron Microsc.* **II**, 279 (1979), LAMMA is a registered trademark of Leybold-Heraus.

[55] P. Feigl, B. Schueler and F. Hillenkamp, *Anal. Chem.* **57**, 2935 (1985).

[56] F. Hillenkamp, in *Ion Formation from Organic Solids, IFOS*, Ed. by A. Bennihoven, Springer Series in Chem. Phys., **25**, 190-205 (1983).

[57] F. Hillenkamp, in *Secondary Ion Mass Spectrpmetry, SIMS V*, Ed. by A. Benningoven, R. J. Colton, D. S. Simmons and H. W. Werner, Springer Series in Chem. Phys. **44**, 471 (1986).

[58] B. Jöst, B. Schueler and F. R. Krueger, *Z. Naturforsch*, **37a**, 18 (1982).

[59] C. L. Wilkins, D. A. Weil, C. L. C. Yang and C. F. Ijames *Anal. Chem.* 57 (1985).

[60] R. B. Van Bremen, M. Snow, R. J. Cotter, *Int. J. Mass Spectrom. Ion Phys.* **49**, 35 (1983).

[61] R. J. Cotter, *Anal. Chem. Acta* **195**, 45 (1987).

[62] F. Hillenkamp, *Advances in Mass Spectrometry*, Ed. by P. Longvialle Vol. **11a**, p.354, Heyden & Sons. London (1989).

[63] E. Schröder, H. Munster, H. Budzikiewicz, *Org. Mass Spectrom.* **21**, 707 (1986).

[64] R. B. Freas, M. M. Ross, J. E. Campana, *J. Am. Chem. Soc.* **107**, 6195 (1985).

[65] K. Walter, U. Boesl and E. W. Schlag. *Int. J. Mass Spectrom Ion Phys.* **71**, 309 (1986).

[66] J. Grotemeyer, U. Boesl, K. Walter and Schlag, *J. Am. Chem. Soc.* **108**, 4233 (1986).

[67] R. Tembreull and D. M. Lubman, *Anal. Chem.* **59**, 1003 (1987).

[68] R. Tembreull and D. M. Lubman, *Anal. Chem.* **59**, 1082 (1987).

[69] R. Tembreull and D. M. Lubman, *Appl. Spectrosc.* **41**, 431 (1987).

[70] F. Engelke, J. H. Hahn, W. Henke and R. Zare, *Anal. Chem.* **59**, 909 (1987).

[71] P. Roepstorff. P. F. Nielsen, K. Klarskov, P. Hojrup, *Biomed. Environm. Mass Spectrom.* **16**, 9 (1988).

[72] R. J. Cotter, *Anal. Chem.* **60**, 781A (1988).

[73] K. Tanaka, Y. Ido, S. A. Kita, Y. Yoshida and T. Yoshida, *Proc. 2nd Japan-China Joint Sympos. On Mass Spectrom.* p. 185 (1987).

[74] K. Tanaka, H. Waki, Y. Ido, S. Akita, Y. Yoshida and T. Yoshida, *Rapid Commun. Mass Spectrom.* **2**, 151 (1988).

[75] M. Karas, D. Bachmann, U. Bahr and F. Hillenkamp, *Int. J. Mass Spectrom. Ion Proc.* **78**, 53 (1987).

[76] M. Karas, D. Bachmann, U. Bahr and F. Hillenkamp, *Anal. Chem.* **57**, 2935 (1985).

[77] M. Karas, F. Hillenkamp, *Anal. Chem.* **60**, 2299 (1988).

[78] M. Karas, U. Bahr and F. Hillenkamp, *Int. J. Mass Spectrom. Ion Processes* **92**, 231 (1989).

[79] M. Karas, U. Bahr, A. Ingendoh, F. Hillenkamp, *Angew, Chem.* Int Ed, Engl. **28**, 760 (1989).

[80] R. C. Beavis, B. T. Chait, *Rapid Commun. Mass Spectrom.* **3**, 233 (1989).

[81] R. C. Beavis, B. T. Chait, *Rapid Commun. Mass Spectrom.* **3**, 432 (1989).

[82] R. C. Beavis, B. T. Chait, *Rapid Commun. Mass Spectrom.* **3**, 436 (1989).

[83] R. C. Beavis, B. T. Chait, *Proceedings of the 38th ASMS Conference on Mass Spectrometry and Allied Topics.* Tucson, Arizona, p. 26, (1990).

[84] M. Yamashita and J. B. Fenn, *J. Phys. Chem.* **88**, 4451 (1984).

[85] M. Yamashita and J. B. Fenn, *J. Phys. Chem.* **88**, 4671 (1984).

[86] C. M. Whitehouse, R. N. Dreyer, M. Yamashita and J. B. Fenn, *Anal. Chem.* **57**, 675 (1985).

[87] M. Dole, L. L. Mach, R. L. Hines, R. C. Mobley, L. P. Ferguson and M. B. Alice, *J. Chem. Phys.* **49**, 2240 (1968).

[88] L. L. Mach, P. Kralik, A. Rheude and M. Dole, *J. Chem. Phys.* **52**, 4977 (1970).

[89] C. K. Mong, M. Mann. J. B. Fenn, *Z. Phys.* **D 10**, 361 (1988).

[90] S. F. Wong, C. K. Meng and J. B. Fenn, *J. Phys. Chem.* **92**, 546 (1988).

[91] J. B. Fenn, M. Mnn. C. K. Meng, S. F. Wong and C. M. Whitehouse, *Science* **246**, 64 (1989).

[92] J. B. Fenn, M. Mnn. C. K. Meng, S. F. Wong, *Mass Spectrom. Rev.* **9**, 37 (1990).

[93] T. R. Covey, R. F. Bonner, B. I. Shushan and J. D. Henion, *Rapid Commun. Mass Spectrom.* 2, 249 (1988).

[94] J. A. Loo, H. R. Udseth and R. O. Smith, *Anal. Biochem.* **179**, 404 (1989).

[95] S. K. Chowdhury, V. Katta and B. T. Chait, *Rapid Commun. Mass Spectrom.* **4**, 81 (1990).

[96] G. P. Jonsson, A. B. Hedin, P. L. Hakansson, B. U. R. Sundqvist, B. G. S. Swe, P. F. Nielsen, P. Roepsdorff, K. E. Johansson, I. Kamensky and M. S. C. Lindberg, *Anal. Chem.* **58**, 1084 (1986).

[97] F. Lafortune, R. Beavis, X. Tang, K. G. Standing and B. T. Chait, *Rapid Commun. Mass Spectrom.* **1**, 114 (1987).

[98] W. E. Stephens. *Phys. Rev.* **69**, 691 (1946).

[99] A. E. Cameron and D. F. Eggers, Jr., *Rev. Sci. Instrum.* **19**, 605 (1948).

[100] J. A. Hipple. H. Sornmer and H. A. Thomas, *Phys. Rev.* **76**, 1877 (1949).

[101] E. D. Courant, M. S. Livingston and H. S. Sngder, *Phys. Rev.* **88**, 1190 (1952).

[102] J. P. Blewett. *Phys. Rev.* **88**, 1197 (1952).

[103] W. Paul and H. Steinwedel, *Z. Naturforsch A*, **8**, 448 (1953).

[104] J. E. Campana, *Anal. Instrum.* **16**, 1 (1987).

[105] D. Price, in *Dynamic Mass Spectrometry*, Ed. by D. Price and J. F. J. Todd, Heyden and Son, London. Vol. **4**, p. 1 (1976).

[106] R. S. Gohlke, *Anal. Chem.* **31**, 535 (1959).

[107] H. S. Katzenstein and S. S. Friedland, *Rev. Sci Instrum.* **26**, 324 (1955).

[108] W. C. Wiley and I. H. Mclaren, *Rev. Sci Instrum.* **26**, 1150 (1955).

[109] J. M. B. Bakker, in *Dynamic Mass Spectrometry*, Eds. by D. Price and J. F. J. Todd, Heyden and Son, London. Vol. **4**, p. 25 (1976).

[110] R. Stein, *Int. J. Mass Spectrom. Ion Process.* **14**, 205 (1974).

[111] D. Price, G. J. Milnes, *Int. J. Mass Spectrom. Ion Process.* **60**, 61 (1984).

[112] B. A. Mamyrin, Doctoral Dissertation. Physico-Technical Institute, Academy of Sciences, USSR. Leningrad (1966); B.A. Mamyrin, Inventors Certificate No. 198034, USSR (1966).

[113] V. I. Karataev, B. A. Mamyrin and D. V. Shmikk, *Sov. Phys. Tech. Phys.* **16**, 1177 (1972).

[114] B. A. Mamyrin, V. I. Karataev, D. V. Shmikk and V. A. Zagulin, *Sov. Phys. JETP* **37**, 45 (1973).

[115] B. A. Mamyrin and D. V. Shmikk, *Sov. Phys. JETP* **49**, 762 (1979).

[116] A. Benninghoven in *Ion Formation from Organic Solids, IFOS II*, Ed. by A. Benninghoven, Springer Series in Chem. Phys., **25**, 64 (1983).

[117] K. Walter U. Boesl and E. W. Schlag, *Int. J. Mass Spectrom. Ion Processes* **71**, 309 (1986); U.Boesl, J. Grotemeyer, K. walter and E. Schlay *Anal. Instrum.* **16**, 151 (1987).

[118] M. Yang and J. P. Reilly, *Anal. Instrum.* **16**, 133 (1987); *Int J. Mass Spectrom. Ion Processes* **75**, 209 (1987).

[119] S. Della-Negra, C. Deprun and Y. LeBeyec, *Rapid Commun. Mass Spectrom.* **1**, 10 (1987).

[120] E. Niehuis, T. Heller. H. Field and A. Benninghoven in *Secondary Ion Mass Spectrometry, SIMS V*, Ed. by A. Benningoven, R. J. Colton, D. S. Simmons and H. W. Werner, Springer Series in Chemical Physics, No. **44**, 188 (1986); *J. Vac. Sci, Technol A.* **A5** 1243 (1987).

[121] X. Tang, R. Beavis, W. Ens, F. Lafortune, B. Schueller and K. G. Standing *Int, J. Mass Spectrom. Ion Processes*, **85**, 43 (1988); also this thesis.

[122] R. Grix, R. Rutscher, G. Li, U. Gruner and H. Wollnik, *Rapid Commun. Mass Spectrom.* **5**, 83 (1988).

[123] K. G. Standing, in *Proc. 6th Int. Conf. Secondary Ion Mass Spectrometry, SIMS VI*, Ed. by A. Benninghoven, A. M. Huber and J. W. Werner, John Wiley & Sons, Chichester, England, p. (1988).

[124] *Secondary Ion Mass Spectrometry, SIMS V*, Ed. by A. Benninghoven, R. J. Colton, D. S. Simmons and H. W. Werneret, Springer Series in Chemical Physics, **No. 44**, Spering-Verlag, Berling (1986).

[125] *Proc. 6th Int. Conf. Secondary Ion Mass Spectrometry, SIMS VI*, Ed. by A. Benninghoven, A. M. Huber and J. W. Werner, John Wiley & Sons, Chichester, England, (1988).

[126] *Ion Formation from Organic Solids, IFOS III*, Springer Proc. Phys. **9** (1986).

[127] *Ion Formation from Organic Solids, IFOS IV*, Ed. by A. Benninghoven, John Wiley & Sons, Chichester, England, (1989).

[128] *Ion Formation from Organic Solids, IFOS V*, Ed. by Hedin, B. U. R. Sundqvist and A.

Benninghoven, John Wiley & Sons, Chichester, England, (1990).

[129] *Analytical instrumentation* **16**, No. 1 (1987).

[130] B. T. Chait and K. G. Standing, *Int. J. Mass Spectrom. Ion Phys.* **40**, 185 (1981).

[131] W. Ens. Ph. D. Thesis, University of Manitoba, Winnipeg, 1984.

[132] R. D. Macfarlane, and D. F. Torgerson. *Int. J. Mass Spectrom. Ion Phys.* **21**, 81 (1976).

[133] W. Ens. R. Beavis and K. G. Standing, *Phys. Rev. Lett.* **50**, 27 (1983).

[134] K. G. Standing, W. Ens, R. Beavis in *Ion Formation from Organic Solids, IFOS*, Ed. by A. Bennighoven, Springer Series in Chemical Physics, **25**, p. 107 (1983).

[135] J. E. Campana, T. M. Barlark, R. J. Colton, J. J. DeCorpo, J. R. Wyatt and B. I. Dunlap, *Phys. Rev. Lett.* **47**, 1046 (1981).

[136] X. Tang, R. Beavis, W. Ens, B. Schueler and K. G. Standing, *Proceedings of the 34th ASMS Conference on Mass Spectrometry and Allied Topics*, Cinicinnati, OH., p. 171 (1986).

[137] K. G. Standing, R. Beavis, G. Bolbach, W. Ens, F. Lafortune, D. Main, B. Schueler. X. Tang and J.B.Westmore, *Anal. Instrum.* **16**, 173 (1987).

[138] F. Lafortune, R. Beavis, W. Ens, X. Tang and K. G. Standing, *Proceedings of the 35th ASMS Conference on Mass Spectrometry and Allied Topics*, Denver, CO., p. 68 (1987).

[139] W. F. Hadden and F. W. McLafferty, *Anal. Chem.* **41**, 31 (1969).

[140] W. W. Hunt, Jr. R. E. Huffman and K. E. McGee, *Rev. Sci Instrum.* **35**, 82 (1964).

[141] B. T. Chait and F. H. Field. *Int. J. Mass Spectrom, Ion Phys.* **41**, 17 (1981); B. T. Chait, *Int. J. Mass Spectrom, Ion Phys.* **53**, 227 (1983).

[142] B. Schueler, R. Beavis, G. Bolbach, W. Ens, D. E. Main and K. G. Standing, *SIMS V*, Springer Ser. Chem. Phys., **44**, 57 (1986).

[143] B. Schueler, R. Beavis, W. Ens, D. E. Main, X. Tang and K. G. Standing, *Int. J. Mass Spectrom. Ion Processes* **92**, 185, (1989).

[144] H. Danigel, H. Jungclas, and L. Schmidt. *Int. J. Mass Spectrom. Ion Phys.* **52**, 223 (1983).

[145] S. Della-Negra and Y. LeBeyec, *Int. J. Mass Spectron. Ion Proc.* **61**, 21 (1984).

[146] S. Della-Negra and Y. LeBeyec, *Anal. Chem.* **57**, 2035 (1985).

[147] S. Della-Negra and Y. LeBeyec, Springer Proc. Phys., **9**, 42 (1986).

[148] W. Ens, R. Beavis, G. Bolbach, D. Main, B. Schueler and K. G. Standing, *Nucl. Instrum. Meth.* **A245**, 146 (1986);

[149] W. Ens, Y. Mao, X. Tang and K. G. Standing, *Proceedings of the 37th ASMS Conference on Mass Spectrometry and Allied Topics*, Miami Beach, p. 1059 (1989).

[150] F.W. Mclafferty, Ed., *Tandem Mass Spectrometry*, John Wiley & Sons, New York, (1983).

[151] K.L. Busch, G.L. Glish and S.A. Mcluckey, *Mass Spectrometry/Mass Spectrometry*, VCH Publishers, New York, (1988).

[152] R. D. Macfarlane and D. F. Torgerson, *Proceedings of the 24th ASMS Conference on Mass Spectrometry and Allied Topics*, San Diego, CA., p. 330, (1976).

[153] R. W. Odom, S. E.Buttrill, Jr. R. H. Fleming, M. Rossi, L. N. Goeller and W. Gohl, *Int. J. Mass Spectrom. Ion Phys.*, **49**, 319 (1983).

[154] W. Gohl, R. Kutscher, H. J. Laue and H. Wollnik, *Int. J. Mass Spetrom. Ion Phys.* **48**, 411 (1983).

[155] U. Boesl. H. J. Neusser, R. Weinkanf and E. W. Schlag, *J. Phys. Chem.*, **86**, 4857 (1982).

[156] H. Kühlewind, H. J.Neusser and E. W. Schlag. *Int. J. Mass Spectrom. Ion Phys.*, **51**, 255 (1983); *J. Chem. Phys.* **82**, 5452 (1985). H. J. Neusser, *Int. J. Mass Spectrom. Ion Processes.* **79**, 141 (1987).

[157] H. J. Neusser, U. Boesl, R. Weinkanf and E. W. Schlag, *Int. J. Mass Spectrom. Ion Processes.* **60**, 147 (1984).

[158] A. Brunelle, S. Della-Negra, J. Depauw, H. Joret and Y. Le Beyec, in *Ion Formation from Organic Solids, IFOS V*, Ed. by Hedin, B. U. R. Sundqvist and A. Benninghoven, John Wiley & Sons, Chichester, England, p. 39 (1990).

[159] P. W. Geno and R. D. Macfarlane, *Int. J. Mass Spectrom. Ion Processes* **77**, 75 (1987).

[160] L. Kelner, S. P. Markey, *Int. J. Mass Spectrom. Ion Processes* **59**, 157 (1984).

[161] C. Berger. *Int. J. Mass Spectrom. Ion Phys.* **46**, 63 (1983).

[162] R. Kutscher, H. Wollnik and W. Gohl. *Verh Dtsch Phys Ges.* **19**, 763 (1984).

[163] R. Frey, G. Weiss, H. Kaminski and E. W.Schlay, *Z. Naturforsch, Teil A* **40**, 1349 (1985).

[164] For the solution of a similar problem, see, for example, W. R. Smythe, *Static and Dynamic Electricity*, McGraw-Hill, New York, Sect. 5.36 (1950).

[165] See, for example, C. J. Tranter, *Bessel Functions with some Physical Applications*, Hart, New York, (1969).

[166] C. J. McNeal, R. F. Macfarelane, E. L. Thurston, *Anal. Chem.* **51**, 2036 (1979).

[167] S. Tamaki, W. Sichtermann and A. Benninghoven. *Jap. J. A. Appl. Phys.* **23**, 544 (1984).

[168] A. Benninghoven, E. Niehues, D. Greifendorf, D. Van Leyen and W. Lange, in *SIMS V*. Ed. by

A. Benninghoven et al, Spring series in Chemical Physics, **44**, p. 497 (1986).

[169] X. Tang, W. Ens, K. G. Standing and J. B. Westmore, *Anal, Chem.* **60**, 1791 (1988).

[170] R. Beavis, W. Ens, M. J. Nemer, K. K. Ogilvie, K. G. Standing and J. B. Westmore, *Int. J. Mass Spectrom. Ion Phys.* **46**, 475 (1983).

[171] E. A. Jordan, R. D. MacFarlane, C. R. Martin and C. J. McNeal, *Int. J. Mass Spectrom. Ion Phys.* **53**, 345 (1983).

[172] M. Alai, P. Demirer, C. Fenselau and R. J. Cotter, *Anal Chem.* **58**, 1303 (1986).

[173] W. Ens, P. Hakansson, B. U. R. Sundqvist in *Proc. 6th Int. Conf. Secondary Ion Mass Spectrometry, SIMS VI*, Ed. by A. Benninghoven, A. M. Huber and J. W. Werner, John Wiley & Sons, Chichester, England, p. 623 (1988).

[174] B. T. Chait, *Int. Mass Spectrom. Ion Processes.* **78**, 237 (1987).

[175] P. Demirer, C. Fenselau and R. J. Cotter, *Int. J. Mass Spectrom. and Ion Processes.* **78**, 251 (1987).

[176] P. Roepstorff, P. F. Nielson, B. U. R. Sundqvist, P. Håkansson and G. Jonsson. *Int. J. Mass Spectrom. Ion Processes.* **78**, 229 (1987).

[177] J. L. Wiza, *Nucl. Instrum. Methods.* **162**, 587 (1979).

[178] A. M. Zebelman, W. G. Meyer, K. Halbach, A. M. Poskanzer, R. G. Sextro, G. Gabor and D. A. Lacdis, *Nucl. Instrum. Methods.* **141**, 439 (1977).

[179] R. D. Macfarlane, J. Hill and D. C. Jacobs, *Anal. Instrum.* **16**, 51 (1987).

[180] S. Della-Negra, I. Lorthois, Y. LeBeyec and R. Macfarlane, Orsay Rep. IPNO-DRE-83-03, Institut de Physique Nucléaire, Orsay, France. S. Della-Negra, M. Dumail and Y. LeBeyec, Orsay Rep. IPNO-DRE-85-33, Institut de Physique Nucléaire, Orsay, France.

[181] S. Della Negra and Y. Le Beyec, *Nucl. Sci Appl.* **1**, 569 (1983).

[182] R. J. Beuhler and L. Friedman, *Nucl. Instrum. Meth.* **170**, 309 (1980).

[183] R. J. Beuhler *J. Appl. Phys.* **54**, 4118 (1983).

[184] A. Hedin, P. Håkansson and B.U.R. Sundqvist, *Int. J. Mass Spectrom. Ion Processes.* **75**, 275 (1987).

[185] P. W. Geno and R. D. Macfarlane, *Int. J. Mass Spectrom. Ion Processes*, **92**, 195 (1989).

[186] K. G. Standing, W. Ens. R. Beavis, G. Bolbach, D. E. Main, B. Schueler and J. B. Westmore, in *Ion Formation from Organic Solids, IFOS III*, Ed. by A Benninghoven, Springer Proc. Phys. **9**, 37 (1986); W. Ens. R. Beavis, G. Bolbach, D. E. Main, B. Schueler and K.G. Standing, in *Secondary Ion Mass Spectrometry, SIMS V*, Ed. by A. Benninghoven, R. J. Colton, D. S. Simmons and H.

W. Werneret, Springer Series in Chemical Physics, No. 44, (1986).

[187] H. Danigel and R.D. Macfarlane, *Int. J. Mass Spectrom. Ion Phys.* **39**, 157 (1981).

[188] F. Riggi, *Nucl. Instrum. Methods B* **22**, 588 (1987).

[189] A. Bertein, *J. Phys. Radium*, **12**, 595 (1951).

[190] M.Y. Berhard, *J. Phys. Radium*, **14**, 381, 451 (1953).

[191] J.L. Verster, *Philips Res. Rep.* **18**, 465 (1963).

[192] O. Becker, *Nucl. Instrum. Methods* **98**, 53 (1982).

[193] S. Widdiyasekera, P. Håkansson and B.U.R. Sundqvist, *Nucl. Instrum. Meth. in Phys. Res B* **33**, 836 (1988).

[194] A. Benninghoven, E. Niehuis, T. Friese, D. Greifendorf, and P. Steffens *Org. Mass Spectrom.* **19**, 346 (1984).

[195] V. Katta, L. Grace, T. Chaudary and B. Chait, *Proceedings of the 36th ASMS Conference on Mass Spectrometry and Allied Topics*, San Francisco, CA. p. 413, (1988).

[196] X. Tang, W. Ens and K. G. Standing, *Proceedings of the 38th ASMS Conference on Mass Spectrometry and Allied Topics*, Tucson, AZ. p. 542 (1990). X. Tang, W. Ens N. Poppe-Schriemer and K. G. Standing in *Methods and Mechanisms for Producing Ions from Large Molecules*, in the NATO ASI Science Series, Ed. by W. Ens and K.G. Standing, Plenum Press (in press).

[197] J.S. Cottrell and S. Evans, *Anal. Chem.* **59**, 1990 (1987).

[198] J.A. Hill, S.A. Martin, J.E. Biller and K. Biemann, *Biomed. Enviroment. Mass Spectrom.* **17**, 147 (1988); J.A. Hill, J.E. Biller, S.A. Martin, K. Biemann, K. Yoshidome and K. Sato, *Int. J. Mass Spectrom. Ion Proc.* **92**, 211 (1989)

[199] K.G. Standing, R. Beavis, W. Ens, X. Tang and J.B. Westmore, in *The Analysis of Peptides and Proteins by Mass Spectrometry*, Ed. by C.J. McNeal, p. 267, John Wiley & Sons, Chichester (1988).

[200] K.G. Standing, W. Ens, F. Mayer, X. Tang and J.B. Westmore, in *Ion Formation from Organic Solids, IFOS V*, Ed. by A. Hedin, B.U.R. Sundqvist and A. Benninghoven, John Wiley & Sons, Chichester, England, p. 93 (1990).

[201] K. G. Standing, W. Ens, X. Tang and J. B. Westmore, in *Mass Spectrometry of Peptides*, Ed. by D.M. Desiderio, CRC press, Florida, p. 159 (1990).

[202] X. Tang, W. Ens and K.G. Standing, *Proceedings of the 37th ASMS Conference on Mass Spectrometry and Allied Topics*. Miami Beach p. 232, (1989).

[203] K. Sato, T. Asada, M. Ishihara, F. kunihiro, Y. Kammei, E. Kubota, C.E. Costello, S.A. Martin, H.A. Scoble and K. Biemann, *Anal. Chem.* **59**, 1652 (1987).

[204] P.C.Bergers, J.L.Holmes, *Rapid Comm. Mass Spectrom.* **3**, 279 (1989).

[205] P. Roepstorff, J. Fohlman, *J. Biomed. Mass Spectrom.* **11**, 601 (1984).

[206] G. Benedek et al, Eds., *Elemental and Molecular Clusters*, Springer Series in Materials Science 6, Spering-Verlag, Berling, (1987).

[207] E.R. Hilf et al, Eds., *PDMS and Clusters*, Lecture Notes in Physics, 269, Springer-Verlag, Berling, (1986).

[208] D. Renner and G. Spiteller, *Biomed. Environ. Mass Spectrom.* **15**, 75 (1988)

[209] R. P. Grese, R.L. Cerny and M. L. Gross, *J. Amer. Chem. Soc.* (in press).

[210] G.C. Thorne and S.J. Gaskell, *Rapid Comm. Mass Spectrom.* **3**, 217 (1989).

[211] W. Kulik, W. Heerma and J.K. Terlouw, *Rapid Comm. Mass Spectrom.* **3**, 276 (1989).

[212] M. Fujioka, I. Sumino, S, koda and T. Yasuda, *Org. Mass Spectrom.*, **25**, 80 (1990).

[213] D.M. Desiderio and M, Kai, *Biomed. Mass. Spectrom.* **10**, 471 (1983).

[214] R.P. Hanzlik, In *Inorganic Aspects of Biological and Organic Chemistry*, Academic press: New York, p 131 (1976).

[215] R. Steinauer, H. Walther and U.P. Schlunegger, *Helv. Chim. Acta* **63**, 610 (1980).

[216] D.M. Desiderio, J.Z. Sabbatini, *J. Z. Biomed. Mass Spectrom.* **8**, 565 (1981).

[217] L.M. Mallis and D.H. Russell, *Anal. Chem.* **58**, 1076 (1986).

[218] S.J. Gaskell, M.H. Reilly and C.J. Porter, *Rapid Comm. Mass Spectrom.* **2**, 142 (1988).

[219] R.D. Macfarlane, personal communicattion.

[220] R. Beavis, Ph.D. Thesis, University of Manitoba, (1987).

[221] S. Della-Negra, Y. Le Beyec and J.C. Tabet, Orsay Report IPNO-DRE-85-22, Institute de Physique Nucleaire, Orsay, France, (1985).

[222] P. Grossmann and H.P. Kellerhals, *Spectrospin Information ICR*, Spectrospin AG, Fallenden, Switzerland, No. 8, p 3, (1986).

[223] K. Biemann, F. Gapp and J. Seibl, *J. Am. Chem. Soc.* **81**, 2274 (1959).

[224] K. Biemann, *Biomed. Environment. Mass Spectrom.* **16**, 99 (1988).

[225] K.G. Standing, W. Ens, Y. Mao, F. Mayer, X. Tang and J.B. Westmore, *J. de physique*, **50, Colloque C2**, 163 (1989).

[226] X. Tang, W. Ens, F. Mayer and K.G. Standing, *Rapid Comm. Mass Spectrom.* **3**, 443

(1989).

[227] S.A. Martin, and K. Biemann, *Int. J. Mass Spectrom. Ion Proc.* **78**, 213 (1987); R.S. Johnson, S.A. Martin, and K. Biemann, *Int. J. Mass Spectrom. Ion Proc.* **86**, 137 (1988).

[228] S.J. Gaskell, P.E. Haroldson and M.H. Reilly, *Biomed. Environment. Mass Spectrom.* **16**, 31 (1988).

[229] E.D. Pauw, *Mass Spectrom. Rev.* **5**, 191 (1986).

[230] K.B. Tomer, M.L. Gross, H,Zappey, R.H.Fokkens and N.M.M. Nibbering, *Biomed. Environ. Mass Spectrom.* **15**, 649 (1988).

[231] N. Poppe-Schriemer, D.R. Binding, W. Ens, J.C. Martens, F. Mayer, K.G. Standing, X. Tang and J.B. Westmore, in *Methods and Mechanisms for Producing Ions from Large Molecules*, in the NATO ASI Science Series, Ed. by W. Ens and K.G. Standing, Plenum Press (in press).

[232] R.E. Tecklenburg, Jr., M.N. Miller and D.H. Russell, *J. Am. Chem. Soc.* **111**, 1161 (1989).

[233] L.M. Nuwaysir and C.L. Wilkins, *Anal. Chem.* **61**, 689 (1989).

[234] G.M. Neumann, M.M. Sheil and P.J.Z. Derrick, *Naturforsch* **39a**, 584 (1984).

[235] B.T. Chait and F.H. Field, *Biochem. Biophys. Res. Commun.* **134**, 420 (1986).

[236] B.T. Chait, T. Chaudhary and F.H. Field, In *Methods in Protein Sequence Analysis*, Ed. by K.A. Walsh, The Humana Press, Clifton, N.J., pp. 483-491, (1987).

[237] M. Barber, L. Tetler, D. Bell, B. Bycroft, J. Monaghan, B.Modren and B.N. Green, *Proceedings of the 35th ASMS Conference on Mass Spectrometry and Allied Topics.* Denver CO, p. 3, ASMS (1987).

[238] R.B. Cody, Jr., I.J. Amster and F.W. Mclafferty, *Proc. Natl. Acad. Sci. USA* **82**, 6367 (1985).

[239] F,Lafortune, M.J.Damha, X.Tang,K.G.Standing, J.B.Westmore and K.K.Ogilvie, *Nucleosides & Nucleotides*, **9(3)**, 445-446 (1990); F,Lafortune, W. Buchannon, G.W. Buchko, F.E. Hruska, K.L. Sadana, K.G.Standing and J.B.Westmore, *Proceedings of the 37th ASMS Conference on Mass Spectrometry and Allied Topics*, Miami Beach p. 730, (1989); F,Lafortune, K.G.Standing, J.B.Westmore M.J.Damha and K.K.Ogilvie, *Org. Mass Spectrom.* **23**, 228 (1988).

[240] M.J. Damha and K.K. Ogilvie, *J. Org. Chem.* **53**, 3710 (1988).

[241] W. Ens, B.U.R. Sundqvist, P. Håkansson, D. Fenyö, A. Hedin and G. Jonsson, *J. de physique*, **50, Colloque C2**, 9 (1989).

[242] B. Blanchard, D. Flotté, P. Juliet, in *Proc. 6th Int. Conf. Secondary Ion Mass Spectrometry, SIMS VI*, Ed. by A. Benninghoven, A. M. Huber and J. W. Werner, John Wiley & Sons, Chichester, England, p. 71 (1988).